The intracellular targeting and regulation of PDE4 cyclic AMP-specific phosphodiesterase enzymes

A thesis submitted to the University of Glasgow for the degree of Doctor of Philosophy in the Faculty of Science

ALEXANDER HOWARD PEDEN B.Sc., A.R.C.S

Division of Biochemistry and Molecular Biology
Institute of Biomedical and Life Sciences (IBLS)
University of Glasgow

September 2000

ProQuest LLC.
789 East Eisenhower Parkway
P.O. Box 1346
Ann Arbor, MI 48106 – 1346

Dedicated to my Wife and my Parents

ABSTRACT

Cyclic adenosine 5': 3' monophosphate (cAMP) is a ubiquitous second messenger in cells which transduces the action of a wide variety of hormones and neurotransmitters. cAMP phosphodiesterase (PDE) enzymes provide the sole route for the degradation of cAMP and are thus placed in a key position for regulating cAMP-dependent processes. The cAMP-specific PDE4 enzyme family are encoded by four genes (PDE4A, -B, -C and -D) which each generate a number of isoenzymes by alternative 5' mRNA splicing. This process gives rise to PDE4 isoenzymes with unique extreme NH_2-terminal splice regions, one or two upstream conserved regions (UCR1/UCR2) and a central to COOH-terminal catalytic unit. The extreme NH_2-terminal splice domains confer distinct modes of regulation and intracellular targeting on the PDE4 isoenzymes. Understanding the distinct physiological roles of individual PDE4 isoenzymes may aid the development of more specific PDE4 inhibitor-based drugs for therapeutic use in a number of disease states.

I have assessed the involvement of PDE4 isoenzymes in the cAMP-dependent effect of growth hormone (GH) on the differentiation of mouse 3T3 F442A preadipocyte cells (Chapter 3). The PDE4-specific inhibitor rolipram had previously been shown to potentiate the GH-promoted differentiation of these cells to adipocytes. Using the reverse transcription-polymerase chain reaction (RT-PCR) with isoenzyme-specific primer pairs, I determined the PDE4 mRNA transcripts expressed in 3T3-F442A preadipocytes, which were PDE4A1, -A5, -B2, -C2, -D3 and -D5. I cloned and sequenced the PCR fragments for murine PDE4A5, -B2 and -D5 to verify their identities. Stimulation with GH caused an increase in the activity of PDE4A. Having identified PDE4A5 as the sole PDE4A splice variant expressed in these cells, I showed that the level of the PDE4A transcript is not affected by GH treatment. This result combined with other studies suggests that challenge with GH results in the specific activation of PDE4A5 via a post-translational modification, rather than an effect on transcription. The GH-dependent activation of PDE4A5 is proposed to serve as a brake on the process of 3T3 F442A differentiation.

In Chapter 4 of this thesis I have analysed the intracellular targeting of the rat PDE4A isoenzymes RNPDE4A1 (RD1) and RNPDE4A5 (rpde6). I have used chimeric constructs to show that the unique NH_2-terminal regions of RD1 (amino acids 1-100) and rpde6 (amino acids 1-256) can confer membrane association on the normally soluble protein glutathione-*S*-transferase (GST). Furthermore, the region between amino acids 103 and 256 on rpde6, which is shared with the other long PDE4A splice variant rpde39

(RNPDE4A6), is sufficient for membrane binding. The NH_2-terminal regions of RD1 and rpde6 bind to components of the P2-membrane fraction that have different thermal stabilities suggesting that they interact with distinct lipid or protein anchoring molecules.

I have further investigated the protein-protein interactions of rpde6 (Chapter 5). Evidence was obtained from yeast-2-hybrid studies that rpde6 might interact with a novel immunophilin-like protein, RB3. I confirmed this interaction *in vitro*, by showing that a purified GST-fusion of RB3 (but not GST) could pull down rpde6 from the cytosolic fraction of transfected COS-7 cells. Subcellular distribution analysis of transfected COS-7 cells showed that RB3 was distributed between the P1 low-speed pellet fraction (~16%) and the cytosolic S fraction and was absent from the high speed P2-membrane fraction, in contrast to rpde6 which was present in all three fractions. This suggests that the *in vivo* interaction between RB3 and rpde6 may be limited to particular subcellular compartments.

The association of GST-RB3 had a marked inhibitory effect on the catalytic activity of cytosolic rpde6 (IC_{50} ~0.2μM), which was also seen with a maltose binding protein (MBP)-tagged RB3, but not with GST or MBP alone. This inhibitory effect was also seen with a GST fusion of the FK506 binding protein FKBP52, the closest homologue of RB3. In contrast to cytosolic rpde6, particulate (P1 and P2) fraction rpde6 was resistant to inhibition by RB3.

I have shown that the COOH-terminal half of RB3 (amino acids 170-330) which contains a 34-amino acid tetratricopeptide repeat (TPR) motif in its COOH-terminal region mediates both the binding and inhibition of cytosolic rpde6. I have mapped the RB3 binding site on rpde6 to amino acids 218-259, which corresponds to the NH_2-terminal half of UCR2. The NH_2-terminal region of rpde6 has previously been shown to interact with the SH3 domains of Src-family tyrosyl kinases such as Lyn. I have shown that that Lyn SH3 does compete with RB3 for interaction with rpde6.

The above studies suggest that the association of RB3 or a similar TPR-containing protein may represent a new mechanism for the regulation and/or intracellular targeting of rpde6 *in vivo*. Alternatively, this interaction may provide a means for the specific regulation of RB3 function by rpde6.

ACKNOWLEDGEMENTS

I would firstly like to thank Prof. Miles Houslay for his friendly and helpful supervision during the course of this Ph.D. I also thank the members of the Gardiner Laboratory for their friendship and technical assistance.

I would also like to acknowledge the Biotechnology and Biological Sciences Research Council for funding my Ph.D studentship.

I am indebted to my wife Kirsty, my Parents and to my wider family for their tolerance and support over the past few years.

CONTENTS

FIGURES INDEX

TABLES LIST

Abbreviations

aa	Amino acid
AC	Adenylyl cyclase
AhR	Aryl hydrocarbon receptor
AIP	Aryl hydrocarbon receptor interacting protein
AKAP	A kinase anchoring protein
5'AMP	adenosine 5' monophosphate
ARA9	Aryl hydrocarbon receptor associated protein 9
ARNT	Aryl hydrocarbon receptor nuclear translocator
ATP	Adenosine 5' trisphosphate
bp	Base pair
BSA	Bovine serum albumin
Ca /CaM	Calcium/calmodulin
cAMP	Cyclic adenosine-3' 5'-monophosphate,
CAT	Chloramphenicol acetyl transferase
CaM	Calmodulin
CBP	CREB binding protein
CDK	Cyclin dependent kinase
cDNA	Complementary DNA
cGMP	Cyclic guanosine-3' 5'-monophosphate
CNS	Central nervous system
Complete KHEM	KHEM buffer including 1 mM DTT and 1 times Complete™ protease inhibitor cocktail (Boehringer Mannheim)
Conc.	Concentration
CRE	cAMP response element
CREB	cAMP response element binding protein
CREM	cAMP response element modulator
CsA	Cyclosporin A
Cyp40	Cyclophilin 40
DAG	Diacylglycerol

DEAE	Diethyl aminoethyl
DEPC	Diethyl pyrocarbonate
DMEM	Dulbecco's modification of Eagle's Medium
DMSO	Dimethyl sulphoxide
DNA	Deoxyribonucleic acid
dNTP	Deoxynucleotide trisphosphate
DRE	Dioxin response element
DTT	Dithiothreitol
ECL	Enhanced chemiluminescence
EDTA	Diaminoethane-tetra-acetic acid
EGF	Epidermal growth factor
EGTA	Ethylene glycol-bis(β-aminoethyl ether)-N,N,N',N'-tetraacetic acid
EHNA	Erythro-9-(2-hydroxy-3-nonyl)adenine
ELISA	Enzyme linked immunosorbent assay
EPAC	Exchange protein directly activated by cAMP
ERK(1/2)	Extracellular signal regulated kinase
EU	Enzyme units, e.g. one unit of PDE activity = 1pmol (cAMP)/min
FCS	Foetal calf serum
FKBP	FK506 binding protein
FRAP	FKBP12 rapamycin associated protein
GC-D	Odorant receptors with guanylate cyclase activity specific to olfactory neurones
GDP	Guanosine 5' diphosphate
GEF	Guanine nucleotide exchange factor
GH	Growth hormone
GPCR	G-protein coupled receptor
G-protein	Guanine nucleotide binding regulatory protein
GR	Glucocorticoid receptor
GRE	Glucocorticoid response element
GRK	G-protein coupled receptor kinase

GSK	Glycogen synthase kinase 3
GST	Glutathione-*S*-transferase
GTP	Guanosine 5' triphosphate
GPDH	Glycerol-3-phosphate dehydrogenase
HEK293	Human embryonic kidney 293 cells
HEPES	N-2-Hydroxyethylpiperazine-N'-2-ethanesulfonic acid
hnRNA	Heterogeneous nuclear RNA
HPLC	High pressure liquid chromatography
HRP	Horse radish peroxidase
Hsp90, Hsp70	Heat shock protein 90, heat shock protein 70
IBMX	Isobutylmethylxanthine
IC_{50}	Concentration of inhibitor yielding 50% inhibition of enzyme.
IGF	Insulin-like growth factor
IL	Interleukin
IPTG	Isopropyl-β-D-thiogalactopyranoside
IRS1/IRS2	Insulin receptor substrate 1 (or 2)
JAK	Janus kinase
Kb	Kilobases
K_d	Dissociation constant
KHEM buffer	50 mM KCl, 50 mM HEPES-KOH pH 7.4, 10 mM EGTA, 1.92 mM $MgCl_2$ buffer
LB	Luria-Bertani
LR	Linker region
MAP kinase	Mitogen activated protein kinase
MBP	Maltose binding protein
MEK	MAP kinase kinase
MOPS	3-[N-morpholino] propanesulfonic acid
mRNA	messenger RNA
MW	Molecular weight
NBCS	New born calf serum

NF-AT	Nuclear factor of activated T-cells
NMDA	*N*-methyl-*D*-aspartate
NMR+	Nuclear magnetic resonance
NO	Nitric oxide
OD_{600}	Optical density (e.g. at 600nm)
ORF	Open reading frame
PA	Phosphatidic acid
PAH	Polycyclic aromatic hydrocarbons
PBS	Phosphate buffered saline
PCR	Polymerase chain reaction
PDE	Phosphodiesterase
PDK	PtdIns(3,4,5)P_3-dependent protein kinase
PH domain	Pleckstrin homology domain
PI3-kinase	Phosphatidylinositol 3-kinase
PKA	cAMP-dependent protein kinase, protein kinase A
PKB	Protein kinase B
PKC	Ca^{2+}/phospholipid-dependent protein kinase, protein kinase C
PKI	PKA inhibitor protein
PMA	Phorbol 12-myristate 13-acetate
PMSF	Phenylmethylsulphonyl chloride
PP5	Protein phosphatase 5
PPIase	Peptidyl prolyl *cis-trans* isomerase activity
PPII helix	Polyproline type II helix
PSD-95	Postsynaptic density protein-95
PtdIns	Phosphatidylinositol
PtdIns(3)*P*	Phosphatidylinositol-3 phosphate
RB3	Rat Brain 3, rat homologue of the protein AIP and the human immunophilin-like protein ARA9
RIPA	Radio-immunoprecipitation assay

RNA	Ribonucleic acid
ROM	Reactive oxygen metabolites
RPMI-1640	Roswell park memorial institute 1640 medium
RT-PCR	reverse transcription-polymerase chain reaction
SD	Standard deviation
SDS	Sodium dodecyl sulphate
SDS-PAGE	Sodium dodecyl sulphate polyacrylamide gel electrophoresis
SE	Standard error
SH2 domain	Src homology 2 domain
SH3 domain	Src homology 3 domain
STAT	Signal transducer and activator of transcription
Sos	Son of sevenless
TAE	Tris/acetate/EDTA
TBS	Tris buffered saline
TCCP	2,3,7,8-tetrachlorodibenzo-*p*-dioxin
TE	Tris/EDTA
TEA	Triethanolamine
TEMED	N,N,N',N'-tetramethyl-ethylenediamine
TNF	Tumour necrosis factor
TPR	Tetratricopeptide repeat
TSH	Thyroid stimulating hormone
UCR1/ UCR2	Upstream conserved regions 1 and 2
UV	Ultraviolet
W/V	Weight(mass) for volume
XAP2	Hepatitis B virus X-associated protein (identical to ARA9)
X-gal	5-bromo-4-chloro-3-indolyl-β-D-galactopyranoside

CHAPTER 1

Introduction

1.Introduction

1.1 The cAMP signalling pathway

Cyclic adenosine 5': 3' monophosphate (cAMP) is a ubiquitous second messenger involved in a wide range of physiological processes such as lipolysis, glycogenolysis (Manganiello et al., 1996), cytoskeletal function, regulation of gene transcription (Daniel et al., 1998), cell growth, proliferation (Dugan et al., 1999), differentiation (Yarwood et al., 1998), neurotransmission, learning and memory (Byers et al., 1981). The cAMP signalling pathway is illustrated in Figure 1.1. cAMP is generated from ATP by the action of the membrane-bound enzyme adenylyl cyclase (AC). The activity of this enzyme is regulated by external stimuli (e.g. hormones or neurotransmitters) via the concerted action of G protein coupled receptors (GPCRs) and heterotrimeric G proteins. The latter consists of guanine nucleotide binding αGs subunit and a tightly associated Gβγ dimer (Hamm and Gilchrist, 1996). The binding of a ligand to a GPCR causes the intracellular domain of this receptor to interact with the αGs subunit. This causes a conformational change in the αGs subunit that results in the release of GDP and its replacement with GTP. αGs-GTP is then released from Gβγ and diffuses within the membrane to activate adenylyl cyclase. In contrast to this, αGi subunits have inhibitory effects on adenylyl cyclase. The Gβγ dimer is also involved in the regulation of adenylyl cyclase activity. For example, Gβγ can have inhibitory effects on the adenylyl cyclase isoform AC-I, but synergises with αGs in the activation of the AC-II and AC-IV isoforms (Taussig and Gilman, 1995). It should be noted that adenylyl cyclase can also be activated by the direct binding of the diterpene agent forskolin (Houslay and Milligan, 1997) and by cholera toxin, which ADP-ribosylates and activates a stimulatory G protein.

The activation of adenylyl cyclase results in an elevation in the intracellular concentration of cAMP. This in turn results in the activation of cAMP-dependent protein kinase (PKA). The PKA holoenzyme is a heterotetramer consisting of two regulatory (R) subunits and two catalytic (C) subunits. Each of the R subunits binds to one molecule of cAMP and this results in the release and activation of the two C subunits. The C subunits phosphorylate and thereby regulate a large number of proteins including ion channels, cytoskeletal elements and metabolic enzymes. The activated C subunits may also translocate to the nucleus where they can phosphorylate and regulate transcription factors such as CREB (cAMP-response element binding protein). PKA-phosphorylated CREB

binds to the co-activator CBP (CREB binding protein) and activates the expression of number of genes by binding to cAMP response elements (CRE) in their promoter regions (Frank and Greenberg, 1994; Lalli and Sassone-Corsi, 1994; Roesler et al., 1988).

The phosphodiesterase (PDE) enzymes represent a crucial component of the cAMP-signalling pathway. PDEs catalyse the hydrolysis of cAMP to 5'AMP (see Figure 1.1) and thus provide the sole route for the degradation of cellular cAMP. The activity of PKA in cells therefore largely depends on the relative activities of adenylyl cyclase and PDEs. The regulation of these two opposing enzyme activities is equally important in the control of cAMP-dependent processes.

PKA enzymes are only activated above a certain threshold cAMP level. Therefore, cells that express adenylyl cyclase isoforms with a high basal level of activity will be more responsive to signals that elevate cAMP by inhibiting PDE activity. Several physiological processes such as lipolysis in adipocytes (Manganiello et al., 1996) and the production of insulin by pancreatic β-cells appear to be regulated by signals that act via PDE isoenzymes (Zhao et al., 1997).

By lowering the local intracellular concentration of cAMP, PDEs provide one mechanism for the desensitisation of cAMP signalling pathways. Other mechanisms for desensitisation exist, including those that involve the uncoupling of adenylyl cyclase from the GPCR. Once such mechanism is the phosphorylation of the GPCR by G-protein coupled receptor kinases (GRK) or by PKA. This is followed by the binding of an arrestin protein to the intracellular domain of GPCR, which then sterically blocks the binding of heterotrimeric G proteins (Luttrel et al., 1999). Other proteins that may be involved in desensitisation are PKIs (PKA-inhibitor proteins) which binds to and inhibit the C subunit of PKA (Daniel et al., 1998).

Figure 1.1 depicts the classical cAMP signalling pathway in which PKA acts as the cAMP sensor protein. Recently a new target protein for cAMP has been cloned, called EPAC (Exchange protein directly activated by cAMP) (De Rooij et al., 1998). EPACs function as cAMP-activated guanine nucleotide exchange factor (cAMP-GEF) (Kawasaki et al., 1998). The EPAC protein contains a cAMP binding domain fused to a GEF domain. These proteins are responsible for the cAMP-dependent activation of the small G protein Rap1, a close relative of Ras. In a similar manner to heterotrimeric G proteins, small G proteins such as Rap1 and Ras are activated by the exchange of a bound GDP molecule for GTP. With small G proteins this process is catalysed by guanine nucleotide exchange

factors (GEFs). The binding of cAMP to EPAC results in the allosteric activation of its GEF domain, which promotes the GDP/GTP exchange on Rap1. Activated Rap1 can phosphorylate a number of proteins including Raf-B, which results in the activation of the Raf-MEK-ERK kinase cascade (Vossler et al., 1997). PKA is not involved in the cAMP-dependent activation of Rap1. Therefore, EPACs represent a new family of cAMP sensors and a new point of cross talk between cAMP signalling and the Raf-MEK-ERK kinase pathways. EPAC may also be negatively regulated by PDEs. The activation of PDEs will result in a decrease in the local concentration of cAMP, which would lead to a decrease in the activity of EPACs. This may be a new mechanism for the down-regulation of the Raf-MEK-ERK pathway.

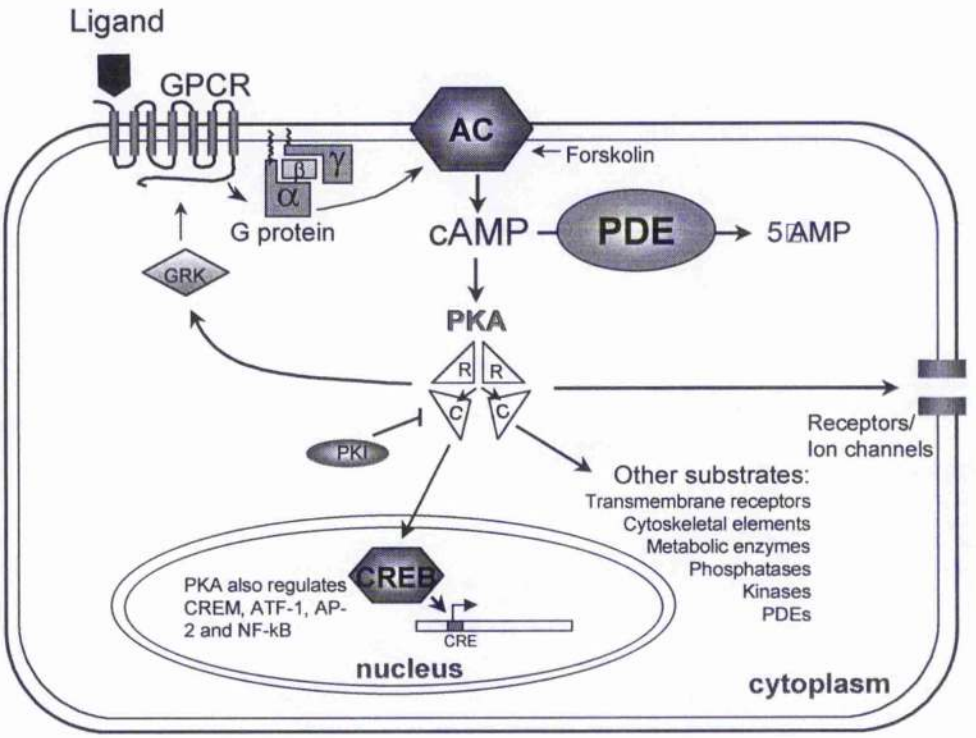

Figure 1.1 cAMP signalling pathway

cAMP is generated by the membrane-bound adenylyl cyclase (AC). The activity of this enzyme is regulated by external stimuli (e.g. hormones or neurotransmitters) which bind to G protein coupled receptors (GPCRs) which are seven-pass transmembrane proteins. The ligand/receptor complexes bind to and activate the αGs subunit of the heterotrimeric G protein Gs. αGs diffuses along the membrane and activates adenylyl cyclase (AC) which catalyses the formation of cAMP from ATP. Adenylyl cyclase is also activated by the direct binding of forskolin. cAMP binds to the R subunits of PKA which results in the release and activation of the C subunits which phosphorylate a broad range of substrate proteins, including transcription factors such as CREB. The breakdown of cAMP to 5'AMP is catalysed by phosphodiesterase (PDE) enzymes.
GRK= G protein coupled receptor kinase, CREB = cAMP response element binding protein, PKI= PKA-inhibitor protein.

1.1.1 The cGMP signalling pathway

Another second messenger with many physiological roles is cyclic guanosine 3': 5' monophosphate (cGMP). These roles include smooth muscle relaxation, inhibition of platelet aggregation, neutrophil degranulation and visual signal transduction (Corbin and Francis, 1999). The cAMP-pathway is analogous to the cGMP-signalling pathway. However, there are several key differences. Firstly, both soluble and transmembrane forms of guanylate cyclase exist, in contrast to adenylyl cyclase isoforms, which are all membrane-associated. The soluble guanylate cyclase exists as a heterodimer and is activated by nitric oxide. The up-regulation of cGMP via this route is involved in processes such as the relaxation of arteriolar smooth muscle (Moreland et al., 1999). In transmembrane guanylate cyclases the binding of a ligand to their extracellular domains results in an activation of their intracellular catalytic domains and the production of cGMP. Examples of this type of guanylate cyclase are the GC-D odorant receptors that are specific to olfactory neurones (Juilfs et al., 1997) and the atrial natriuretic peptide receptor. In contrast to the tetrameric PKA enzyme, its counterpart in the cGMP pathway, PKG (cGMP-dependent protein kinase) is a single polypeptide that contains a regulatory domain for binding cGMP and a catalytic domain. As discussed below (see section 1.3) certain PDE families catalyse the breakdown of cGMP to 5'GMP. One such family, PDE6, is a central component of the visual signalling pathway (Korschen et al., 1999).

1.2 Isoform multiplicity and intracellular targeting of the components of the cAMP signalling pathway

Isoform multiplicity occurs at all levels of the cAMP signalling pathway. The multitude of physiological responses that can be elicited by the activation of the cAMP signalling pathway in different cells is based on the selective expression of these isoforms. This is firstly seen at the level of the G-protein coupled receptors (GPCRs) of which there are many isoforms including those for amines, peptides, eicosanoids, light and odorants. Secondly, a considerable variety of heterotrimeric G protein complexes are possible from a choice of at least 20 α isoforms, 5 β isoforms and 12 γ isoforms (Clapham, 1996; Hamm and Gilchrist, 1996). The α subunits from different G proteins have a variety of effects, which include the stimulation (αGs) or inhibition (αGi) of adenylyl cyclase, or association with specific GPCRs, such as the odorant receptors (Golf) (Juilfs et al., 1997).

At least nine adenylyl cyclase (AC) isoenzymes exist, which show different patterns of regulation. For example AC-I, -III and -VIII are stimulated by Ca^{2+}/calmodulin (Ca^{2+}/CaM), whereas AC-V and AC-VI are inhibited by Ca^{2+}/CaM. The diversity of adenylyl cyclase isoenzymes is increased further by alternative mRNA splicing. For instance, AC-VIII produces three splice variants with different Ca^{2+}/CaM sensitivities. Certain adenylyl cyclase isoenzymes are also phosphorylated by PKA (AC-V) and phosphorylation by PKC can activate the AC-I/II/III isoforms (Houslay et al., 1997). Therefore, the adenylyl cyclase isoenzymes expressed by a cell will affect the integration of intracellular Ca^{2+} and cAMP signals. Although all adenylyl cyclase isoenzymes are activated by the αGs subunit of stimulatory G proteins, the other αGs subunits, (including αGp and αGi), have different effects on different adenylyl cyclase isoenzymes. In addition, certain adenylyl cyclase isoenzymes appear to have distinct patterns of intracellular localisation. For example, ACIII is exclusively found in the cilia of olfactory neurones (Juilfs et al., 1997) and other work has suggested the co-localisation of the Ca^{2+}-sensitive isoenzymes ACI and ACVIII with plasma membrane Ca^{2+} channels (Fagan et al., 1996).

Isoform multiplicity also occurs at the level of the PKA holoenzyme. Two forms of R subunit were originally identified, with RI being mostly cytoplasmic and RII being associated with the particulate fraction of cells. Four separate gene products, RIα, RIβ, RIIα and RIIβ have now been identified, with additional isoforms of RIα arising through alternative mRNA splicing (Daniel et al., 1998). Three forms exist for the C subunit as well, namely Cα, Cβ and Cγ and mRNA splice variants have been reported for the Cα and Cβ genes. These subunits can give rise to a considerable number of R_2C_2 combinations that display different cAMP sensitivities (Daniel et al., 1998).

The intracellular localisation of PKA is determined by the association of their R subunit dimers with A-kinase anchoring proteins (AKAPs). The AKAPs are an increasingly large family of proteins that are responsible for targeting PKA to a diverse range of intracellular locations such as the nucleus (AKAP350), mitochondria (AKAP84), microtubules (MAP2) and the plasma membrane (AKAP79) (Edwards and Scott, 2000). The association of R subunits with AKAPs restricts the action of PKA to specific regions of the cell and limits its access to substrates. In this way, the AKAPs confer specificity on a multi-functional kinase that has a very broad range of substrate proteins (Cheley et al., 1994). The first AKAP proteins to be identified all associated with the RII subclass of proteins. These associations were high affinity, in the nanomolar range (Carr et al., 1992).

More recently, novel AKAPs have been discovered that can associate with the both RI and RII subunits (Huang et al., 1997). The association with RI is of a lower affinity, in the micromolar range. This interaction is likely to be physiologically relevant when RII concentrations are limiting (Burton et al., 1997). Targeting domains have been identified on a number of AKAPs including a mitochondrial membrane targeting sequence in AKAP84 and spectrin-like repeats in mAKAP that direct it to the perinuclear region (Colledge and Scott, 1999).

The isoform diversity seen for the above proteins is also clearly seen in the phosphodiesterase (PDE) family, which is the main subject of this thesis. At least 10 PDE families have been identified to date containing over 30 isoenzymes in total. As discussed below in section 1.3 the different PDE isoenzymes show distinct patterns of regulation and intracellular targeting. The PDE isoenzymes expressed by a cell will profoundly effect the response to stimuli that act via cAMP or cGMP.

1.2.1 The compartmentalisation of cAMP

As discussed in the previous section, multiple isoforms with different patterns of regulation and intracellular targeting exist at each level of the cAMP signalling pathway. The combination of isoforms expressed by a cell will affect the duration and the magnitude of the cAMP response. However, this does not explain how the cAMP signalling pathway can be used by two different signals to produce two different effects in the same cell. An early example of this was the effect of isoproterenol and prostaglandin E_1 on cardiac myocytes (Hayes et al., 1982). Both these agents caused an increase in intracellular cAMP, which led to the activation of PKA. However, stimulation with isoproterenol resulted in the increased phosphorylation of ~16 proteins that were not phosphorylated upon stimulation with prostaglandin E_1.

An hypothesis put forward to explain this was that the different hormones affect different intracellular pools of cAMP (Hohl and Li, 1991). The components of cAMP signalling pathway that are involved in the generation of cAMP (i.e. the GPCRs and adenylyl cyclase) are localised to specific regions of plasma membrane. In addition, both PKA (which detects cAMP) and PDE (which degrades cAMP) are targeted to specific regions within the 3-D matrix of the cell. Therefore, a system is in place whereby the activation of certain GPCRs can result in an increase the concentration of cAMP within discrete compartments within the cell. This results in the activation of specific sub-

populations of PKA enzymes that are targeted to these compartments by their association with AKAP anchoring proteins. These targeted PKAs will only phosphorylate substrates in their vicinity. Different stimuli affect distinct cAMP compartments and thereby cause unique physiological responses. The cAMP levels in these various compartments could be differentially regulated by specifically targeted PDEs which breakdown cAMP.

Several studies have identified a role for PDE isoenzymes in the compartmentalisation of cAMP. For example, Jurevicius and Fischmeister have studied the cAMP-dependent activation of Ca^{2+} channels by β2-adrenoceptor agonists in frog cardiac myocytes (Jurevicius and Fischmeister, 1996). In this system, the β2-adrenoceptor agonist, isoprenaline causes an elevation in cAMP and the activation of PKA (as described in section 1.1), which phosphorylates and activates the L-type Ca^{2+} channels in the plasma membrane (Hartzell et al., 1991). Jurevicius and Fischmeister showed that the 'local' stimulation of Ca^{2+} channels in the half of the cell exposed to the agonist was 40-fold greater than the 'distant' stimulation in the other half of the cell that had not been exposed to agonist. The prevalence of the local effect of the agonist over its distant effect was significantly diminished by the presence of the PDE inhibitor, IBMX (Jurevicius and Fischmeister, 1996). Further analysis with PDE family-specific inhibitors (see section 1.3 below) suggested that the localised activation of the Ca^{2+} channels was due, at least in part, to the compartmentalisation of cAMP by PDE3 and PDE4 (Jurevicius et al., 1997).

Several groups have uncovered evidence for the existence of two distinct pools of cAMP in the same cell that are regulated by different PDE isoenzymes. For instance, Dousa and coworkers have studied two cAMP-regulated processes in the mesangial cells of the kidney glomeruli. One of these processes is the generation of superoxide during the respiratory burst, which is a factor in the pathogenesis of glomerulonephritis (Dousa, 1999). This process was inhibited by PDE4-specific inhibitors, such as rolipram, but not by the PDE3-specific inhibitor, cilostamide (Chini et al., 1994; Chini et al., 1997). Another cAMP-dependent process in mesangial cells is the mitogenic stimulation of DNA synthesis, which was inhibited by PDE3 inhibitors, but unaffected by PDE4 inhibitors. This implied that two different PDE isoenzymes compartmentalise two separate pools of cAMP that regulate DNA synthesis or superoxide generation. The specific involvement of PDE4 in the regulation of the respiratory burst suggests that PDE4 inhibitors might be developed for use in treating inflammatory glomerulopathies without affecting DNA synthesis (Dousa, 1999).

The above studies have demonstrated that PDE isoenzymes play a crucial role in the compartmentalisation of cAMP. A greater understanding of this process will be gained from identifying the specific PDE isoenzymes that are involved. Information on the intracellular localisation, protein-protein interactions and regulation of these PDE isoenzymes may aid the design of drugs that target specific pools of cAMP within cells. These drugs may have more effective therapeutic actions with fewer side effects.

1.3 The phosphodiesterase superfamily

The PDE superfamily is large and complex (Beavo et al., 1994). At the present time it consists of at least 11 families that catalyse the hydrolysis of cAMP, cGMP or both. These PDE families can be further distinguished according to their primary structures, their modes of regulation and their inhibition by specific inhibitors. Each of the PDE families contains one to four genes and many of these genes generate several isoenzymes by alternative 5' mRNA splicing and the use of different transcription initiation sites. This results in PDE isoenzymes with common central and COOH-terminal regions and variable NH_2-terminal regions. In addition, alternative 3' mRNA splicing has been observed for members of the PDE1 family. The isoenzymes within each of these PDEs families show distinct patterns of expression in different tissues and have different characteristics. A summary of the general characteristics of each of the 11 families is given Table 1.1.

The focus of this thesis will be the PDE4 cAMP-specific family. A major theme will be the intracellular targeting, proteins-protein interactions and regulation of certain isoenzymes within this gene family. In order to understand the properties and functions of the PDE4 isoenzymes, it is necessary to review the PDE superfamily as a whole.

1.3.1 PDE nomenclature

A system of nomenclature has been developed to cope with the complexity of the PDE superfamily (Beavo et al., 1994). This can be explained with the following example of HSPDE4A5 where 'HS' refers to the species of origin (in this case *Homo sapiens*), 'PDE4' refers to the gene family, 'A' refers to the gene and '5' refers to the splice variant. A letter sometimes given after the splice variant number refers to the specific GenBank report for a splice variant that has been cloned separately by two or more groups.

1.3.2 Structure and regulation of PDE isoenzymes

All PDE isoenzymes have the same general structure, which is shown in the first column of Table 1.1. The catalytic units of PDEs generally occupy the central to COOH-terminal region of these enzymes. This region is conserved between members of the same gene family. However, the NH_2-terminal regions of PDEs are variable and contain sequence motifs involved in the regulation of PDE catalytic activity. For instance, the PDE1 isoenzymes have two putative Ca^{2+}/calmodulin (Ca^{2+}/CaM) binding domains in their NH_2-terminal regions. The binding of Ca^{2+}/CaM causes the activation of these isoenzymes, which can hydrolyse both cAMP and cGMP. The PDE1 family contains 3 genes and the diversity of this family is further increased by 5' and 3' alternative mRNA splicing which results in isoenzymes which differ at the NH_2- and COOH-termini. One consequence of the 5' alternative mRNA splicing is the generation of splice variants with different Ca^{2+}/CaM binding affinities. For instance, the NH_2-terminal regions of PDE1C2 and the other PDE1C splice variants diverge at a point midway between the two Ca^{2+}/CaM binding domains. As a result, PDE1C2 has a significantly greater sensitivity to Ca^{2+} when compared with PDE1C1, -3, -4 and -5 (Yan et al., 1996). The NH_2-terminal regions of PDE1C isoenzymes also contain sites for regulation by phosphorylation. PKA-phosphorylation of PDE1A1 and 1A2 reduces the affinity of these isoenzymes for Ca^{2+}/CaM (Beavo, 1995). Therefore PDE1 isoenzymes provide a means of cross talk between the cAMP and Ca^{2+} signalling systems.

The PDE2, PDE5, PDE6, PDE10 and most recently identified PDE11 families all contain two GAF domains within their NH_2-terminal regions (see Table 1.1) (Fawcett et al., 2000; Soderling et al., 1999; Soderling and Beavo, 2000). GAF domains have been identified in a diverse range of proteins, including those from plants, bacteria and vertebrates (Aravind and Ponting, 1997). The name GAF stands for three proteins that contain these conserved domains: cGMP-specific phosphodiesterases, cyanobacterial *Anabaena* adenylyl cyclase and the *Escherichia coli* transcriptional regulator FhlA. In PDE5 and 6, these GAF domains have been shown to bind cGMP (Granovsky et al., 1998). The cAMP and cGMP hydrolysing activities of the GAF-containing PDE2 isoenzymes are activated by the allosteric binding of cGMP (Beavo, 1995). Therefore, PDE2 may mediate cross talk between cAMP and cGMP signalling pathways. For instance, in a certain subset of olfactory neurones activation of transmembrane guanylate cyclase may result in the

activation of PDE2 which may result in a down-regulation of the cAMP signalling pathway activated by odorant receptors (Juilfs et al., 1997).

The cGMP-specific PDE6 has a very specialised function in the visual signal transduction pathway and is exclusively expressed in the rod and cone photoreceptors of the retina. PDE6 differs from the other PDEs in that it is a multi-subunit protein. In bovine rod photoreceptors the PDE6 holoenzyme consists of the catalytic subunits (α and β) in association with two inhibitory γ subunits (Stryer, 1991). The α and β subunits correspond to PDE6A and PDE6B,respectively (see Table 1.1). The visual signalling pathway in rod photoreceptors is initiated by a photon-induced change in the conformation of the rhodopsin receptor in the internal disc membranes. This results in the activation of the heterotrimeric G protein transducin. The α subunit of transducin interacts with the PDE6 holoenzyme and causes the release of the α and β catalytic subunits from the inhibitory γ subunit. The activation of these catalytic subunits results in a drop in the levels of cGMP. This in turn results in the closure of cGMP-gated ion channels in the rod photoreceptor plasma membrane, membrane hyperpolarisation and a decrease in neurotransmitter release (Chabre and Deterre, 1989; Yarfitz and Hurley, 1994). PDE6A and PDE6B may be regulated by the association of cGMP with their NH_2-terminal GAF domains (Granovsky et al., 1998). The binding of cGMP to rod photoreceptor PDE was increased in the presence of the γ subunit, whereas activated rod PDE had a reduced affinity of cGMP (Yamazaki et al., 1982).

The cGMP-specific PDE5 shares certain structural similarities with PDE6. The binding of cGMP to the NH_2-terminal GAF domains of PDE5 results in a conformational change that allows phosphorylation and activation by PKG and PKA (Turko et al., 1998). The exact physiological role of this phosphorylation is unclear. However, Lochhead et al have provided evidence that two binding proteins form a regulatory complex with PDE5 in airway smooth muscle cells (Lochhead et al., 1997). Interestingly, these proteins, which run at 14 and 18kDa on SDS-PAGE, can be detected in the membranes of these cells using an antibody raised against the 24-46 region of the inhibitory γ subunit of PDE6. A peptide corresponding to this 24-46 region and full-length recombinant γ both prevented the PKA-induced activation of PDE5. This suggests that an epitope common to the 14 and 18kDa proteins and the γ subunit interacts with PDE5 and prevents its activation by PKA. Therefore, regulation by both protein-protein interactions and phosphorylation are common characteristics of members of the PDE superfamily.

As discussed in section 1.4, the PDE4 isoenzymes also have two conserved regions (UCR1 and UCR2) at their extreme NH_2-termini that appear to be involved in the regulation of enzyme activity. These are similarly placed to the paired GAF domains in PDE2, -5, -6 and -10 and the paired Ca^{2+}/CaM binding domains in PDE1. Therefore, a general theme of PDE regulation is that conformational changes in the NH_2-terminal, caused by phosphorylation, protein- or cyclic nucleotide-interaction, can affect the function of the catalytic unit.

Table 1.1 Phosphodiesterase superfamily

PDE family	Genes	Substrate specificity	Inhibitors	Examples of regulation
PDE1 	PDE1A PDE1B PDE1C	cGMP and cAMP	Nicardipine, Methoxymethyl-IBMX Vinpocetine, KS-505a	Stimulated by Ca^{2+}/calmodulin Phosphorylated by PKA/PKG
PDE2 	PDE2	cGMP and cAMP	EHNA	Stimulated by cGMP
PDE3 	PDE3A PDE3B	cAMP specific	Cilostamide, milrinone, enoximone Siguazodan	Competitively Inhibited by cGMP. Activated by Insulin in adipocytes
PDE4 	PDE4A PDE4B PDE4C PDE4D	cAMP specific	Rolipram, Ro-20-1724, CDP840, RP 73401, CP80633	Phosphorylated by PKA, Phosphorylated by ERK2
PDE5 	PDE5	cGMP specific	Zaprinast Sildenafil	cGMP binding results in phosphorylation by PKA/PKG
PDE6 	PDE6A PDE6B PDE6C	cGMP specific	Zaprinast, dipyridamole	Stimulated by photons, via rhodopsin and transducin. Inhibited by γ subunit.
PDE7 	PDE7A	cAMP specific		
PDE8 	PDE8A PDE8B	cAMP specific	Dipyridamole (Ki=4.5μM)	
PDE9 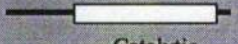	PDE9A	cGMP specific	SCH 518666 Zaprinast	
PDE10 	PDE10A	cAMP and cGMP		
PDE11 	PDE11A	cAMP and cGMP	Zaprinast, dipyridamole	

1.3.3 Intracellular targeting of PDEs

As discussed in the previous section, numerous mechanisms exist for the regulation of PDE isoenzymes. Different PDE isoenzymes also show distinct patterns of intracellular localisation. In many cases these differences have been attributed to the unique NH_2-terminal regions of PDE isoenzymes. The targeting of PDE isoenzymes in the cell is likely to be a crucial aspect of their function, particularly in the compartmentalisation of cAMP. For instance, in olfactory neurones the splice variant PDE1C2 co-localises with the adenylyl cyclase isoform ACIII in the cilia that extend from the dendrites into the nasal epithelium (Juilfs et al., 1997). ACIII and PDE1C2 are believed to be responsible for the rapid, transient cAMP response to odorants that bind to the G-protein coupled receptors in the cilial plasma membrane. PDE1C2 and ACIII are not found in other parts of the neurone, such as the axons and the cell body. However, olfactory neurones express an undefined PDE4A isoenzyme that is found only in the axons and the cell body. This PDE4A splice variant may be involved in the transmission of signal through the neurone to the olfactory bulb. The presence of two uniquely targeted PDE isoenzymes in one cell strongly suggests the existence of two separately regulated pools of cAMP in olfactory neurones.

PDE3 provides an example of the way in which the NH_2-terminal regions of PDE isoenzymes can determine their intracellular localisation. So far, two PDE3 genes have been identified, A and B. These genes have been shown to generate at least three isoenzymes: PDE3A1, PDE3A2 and PDE3B (Kasuya et al., 1995; Meacci et al., 1992; Taira et al., 1993). PDE3A1 and PDE3B may correspond to the 130-135kDa species observed in the sarcoplasmic reticulum fraction of cardiac myocytes and the endoplasmic reticulum fraction of adipocytes (Degerman et al., 1990; Smith et al., 1993). These two isoenzymes contain a hydrophobic segment in their NH_2-terminal regions that is predicted to form six transmembrane helices (Degerman et al., 1997). This may explain why these isoenzymes are targeted to the membrane fractions of adipocytes and cardiac myocytes (Degerman et al., 1990; Smith et al., 1993). Recombinant PDE3A1 and 3B are both associated with the particulate fractions of Sf9 cells (Kasuya et al., 1995; Leroy et al., 1996). However, truncated species that lacked the NH_2-terminal hydrophobic domain were cytosolic (Degerman et al., 1997). Similarly, the PDE3A2 isoenzyme has a very short NH_2-terminal splice domain that lacks the hydrophobic region. As expected, recombinant

PDE3A2 was found in the cytosolic fraction of Sf9 cells (Kasuya et al., 1995). Therefore, it has been hypothesised that the NH_2-terminal hydrophobic region targets PDE3A1 and 3B to the membrane fraction of cells (Degerman et al., 1997). This could be tested by expressing the hydrophobic region as a fusion to a normally soluble protein and then assessing the ability of this fusion to bind to membrane preparations. This technique was used to characterise the membrane-association region of PDE4A1 as described in section 1.8.1 below.

The targeting of PDE3B to intracellular membranes or the plasma membrane may play an important role in the compartmentalisation of cAMP pools in lipolysis. PDE3B mediates the inhibitory effects of insulin on lipolysis in adipocytes (Manganiello et al., 1996). Insulin acts via a pathway that involves IRS-1, PI3-kinase and an unidentified PDE3 kinase (PDE3IK) which activates PDE3B by phosphorylation at Ser302. Activation of PDE3B results in a drop in the level of cAMP and a reduction in the activity of PKA. This results in net dephosphorylation and inactivation of hormone-sensitive lipase (HSL) and a decrease in the hydrolysis of stored triglyceride (Degerman et al., 1997). It is possible that membrane-associated PDE3B is targeted to a region within the cell where it is in close proximity to an AKAP-anchored PKA and HSL. In this way, PDE3B could control a pool of cAMP that specifically regulates lipolysis via PKA and HSL. This would explain why PDE3 inhibitors and not PDE4 inhibitors prevent the inhibitory effects of insulin on lipolysis in adipocytes.

The effect of alternatively spliced NH_2-terminal regions on the intracellular targeting of PDE isoenzymes is also seen for members of the cAMP-specific PDE7 family. Two splice variants have been cloned for this family: PDE7A1, which is found in multiple tissues and PDE7A2, which is expressed mainly in skeletal muscle and cardiac myocytes (Han et al., 1997). The NH_2-terminal region of PDE7A2 contains hydrophobic sequences. As a result, PDE7A2 is predominately found in the particulate subcellular fraction of tissues. In contrast, the NH_2-terminus of PDE7A1 contains a large number of polar and positively charged residues. The intracellular localisation of PDE7A1 is more complex. For example, in foetal skeletal muscle PDE7A1 is mainly soluble, whereas in brain it is distributed between the soluble and the particulate fractions (Han et al., 1997). One explanation for these differences is that PDE7A1 interacts with one or more targeting proteins with tissue-specific patterns of expression.

A recent study has suggested that PDE6A and B (α and β) may associate with a signalling complex in the outer segments of rod photoreceptor cells. The formation of this complex is mediated by glutamic-acid-rich proteins (GARPs) (Korschen et al., 1999). The GARP proteins GARP1 and GARP2 bind tightly to the membrane fraction of rod outer segments and provide a scaffold for the binding of PDE6, guanylate cyclase and the ATP-binding cassette transporter (ABCR). In many ways GARP proteins are similar to the scaffold proteins described in section 1.10.2, which bind to a number of proteins in the same signalling pathway and thereby increase the efficiency of signal transduction. However, the association of light-activated PDE6 with GARP results in an inhibition of PDE activity. This led to the suggestion that the association of guanylate cyclase and PDE6 prevents the unnecessary cycling of cGMP in rod photoreceptors that have been saturated by high light conditions (Korschen et al., 1999). The association of PDE isoenzymes with scaffold proteins may thus turn out to be recurrent theme in the PDE superfamily.

So far, not much information has been obtained on the regulation and targeting of the newly discovered families PDE8, -9, -10 and –11 (see Table 1.1). All four of these families show broad but unique patterns of tissue expression. The isoenzymes generated by PDE8 genes are cAMP-specific and are expressed in a number of tissues including testis, ovary and intestine (Soderling et al., 1998). Interestingly, these isoenzymes contain Per-ARNT-Sim (PAS) homology domains in their NH_2-terminal regions (Soderling and Beavo, 2000). These domains have been shown to mediate the homo- and hetero-dimerisation of a number of proteins including the *Drosophila* proteins Per and Sim (Huang et al., 1995; Huang et al., 1993). The association of the aryl hydrocarbon receptor (AhR) with the Ah receptor nuclear translocator (ARNT) is mediated by their PAS domains (Fukunaga et al., 1995; Schmidt and Bradfield, 1996). In addition, PAS domains are also believed to mediate the hetero-dimerisation of White collar 1 and 2 which are involved in blue-light signal transduction in the fungus *Neurospora crassa* (Linden and Macino, 1997). Therefore, PAS domains may be involved in the protein-protein interactions or intracellular targeting of PDE8 isoenzymes. The PDE10 and PDE11 isoenzymes have dual cAMP/cGMP hydrolysing activity and contain GAF domains in their NH_2-terminal regions (Fawcett et al., 2000; Soderling et al., 1999). These are potential allosteric binding sites for cGMP, which may be involved in the regulation of these isoenzymes.

The above two sections have given an overview of the diverse mechanisms of regulation and intracellular targeting in the PDE superfamily as a whole. The following

sections focus on the cAMP-specific PDE4 family. Studies using specific inhibitors have identified PDE4 as a potential target in the treatment of a number of conditions, including inflammatory diseases such as asthma and atopic dermatitis (see section 1.9). The multiple isoenzymes in this family again show diverse patterns of tissue expression, regulation and intracellular targeting. A major research aim is to determine the *in vivo* functions of these isoenzymes, which may aid the development of novel therapeutic agents.

1.4 PDE4 cAMP-specific phosphodiesterases: structure and alternative 5' mRNA splicing

The mammalian PDE4 cAMP-specific phosphodiesterases are a complex family of at least 16 isoenzymes that are specifically inhibited by the anti-depressant drug rolipram (Henkel-Tigges and Davis, 1989). The PDE4 isoenzymes show considerable homology to the *dunce* family of phosphodiesterases of *Drosophila melanogaster* (Chen et al., 1986) which are essential for learning and memory in this organism (Dudai et al., 1976). The first member of the mammalian PDE4 family to be cloned (PDE4A1) was isolated in a screen of a rat brain cDNA library using dunce cDNA as a probe (Davis et al., 1989). Other PDE4 isoenzymes have been cloned by low-stringency cDNA library screening, using as probes the cDNA clones isolated in previous screens (Bolger et al., 1993; Livi et al., 1990; McLaughlin et al., 1993).

The PDE4 isoenzymes are derived from four genes A, B, C and D in rats, humans and mice. These genes are highly conserved between species. Indeed, each of the four human PDE4 genes are more related to their rat counterparts than they are to each other (Bolger et al., 1994; Bolger, 1994). The human chromosomal loci of these genes have been defined by screening somatic cell hybrids and by fluorescence *in situ* hybridisation. PDE4A and PDE4C are both located on chromosome 19, at positions p13.2 and p13.1, respectively (Horton et al., 1995; Milatovich et al., 1994; Sullivan et al., 1999). PDE4B is found on chromosome 1, region p31 and PDE4D maps to chromosome 5, region q12 (Szpirer et al., 1995).

The diversity of PDE4 isoenzymes comes from the use of alternative promoters for the initiation of transcription and the process of alternative 5' mRNA splicing (Chabot, 1996; Lopez, 1998). In the latter process the 3' exons that encode the core region are spliced to a range of alternative 5' exons (Bolger, 1994; Obernolte et al., 1993). This generates for each gene a number of isoenzymes that have shared central and COOH-

terminal core regions and unique NH_2-terminal regions (Figure 1.2). As discussed below, these unique NH_2-terminal domains appear to confer distinct modes of targeting and regulation on the PDE4 isoenzymes. A number of screening studies have shown that different tissues and cell lines express different combinations of PDE4 isoenzymes (Bolger, 1994; Erdogan and Houslay, 1997; MacKenzie and Houslay, 2000; Muller et al., 1996; Torphy et al., 1995). The complement of PDE4 isoenzymes expressed in a cell will clearly affect the spatial and temporal nature of the cAMP signal.

In PDE4 genes A, B and D there are two major splice junctions, (labelled 1 and 2 in Figure 1.2). Alternative splicing at the first junction (1) gives rise to 'long forms' whereas splicing at the downstream junction (2) gives rise to the 'short forms'. The relative positions of these splice junctions are conserved in PDE4B and PDE4D (Figure 1.3) (Monaco et al., 1994; Sullivan et al., 1998). However, the PDE4A gene is different in that the splice junction for the short splice variant, PDE4A1 (RD1) is shifted slightly downstream relative to the splice junctions for the short splice variants of PDE4B and PDE4D (see Figure 1.3). In addition, the alternative splicing of the PDE4C gene differs from the other 3 genes and short PDE4C forms comparable to the 4A, B and D short forms have not been identified (Obernolte et al., 1997; Sullivan et al., 1999). The general pattern of alternative 5' mRNA splicing shown by the mammalian PDE4 genes is conserved between species. For example, the primary transcript of the *Drosophila dunce* gene is alternatively spliced at the same relative positions as the mammalian PDE4A, B and D transcripts (Bolger et al., 1993; Davis et al., 1989; Henkel-Tigges and Davis, 1989; Qui et al., 1991; Swinnen et al., 1989).

Three regions show striking sequence conservation within the PDE4 family. These are the catalytic unit in the core region and two Upstream Conserved Regions (UCRs) found towards the NH_2-terminal ends of the PDE4 isoenzymes (Bolger et al., 1994; Bolger, 1994) (see Figure 1.2). These regions are very highly conserved between species and >80% amino acid identity is observed between the corresponding regions of rat PDE4 and *Drosophila* dunce isoenzymes (Davis et al., 1989; Houslay et al., 1998). The positions of the two splice junctions shown in Figure 1.2 and Figure 1.3 mean that all long PDE4 forms contain both UCR1 and UCR2 whereas the short forms of PDE4A, 4B and 4D lack UCR1. An exception is PDE4A1, which also lacks the NH_2-terminal half of UCR2.

It should be noted that these three conserved regions are flanked by variable regions, shown as heavy black bars in Figure 1.2 and Figure 1.3. The variable region

between UCR1 and UCR2 is referred to as LR1 (Linker Region 1) whereas the region between UCR2 and the catalytic unit has been named LR2. The extreme COOH-terminal regions of PDE4 isoenzymes are also variable. This feature of the PDE4 isoenzyme family has been exploited to produce antibodies that are specific for the splice variants derived from a single PDE4 gene (Erdogan and Houslay, 1997) (Houslay et al., 1998). Antibodies raised against these extreme COOH-terminal regions can therefore be used as probes in western blotting experiments to identify the presence of the PDE4 splice variants of a particular gene, by comparison of their observed molecular weights with recombinant protein standards (MacKenzie and Houslay, 2000).

Various attempts have been made to clearly define the catalytic unit in PDE4 isoenzymes. A definition based on sequence similarity suggests that it is around 360-390 amino acids in length (Houslay et al., 1998). Within this region the amino acid residues that are essential for catalytic function are His433, His437, His473, His474, His477, His505 and Thr544 (numbering based on HSPDE4A4B) (Jacobitz et al., 1997; Jin et al., 1992). 3D structural analysis of the PDE4 enzyme will be needed for a full understanding of the catalytic mechanism. Although the COOH-terminal catalytic unit is highly conserved throughout the PDE4 family, some sequence differences do occur between genes in the core region. These differences have allowed the generation of gene- and isoenzyme-specific primers for RT-PCR analyses of the isoenzymes expressed in different cell lines (Erdogan and Houslay, 1997; Kostic et al., 1997) (see Chapter 3).

The two upstream conserved regions UCR1 and UCR2 have very different primary structures. The ~55 amino acids of UCR1 can be divided into two subdomains. The NH_2-terminal half of UCR1 is polar and contains a high proportion of charged residues whereas the COOH-terminal half is hydrophobic. In contrast, UCR2 is entirely polar. Secondary structure predictions on this ~76 amino region suggest that it can be divided into three helical subdomains. The NH_2- and COOH-terminal subdomains are negatively charged, whereas the central domain has an overall positive charge (Houslay et al., 1998).

The very high conservation of the UCRs between species suggests that these regions are functionally significant. The function of these regions has recently been investigated. Studies on HSPDE4D3, using yeast two-hybrid and 'pull-down' constructs expressing various portions of UCR1 and UCR2, have shown that an interaction occurs between these regions (Beard et al., 2000). The fact that this interaction was observed using a number of different fusion constructs for both UCR1 and UCR2 suggests that these

regions are self-folding protein domains. The UCR1:UCR2 interaction was blocked by the alanine substitution of the acidic residues Glu146, Glu147 and Asp149 within the NH_2-terminal half of UCR2. This interaction was also blocked by the alanine substitution of positively charged amino acids, (Arg98 and Arg101 in PDE4D3), found towards the COOH-terminal end of UCR1. It was therefore proposed that an intramolecular interaction occurs between UCR1 and UCR2 that is mediated by oppositely charged residues.

Significantly, the phosphorylation of Ser54 (in PDE4D3) at the NH_2-terminal end of UCR1 also disrupted the interaction with UCR2 (Beard et al., 2000). The mutation of Ser54 to Asp, which mimics phosphorylation, had a similar effect. Interestingly, the phosphorylation of PDE4D3 at Ser54 by PKA is known to cause both enzyme activation and an alteration in the sensitivity of this isoenzyme to rolipram inhibition (Hoffmann et al., 1998). Therefore, the UCR domains may form an intramolecular module that regulates the function of the catalytic unit (discussed further in section 1.7.2).

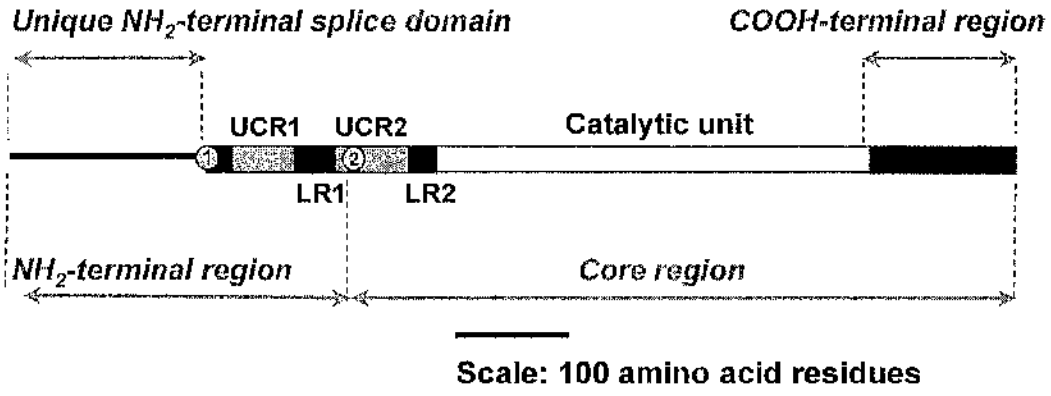

Figure 1.2 PDE4 general structure

The general domain structure of a long PDE4 splice variant is shown. Grey bars mark the positions of the upstream conserved regions (UCR1 and UCR2). The catalytic unit is shown by a white bar. The thick black line represents the unique NH_2-terminal splice domain and grey circles mark the splice junctions. The region downstream of the second splice junction is shared by all the isoenzymes from one gene and is thus referred to as the core region. The NH_2-terminal regions of long PDE4 isoenzymes contain an extreme NH_2-terminal splice domain that is unique to each isoenzyme and a region between the first ('1') and second ('2') splice junctions that is common to all the long forms within a single gene subfamily.

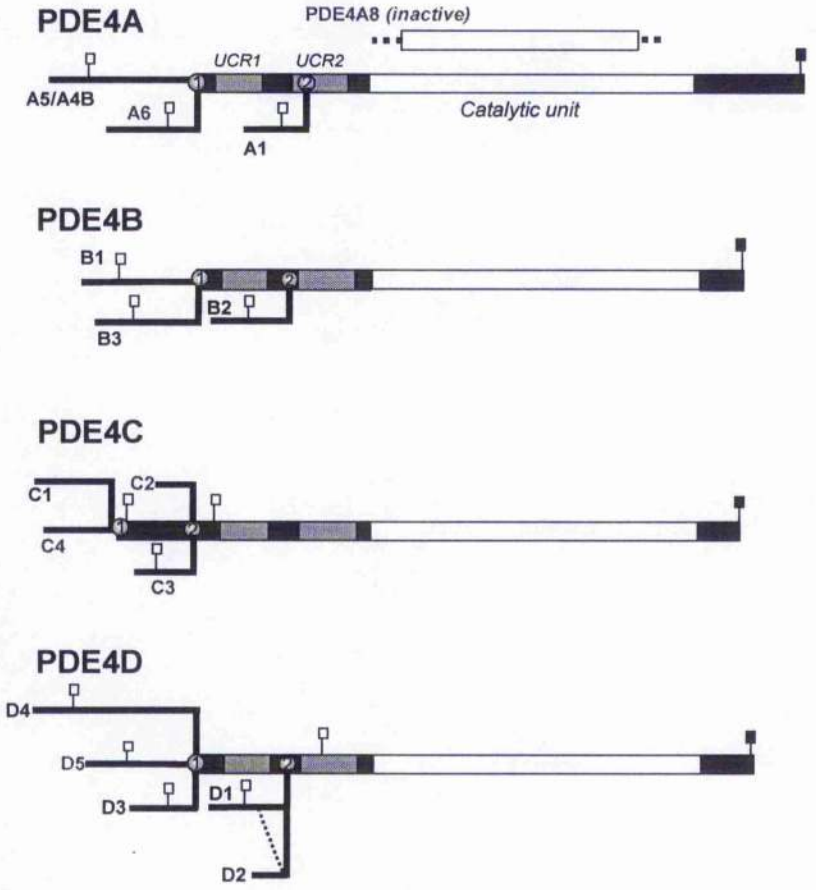

Figure 1.3 Structure of mRNA transcripts of PDE4 splice variants

This figure shows a schematic diagram of the mRNA transcripts that encode the PDE4 splice variants in rats and humans. The positions of the ATG initiator methionine codons are marked with white squares, whereas the termination codons are marked with black squares. Grey and white bars mark the positions of the upstream conserved regions (UCR1 and UCR2) and the catalytic unit, respectively. Black lines represent the unique NH_2-terminal splice domains and grey circles, numbered 1 and 2, mark the splice junctions. It should be noted that the rat homologues of the human splice variants PDE4A6, PDE4A8, PDE4C2, PDE4C3, PDE4C4 and PDE4D5 have not yet been cloned. The inactive, truncated splice variant HSPDE4A8 (2el) has been shown separately.

1.5 Tissue distribution of PDE4 isoenzymes

PDE4 isoenzymes show distinct patterns of expression in tissues, which suggest that they have specific roles in cells (Muller et al., 1996). There are several methods for assessing the expression of PDE4 isoenzymes in different tissues. The first method is the reverse-transcription polymerase chain reaction (RT-PCR) using specific oligodeoxynucleotide primer pairs for the detection of the transcripts of PDE4 isoenzymes (this method is discussed in detail in chapter 3). A second method is RNase protection analysis, in which the presence of PDE4 isoenzyme transcripts are detected by their ability to hybridise with specific antisense probes, to form RNA:RNA duplexes that are resistant to RNase-degradation. The third strategy that is employed for the detection of PDE4 isoenzymes is western blotting using antibodies that are specific for the isoenzymes derived from a single PDE4 gene (see section 1.4 above). The advantage of the latter method is that is detects the PDE4 isoenzymes that are actually expressed, as opposed to those that are merely transcribed.

A number of studies have examined the expression of the PDE4 genes (A, B, C and D) in various cell lines and tissues. Most of the tissues studied expressed PDE4A, PDE4B and PDE4D (Engels et al., 1994; Muller et al., 1996). However, PDE4C expression was restricted to only adipocytes, lung and brain, which suggests that PDE4C isoenzymes have specialised functions. The range of tissues that have been screened for the individual PDE4 isoenzymes is more limited. A particularly good source of PDE4 isoenzymes is rat brain which expresses PDE4A1, 4A5, 4A6, 4B1, 4B2, 4C2, 4D1, 4D2, 4D3, 4D4 and 4D5 (Beard et al., 1999; Bolger et al., 1997; Houslay et al., 1998). However, these isoenzymes are differentially expressed in the various brain regions (Lobban, 1994; McPhee et al., 1995). A few cell lines such as U937 monocytes (MacKenzie and Houslay, 2000) and Jurkat T-cells (Erdogan and Houslay, 1997) have also been screened for individual PDE4 isoenzymes. A comparison of these two cell lines illustrates the fact that different cell types express very unique combinations of PDE4 isoenzymes, which define the cell's response to signals mediated via cAMP.

1.6 Regulation of PDE4 expression

The chronic stimulation of certain cells with hormones has been shown to alter the expression pattern of PDE4 isoenzymes. A prime example of this is the induction of the

short forms PDE4D1 and PDE4D2 which has been observed in a number of cell lines (Conti and Jin, 2000). The transcription of these isoenzymes is controlled from one intronic promoter (Vicini and Conti, 1997). As shown in Figure 1.3, PDE4D2 differs from PDE4D1 by the deletion of an 86 nucleotide section downstream of the PDE4D1 start codon. This results in a frame shift, which shifts the start of translation to a methionine in the middle of UCR2 (Monaco et al., 1994).

The induction of these isoenzymes was first demonstrated in rat Sertoli cells treated with follicle stimulating hormone (FSH). The increase in the mRNA levels and transcription rates for PDE4D1/PDE4D2 in the Sertoli cells was observed after 1h and reached a maximum after 3h (Conti et al., 1995; Swinnen et al., 1989; Swinnen et al., 1991). A similar effect was observed with the non-hydrolysable cAMP analogue N^6, O^2,-dibutyryl cAMP (Bt_2cAMP) and the adenylyl cyclase activator forskolin indicating that the induction was a cAMP-dependent process. Therefore, chronic (>1h) elevation of cAMP in Sertoli cells switches on transcription of both PDE4D1 and PDE4D2 from an intronic promoter (Verghese et al., 1995).

The induction of PDE4D1 and PDE4D2 expression by an increase in intracellular cAMP has been observed in a number of other cell lines, including FRTL-5 thyroid cells (Jin et al., 1998; Sette et al., 1994), Jurkat T-cells (Erdogan and Houslay, 1997), Mono Mac 6 monocytic cells (Verghese et al., 1995) and rat skeletal myoblasts (Kovala, 1994). In FRTL-5 thyroid cells the induction of PDE4D1 and PDE4D2 expression occurred after chronic (24h) stimulation of these cells with thyroid stimulating hormone (TSH). This induction followed the acute activation of the constitutively expressed PDE4D3 isoenzyme, which was seen after a 15min incubation with TSH (Sette et al., 1994). As discussed in section 1.7.1, this activation is a result of phosphorylation by PKA. Unlike PDE4D1 and PDE4D2, the expression level of PDE4D3 was not affected by elevated levels of cAMP in these cells. This demonstrates the fact that separate promoters control the expression of different isoenzymes derived from a single PDE4 gene. Four putative promoter regions have been identified in the RNPDE4D (Conti and Jin, 2000). The existence of such multiple promoters allows different combinations of PDE4 isoenzymes to be expressed under different conditions.

In contrast to the long PDE4D isoforms 4D3, 4D4 and 4D5 which are found in the particulate and soluble fractions of cells, the short forms 4D1 and 4D2 are found entirely within the soluble, cytosolic fraction (see section 1.8 below). From this one would infer

that the long and short PDE4D isoenzymes occupy distinct compartments within the cell and they may therefore regulate different cellular functions. Therefore, the long-term hormonal induction of PDE4D1 and PDE4D2 may result in a profound change in the control of intracellular compartmentalised pools of cAMP.

Changes in intracellular cAMP levels can regulate the expression of other transcripts apart from PDE4D1 and PDE4D2. The cAMP-dependent induction of the short PDE4B form PDE4B2 has been observed in a number of cells, including U937 cells (Torphy et al., 1995) and monocytes (Verghese et al., 1995). In Jurkat T-cells, the cAMP-dependent increase the transcription of short PDE4D isoenzyme was accompanied by a drop in the level of a novel, as yet unidentified PDE4A transcript (Erdogan and Houslay, 1997). Therefore, the hormonal treatment of cells has dichotomous effects on the expression of PDE4 isoenzymes.

1.7 Regulation of PDE4 activity

As discussed in section 1.4 most of the structural diversity within the PDE4 family occurs at extreme NH_2-terminal ends of the isoenzymes, as a result of alternative 5'mRNA splicing. It has been hypothesised that the extreme NH_2-terminal regions confer distinct modes of intracellular targeting and regulation on PDE4 isoenzymes *in vivo* (Houslay, 1995; Houslay et al., 1995). The effect of these NH_2-terminal splice domains on the acute regulation of PDE4 activity is discussed in the following sections.

1.7.1 Phosphorylation of PDE4D3 by PKA and ERK2

The activity of the PDE4 isoenzymes can be regulated in a rapid and transient fashion by phosphorylation at certain key sites. This mode of regulation has been most extensively studied in the PDE4D3 isoenzyme. As mentioned in section 1.6, Conti and co-workers originally showed that this isoenzyme was phosphorylated and activated by PKA in rat thyroid FRTL-5 cells in response to an acute (15min) stimulation with TSH (Sette and Conti, 1996; Sette et al., 1994). This preceded the induction of PDE4D1 and PDE4D2 observed after a 24h treatment with TSH (Sette et al., 1994). Therefore, TSH produces both an acute and a long-term effect on PDE4D activity in thyroid cells. Both forms of regulation must be taken into consideration in assessing the effect of hormones on PDE4 activity in cells.

There are two sites of PKA phosphorylation in PDE4D3, Ser13 and Ser54 (see Figure 1.4). However, the phosphorylation of Ser54 at the beginning of UCR1 was concurrent with enzyme activation (Sette and Conti, 1996). This was confirmed by the replacement of Ser54 with an aspartate residue which mimicked phosphorylation at this site and led to a 3-fold increase in catalytic activity (Hoffmann et al., 1998). In addition, the activated, phosphorylated form of wild-type PDE4D3 and the Ser54→ Asp mutant both showed an increased affinity for the PDE4-specific inhibitor, rolipram. This increase in rolipram affinity was just one aspect of an overall change in the kinetics of rolipram inhibition, which implied a conformational change in the catalytic unit. The phosphorylated form of PDE4D3 showed the characteristics of partial competitive inhibition, whereas the non-activated form displayed simple competitive inhibition with rolipram (Hoffmann et al., 1998).

In addition to being activated by PKA phosphorylation in its NH_2-terminal region, PDE4D3 is inhibited by an ERK2-dependent phosphorylation at the COOH-terminal end of the catalytic unit (see Figure 1.4). Epidermal growth factor (EGF), which activates the Raf-MEK-ERK signalling pathway (Blumer and Johnson, 1994), resulted in a rapid (within 5min) drop in the activity of recombinant PDE4D3 expressed in COS-1 cells (Hoffmann et al., 1999) which was accompanied by an elevation of intracellular cAMP. This effect of EGF treatment was also seen in 3T3 F442A and HEK293 cells where PDE4D3 is expressed endogenously. The inhibition of PDE4D3 was the result of phosphorylation by the MAP kinase ERK2 at Ser579. Closer examination of the sequence surrounding this phosphorylation site in the COOH-terminal region of the catalytic unit revealed the presence of 'KIM' and 'FQF' docking sites for the association of ERK2 (MacKenzie et al., 2000) (see Figure 1.4). Mutational analysis confirmed that these sites mediated association with ERK2. As discussed in section 1.8, PDE4D3 associates with the particulate fraction of cells, which suggests that it may be specifically targeted. Therefore, PDE4D3 represents a means by which the Raf-MEK-ERK2 pathway can modulate discrete pools of cAMP within cells.

The inhibitory effect of EGF treatment on PDE4D3 activity was reversed within 20min. This recovery was due to the feedback activation of PKA, which activates PDE4D3 by phosphorylation at Ser54. Therefore PKA and ERK2 have opposing effects of PDE4D3 activity. Therefore, PDE4D3, which is expressed in a broad range of cells, represents a point of cross talk between the Raf-MEK-ERK pathway and cAMP pathway.

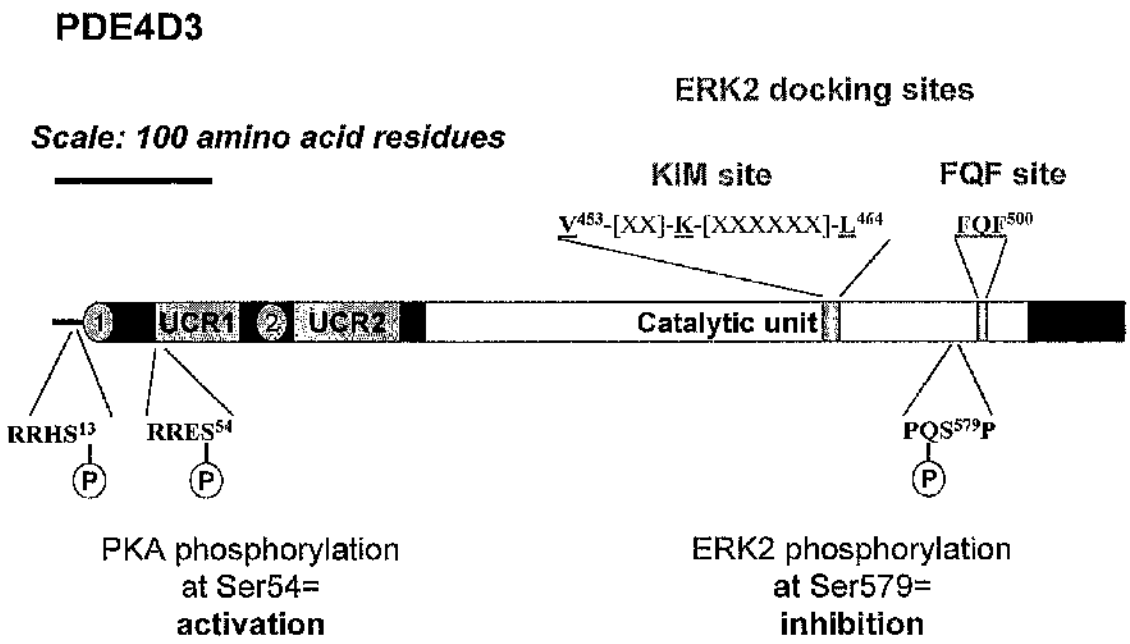

Figure 1.4 PKA and ERK2 phosphorylation sites and ERK2 docking sites in PDE4D3
PDE4D3 has two phosphorylation sites for PKA (Ser13 and Ser54) and one phosphorylation site for the MAP kinase ERK2 (Ser579). PKA phosphorylation at Ser54 results in the activation of the enzyme, whereas ERK2 phosphorylation at Ser579 results in inhibition. The positions of the 'KIM' and 'FQF' docking sequences for the association of ERK2 and the conserved residues with these motifs are also shown. X represents any amino acid.

1.7.2 Phosphorylation of other PDE4D isoenzymes

The short forms PDE4D1 and PDE4D2 lack the UCR1 region that contains the site for phosphorylation and activation by PKA. This again suggests that the expression of PDE4D1 and PDE4D2 in cells may have a profound effect on the response to signals that act via the cAMP pathway. The ERK2 phosphorylation site (PXSP) at the COOH-terminal end of the catalytic unit is present in all PDE4D isoenzymes and is conserved in PDE4B and PDE4C. However, PDE4A isoenzymes contain the slightly different sequence (RXSP) which does not appear to be a substrate for ERK2 action (Hoffmann et al., 1999). Intriguingly, ERK2 phosphorylation had different effects on the activities of the short and long PDE4D isoenzymes (MacKenzie et al., 2000). As shown in Figure 1.5, these isoenzymes contained different portions of the upstream conserved regions UCR1 and UCR2. The different responses of these isoenzymes to ERK2 phosphorylation suggested that the UCR domains had a regulatory role. The long isoenzymes, PDE4D3 and PDE4D5, which contained both UCR1 and UCR2, were both inhibited by ERK2 phosphorylation. In contrast, the species that lacked UCR1 but contained an intact UCR2 (i.e. PDE4D1 and the UCR2 + CAT NH_2-terminal truncate) were stimulated upon ERK2 phosphorylation. However, PDE4D2, which lacks all of UCR1 and the first 32 amino acid residues of UCR2, was inhibited by ERK2 phosphorylation, but to a lesser degree than that observed with the long forms (MacKenzie et al., 2000).

Therefore, it would appear that ERK2 phosphorylation has an intrinsic inhibitory effect on the core catalytic unit. This inhibitory effect is amplified in long isoenzymes that contain both UCR1 and UCR2. However, in the absence of UCR1, UCR2 directs the stimulation of catalytic activity in response to ERK2 phosphorylation. This is abolished by the removal of the NH_2-terminal half of UCR2. It has therefore been proposed that the UCR1 and UCR2 domains form an intramolecular module that regulates the response of the catalytic unit to phosphorylation by ERK2 (MacKenzie et al., 2000).

The above analysis of PDE4D3 phosphorylation has touched on several important aspects of PDE4 regulation that will be explored later in this thesis. Firstly, the above study has shown that alterations to the structure of the NH_2-terminal ends of PDE4 isoenzymes, such as phosphorylation at Ser54, can severely affect the activity of catalytic unit and its conformational state, shown by a change in rolipram affinity. Secondly, the activation or inhibition of various PDE4D isoenzymes by ERK-phosphorylation has shown that the

UCR1 and UCR2 regions affect the regulation of the catalytic unit. The different effects of ERK2 and PKA on different PDE4D isoenzymes also implied that the selective expression of different isoenzymes in cells could potentially be used to tailor cAMP responsiveness.

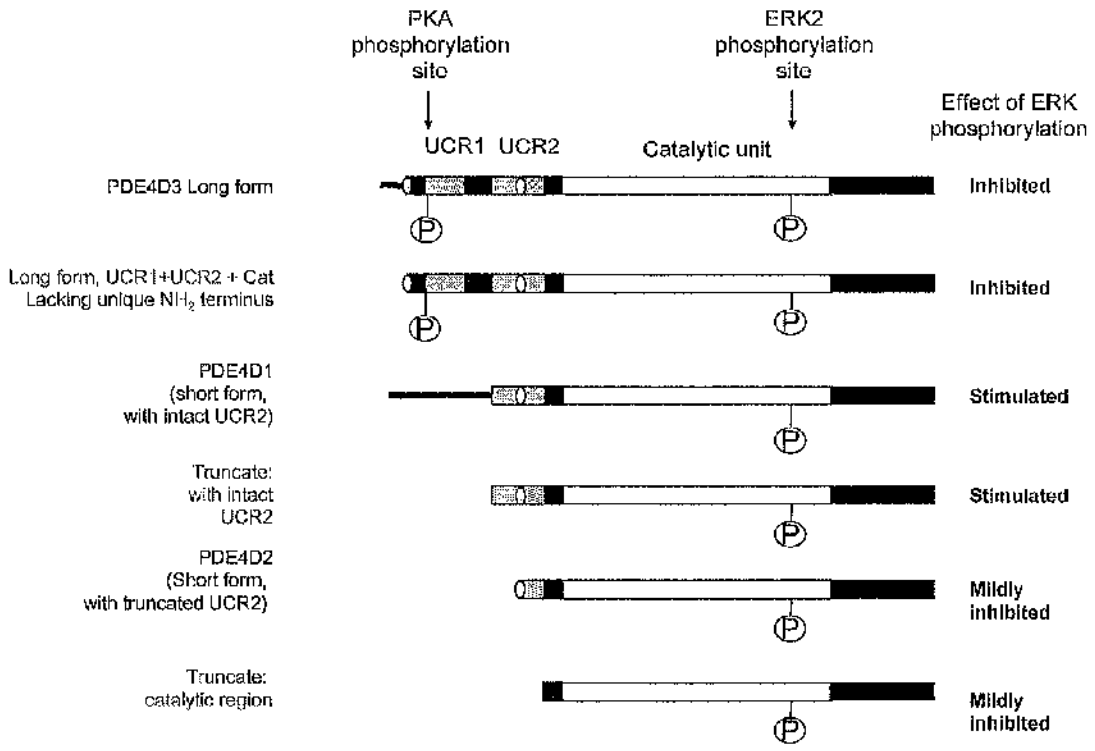

Figure 1.5 Effect of ERK2 phosphorylation on a range of PDE4D substrates

This figure summarises the effect of ERK2 phosphorylation on the activity long and short PDE4D isoenzymes and NH_2-terminal deletion mutants (MacKenzie et al., 2000). These species contain various portions of the UCR1 and UCR2. The positions of the ERK2 and PKA phosphorylation sites are indicated. The key to this schematic diagram is the same as that used in Figure 1.2 with thinner black lines representing the unique NH_2-terminal splice domains of the PDE4D splice variants. Grey circles represent the splice junctions.

1.7.3 Effect of phosphatidic acid on PDE4 activity

Another mechanism for the acute regulation of PDE4 via their NH_2-terminal regions is activation by phosphatidic acid (PA). PA is a phospholipid that accumulates in a number of cells in response to mitogenic or hormonal stimulation. PA can be produced by a number of biosynthetic routes (Athenstaedt and Daum, 1999). For example, PA can be produced the action of diacylglycerol kinase on diacylglycerol (DAG) which is a product of the hydrolysis of phospholipids by phospholipase C (PLC). Alternatively, PA can be produced by the direct action of phospholipase D (PLD) on various phospholipids. PA has been suggested to act as an intracellular second messenger and can modulate a number of signalling proteins including Raf-1 kinase and PKC (ElBawab et al., 1997).

The mitogenic stimulation of rat thymocytes with concanavalin A led to an accumulation of PA and the activation of PDE4 and a resultant drop in the level of intracellular cAMP (ElBawab et al., 1997). As discussed later in section 1.9.1, elevated cAMP levels have an inhibitory effect on the immune response of a number of cells. Therefore, the PA-induced drop in cAMP levels may be a mechanism for the activation of certain immune responses such as the proliferation of T lymphocytes (Savany et al., 1996). Studies with a range of PA-like molecules showed that the negatively charged phosphate group was essential for maximal PDE4 inhibition. Studies of the effect of PA on various recombinant PDE4 isoenzymes showed that PA specifically activated the long forms, while having no affect on the short forms (Nemoz et al., 1997). A distinguishing feature of the long PDE4 forms is the presence of UCR1 in their NH_2-terminal regions. As mentioned in section 1.4, the NH_2-terminal half of UCR1 is highly polar with an overall positive charge, whereas the COOH-terminal half of this region is hydrophobic. This may present an ideal binding surface for interaction with the amphipathic PA molecules, with the negatively charged phosphate group of PA interacting with UCR1. By affecting the intramolecular interactions of UCR1, the binding of PA may cause a conformational change that results in the activation of the PDE4 catalytic unit. This would be compatible with the mechanism proposed for the activation of PDE4D3 by phosphorylation at Ser54 and the theory that UCR1 and UCR2 form an intramolecular module that regulates the activity of the catalytic unit (see section 1.7.2 above).

1.8 Intracellular targeting of PDE4 isoenzymes

A crucial step in understanding the function of signalling enzymes, including PDE4, is to determine their intracellular localisation. A common method used in the initial characterisation of new PDE4 isoenzymes is transient expression in COS cells (Shakur et al., 1993; Sullivan et al., 1994). These cells allow high expression of transfected proteins and have very low levels of endogenous PDE4 activity (Scotland et al., 1998).

Information on the intracellular localisation of PDE4 isoenzymes can at first be obtained from their distribution between particulate and soluble fractions of these cells. A low speed (1000*g*) P1-pellet fraction, a high-speed (100,000*g*) P2-pellet fraction and a high-speed supernatant S fraction are usually prepared for this purpose. The P1-pellet fraction is generally composed of nuclear and cytoskeletal components, the P2-pellet fraction contains plasma membranes, endoplasmic reticulum, Golgi stacks, endosomes and lysosomes and cytoskeletal components (Scotland et al., 1998) and the S fraction contains 'soluble' cytosolic proteins. Table 1.2 shows that the distribution of PDE4 isoenzymes between these fractions varies considerably in transiently transfected COS-7 cells. In this table, the presence of a PDE4 isoenzyme within a particular fraction is indicated with a tick. Quantitative analyses of the distribution of the certain PDE4 isoenzyme have also been presented.

Variation is seen not only in the relative association of PDE4 isoenzymes with the particulate fractions but also in the susceptibility of these associations to the detergent Triton X-100 and high salt concentrations, which disrupt hydrophobic and electrostatic interactions, respectively. Susceptibility to either salt or detergent might indicate an interaction with an integral membrane protein, a membrane-associated protein or a phospholipid. Resistance to solubilisation with detergent often indicates an association with the cytoskeletal fraction (El Benna et al., 1999; Jung and Moroi, 1988; Slusarewicz et al., 1994; Yan et al., 1995). As shown in Table 1.2, subtle differences are observed between the PDE4 isoenzymes derived from the same gene, in terms of the effects these agents have on their association with the particulate fractions, which suggests that they interact with distinct anchoring components. The PDE4 isoenzymes derived from a single gene differ only in their extreme NH_2-terminal splice domains (see Figure 1.3). This further suggests that the distinct patterns of intracellular targeting shown by the different PDE4 isoenzymes are predominantly determined by their unique NH_2-terminal alternatively spliced regions.

Table 1.2 Subcellular distribution data for PDE4 isoenzymes in transfected COS-7 cells

This table summarises the distribution of PDE4A, 4B, and 4D isoenzymes between the low-speed pellet (P1), high-speed pellet (P2) and S fractions of transfected COS-7 cells. No data has been obtained for PDE4C isoenzymes. In some cases quantitative analyses were carried out and the percentage values are given. Pellet-associated PDE4 isoenzymes are either resistant (*R*) or susceptible (*S*) to solubilisation with 1M NaCl or 5% Triton X-100. The particulate isoenzymes that can only be solubilised with a combination of both Triton and NaCl are indicated as {Triton + NaCl} *S*

PDE4 isoenzyme	Subcellular distribution in transfected COS-7 cells ✓ = isoenzyme present ✗ = isoenzyme absent			Refs
	P1	P2	S	
RNPDE4A1 *short* (also known as RD1)	✗	✓ Triton *S* NaCl *R*	✗	(Pooley et al., 1997; Shakur et al., 1995)
RNPDE4A5 *long* (also known as rpde6)	✓ 21% Triton *R* NaCl *R*	✓ 28% Triton *R* NaCl *R*	✓ 51%	(McPhee et al., 1999) (Huston et al., 2000)
HSPDE4A5B *long* (also known as pde46)	✓ 19% Triton *R* NaCl *R*	✓ 26% Triton *R* NaCl *R*	✓ 55%	(McPhee et al., 1999) (Huston et al., 1996)
RNPDE4A6 *long* (also known as rpde39)	✗	✓ Triton *R* NaCl *R*	✓	(Bolger et al., 1996)
HSPDE4B1 *long*	✓ 17% Triton *R* NaCl *S*	✓ 11% Triton *S* NaCl *R*	✓ 71%	(Huston et al., 1997)
HSPDE4B2 *short*	✓ 26% Triton *S* NaCl *S*	✓ 12% Triton *S* NaCl *R*	✓ 61%	
HSPDE4B3 *long*	✓ 23% Triton *S* NaCl *S*	✓ 17% Triton *R* NaCl *R*	✓ 58%	

Table 1.2 *continued*

PDE4 isoenzyme	Subcellular distribution in transfected COS-7 cells ✓ = isoenzyme present ✗ = isoenzyme absent			Refs
	P1	P2	S	
HSPDE4D1 *short*	✗	✗	✓	(Bolger et al., 1997)
HSPDE4D2 *short*	✗	✗	✓	
HSPDE4D3 *long*	✓ 11%	✓ 20% {Triton +NaCl} S	✓ 69%	
HSPDE4D4 *long*	✓ 20%	✓ 40% {Triton +NaCl} S	✓ 40%	
HSPDE4D5 *long*	✓ 18%	✓ 15% {Triton +NaCl} S	✓ 67%	

1.8.1 Membrane targeting of RNPDE4A1 (RD1)

The short splice variant RNPDE4A1 (RD1) provides a clear example of the profound influence the unique NH_2-terminal splice domains have on the targeting of PDE4 isoenzymes. RNPDE4A1 has only been detected in rat brain, which suggests that it may have a specific neuronal role (Bolger et al., 1996). This isoenzyme is found entirely within the high-speed pellet (P2) fraction in both brain and transiently transfected COS-7 cells (McPhee et al., 1995; Shakur et al., 1993). It can be solubilised from this fraction by low (<0.1%) concentrations of the detergent Triton X-100 (see Table 1.2). Analysis by confocal immunofluorescence microscopy showed that RNPDE4A1 was associated with the plasma membrane, the Golgi apparatus and punctate vesicle-like structures adjacent to the plasma membrane in COS-7 cells (Shakur et al., 1995). Interestingly, the distribution of RNPDE4A1 in the stably transfected FTC thyroid carcinoma cells was slightly different in that it associated almost exclusively with the Golgi apparatus. These observations in COS cells and FTC cells suggested that RNPDE4A1 might have a role in the intracellular trafficking of vesicles between the Golgi apparatus and the plasma membrane (Houslay, 1996). Vesicular traffic along the exocytotic route has been shown to be a cAMP-dependent process (Muniz et al., 1996).

A major step in understanding the intracellular targeting of RNPDE4A1 came from the finding that the removal of the 25 amino acid NH_2-terminal splice domain of RNPDE4A1 completely abolishes its association with the P2-membrane fraction. The truncated species Met^{26}RD1, which corresponds to the core region of PDE4A beginning at the second splice junction, was found entirely within the cytosolic S fraction of transfected COS cells. Confocal immunofluorescence microscopy showed that Met^{26}RD1 had a diffuse cytosolic distribution (Shakur et al., 1995). This suggested that the unique NH_2-terminus of RNPDE4A1 contained a motif for interaction with the P2 (membrane) fraction. This was confirmed by Scotland and Houslay who showed that the fusion of this domain to chloramphenicol acetyl transferase (CAT) conferred membrane association on this normally soluble bacterial protein (Scotland and Houslay, 1995; Scotland and Houslay, 1998). The NH_2-terminal splice domain of RNPDE4A1 is therefore crucial to any function of this isoenzyme that would require its precise localisation in cells, such as the compartmentalisation of cAMP.

The mechanism of targeting of the RNPDE4A1 NH_2-terminal splice domain has not yet been established. The unique NH_2-terminal splice domain bears no homology to any other known protein. Its solubilisation from the P2 fraction with detergent suggests that it may interact with a lipid component. However, RNPDE4A1 appears to only associate with certain cellular membranes. Therefore, the interacting component must also be specifically localised within the cell.

In order to assess the feasibility of a lipid interaction, the 3-D structure of the RNPDE4A1 splice domain was determined by ^{1}H-NMR (Smith et al., 1996). This identified the presence of two helical regions separated by a hinge. The first helical region, Leu3-Cys11, is amphipathic in nature, and contains the polar residues Asp5, Cys8, Glu9, Thr10, and Cys11. The second of these helical regions, Pro14-Lys24 contains a compact unit of hydrophobic residues, Pro14-Trp20. The bulky side chains of the three tryptophans at positions 15, 19 and 20, and the leucine at position 16 interact to form a hydrophobic cluster. Interesting, deletion of region 14-20 abolished membrane association, in contrast to the deletion of regions 2-7, 8-13 and 21-25. Therefore, it is possible the region 14-20 provides a hydrophobic surface for interaction with membrane lipids, or alternatively a membrane-associated protein. The nature of the interacting component is investigated later in this thesis (Chapter 4).

1.8.2 Interaction of RNPDE4A5 (rpde6) with SH3 domains

The targeting of PDE4 isoenzymes by their extreme NH_2-terminal regions is further illustrated by a comparison of the intracellular localisation of the short PDE4A isoenzyme RNPDE4A1 with that of the long isoenzyme RNPDE4A5 (rpde6). This isoenzyme has been detected in a number of specific regions of the rat brain and in a range of cell lines including thymocytes (ElBawab et al., 1997; Nemoz et al., 1997), Jurkat T-cells (Seybold et al., 1998), pheochromocytoma (PC12) cells and U937 human monocytes (MacKenzie and Houslay, 2000). It is found in all fractions (P1, P2 and S) of transfected COS-7 cells and brain. In contrast to RNPDE4A1, RNPDE4A5 could not be solubilised from rat brain membranes with Triton X-100. This suggested that RNPDE4A5 interacted with the detergent insoluble cytoskeletal fraction (Yan et al., 1995). This was supported by immunofluorescence analysis in COS-7 cells that showed RNPDE4A5 to associate with a network extending throughout the cell with a concentration in the perinuclear region (Huston et al., 2000).

Analysis of the sequence of the unique NH_2-terminal splice domain of RNPDE4A5 revealed the presence of three proline-rich motifs (see Figure 1.6). These were reminiscent of the sites for high-affinity binding of Src homology 3 (SH3) domains. SH3 domains are self-folding globular protein modules of around 50 amino acids that mediate protein-protein interactions in signalling networks (Pawson, 1995). These domains bind to left-handed polyproline type II structures with the core motif PXXP (Alexandropoulos, 1995; Mayer and Eck, 1995). These motifs are also characterised by the presence of adjacent arginine residues. SH3 domains found in a wide variety of proteins including the cytoskeletal elements myosin and fodrin (Mayer, 1993), adaptor proteins such as Grb2, Crk and SHC (Buday, 1999) and the Src family of cytoplasmic tyrosyl kinases (Cooper and Howell, 1993; Sicheri et al., 1997). The latter are involved in a large number of signalling pathways including those downstream of growth factor and cytokine receptors (Abram and Courtneidge, 2000; Erpel and Courtneidge, 1995; Tatosyan and Mizenina, 2000).

Pull down experiments using a panel of SH3 domains fused to GST did indeed show an interaction between RNPDE4A5 and certain SH3 domains (O' Connell et al., 1996). The best binders were the SH3 domains of Src family tyrosyl kinases Lyn, Fyn and Src. Only very weak association was observed with the SH3 domains of the adaptor proteins Grb2 and Crk. The binding of RNPDE4A5 to the Src family tyrosyl kinase SH3 domains was resistant to dissociation with Triton X-100. Interaction with SH3 domains was not seen with the other PDE4A splice variants RNPDE4A6 (rpde39) and RNPDE4A1 indicating that binding was determined by motifs in the 103 amino acid unique NH_2-terminal domain of RNPDE4A5 (O' Connell et al., 1996).

The interaction of RNPDE4A5 with SH3 domains may target RNPDE4A5 to the cytoskeleton. A number of cytoskeletal proteins, such as fodrin or cortactin contain SH3 domains. Association with SH3 domain proteins may bring RNPDE4A5 into close proximity with a regulatory kinase or phosphatase. Alternatively, interaction of RNPDE4A5 with Src tyrosyl kinase domains may allow signal transduction pathways activated through Src, such as the Ras pathway and the MAP kinase cascade, to 'cross-talk' with the cAMP signalling pathways.

The observed interaction of RNPDE4A5 with SH3 domains also opens up new possibilities for the involvement of PDE4 in the regulation of superoxide generation by NADPH oxidase in a number of cell types. The assembly and activation of the NADPH-oxidase complex requires the interaction the p47-phox and p67-phox (McPhail, 1994)

which contain SH3 domains. Inhibition of PDE4 inhibits the respiratory burst in eosinophils, neutrophils (Spina et al., 1998) and kidney glomeruli cells (Chini et al., 1994) (see section 1.2.1) and PDE4 isoenzymes have recently been shown to be targeted to the forming phagosome, the site of superoxide generation in neutrophils and macrophages (Pryzwansky et al., 1998). Therefore, the interaction between RNPDE4A5 and SH3 domains illustrates the importance of finding protein interaction partners for PDE4 isoenzymes in order to identify their possible roles in signalling cross-talk or the compartmentalisation of cAMP.

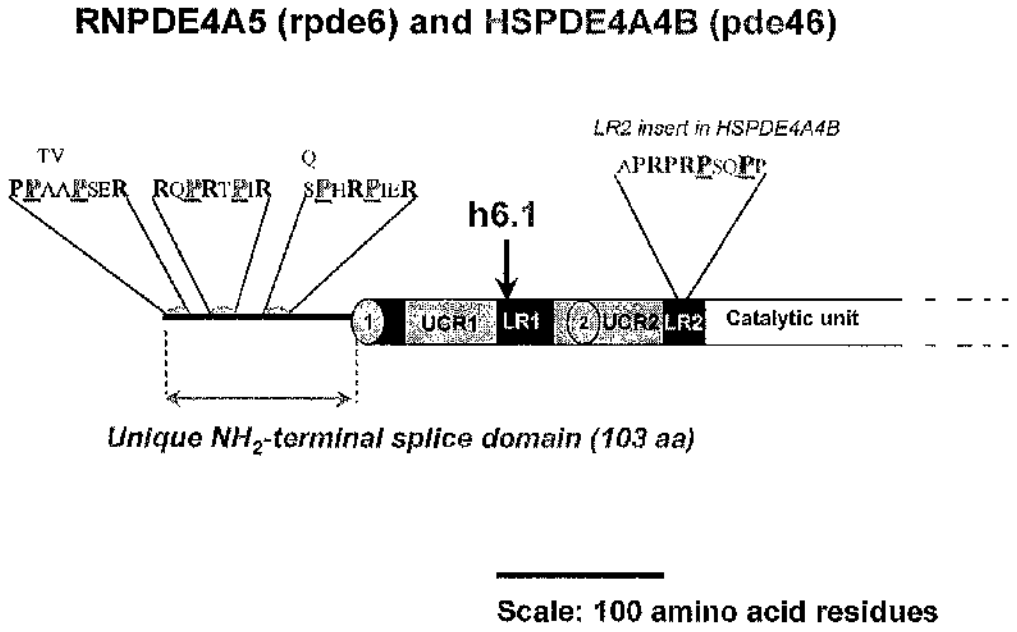

Figure 1.6 The putative SH3 domain-binding motifs in RNPDE4A5 (rpde6) and its human homologue HSPDE4A4B (pde46)

The domain structure of RNPDE4A5 and its human homologue HSPDE4A4B is shown. The position of the start of HSPDE4A4C (h6.1) is indicated with an arrow. This species is essentially a truncated version of HSPDE4A4B with a unique nine-residue section at its NH_2-terminus. The sequences of the three putative SH3 domain-binding motifs in the unique NH_2-terminal splice domains of RNPDE4A5 and HSPDE4A4B are shown above the structure. The positions the two key proline residues of the PXXP motif and adjacent proline and arginine residues in these sequences are indicated in bold. Sequence differences in HSPDE4A4B are shown above the RNPDE4A5 sequences. The HSPDE4A4B homologue contains an additional proline-rich insertion in its LR2 region that constitutes a further putative SH3 domain-binding site.

1.8.3 Interaction of HSPDE4A4B (pde46) with SH3 domains

The SH3 binding motifs observed in the unique NH_2-terminal splice domain of RNPDE4A5 are conserved in the human homologue of this splice variant, HSPDE4A4B (pde46) (see Figure 1.6). Like RNPDE4A5, HSPDE4A4B also interacts with the SH3 domains of Src family tyrosyl kinases, with a preference for Lyn SH3 (McPhee et al., 1999). HSPDE4A4B is also found in both the cytosolic and particulate fractions of COS-7 cells and its immunofluorescence pattern suggests that it associates with the cytoskeleton in the perinuclear region and also at distinct cortical regions near the cell periphery (Huston et al., 1996). Furthermore, immunofluorescence analysis showed that HSPDE4A4B and Lyn co-localised to the same subcellular structures.

The alignment of the sequences of HSPDE4A4B and RNPDE4A5 has identified the presence of a proline-rich insert in the variable LR2 region of HSPDE4A4B that contains an additional SH3-domain binding motif (see Figure 1.6). When expressed as a GST fusion, this LR2 insert could be co-immunoprecipitated with Lyn SH3, indicating a direct interaction. This region also mediated the association of a truncated species, HSPDE4A4C (h6.1) with Lyn SH3, in contrast with the rat PDE4A NH_2-terminal truncate Met^{26}RD1, which does not bind to SH3 domains.

Differences were observed between the particulate and soluble forms of HSPDE4A4B in COS-7 cells, in terms of their kinetics of inhibition by the PDE4-specific inhibitor rolipram. Particulate HSPDE4A4B showed complex partial competitive inhibition by rolipram with an increased affinity for this inhibitor in comparison to cytosolic HSPDE4A4B, which displayed simple competitive inhibition (Huston et al., 1996). These results suggested that the particulate and soluble forms of HSPDE4A4B had different conformational states. In contrast, the cytosolic and particulate forms of the rat homologue RNPDE4A5 both displayed simple competitive inhibition, suggesting they had the same conformation.

In order to explain this fundamental difference between HSPDE4A4B and RNPDE4A5, it was hypothesised that the altered conformation of HSPDE4A4B observed in the particulate fraction was induced by the association of an SH3-domain containing protein with the LR2 insert region. Therefore, the effect of Lyn SH3-association on the kinetics of rolipram inhibition was assessed. The binding of Lyn SH3 to cytosolic HSPDE4A4B did indeed switch the kinetics of rolipram inhibition from simple

competitive to partial competitive, with a concomitant increase in rolipram affinity. A similar switch was observed for HSPDE4A4C (h6.1) after association with Lyn SH3. Deletion mutants that lacked all or part of the proline-rich insert region also associated with Lyn SH3, presumably via the putative SH3 domain binding sites within the unique NH_2-terminal splice domain. However, these mutants did not show the aberrant kinetics of rolipram inhibition on binding to Lyn SH3, indicating that it was the specific interaction of Lyn SH3 with the LR2 region that induced the conformational change. Therefore, the interaction of HSPDE4A4B with SH3 domains causes the same conformational switch as that observed for HSPDE4A4B in the particulate fraction of transfected COS-7 cells.

This SH3 domain-induced conformational switch is in HSPDE4A4B similar to the switch observed when PDE4D3 is phosphorylated and activated by PKA. However, the binding of an SH3 domain to HSPDE4A4B does not result in the activation of catalytic unit. The above study highlights a potential mode of regulation in which the interaction of a protein with a specific PDE4 isoenzyme can induce a conformational change in the PDE catalytic unit. Understanding the mechanisms involved in these interactions may aid the design of drugs that inhibit the targeting of PDE4 isoenzymes to specific subcellular compartments and the attainment of one or other conformational state.

1.8.4 Interaction of HSPDE4D4 with SH3 domains

The long HSPDE4D4 splice variant also interacts with SH3 domains (Beard et al., 1999). Like RNPDE4A5 and HSPDE4A4B, this isoenzyme shows a preference for association with the SH3 domains of Src-tyrosyl kinases. These interactions are again directed by the unique NH_2-terminal splice domain of HSPDE4D4, which contains proline-rich sequences. In contrast to the PXXP motifs seen in the NH_2-terminal domains of RNPDE4A5 and HSPDE4A5, the NH_2-terminal region of HSPDE4D4 contains several polyproline stretches, 6-7 residues in length. These differences may explain the slightly different pattern of SH3-domain interactions shown by HSPDE4D4. For instance, HSPDE4D4 associates with Lyn-, Src- and Fyn-SH3 domains with roughly equal efficiency, whereas RNPDE4A5 and HSPDE4A4B show a distinct preference for Lyn SH3 (Beard et al., 1999).

These SH3-domain interacting isoenzymes are all expressed in brain (Bolger et al., 1997). This suggests that the association of PDE4 isoenzymes with SH3 domains may have an important function in neurones. The associations of HSPDE4D4 with SH3 domains

does not alter its catalytic activity or rolipram affinity. Therefore, the functional importance of this interaction may simply be the targeting of HSPDE4D4 to a specific compartment within the cell.

1.8.5 Intracellular targeting of HSPDE4D5: interaction with the anchoring protein RACK1

The PDE4D5 isoenzyme is expressed in numerous mammalian cell lines and also the brain (Bolger et al., 1997; MacKenzie and Houslay, 2000). Like the other long PDE4D isoenzymes, PDE4D5 is distributed between the particulate and soluble fraction of transfected COS-7 cells (see section 1.8). The yeast-2-hybrid technique has been used to successfully identify a protein binding partner for the HSPDE4D5 isoenzyme. The Receptor for Activated C Kinase (RACK1) was identified in a screen of a HeLa cell two hybrid cDNA library using HSPDE4D5 as bait (Yarwood et al., 1999). Subsequently it was shown that these two proteins have a very similar subcellular distribution patterns in transfected COS-7 cells and their interaction was confirmed by their co-immunoprecipitation from a number of cell lines. Binding studies with purified recombinant RACK1 and PDE4D5 indicated the interaction was high affinity and did not require intermediary proteins. The residues Asn22, Pro23, Trp24 and Asn26 within the unique NH_2-terminal splice domain of PDE4D5 were found to be essential for interaction with RACK1.

RACK1 (36kDa) is a member of the WD40-repeat family of proteins, which perform a wide range of functions (Neer et al., 1994). RACK1 is homologous to the β subunit of the stimulatory heterotrimeric G protein (Ron et al., 1994). The β subunit has a 'propeller-like' structure that consists of seven 'blades' that are believed to mediate interaction with proteins such as β-adrenergic receptor kinase (βARK) (Lambright et al., 1996; Wall et al., 1995). It is probable that RACK1 has a similar three-dimensional structure and PDE4D5 may indeed associate with one of its propeller blades.

RACK1 was originally discovered as a protein binding partner for protein kinase C (PKC) (Mochly-Rosen et al., 1991). RACK1 is necessary for the translocation of PKC from the cytosol to the particulate fraction of cells upon activation with Ca^{2+} and PMA (phorbol 12-myristate 13-acetate). Other proteins have been shown to interact with RACK1, including phospholipase Cγ, (Disatnik et al., 1994), Src tyrosyl kinase (Chang et al., 1998) and β-integrin (Liliental and Chang, 1998).

The binding region for RACK1 on PKC is contained the within the C2 domain of the 'conventional' subfamily of PKCs which is exposed upon activation with Ca^{2+} and PMA (Mochly-Rosen, 1995). The unique NH_2-terminal splice domain of PDE4D5 does not contain any regions with homology to the C2 region and no PMA-induced conformational change was necessary for the association of PDE4D5 with RACK1. Furthermore, the association with RACK1 does not affect the catalytic activity or rolipram affinity of PDE4D5. Rather than regulating PDE4D5, RACK1 may be acting as an anchor protein. The simultaneous association of RACK1 with PDE4D5 and other signalling proteins such as PKC and PLCγ may allow more efficient cross talk between signalling pathways. Alternatively, the association with RACK1 may localise PDE4D5 within the cell so that it can modulate a specific pool of cAMP. In this way PDE4A5 may regulate the activity of PKA and substrates of PKA in the vicinity of the RACK1 complex.

1.9 Pharmacological importance of PDE4

As mentioned previously, PDE4 isoenzymes have been identified as potential targets in a number of diseases. The PDE4-specific inhibitor rolipram was originally discovered in the search for novel treatments for depression. Although early phase clinical trials indicated that rolipram was an effective anti-depressant, they also showed a number of side effects, including nausea and vomiting. These side effects are a recurring problem in the use of PDE4 inhibitors as therapeutic agents. PDE4 inhibitors have also been shown to have anti-inflammatory effects. The potential use of PDE4 inhibitors in a number of disease states and possible approaches to developing more specific PDE4 inhibitor-based drugs are discussed in the following sections.

1.9.1 inflammatory diseases: asthma and atopic dermatitis

A potential use for the anti-inflammatory property of PDE4 inhibitors is in the treatment of asthma. This disease is characterised by an inflammatory response to inhaled allergenic or irritative substances, that results in bronchoconstriction, bronchial oedema and increased tone of airway smooth muscle (Spina et al., 1998). Asthma is a complex multifactorial condition. The inflammatory response involves the recruitment and activation of inflammatory cells to the airway. These include eosinophils, neutrophils, mast cells and T lymphocytes (Torphy, 1998). Once activated these cells generate of large number of different pro-inflammatory substances including cytokines, leukotrienes, and

cytotoxic superoxide (generated in the respiratory burst by activated NADPH oxidase). The infiltration and activation of all of these cells are suppressed by an increase in the intracellular levels of cAMP (Spina et al., 1998).

β-adrenoceptor agonists (e.g. salbutamol), which cause bronchodilation by the relaxation of airway smooth muscle, are commonly used in the treatment of asthma. This effect is mediated, at least in part, by the activation of PKA via the cAMP signalling pathway (Giembycz, 1996; Torphy et al., 1995). Another commonly used drug is the non-specific PDE inhibitor theophylline. The mechanism of action of theophylline is unclear as it has other actions apart from PDE inhibition, such as the activation of adenosine receptors (Essayan, 1999).

Studies have shown that a major component of the PDE activity in the pro-inflammatory cells mentioned above is PDE4 (Spina et al., 1998; Torphy, 1998). This provides a rationale for developing PDE4 inhibitors as anti-asthma drugs. PDE4 inhibitors, such as rolipram and Ro 201724, are effective at suppressing the activity of many inflammatory cells. For instance, they suppress superoxide generation and leukotriene production by neutrophils and eosinophils and they suppress IgE induced degranulation in mast cells (Essayan, 1999). PDE4 inhibitors also reduce the infiltration of inflammatory cells to the airway epithelium, by reducing the production of chemotactic mediators and by inhibitory effects on cell trafficking (Torphy, 1998).

PDE4 enzymes are expressed in airway smooth muscle and selective PDE4 inhibitors appear to have a relaxant effect on these smooth muscle cells (Polson and Strada, 1996). These effects of PDE4 inhibits are potentiated by the presence of PDE3 inhibitors. Therefore, both PDE3 and PDE4 isoenzymes appear to be involved in the regulation of airway smooth muscle tone.

A major disadvantage of the use of PDE4 inhibitors in the treatment of asthma and other diseases is their side effects of nausea and vomiting. This highlights the importance of developing PDE4 inhibitors with greater specificity. Studies on the function of PDE4 in inflammatory cells have suggested that PDE4 isoenzymes can adopt one of two conformational states, which can be distinguished by their relative affinities for the inhibitor rolipram. These states have been noted for the isoenzymes PDE4D3 (see section 1.7.1) and HSPDE4A4B (see section 1.8.3). The balance between these two states varies from cell to cell. The major functional PDE4 in eosinophils was in the high-affinity state (Souness and Scott, 1993). However, the PDE4 isoenzymes that regulated TNFα

production in human monocytes were in the low-affinity state. Compounds that preferentially inhibit the catalytic activity of one these two PDE4 conformational states may have more specific therapeutic actions with fewer side effects. The PDE4-selective inhibitor CDP840 preferentially inhibits the low rolipram affinity conformational state. This drug appears to have an anti-inflammatory action that ablates the asthmatic late-phase response to allergen, without any side-effects (Harbinson et al., 1997). An understanding of this conformational switch may aid the development of compounds that favour the adoption of one or other state and these may be of therapeutic value.

The high- and low-affinity PDE4 conformational states are believed to be interconvertible. In the case of HSPDE4A4B, interaction with the SH3 domains of Src tyrosyl kinases with the LR2 region of this isoenzyme caused the catalytic region to switch from the low- to the high-affinity state (see section 1.8.3). Other protein-protein interactions may govern the switch between PDE4 conformational states. Identifying these binding proteins and their mechanisms of interaction may be an important step in drug development.

Another approach to developing drugs with better tissue specificity is the search for compounds that specifically inhibit the isoenzymes derived from a single PDE4 gene (A, B, C or D). This is based on the fact that different tissues show distinct patterns of expression for each of the four genes. In this regard, the identification of the precise PDE4 isoenzymes expressed in inflammatory cells and airway smooth muscle is imperative. Interestingly, the inhibitor SB207499 shows selectivity for the PDE4D subfamily. SB207499 lacks the side effects of nausea and vomiting seen with rolipram (Barnette et al., 1998).

Another inflammatory disease where PDE4 inhibitors may be of therapeutic importance is atopic dermatitis (Spina et al., 1998). This condition is characterised by emergence of skin lesions after exposure to various allergens. As in asthma, the development of atopic dermatitis involves the infiltration of T-lymphocytes and other leukocytes to the sites of inflammation. The molecular basis of atopic dermatitis is unclear although it appears to involve aberrant levels of cAMP PDE activity in pro-inflammatory cells. Early clinical trials suggest that PDE4 inhibitors may be effective treatments for this disease. The PDE4-specific inhibitor CP-80633 appeared to have a therapeutic effect on this condition and inhibited many aspects of the inflammatory response, including superoxide production, eosinophil chemotaxis and TNFα release (Cohan et al., 1996).

1.9.2 Other conditions: Parkinson's disease and diabetes insipidus

Another condition where PDE4 inhibitors could be exploited is in Parkinson's disease. This condition is characterised by loss of dopaminergic neurones in the substantia nigra region within the brain. PDE4 inhibitors protected dopaminergic neurones from the pro-apoptotic effects of 1-methyl-4-phenyl-1, 2, 3, 6-tetrahydropyridine (MPTP) both in culture and in the substantia nigra of mice (Hulley et al., 1995). This highlights the potential use of PDE4-inhibiting drugs in the treatment of a major neurodegenerative disease.

PDE4 enzymes have also been implicated in the rare disease nephrogenic diabetes insipidus. In mouse models of this condition the cells of the medullary collecting duct in the kidney show a poor response to the antidiuretic hormone vasopressin, which activates the cAMP pathway. Although the ability of vasopressin to stimulate adenylyl cyclase was unaffected, the cells from diseased state mice failed to accumulate sufficient cAMP (Takeda et al., 1991). This condition was ameliorated with the PDE4-specific inhibitor rolipram, which suggested that the abnormal response to vasopressin might be due to the over-expression of certain PDE4 isoenzymes in the collecting duct cells. Identifying the precise PDE4 isoenzymes involved is again crucial for our understanding of the molecular basis of this condition and for the development of novel drugs (Houslay et al., 1998).

1.10 Anchoring and scaffold proteins

As mentioned above, the identification of the protein-binding partners for PDE4 isoenzymes may be an important step in drug development. Although potential protein-binding partners have been found for PDE4A4/5, PDE4D4 and PDE4D5 there are many other PDE4 isoenzymes for which protein interaction partners need to be defined. The association of PDE4 isoenzymes with protein complexes may turn out to be a common theme of this family. In these complexes the PDE4 isoenzymes may associate with more than one protein. Two overlapping classes of protein that serve as 'molecular glue' for signalling complexes have been defined by Faux and Scott (Faux and Scott, 1996). These are the scaffold proteins and anchoring proteins. The possibility that these proteins are intracellular targets for PDE4 isoenzymes is discussed below.

1.10.1 Anchoring proteins

Anchoring proteins target one or more signalling proteins to specific locations within the cell. A prime example is RACK1, which has been shown to associate with PKC, PLCγ, integrin β-subunit, Src tyrosyl kinase and PDE4D5. A number of experiments have shown that the correct intracellular targeting of PKC isoforms via RACK1 is essential for their function. For example, a peptide corresponding to the RACK1 binding site on εPKC blocked the translocation of εPKC to specific subcellular sites in cardiac myocytes and prevented the regulation of contraction by noradrenaline (Johnson et al., 1996). Similarly, peptides that blocked the interaction of PKCβ with RACK1 in pancreatic β cells blocked the glucose-induced translocation of PKCβ to the cell periphery and reduced the production of insulin by these cells in response to glucose (Yedovitzky et al., 1997). In a similar manner, the precise intracellular localisation of PDE4D5 is probably essential for its function *in vivo*.

Other examples of anchoring proteins are the AKAPs, which were described in section 1.2. AKAPs are a growing family of proteins that target PKA to various subcellular compartments. In addition to associating with the R subunits of PKA, AKAP79 has been shown to bind to PKC and protein phosphatase 2B (calcineurin) (Coghlan et al., 1995; Klauck et al., 1996). These three proteins bind to separate sites on AKAP79 and can associate simultaneously in any combination (Klauck et al., 1996). In neurones, AKAP79 is targeted to the postsynaptic density. Multivalent complexes such as this may allow the efficient co-ordination of signalling events at the synapse. The opposing actions of kinases and phosphatases may be tightly integrated through their association with AKAPs. For instance, an AKAP called Yotaio binds to PKA, protein phosphatase 1 (PP1) and the *N*-methyl-*D*-aspartate (NMDA) receptor (Westphal et al., 1999). Under basal conditions, this complex is believed to maintain the NMDA receptor in an inactive, dephosphorylated state. However, this situation is rapidly reversed by treatments that activate PKA (Westphal et al., 1999). Therefore, AKAPs conform to the 'targeting hypothesis' in which it proposed that phosphorylation events are partly regulated by 'targeting subunits' which bring kinases and phosphatases into close proximity with their substrates (Hubbard and Cohen, 1993).

In a similar manner to the association of PKC with RACK1, several studies have shown that the correct association of PKA with AKAPs is essential for certain physiological functions. Intracellular perfusion of a peptide corresponding to the conserved RII subunit binding region (Ht31) of AKAP79 into hippocampal neurones prevented the

association of PKA with AKAP79 and abolished the PKA-dependent modulation of AMPA/kainate channels (Rosenmund et al., 1994). In another example disruption of the interaction of RII with AKAPs (Lester et al., 1997) blocked insulin secretion in pancreatic β islet cells.

Other anchoring proteins may exist that target PDE4 isoenzymes to specific intracellular locations. Identifying these anchoring species is a major research aim as compounds that block these interactions may be an effective way of inhibiting the function of specific PDE4 isoenzymes and these may be of pharmacological importance.

1.10.2 Scaffold proteins

Examples have been shown of proteins that provide a scaffold for the binding and spatial organisation of proteins that occupy sequential positions in a single signal transduction pathway. A prime example of this in mammals is the organisation of the cytokine/stress activated JNK/SAPK pathway. The components of this cascade MKK7, MLK3 and HPK1 and JNK bind to the multivalent scaffold protein, JIP1 (Pawson and Nash, 2000; Schillace and Scott, 1999). These components bind to separate sites on JIP1 and the over-expression of JIP1 increases the efficiency of the signal transduction process.

Scaffold proteins may be a widespread phenomenon for the organisation of signal-transduction pathways. One function of these scaffold proteins may be to segregate separate signal transduction processes (Faux and Scott, 1996). The association of PDE4 isoenzymes with these scaffold proteins might provide a mechanism for controlling the levels of cAMP in the vicinity of the components of a signal transduction pathway. In this way, PDE4 isoenzymes could affect the regulation of signal transduction pathways by PKA.

1.11 Protein-protein interaction modules

As discussed in section 1.8 PDE4A4/5 and PDE4D4 both associate with the SH3 domains of Src-family tyrosyl kinases. The SH3 domains are just one example of a number of conserved protein modules that have been defined, including SH2, PDZ, PH, PTB and TPR domains. These are all independently folding, globular domains that are found in a range of proteins in various different combinations. These modules mediate protein-protein interactions and play an important role in the intracellular localisation of signalling molecules. The intracellular targeting of many other PDE4 isoenzymes, in addition to

PDE4A4/5, may be determined by these modules. The main characteristics of these modules are discussed below.

1.11.1 SH2 and SH3 domains

The Src homology domains SH2 and SH3 are self-folding modules of around 100 and 50 amino acids, respectively. SH3 domains specifically recognise proline-rich motifs with the core sequence PXXP that adopt left-handed polyproline type II helices. The implications of the association of SH3 domains with PDE4A4/5 and PDE4D4 were discussed in section 1.8. The SH2 domains specifically recognise short peptide motifs containing phosphotyrosine (pTyr). The 3-5 residues on the COOH-terminal side of the phosphotyrosine confer specificity for different SH2 domains (Pawson and Gish, 1992). The SH2 domains mediate the interaction of the protein components of tyrosine kinase signalling pathways. This is seen for the signalling pathways downstream of transmembrane receptor tyrosine kinases (RTKs) for peptide growth factors such as EGF and PDGF. The binding of ligands results in the oligomerisation of these receptors, which causes the autophosphorylation of a number of tyrosine residues in their intracellular domains. This causes the recruitment of SH2 domain-containing signalling proteins including PLCγ, adaptor proteins and the p85 subunit of PI3-kinase (Mayer, 1993).

The SH2 and SH3 domains are often found together in proteins that act as integrators of signalling pathways (Pawson, 1995). The adaptor proteins such as Grb2 and Crk consist almost entirely of SH2 and SH3 domains. These proteins function as co-ordinators of signalling complexes. For instance, the SH2 domain of Grb2 associates with pTyr sites on activated receptor tyrosine kinases. Simultaneously, the SH3 domain of Grb2 associates with proline-rich sites on Sos (Mayer and Gupta, 1998). The later activates Ras, which in turn leads to the activation of the Raf-MEK-ERK pathway. Other SH2 and SH3 domain-containing proteins are involved in processes such as the organisation of the cytoskeleton and the control the cell movement. For example, Nck is an adaptor protein that co-ordinates the components of signalling pathways downstream of Eph receptors which control axon guidance during the development of the mammalian CNS (Pawson and Nash, 2000).

1.11.2 PTB and WW domains

Another protein module that binds to pTyr motifs in addition to SH2 is the PTB (pTyr binding) domain (FormanKay and Pawson, 1999). These domains preferentially interact with the NPXY motif and in contrast to SH2 not all PTB domains require the phosphorylation of the tyrosine in this motif for high-affinity binding. PTB domains are often found in 'docking proteins' such as IRS1 and Shc. These proteins associate with receptor tyrosine kinases that lack binding sites for SH2 domains. The RTKs phosphorylate the docking proteins at key tyrosine residues that provide binding sites for the SH2 domains of proteins such as Grb2 and PI3-kinase. The functions of many PTB - containing docking proteins overlap those of the adaptor proteins described above in that they physically bring together proteins that occupy successive positions in signalling pathways.

WW domains are analogous to SH3 domains in that they associate with proline-rich sites. These are relatively small domains of 35 to 40 amino acid residues and associate with PPXY or PPLP motifs (Pawson and Scott, 1997). The WW domains of the ubiquitin protein ligase Nedd4 mediate its association with epithelial Na^+ channels in the kidney. No association was seen between the WW domain of Nedd4 and PDE4A4/5 or PDE4D4 (Beard et al., 1999). However, this does not exclude the possibility that other PDE4 splice variants interact with WW domains.

1.11.3 PDZ domains

Another recently identified protein module is the PDZ domain. These modules recognise E(S/T)DV motifs which are often found at the COOH-terminal ends of transmembrane ion channels subunits and receptors (Pawson and Scott, 1997). PDZ domains play an important role in the spatial organisation ion channels and receptors at the synapse. For instance, a major organiser protein of the post-synaptic density, PSD-95, contains three PDZ domains that bind to the NMDA channel receptor subunit NR2B and the Kv4.1 potassium channel. In this way, PSD-95 mediates the clustering of these ion channels in the postsynaptic membrane. Other PDZ proteins, such as GRIP and Homer act as adaptor proteins and mediate the clustering of certain receptors and their association with signalling proteins and cytoskeletal components (Schillace and Scott, 1999). A considerable number of PDE4 isoenzymes are expressed in the brain (section 1.5). Some of these isoenzymes, including PDE4A4/5 and PDE4A6, are found to associate with the

cytoskeletal fraction of cells. PDZ proteins may be involved in the organisation of PDE4 isoenzymes at the synapse.

As mentioned in section 1.1 many ion channel receptors are regulated by PKA-phosphorylation both in neurones and other cells. Several studies have shown that PKA is targeted to these ion channels by its association with AKAP anchoring proteins, such as AKAP79, which regulates AMPA/kainate receptors in hippocampal neurones (Rosenmund et al., 1994). In airway epithelial cells the cystic fibrosis transmembrane conductance regulator (CFTR) Cl^- channel is regulated by PKA phosphorylation (Schillace and Scott, 1999). A PDZ protein EBP50/NHERF binds to both the CFTR Cl^- channel and the AKAP protein ezrin (Short et al., 1998). This example shows that PDZ domains appear to be involved in both the spatial organisation of receptor ion channels and the regulation of these channels by PKA. The PKA enzymes that are targeted to these ion channels may be regulated by distinct pools of intracellular cAMP. Furthermore, the compartmentalisation of these cAMP pools may require the co-localisation of cAMP-specific PDEs such as PDE4. Protein modules such as PDZ proteins may directly mediate the targeting of PDE4 isoenzymes to these compartments.

1.11.4 TPR domains

Another module that is involved in protein-protein interactions is the tetratricopeptide repeat (TPR). The TPR motif is a 34 amino acid motif found in proteins involved in a wide range of cellular processes. These include cell cycle regulation (Lamb et al., 1995), peroxisomal and mitochondrial membrane transport (Terlecky et al., 1995; Yano et al., 1998), the organisation of the cytoskeleton and the generation of superoxide during the respiratory burst in phagocytes (Ponting, 1996). Some TPR proteins, such as the anaphase promoting complex subunit cdc27 (Ollendorff and Donoghue, 1997) and the postsynaptic cytoskeletal protein rapsyn (Ponting and Phillips, 1996) interact with multiple proteins.

The crystal structure of the TPR domain of protein phosphatase 5 (PP5) has been determined (Das et al., 1998). PP5 contains 3 TPRs arranged in tandem. The individual TPRs essentially fold into two antiparallel alpha helices (A and B). The tandem arrangement of TPR motifs in PP5 results in the formation of a concertina-like arrangement of A and B helices. This appears to form a right-handed helical superstructure.

In proteins with several TPRs in tandem such a rapsyn (Ponting and Phillips, 1996), this would be extended to provide an ideal scaffold for the association of a number of proteins.

The amino acid sequences of TPRs are highly degenerate with weak conservation between species. However, there are a number of conserved positions which appear to help maintain the 3D structure of the TPR (Das et al., 1998). A proline residue is commonly observed at position 32 at the end of helix B. Small hydrophobic residues often occur at positions 8 and 20, which are the closest points of contact being helix A and helix B. Large hydrophobic residues are frequently seen at positions that form the interface between the two helices. The TPR domains of a number of proteins including PP5 and the immunophilins Cyp40 and FKBP52 mediate their association with the molecular chaperone heat shock protein 90 (hsp90). Site directed mutagenesis studies showed that the basic residues (Lys97 and Arg101) at the NH_2-terminal end of TPR domain 3 in PP5 were essential for interaction with hsp90 (Russell et al., 1999). Further analysis by Russell et al indicated that the replacement of three acidic residues in the EEVD motif at the COOH-terminal end of hsp90 reduced the association with PP5. This suggested that the association of a TPR-containing protein with hsp90 was mediated by electrostatic interactions between oppositely charged residues.

Certain TPR proteins may be involved in the intracellular targeting of proteins. For example, the immunophilin proteins Cyp40 and FKBP52 form complexes with the molecular chaperone hsp90 and steroid hormone receptors such as the glucocorticoid receptor (GR). Pratt and co-workers have a proposed a model where a chaperoned protein, such GR, is targeted to a specific region of the cell by a TPR protein that binds to hsp90 (Owens-Grillo et al., 1996). Different TPR proteins, such as Cyp40 and FKBP52 have been shown to compete for interaction with the TPR acceptor site. The various TPR proteins confer different patterns of intracellular targeting on the resultant complexes (Owens-Grillo et al., 1996).

1.11.5 PH domains

Not all protein modules associate with peptide targets. For instance, pleckstrin homology (PH) domains are targeted to the membrane lipid bilayer by their association with the charged head groups of specific polyphosphoinositides PI-4,5-P_2 and PI-3,4,5-P_3. The latter are generated by the action of phosphatidylinositol kinases. PH domains are found in a large number of proteins including the kinases Akt/PKB and PDK1, PLC

isoforms, cytoskeletal proteins and the regulators of small G proteins. One function of PH-domain proteins may be to link the action of phosphatidyl inositol kinases with downstream signalling pathways. For instance, PI-3,4,5-P_3, which is generated by PI3-kinase, binds to the PH domain of Grp1. The latter acts as a GEF for the small G protein Arf which controls vesicle trafficking. In this way, the activation of PI3-kinase by receptor tyrosine kinases (RTKs) is linked with the regulation of vesicle trafficking by Arf.

Several other protein modules have been shown to exist in addition to the ones described above (Pawson and Nash, 2000). These modules occur in many different combinations in proteins, which allows the integration of a number of signalling pathways. A common feature of these protein-protein interaction modules described above is their association with short sequence motifs on the target proteins. Peptide mimetic compounds could potentially block these interactions. Therefore, the identification of the protein modules that interact with PDE4 isoenzymes may lead the way to novel pharmacological agents that block the function of specific PDE4 isoenzymes.

1.12 Summary

Considerable isoform diversity occurs at all levels of the cAMP signalling pathway. The selective expression of these isoforms allows cells to tailor their responsiveness to stimuli that act via cAMP. This isoform diversity is particularly apparent in the cAMP-specific PDE4 family. This is partly the result of alternative 5' mRNA splicing, which generates isoenzymes with shared catalytic core regions and unique NH_2-terminal splice domains. One effect of these NH_2-terminal regions is to confer distinct patterns of regulation on the individual isoenzymes. An example of this is shown by the different effects of ERK2 phosphorylation on the activity on the long and short PDE4D splice variants (see section 1.7.1).

An important goal in PDE4 research is the elucidation of the roles of individual PDE4 isoenzymes in cAMP-dependent processes. This will allow us to make predictions on the cAMP-responsiveness of cells, based on the PDE4 isoenzymes that they express. It may also help in the identification of the appropriate targets for the design of drugs to treat diseases where PDE4 has been implicated, such as asthma and atopic dermatitis. One approach is to use a model cell system where we can analyse a measurable cAMP-dependent process that is regulated by PDE4. One such system is the positive effect of

growth hormone (GH) on the differentiation of 3T3 F442A preadipocytes, which is potentiated by the PDE4 specific inhibitor rolipram. In Chapter 3 I have determined the PDE4 isoenzymes expressed in these cells by RT-PCR and sequencing. Further analysis showed that GH specifically activated the PDE4A5 isoenzyme via PI3-kinase and p70S6 kinase and this activation was suggested to act as a break on the process of differentiation. Therefore, an initial screen of PDE4 isoenzymes expressed by a cell is a key step in elucidating the physiological role of individual isoenzymes.

Studies have suggested that PDE4 isoenzymes may be involved in the regulation of compartmentalised pools of cAMP. The precise localisation of these isoenzymes within the 3D matrix of the cell is likely to be a crucial aspect of this function. The distinct patterns of intracellular localisation shown by PDE4 isoenzymes may be due to targeting motifs within their unique NH_2-terminal splice domains. In Chapter 4 I test this hypothesis by expressing the NH_2-terminal domains of PDE4A1 and PDE4A5 as fusions to GST. These NH_2-terminal domains do indeed confer particulate fraction association on the normally soluble GST. Further analyses using these constructs suggested that PDE4A1 and PDE4A5 interact with distinct components of the particulate fraction.

A number of signalling proteins are targeted to specific regions of the cell by their association with scaffold and anchoring proteins. Recently, PDE4D5 has been shown to associate with the RACK1 anchoring protein, which also associates with PKC and PLCγ. This complex may thus allow the co-ordination of Ca^{2+} and cAMP signalling pathways. Subcellular distribution analyses suggest that many other PDE4 isoenzymes may be specifically targeted by anchoring proteins or lipids.

The formation of signalling complexes is often mediated by protein-protein interaction modules, including SH2, SH3, PDZ and TPR domains. The majority of these modules recognise short sequence motifs in their target proteins. The PDE4A4/5 and PDE4D4 isoenzymes can both bind to the SH3 domains from Src family tyrosyl kinases. Modules such as these may localise PDE4 isoenzymes to signalling proteins or complexes where they can modulate the local activity of PKA. PDE4 isoenzymes may well associate with two or more proteins, either separately or as complexes. In Chapter 5 I show that RNPDE4A5 associates with a novel immunophilin-like protein RB3. This interaction appears to be mediated by the COOH-terminal half of RB3, which contains a TPR domain. Intriguingly, this interaction inhibits the catalytic activity of RNPDE4A5, which suggests that RB3 may modulate PDE4 function *in vivo*.

CHAPTER 2

Materials and Methods

2.Materials and Methods

Throughout the following methods the names of the companies used for the purchase of specific reagents or materials are given in parentheses. Where no company is mentioned, the reagent was purchase from Sigma-Aldrich. All reagents were of analytical grade.

CELL CULTURE TECHNIQUES

2.1 Cell culture

All cells were routinely cultured in 75cm^2 flasks at 37°C in 95% air/5% CO_2 in a humidified incubator. The media and sera used to culture these cells were obtained from Gibco BRL (UK).

2.1.1 Adherent cells

2.1.1.1 COS cells and HEK293 cells

The COS cells lines, including COS-1 and COS-7 are derived from the CV-1 cell line, which was originally established from simian kidney (African Green Monkey, *Cercopithecus aethiops*) (Gluzman, 1981; Scotland et al., 1998). These cells were transformed with an origin-defective mutant of SV40 DNA, which encoded the T antigen. The presence of the T-antigen allows vector plasmids, such as pcDNA3 and pSV-SPORT, which contain the SV40 origin of replication, to evade the normal block on DNA re-replication. Therefore, COS cells are able to support the expression of high copy numbers of these vectors and thus high levels of expression from cDNA carried by these vectors.

COS-1 and COS-7 cells were cultured as monolayers in DMEM with 0.2mM glutamine, 10% FCS, 200units/ml penicillin and 200µg/ml streptomycin. The adherent cells used in these studies were passaged when they were ~90% confluent (once every 2-4 days) and were split 1:3 to 1:6.

2.1.1.2 3T3 F442A preadipocytes and HEK293

The preadipocyte mouse fibroblast cell line 3T3 F442A (MacKenzie et al., 1998) and the human embryonic kidney cells (HEK293) (Brunn et al., 1997; Von Manteuffel et al., 1996) were cultured in an identical manner to COS cells (see previous subsection).

However, 3T3 F442A preadipocytes were cultured using DMEM containing 0.2mM glutamine, 10% NBCS, 200units/ml penicillin and 200µg/ml streptomycin

2.1.2 Suspension cell lines

2.1.3 MOLT3, Jurkat T, B, and U937

The suspension cell lines used were as follows: Daudi B-cells (Hewitt et al., 1997), Jurkat T-cells (Erdogan and Houslay, 1997; Seybold et al., 1998), U937 human monocytes (Torphy et al., 1995) and murine MOLT3 T-lymphoblastic cells (Hayon et al., 1999). These lines were all cultured in RPMI-1640 medium containing 0.2mM glutamine, 10% FCS, 200units/ml penicillin and 200µg/ml streptomycin and were passaged every 2-4 days. The cells were harvested by centrifugation (5min, 1000*g* at room temperature) when their density reached $2x10^6$ cells/ml.

2.1.4 Stimulation of cell lines with biochemical agents

All treatments were carried out under normal growth conditions (37°C, 5% CO_2 humidified incubator). The stock solutions of PMA, GH and IBMX were prepared in 100% DMSO. To treat the cells, these effectors were diluted in the appropriate cell growth media to yield the final concentrations given below. The final concentration of DMSO in the growth medium was always ≤ 0.1%, which has been shown to have no effect on cell PDE activity or expression (Erdogan and Houslay, 1997).

2.1.4.1 Stimulation of 3T3 F442A preadipocytes with GH, PMA and wortmannin

At ~90% confluence, 3T3 F442A mouse preadipocytes were serum starved for 16h. These cells were then left untreated (control) or incubated for 30min with 25nM GH, 25nM PMA or 2nM wortmannin. These treatments were terminated by washing the cells with ice-cold PBS (ICN Biomedicals, see section 2.7.1 for composition) and proceeding with RNA extraction as described in section 2.6.1.

2.1.4.2 Stimulation of COS7 cells with IBMX, forskolin and PMA

In order to effect an increase in the total intracellular concentration of cAMP, and thus bring about an activation of PKA, cells at ~90% confluence were treated with a combination of forskolin, which activates adenylyl cyclase (Houslay and Milligan, 1997) and IBMX, which prevents the breakdown of cAMP by inhibiting PDEs. COS-7 cells were

treated for 20min with 100μM IBMX prior to the addition of 100μM forskolin and a further 20min incubation.

In order to activate both PKC, and ERK (activated downstream of PKC (MacKenzie et al., 1997)) in COS-7 cells, they were stimulated with 100μM PMA for 5mins. This treatment is known to produce an optimal ERK2-dependent stimulation of PDE4D3 activity (MacKenzie et al., 2000).

2.2 Transfection of COS cells with plasmid DNA

Table 2.1 Buffers used for transfection of COS cells with DNA

TE buffer	10 mM 0.1mM	Tris-HCl, pH8.0 EDTA
DEAE-dextran	10mg/ml	DEAE-dextran in PBS

COS cells (COS-1 or COS-7) were seeded at a density of approximately 50% confluency onto 100mm diameter plates 18h before transfection. Immediately before transfection the culture medium was replaced with DMEM containing 10% (v/v) NBCS and 0.1mM chloroquine to minimise DNA degradation (Sambrook et al., 1989). For each 100mm plate a DNA solution was prepared by diluting 10μg of the plasmid to a final volume of 250μl in TE buffer and adding 200μl of a 10mg/ml DEAE-dextran solution. This mixture was incubated at room temperature for 15min prior to the addition to the COS cell culture. Cultures were incubated for 3-4h at 37°C in a humidified incubator before the medium was aspirated and the cells shocked for 2min with 10% DMSO in PBS. The cultures were then rinsed once in PBS before the addition DMEM containing 10% FCS. The cultures were incubated in a humidified incubator for 72h before analysis by SDS-PAGE/western blotting or PDE assay.

2.3 Agarose gel electrophoresis of DNA

Table 2.2 Buffers used for the separation of DNA by agarose gel electrophoresis

TAE running buffer	40 mM 20mM 1mM	Tris-HCl, pH8.0 Acetic acid EDTA
Agarose gel (0.7-2%) in TAE buffer	0.7-2% (w/v) 0.5µg/ml	Agarose Ethidium bromide TAE buffer

DNA was separated and visualised by electrophoresis on 0.7-2% agarose gels in the presence of ethidium bromide. The agarose gel mix was prepared as described above. The concentration of agarose was selected according to the size range of the DNA fragments to be separated (see Table 2.3 below). Appropriate volumes of 6x blue/orange loading dye (Promega, UK) were added to the DNA samples to give a final concentration of 1x. These samples were applied to the gel and separated by electrophoresis in TAE runnning buffer at 100V. The presence of the intercalating dye, ethidium bromide, allowed the visualisation of the separated DNA bands under UV transillumination. The DNA fragments were sized by comparison to the ΦX174 *Hae*III molecular weight standard (Boehringer Mannheim, UK), which contained fragments of the following sizes: 1353, 1078, 872, 603, 310, 281, 271, 234, 194, 118, and 72bp. These standards were used to generate a plot of distance migrated versus Log [MW (bp)]. The resultant curve was used to determine the molecular weights of the PCR standards from their distances of migration on the agarose gel.

Table 2.3 Relationship between the range of separation and agarose gel concentration.

Based on table 6.1 in (Sambrook et al., 1989).

Agarose concentration (%[w/v])	Efficient size range of separation of DNA molecules (kbp)
0.7	0.8-10
1.2	0.4
2	0.1-2

2.4 Preparation of plasmid DNA

Plasmid DNA was prepared from transformed *E. coli* cultures using the Qiagen or Promega (Wizard™) DNA purification systems. Miniprep and maxiprep kits from both companies were used for small-scale and large-scale preparations of plasmid DNA, respectively. DNA purifications were carried out according to the instructions provided by the manufacturers.

2.5 Transformation of *Escherichia coli* with plasmid DNA

2.5.1 Preparation of heat-shock competent *E. coli*

Table 2.4 Media and buffers used for the preparation of heat-shock competent *E. coli*

SOB liquid media	20g/l 5g/l 10mM 2.5mM	Bacto-tryptone Bacto-yeast NaCl KCl
RF1 (pH adjusted to 5.8 with 0.2M acetic acid)	100mM 50mM 30mM 10mM 15% (w/v)	RbCl $MnCl_2$ Potassium acetate $CaCl_2$ Glycerol
RF2 (pH adjusted to 6.8 with 0.2M NaOH)	10mM 10mM 75mM 15% (w/v)	RbCl MOPS $CaCl_2$ Glycerol

To prepare 'heat-shock' transformation-competent *Escherichia coli*, a colony of the desired strain, (either JM109 or BL21) grown on LB-agar plates, was picked and used to inoculate a SOB culture. This culture was grown at 37°C until its absorbance at 550nm (OD_{550}) was 0.5-0.55. The culture was cooled on ice (30min) and pelleted by centrifugation at 600*g* for 15min. The cells were then resuspended in ice-cold buffer RF1, and

incubated for 15min on ice prior to centrifugation at 2500rpm for 9min at 4°C. The supernatant was removed and the pelleted cells were resuspended in ice-cold buffer RF2 and incubated on ice for 15min. The cells were then aliquoted, snap frozen in a dry ice/ethanol bath and stored at -80°C.

2.5.2 Heat-shock transformation of competent *E. coli.*

Table 2.5 Media and buffers used for the transformation of competent *E. coli*

SOC liquid media	2% (w/v) 0.5% (w/v) 10mM 2.5mM	Bacto-tryptone Bacto-yeast NaCl KCl
LB agar plates (containing ampicillin)	2% (w/v) 0.5% (w/v) 170mM 2% (w/v) Ampicillin	Bacto-tryptone Bacto-yeast NaCl Agar 50μg/ml

Competent *E. coli* were transformed with plasmid DNA using the heat shock method described in (Sambrook et al., 1989). A sample of the plasmid DNA (1μl) was gently mixed with an aliquot (20μl) of the heat-shock competent cells prepared as described in the previous section. This mixture was incubated on ice for 30min. It was then heat-shocked at 42°C for 40s and returned to ice for a further 2min. SOC buffer (80ml) was then added to the cells and they were shaken at 225rpm for 1h at 37°C. The cells were then spread onto an LB agar plate containing 50μg/ml ampicillin and incubated overnight at 37°C in order to obtain ampicillin resistant colonies (NB all the plasmids used in this study contained an ampicillin resistance gene for selection).

2.6 Reverse-transcription polymerase chain reaction (RT-PCR)

2.6.1 RNA extraction and purification from 3T3 F442A cells

Total RNA was extracted using the Tri reagent method. The medium was removed from confluent 3T3 F442A mouse preadipocytes and the cells were washed once with sterile PBS. The cells were scraped into 1ml of Tri reagent and homogenised by passing through a 0.45mm syringe needle 10 times.

The homogenate was centrifuged at 12000*g* for 10min at 4°C to remove cell debris. The supernatant was transferred to a fresh tube and 0.2 volume chloroform was added. This mixture was vortexed for 15s, stored at room temperature for 3min and then centrifuged at 12000*g* for 15min at 4°C. The aqueous phase was transferred to a new eppendorf tube and 0.5ml of propan-2-ol was added for every 1ml of Tri reagent used initially. This was stored at room temperature for 5-10min. The precipitated RNA was pelleted by centrifugation at 12000*g* at 4°C for 10min. The supernatant was removed and the RNA was washed by resuspending the pellet in 75% ethanol (containing 0.025% DEPC) followed by centrifugation at 7500*g* for 5min at 4°C. The supernatant was removed and the pellet was dried and then resuspended in 0.1% DEPC-treated water.

2.6.2 RNA extraction and purification from mouse brain

The brain of a mature male Balb-c mouse was removed, frozen in liquid nitrogen and weighed. The brain was then ground to a slurry in liquid nitrogen using a pestle and mortar. Tri reagent was added to the slurry (1ml per 150mg of organ). The mixture was vortexed and then homogenised by 10 strokes on a rotary homogeniser. Total RNA was extracted from this homogenate using the Tri reagent method described above.

2.6.3 DNase treatment of RNA

To eliminate contamination by genomic DNA, the aqueous suspension of RNA was treated with RNase-free DNase (10 units/20ug RNA) for 15min at 37°C. The DNase treated RNA was then purified by phenol: chloroform extraction and ethanol precipitation as follows. One volume of acid (pH 4.5) 25:24:1 phenol: chloroform:isoamylalcohol was added to the aqueous suspension of RNA and the mixture was vortexed for 1min and then centrifuged at 12,000*g* at 4°C for 2min. The aqueous (upper) phase containing the RNA was transferred to a new tube. One volume of 24:1 chloroform:isoamylalcohol was added and the mixture was vortexed for 1min and then centrifuged at 12,000*g* at 4°C for 2min. The aqueous phase was transferred to a new tube. RNA was precipitated by incubating with 0.5 volume of 7.5M ammonium acetate and 2.5 volumes of 100% ethanol at -80°C overnight. The precipitated RNA was pelleted by centrifugation at 12000*g* at 4°C for 5min. The pellet was washed with 70% ethanol and the RNA was resuspended in 0.1% DEPC-treated water. RNA solutions of an acceptable purity gave a 260nm/280nm ratio of 1.7 to 2.

2.6.4 First strand cDNA synthesis

First strand cDNA synthesis was carried out according to the instructions supplied with the First strand cDNA-kit (Amersham Pharmacia Biotech, Amersham, UK) using a total reaction volume of 33µl. DNase treated RNA (5µg) was denatured at 65°C for 10min and then incubated with reverse transcriptase, 6mM dithiothreitol, 6mM of each dNTP and 0.2µg of poly (dT) primer [*Not* 1-d$(T)_{18}$] for 60min at 37°C. The cDNA was stored at -80°C until it was required.

2.6.5 Polymerase chain reaction

All components of the PCR reaction, except for the primers, were obtained from Promega. Amplification was performed in 1 x PCR buffer (50mM KCl, 20 mM Tris-HCl pH 9.0, 0.1% Triton X-100) containing 200µM of each dNTP, 500nM of each primer and 1.5mM $MgCl_2$. 2.5 units of Taq DNA polymerase were added to each 25µl reaction just before the start of cycling. Amplification was performed on 0.5µl of template cDNA prepared as described above (see section 2.6.4). The sequences of the oligodeoxynucleotide (ODN) primers used are given in the appropriate sections. As a positive control for the PCR amplifications to detect splice variants PDE4B2, PDE4D1 and PDE4D2, where no expression plasmid was available, 0.5µl of mouse brain cDNA was used as template. For all other splice variants, 0.5ng of a plasmid containing the appropriate clone was used as a template. After the indicated cycles of denaturation and extension, a 9µl aliquot from each of the PCR reactions was resolved by electrophoresis on a 2% agarose gel. The ΦX174 *Hae*III molecular weight standards (Boehringer Mannheim, Lewes, UK) were used to determine the size of the PCR fragments as described in section 2.3.

2.6.6 TA cloning of PCR fragments

The cloning and sequencing of amplified PCR fragments is aided by the single-base A overhangs left by Taq polymerase at their 3' ends. This allows their direct insertion into a pCR2.1 vector (Invitrogen), which in its linearized form has overhanging Ts at the 3' ends of each of its DNA strands. The principles of TA cloning are described in Figure 2.1. The system exploits the ability of the enzyme β-galactosidase to metabolise the colourless substrate X-gal to form a blue product. *E.coli* bacteria that contain a plasmid that expresses a functional β-galactosidase will form blue colonies on LB-agar plates that contain X-gal.

However, *E. coli* that carry a plasmid containing an insert that disrupts the β-galactosidase coding region, will form white colonies. Once the PCR products have been cloned into pCR2.1 the inserts can then be sequenced using primers that anneal to sites on pCR2.1 that flank the insertion site.

RT-PCR products were cloned into the vector pCR2.1 using the Original TA Cloning™ Kit (Invitrogen). Ligations were performed by incubating 1μl of the PCR product in a 10μl reaction mix containing 50ng of linearized pCR2.1, 1x Ligation buffer (Invitrogen) and 4 units T4 DNA ligase. The ligation reactions were incubated overnight at 14°C.

The *E. coli* strain INVαF', provided with the kit, was used for the transformation and propagation of insert-containing pCR2.1 plasmids. Transformation was carried out as described in the manufacturer's instruction. In brief, 50μl aliquots of the INVαF' cells were incubated with 2μl samples of the above ligation reaction in the presence of 20mM β-mercaptoethanol for 30min on ice. The cells were then heat-shocked at 42°C and incubated with SOC medium as described in section 2.5.2. They were then plated on LB-agar plates containing 50μg/ml ampicillin and spread with 40mg/ml X-gal dissolved in N,N dimethylformamide (40ml per 100mm plate). These plates were then incubated overnight at 37°C in order to obtain, white, ampicillin resistant colonies of *E. coli* transformed with insert-containing pCR2.1 plasmids.

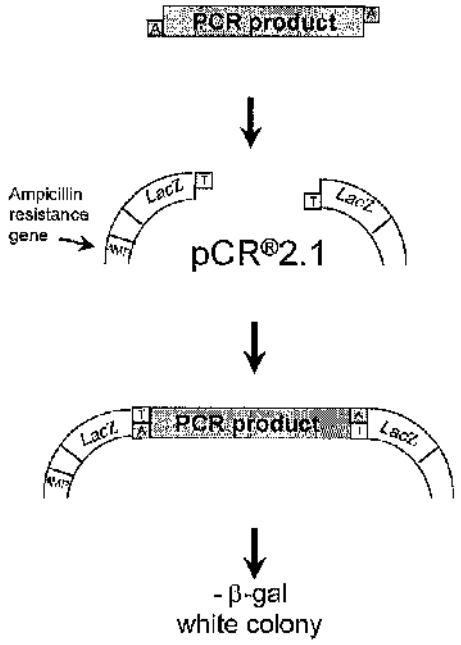

Figure 2.1 Principles of the Invitrogen™ TA method for cloning PCR amplified fragments.

One feature of Taq DNA polymerase is that it appends an A-base overhang to the 3' end of each strand of the PCR product. This allows the direct insertion of PCR products into the pCR2.1 vector (Invitrogen), which is supplied in a linearized form, with overhanging Ts at the 3' ends of each of its DNA strands. The PCR products are inserted within the α-peptide coding region (*LacZα*) of the enzyme β-galactosidase. Therefore, upon transformation into *E. coli* INV-αF' cells, recircularised pCR2.1 vectors that lack an insert express β-galactosidase and produce blue ampicillin-resistant colonies on plates containing X-gal. However, insert-containing pCR2.1 vectors will be unable to express functional β-galactosidase and will therefore produce white ampicillin-resistant colonies on X-gal plates. In this way vectors containing the PCR product can be isolated and used for sequencing. The inserts are sequenced using ODN primers that anneal to either side of the insertion point.

2.6.7 Sequencing of PCR fragments

Plasmid DNA was purified as described in section 2.4. The inserts were sequenced using the M13 forward and reverse primers, provided by Invitrogen that anneal to either side of the insert site in pCR2.1. Sequencing was carried out using the ABI PRISM Dye Terminator Cycle Sequencing Ready Reaction Kit (Perkin-Elmer, UK). Sequencing reactions were set up in a total volume of 20µl, with 0.16µM primer, 20ng/µl plasmid and 8µl of terminator ready reaction mix. The following cycle conditions were used for the sequencing reaction (25 cycles): denaturation, 96°C for 10s; annealing, 50°C for 15s; extension, 50°C for 4min. The extension products were precipitated by the addition of 0.1 volume of 3M sodium acetate (pH4.3) and 2 volumes of ethanol. The precipitated products were pelleted by centrifugation and washed with 70% ethanol. Analysis of the sequencing products was performed on a model 373 automated sequencer (Applied Biosystems, UK).

2.7 Over-expression and purification of GST and MBP fusion proteins

2.7.1 Over-expression of GST and MBP fusion proteins

Table 2.6 Media and buffers used for the over-expression of GST and MBP-fusion proteins

Luria Bertani (LB) medium	170mM 0.5% (w/v) 1 % (w/v)	NaCl Bacto-Yeast Extract Bacto-Tryptone
IPTG		0.1M stock solution (stored at -20°C)
Complete PBS (PBS +protease inhibitors and DTT)	137mM 2.7mM 4mM 0.15mM 1x 1mM	NaCl KCl Na_2HPO_4 NaH_2PO_4 (pH 7.4) Complete™ EDTA-free protease inhibitor cocktail (Boerhinger mannheim, UK) DTT

E. coli (BL21 or JM109 strain) was transformed with either pGEX-2T (for the production of GST), pMAL-C2, (for the production of MBP), a recombinant pGEX vector containing species engineered to form in-frame fusions with GST, or recombinant pMALN containing species engineered to form in-frame fusions with MBP. These transformed

bacteria were grown overnight at 37°C, with agitation, in LB medium containing 50μg/ml ampicillin. Overnight cultures were diluted 1:30 in the same medium (2g/l glucose was included for MBP fusions) and these were grown at 37°C, with agitation, until the OD at 600nm reached 0.6 - 1.0. Expression of the fusion protein was then induced by adding IPTG to a final concentration of 0.5mM (0.1mM for MBP-fusions) and growth was continued for a further 3-4h at 37°C (or 3h at 30°C for MBP-fusions) with agitation. The bacteria were harvested by centrifugation at 4000*g* for 10min in a refrigerated centrifuge and then resuspended in 20ml phosphate buffered saline (PBS) containing 1mM-dithiothreitol (DTT) and Complete™ protease inhibitor cocktail (Boehringer Mannheim (UK), Ltd., Lewes, UK). Resuspended bacteria were stored, as 4ml aliquots, at -20°C. Freezing at this stage assists the lysis of the bacteria.

2.7.2 Purification of GST and MBP fusion proteins expressed in *E. coli*

Table 2.7 Buffers and materials used in the purification of GST- and MBP-fusion proteins expressed in *E. coli*

Elution buffer: GST-fusion proteins	10mM 50mM	Glutathione Tris-HCl, pH 8.0
Elution buffer: MBP-fusion proteins	10mM	Maltose in PBS
PBS and complete PBS		See Table 2.6
Glutathione Sepharose 4B Amylose resin		(Amersham pharmacia biotech, UK) (New England Biolabs)
Dialysis buffer	20mM	Tris pH 8.0

2.7.2.1 Procedure 1: Batch purification

Purification of GST- or MBP-fusion proteins was carried out as described in (Smith and Johnson, 1988). Frozen aliquots of bacteria expressing GST- or MBP- fusion proteins (see above) were thawed at room temperature then held on ice and sonicated for 100s in 20s pulses, separated by 20s intervals. Bacterial debris was then pelleted by centrifugation for 30min at 9000g in a refrigerated centrifuge and the supernatant was transferred to a fresh tube. Glutathione Sepharose beads (for GST-fusions) or amylose resin (for MBP-fusions) were equilibrated by washing twice with 20 bed volumes of ice cold PBS and once with 10 bed volumes of complete PBS (containing 1mM DTT and protease inhibitor

cocktail). The equilibrated beads were added to the above sonicated bacterial supernatant (200µl bed volume Sepharose beads per 4ml supernatant) and incubated end over end at 4°C for 2h. Following incubation, the beads were collected by centrifugation for 5min at 2000*g* in a Jouan C312 'swing-out' centrifuge and the supernatant was discarded. The beads were washed 4 times with 10 bed volumes of ice cold complete PBS per wash. Each wash step was carried out end over end for 30min at 4°C. Purified fusion protein was eluted by incubating the beads with one bed volume of elution buffer (see above table) 3 times at 4°C for 15min.

2.7.2.2 Procedure 2: column purification

Certain GST-fusion proteins (GST-rpde6$^{1-256}$ and GST-RD1$^{1-100}$) were purified using a modification of the above procedure, carried out at 4°C. An equivalent amount of glutathione Sepharose beads were placed in a 20ml column supported on glass wool. The beads were equilibrated with 10 bed volumes of complete PBS. The bacterial sonicated supernatant (see above) was passed through this column twice. The beads were washed with 30 bed volumes of complete PBS. Bound protein was eluted by three separate 10min incubations with 1 bed volume of glutathione elution buffer (Table 2.7).

2.7.2.3 Dialysis of eluates

The glutathione eluates of purified GST-fusions for use in PDE4 activity studies were dialysed against 20mM Tris-HCl pH8.0. This was necessary as glutathione may affect PDE activity (Souness and Scott, 1993). The eluates were combined and dialysed twice against 1 litre of 20mM Tris-HCl pH8.0 for 2h and once against 1 litre of the same buffer overnight. All dialysis steps were carried out at 4°C. The dialysed protein was protein assayed (section 2.8), aliquoted, snap frozen in liquid N_2 and stored at -80°C until required.

2.7.3 Measures taken to increase the yield of soluble protein expressed in *E. coli* strains

A number of factors can prevent successful purification of GST- or MBP- fusion proteins. Using the system described in sections 2.7.1 and 2.7.2, the peptides fused to the GST or MBP affinity tags can undergo proteolytic degradation by bacterial proteases. Alternatively, certain fusion proteins may be insoluble (Shi et al., 1997). This is more likely for large or hydrophobic proteins (Harris, 1998). One way of avoiding this is to

reduce the temperature at which the bacteria are grown (Hengen, 1996) from 37°C to 30°C or room temperature. This modification was used successfully by Nair et al and Chen et al to express soluble forms of FKBP52 and protein phosphatase 5 (PP5) respectively (Chen and Cohen, 1997; Nair et al., 1997). Leverson and Ness also used this strategy to purify GST-Cyp40 (Leverson and Ness, 1998).

In order to purify the large GST fusion proteins, e.g. GST-FKBP52 (see section 5.13) with minimal proteolytic degradation problems, I used the following modifications to the methods set out in sections 2.7.1 and 2.7.2. The plasmids encoding the GST-fusion proteins were transformed into *E. coli* strain BL21 rather the JM109. This BL21 strain is recommended for use as it lacks a number of endogenous proteases that exist in other strains. The cultures were grown up at 30°C and induced when they were in late log phase, i.e. when the OD_{600} was close to 1. The cultures were then induced with 0.1mM IPTG for the minimum time of 3h at room temperature. The lower growth temperature and shorter induction time were used to reduce the effect of proteases (Hengen, 1996) and to decrease the problem of insolubility. To reduce proteolytic degradation during the binding of the GST-fusion proteins to the glutathione Sepharose, the incubation time here was reduced from 2h to 1h.

2.8 Protein assay

Protein was routinely measured by the method of Bradford (Bradford, 1976). Protein assay dye concentrate (Bio-Rad) was diluted 1:4 with water to produce the protein assay dye solution. Samples were diluted with water and 1 volume of diluted sample was incubated with 4 volumes of protein assay dye solution for 5min at room temperature. The absorbance was then measured at 595nm (A_{595}). Bovine serum albumin (BSA) was used as a standard to construct a curve of A_{595} versus protein concentration. This curve was linear between protein concentrations of 20μg/ml and 120μg/ml.

2.9 SDS polyacrylamide gel electrophoresis (SDS-PAGE) of proteins

Table 2.8 Buffers and solutions for SDS-PAGE

Resolving gel (10-12%)	10-12% (w/v)	29:1 acrylamide:N,N'-methylenebisacrylamide*
	0.375M	Tris-HCl, pH8.8
	0.1%	SDS
	0.1%	Ammonium persulphate
	0.04%	TEMED
Stacking gel (5%)	5% (w/v)	29:1 acrylamide:N,N'-methylenebisacrylamide
	0.125M	Tris-HCl (pH6.8)
	0.1%	SDS
	0.1%	Ammonium persulphate
	0.1%	TEMED
Tris-glycine running buffer	0.2M	Glycine
	25mM	Tris
	1% (w/v)	SDS
5X SDS loading buffer (Laemmli buffer)	0.26M	Tris-HCl (pH6.7)
	55.5%	Glycerol
	8.8%	SDS
	11.1%	β-mercaptoethanol
	0.007%	Bromophenol blue
Coomassie blue stain	5% (v/v)	Glacial acetic acid
	45% (v/v)	Methanol
	1% (w/v)	Coomassie brilliant blue
Destain		As above, but no Coomassie

* Referred to as acrylamide in the text.

Proteins were separated according to their size by Tris–glycine SDS PAGE, following the method of Laemmli (Laemmli, 1970). The samples to be separated were diluted with Laemmli buffer (5x) to give a final concentration of 1x. These samples were boiled for 5min prior to storage and/or separation. Samples were separated by downward migration through a vertical two-phase gel consisting of a stacking gel (top) and a resolving gel (bottom). The gel apparatus was obtained from Bio-Rad. The gel was suspended between two separate reservoirs of Tris-glycine running buffer. A cathode and anode were placed in the top and bottom reservoirs respectively. Proteins were separated at 40mA

constant current for 4-5h (30ml resolving gel) or 1h (5ml resolving gel). A 10% (w/v) acrylamide resolving gel was used for the separation of 21-100kDa proteins, whereas a 12% (w/v) acrylamide resolving gel was used for the separation of 10-40kDa proteins (Sambrook et al., 1989). The prestained, broad range protein molecular weight markers used were obtained from New England Biolabs or Bio-Rad. Separated proteins were visualised by Coomassie blue staining (20min stain followed by 1h destain) or were transferred onto nitrocellose membrane for analysis by western blotting.

2.10 Western blotting

Table 2.9 Buffers for western blotting

Transfer buffer	0.2M Glycine 25mM Tris 1% SDS 20% Methanol
TBS-Tween	137mM NaCl 20mM Tris-HCl pH 7.6 0.1% Tween-20

Proteins were transferred from SDS-PAGE gels to nitrocellulose membranes (Protean) by electroblotting in transfer buffer at 1A constant current for 90min. The nitrocellulose membranes were blocked by incubation with 5% skimmed milk in TBS-Tween for 1h shaking at room temperature. They were then incubated with primary antibody, diluted in 1% skimmed milk in TBS-Tween, either shaking at room temperature for 2h or at 4°C overnight. The antibody dilutions that were used are shown in Table 2.10 below. After three 10min washes in TBS-Tween, the nitrocellulose membranes were incubated with horseradish peroxidase (HRP) conjugated secondary antibody, diluted in 1% skimmed milk in TBS-Tween, for 1h shaking at room temperature. The membranes were washed in TBS-Tween as before, rinsed with Milli-Q pure water and developed using the enhanced chemiluminescence (ECL) kit (Amersham Pharmacia Biotech, UK) following the manufacturer's instructions. Immediately after treating the membranes with ECL reagent, they were exposed to Kodak X-ray film for various lengths of time (10sec-30min).

Table 2.10 Table of antibodies and the dilutions used for western blotting

Specific for:	Name	Primary or secondary	Monoclonal/ Polyclonal	Dilution for western blotting
GST	83	Primary	Polyclonal	1:1000
RNPDE4A (generic)	651	Primary	Polyclonal	1:1000
V5-tagged* proteins	Anti V5	Primary	Monoclonal	1:30,000
RB3	574	Primary	Polyclonal	1:1000
Mouse IgG (whole molecule)	Anti mouse IgG	Secondary (HRP-conjugated)	Monoclonal	1:10,000
Rabbit IgG (whole molecule)	Anti rabbit IgG	Secondary (HRP-conjugated)	Monoclonal	1:10,000

* The anti-V5 antibody (Invitrogen) recognised the epitope GKPIPNPLLGLDST

2.11 Homogenisation and fractionation of cells

Table 2.11 Buffer used for the homogenisation of cells

KHEM buffer	50 mM	KCl
	50 mM	HEPES-KOH, pH7.2
	10mM	EGTA
	1.92 mM	$MgCl_2$

2.11.1 Preparation of cell lysates for analysis by SDS-PAGE/western blotting

Confluent adherent cells (COS-7, COS-1 and HEK293 cells) were washed twice with ice cold incomplete KHEM buffer and then scraped into complete KHEM buffer (+ 1mM DTT and protease inhibitors) containing 0.5% Triton-X-100. Suspended cells (e.g. MOLT3 monocytes, U937 and B-cells) were centrifuged and washed twice with ice-cold KHEM buffer before being resuspended in ice-cold complete KHEM buffer containing 0.5% Triton-X-100. All cell lines were homogenised using 10 strokes through a 26G needle (Microlance). The homogenates were assayed for protein (section 2.8) and then mixed with 5x Laemmli buffer to give a final concentration of 1x (Table 2.8). The homogenates were then boiled for 3min.

2.11.2 Subcellular fractionation of cells

Confluent, adherent cells were washed twice with ice-cold KHEM buffer. The cells were then incubated on ice with complete KHEM buffer (KHEM buffer plus 1x Complete™ protease inhibitors [Boehringer Mannheim] and 1mM DTT) for 15min. The majority of complete KHEM buffer was removed by aspiration and the cells were scraped into the residual complete KHEM buffer. The harvested cell suspension was disrupted by 50 strokes of a pestle in a glass Whatman homogeniser.

The P1-pellet fraction, which is composed of nuclear and cytoskeletal components (Scotland et al., 1998), was generated by centrifuging the cell homogenate at 4°C for 10min at 1000*g*. The supernatant was retained and centrifuged at high speed (1h at 100,000*g* at 4°C) to obtain a second high-speed pellet fraction (P2) and a high-speed supernatant fraction (S). The P2-pellet fraction contains plasma membranes, endoplasmic reticulum, Golgi stacks, endosomes and lysosomes and cytoskeletal components (Scotland et al., 1998) whereas the S fraction contains 'soluble' cytosolic proteins. The P1 and P2 pellets were washed twice in complete KHEM buffer, by resuspension using 10 passes

through a 26G needle. The volumes of the P1 and P2 fractions were then equalised to the volume of the S fraction with complete KHEM buffer. The fractions (P1, P2 and S) were then aliquoted, snap frozen in liquid N_2 and stored at -80°C.

2.12 Subcellular distribution analysis by western blotting

The distribution of a specific proteins of interest, (e.g. RB3), between the P1, P2 and S subcellular fractions was determined by western blotting (Bolger et al., 1997; Huston et al., 1997). A range of sample volumes (e.g. 5, 10, 15, 20 and 25µl) for each of the fractions were separated by SDS-PAGE (section 2.9) and transferred onto nitrocellulose. The nitrocellulose membranes were immunoblotted using a primary antibody specific for the protein of interest. The membranes were then developed by ECL and exposed to X-ray film (section 2.10). The net intensities of the bands corresponding to the protein of interest were determined by densiometry using the Kodak 1D image analysis software. For each fraction, the net intensity values were plotted against the fraction volume originally loaded on the SDS-PAGE gel to yield linear graphs (see Figure 2.2). The gradients of these graphs gave values for the intensity units per µl of sample. As the P1, P2 and S fractions had been normalised the same volume (see previous section), these gradients were directly proportional to the relative amounts of the protein of interest in the three fractions. Therefore, for each of the fractions, the relative levels of the protein of interest (in Intensity Units/µl) were expressed as a percentage of the total amount in the cell homogenate (which is equivalent to the P1, P2 and S fractions combined). This method is illustrated in Figure 2.2.

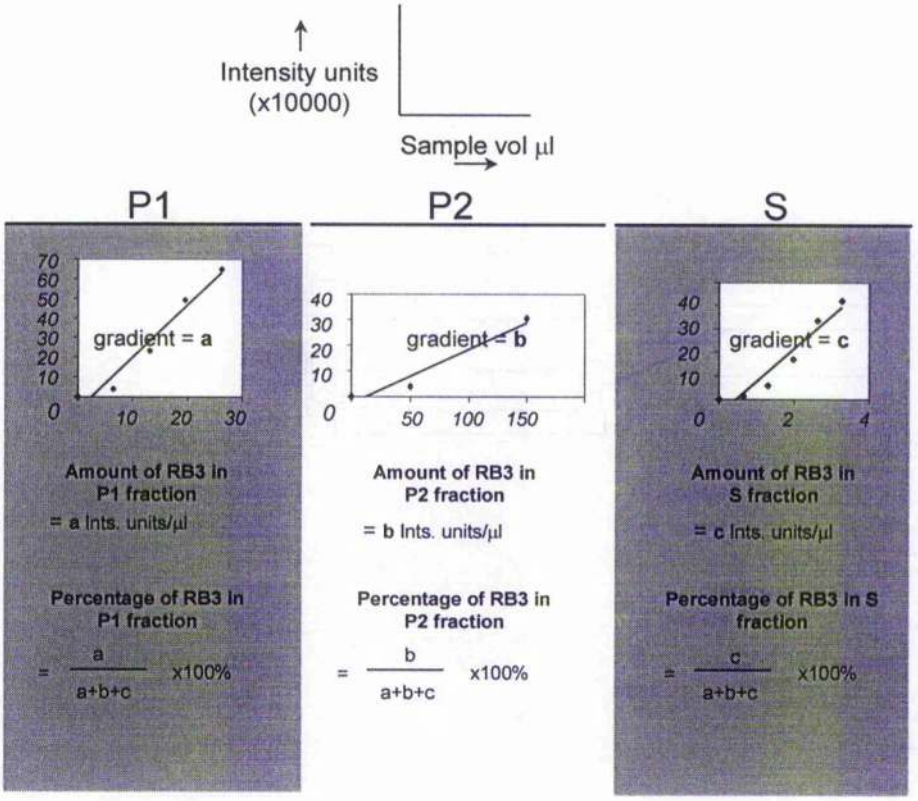

Figure 2.2 Determination of the percentage distribution of a specific protein between the P1, P2 and S subcellular fractions

The example given here is the determination of the percentage distribution of RB3 between the P1, P2 and S fractions of transfected COS-7 cells. Samples of these fractions were separated by SDS-PAGE and immunoblotted using anti-RB3 specific antisera. For each of the fractions, the intensity values of the bands obtained were plotted against sample volume. The gradients of the resulting graphs gave the relative amounts of RB3 in the three fractions (in Intensity Units/µl). These amounts were expressed as a percentage of the total amount of protein in the cell homogenate (P1+P2+ S).

2.13 Membrane association of GST-PDE4 NH_2-termini fusion proteins

GST-PDE4 NH_2-termini fusion proteins (e.g. GST-RD1$^{1-100}$ and GST-rpde6$^{1-256}$) were purified and eluted with glutathione buffer as described in section 2.7.2. Samples of the resuspended P2-'membrane' fraction of COS-7 cells (see section 2.11.2) were centrifuged at 4°C for 30min at 100,000*g*. The P2 pellets were resuspended to a final concentration of 1mg/ml protein in complete KHEM buffer (Table 2.11) containing purified GST-PDE4 NH_2-termini fusion protein (50µg/ml). After incubation on ice for 1h this mixture was then centrifuged again as before. The pellets were washed 3 times in ice-cold complete KHEM buffer. They were then resuspended in complete KHEM buffer, transferred to a fresh tube and boiled in Laemmli buffer (final conc. = 1x) for 5min. The samples were separated on a 10% (w/v) acrylamide SDS-PAGE gel (see section 2.9). After separation, the proteins were transferred onto nitrocellulose membranes and immunoblotted using GST-specific antisera (see antibody Table 2.10, section 2.10) to determine the percentage binding of the fusion protein to the P2 membranes.

2.13.1 Effect of Triton X-100 and NaCl on the membrane association of GST-PDE4 NH_2-termini fusion proteins

Samples of the P2 pellet fraction were incubated with purified GST-PDE4 NH_2-termini fusion protein and washed 3 times with complete KHEM buffer as described above. The P2-pellets were then resuspended in 2M NaCl or 5% Triton X-100 in complete KHEM buffer and incubated on ice for 30min. Afterwards the P2-pellet was recovered by centrifugation (100,000*g*, 30min, 4°C), separated by SDS-PAGE and immunoblotted using anti-GST antisera as primary reagent as described in the previous section.

2.13.2 Membrane association assay for binding of PDE4 NH_2-terminus-GST fusion proteins to thermally denatured P2 fraction

Samples of the COS-7 cell P2-membrane fraction were incubated at 50°C for the time periods indicated in the appropriate figures. The samples were then incubated with purified GST-PDE4 NH_2-termini fusion protein and washed 3 times with complete KHEM as described in section 2.13 above. The P2 pellets were then separated by SDS-PAGE and transferred onto nitrocellulose. The relative amounts of GST-fusion protein associated with

the membrane samples were analysed by immunoblotting with anti-GST antiscra as primary reagent as described above.

2.14 Generation of a polyclonal antiserum to the GST-RB3$^{1-330}$ fusion protein

A fusion of full-length RB3 to the COOH-terminus of GST (GST-RB3$^{1-330}$) was used to raise antisera against RB3 in rabbits. GST-RB3$^{1-330}$ was over-expressed and purified on glutathione Sepharose beads as described in section 2.7. The purified protein was eluted with 10mM glutathione, 50mM Tris-HCl pH8.0, aliquoted, snap frozen and stored at -80°C. Two New Zealand White rabbits (No.s 574 and 575) were immunised by subcutaneous injection at two separate sites with 50µg of GST-RB3$^{1-330}$ in complete Freud's adjuvant. The rabbits were given an initial booster injection with the same amount of fusion protein in incomplete Freud's adjuvant after 9 days and another identical boost after a further 12 days. Sample bleeds were taken 11 days after each booster injection. The final bleed was taken 15 days after the second boost. The serum was aliquoted at stored at -80°C.

2.15 Phosphodiesterase (PDE) assay

Table 2.12 Buffers used in PDE assay

PDE assay buffer	20mM 10mM	Tris-HCl (pH7.4) $MgCl_2$
Cyclic AMP Stock solution	1mM	cAMP (prepared in PDE assay buffer)
Snake venom stock solution	10mg/ml	Snake venom (*Ophiophagus hannah*)
Dowex 1x 8-400	(prepared as described below)	

2.15.1 Principle of the PDE assay

Cyclic AMP-specific PDE activity was assessed by a modification of the radioassay procedure of Thompson and Appleman (Thompson and Appleman, 1971) and Rutten et al (Rutten et al., 1973) as described previously (Marchmont and Houslay, 1980). The principles of this two-step assay are illustrated in Figure 2.3. In the first step, the samples to be assayed were incubated with 1µM 8-[^{3}H]-labelled cAMP substrate. In the second step

the [^{3}H]-labelled product of cAMP hydrolysis, 5'AMP, was dephosphorylated to adenosine by incubation with 0.2mg/ml snake venom. The negatively charged unhydrolysed cAMP was then separated from the uncharged adenosine by incubation with Dowex ion exchange resin. The amount of unbound [^{3}H]-adenosine in the supernatant was determined by scintillation counting in order to calculate the rate of cAMP hydrolysis.

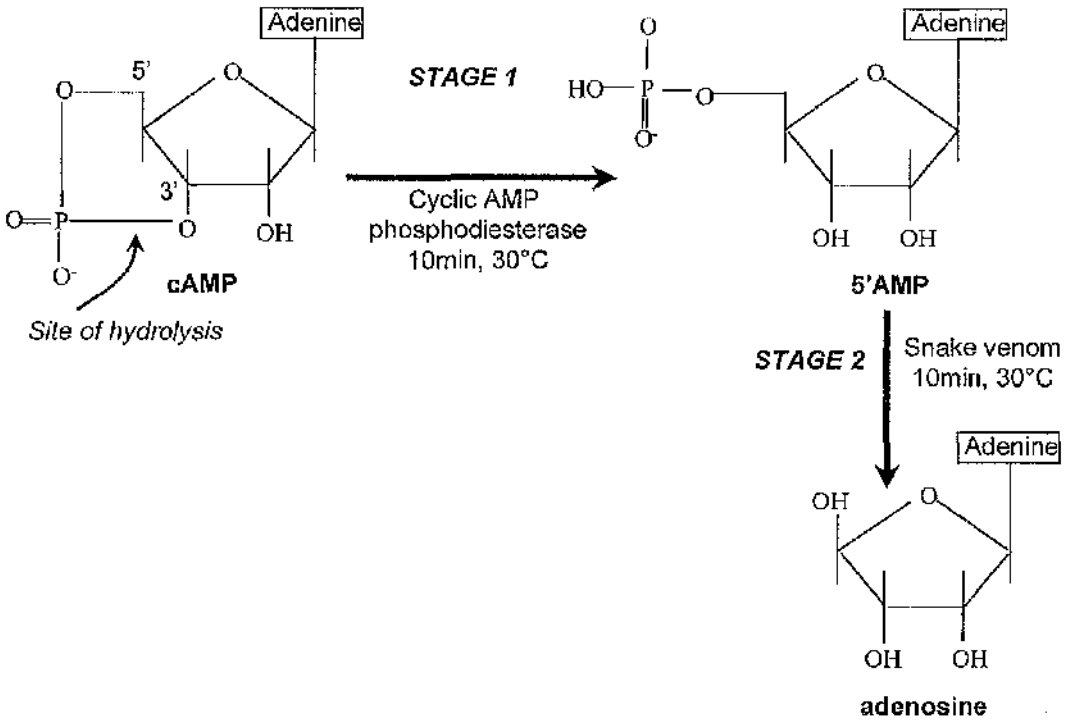

Figure 2.3 Two step PDE assay

In the first stage, the samples to be assayed were incubated with 8-[^{3}H]-labelled cAMP at 30°C for 10min. In the second stage the [^{3}H]-labelled product of cAMP hydrolysis, 5'AMP, was dephosphorylated to adenosine by incubation with snake venom at 30°C for 10min. The negatively charged unhydrolysed cAMP was separated from the uncharged adenosine by incubation with Dowex ion exchange resin. The amount of [^{3}H]-labelled adenosine product in the supernatant was measured in a scintillation counter.

2.15.2 Preparation of reagents

2.15.2.1 8-[^{3}H]-labelled cAMP substrate

A 2μM solution of unlabelled cAMP was prepared by dilution of a 1mM stock in PDE assay buffer. Immediately prior to use, 8-[^{3}H]-labelled cAMP (Amersham Pharmacia Biotech) was added to this solution to a final concentration of 3μCi/ml.

2.15.2.2 Snake venom

A 1mg/ml solution of snake venom (*Ophiophagus hannah*) was prepared by dilution of a stock solution with Milli-Q pure water.

2.15.2.3 Dowex

Dowex 1x 8-400 was prepared by washing the resin once in 1M NaOH for 15min, followed by extensive washing with Milli-Q pure water until the pH of the eluate fell to 7. The resin was then washed with 1M HCl for 15min and rinsed several times with water until the pH rose to 3. The Dowex resin was then resuspended in 1 volume of water and stored at 4°C. Immediately prior to use ethanol was added to a (Dowex:1H_2O:ethanol) ratio of (1:1:1).

2.15.3 Procedure in detail

The first step of the PDE assay was carried out in a total reaction volume of 100μl and at a final concentration of 1μM 8-[^{3}H] cAMP (0.15μCi). The samples to be assayed were incubated with 1μM cAMP for 10min at 30°C. The sample sizes were chosen to give initial reaction rates that were within the linear range for assay. The sample sizes were assumed to be within the linear range if <10% of the cAMP substrate had been consumed during the 10min assay. The assay was commenced by the addition of 50μl of 2μM 8-[^{3}H]-labelled cAMP to 25μl of appropriately diluted sample plus 25μl PDE assay buffer. Incubation was terminated by boiling for 2min.

In the second step the [^{3}H]-labelled product of cAMP hydrolysis, 5'AMP, was dephosphorylated to adenosine by the addition of 25μl of 1mg/ml snake venom to each 100μl reaction and incubation at 30°C for 10min. The negatively charged, unhydrolysed cAMP was separated from the uncharged adenosine by the addition of 400μl

Dowex:ethanol:water (1:1:1) and incubation at 4°C for 15min. The samples were vortexed at 5min intervals during this incubation to keep the Dowex in suspension. The samples were then centrifuged (13000*g*, 3min) and samples of the supernatant (150µl) were added to 1ml of Optiflow Safe 1 liquid scintillation cocktail (Fisons Chemicals Ltd). The [^{3}H]-adenosine in these samples was then counted for 1min in a Wallac scintillation counter. The cpms for each sample were corrected for a background using a blank reaction (containing no PDE). The corrected counts were used to determine the initial rate of reaction (pmol cAMP hydrolysed/min). Determination of the protein content of the samples (section 2.8) allowed the results to be expressed in units of pmol cAMP/min/mg protein (=EU).

2.16 Effect of GST- or MBP-RB3 fusion proteins on the activity of PDE isoenzymes *in vitro*

The effect of the presence of GST- or MBP-fusions of the immunophilin RB3 on the activity of a variety of PDE species was determined by assaying equal amounts of the PDE4 species in question in the presence of increasing concentrations of purified fusion protein. The GST- or MBP-fusion proteins were purified on glutathione Sepharose or amylose resin, eluted with the appropriate elution buffer and dialysed into 20mM Tris-HCl pH8.0 as described in section 2.7. These proteins were diluted with 20mM Tris-HCl pH8.0 as 4x stocks. Sample of the high-speed supernatant (S) fractions of COS-7 cells transfected with the plasmid expressing the appropriate PDE4 species were diluted in complete KHEM buffer. The assay was carried out in a final volume (after the addition of 8-[^{3}H-cAMP]) of 100µl as described in section 2.15. In the first stage 25µl of the diluted S fraction (containing a PDE activity of approx. 1EU [=pmol/min/mg]) was mixed with 25µl of a 4x stock of the purified fusion protein and incubated for 1h on ice. The PDE assay was commenced by the addition of 50µl of a 2µM solution of 8-[^{3}H]-labelled cAMP and incubation for 10min at 30°C as described in section 2.15.

Dose-effect studies were carried out using a range of concentrations (usually 0.01-1 µM) of fusion protein. The molar concentrations referred to here are the final concentrations in the 100µl reaction mixtures after the addition of 8-[^{3}H]-cAMP. The molar concentrations of the fusion proteins used were determined from their predicted molecular weights (see Table 2.13). All recombinant GST-fusion constructs were prepared using the vector pGEX5X-3 and the DNA encoding the recombinant peptide was inserted

at the *Not*1 site. Therefore, the predicted molecular weights of the fusion proteins were the sum of the predicted molecular weights of GST-5X-3 (up to the *Not*1 site) and the peptide to be fused.

Table 2.13 Actual molecular weights of GST- and MBP-fusion protein

Protein	Molecular weight (g/mol ≡ Daltons)
GST (2T)	26884
GST (5X-3) up to Not1 site	27441
GST-FKBP52	78921
GST-PP5$^{16-181}$	46728
GST-RB3$^{1-169}$	46568
GST-RB3$^{1-330}$	65638
GST-RB3$^{170-330}$	45940
GST-RD1$^{1-100}$	39034
GST-rpde6$^{103-256}$	44038
GST-rpde6$^{1-256}$	55410
Lyn SH3-GST	34562
MBP (C2)	50848
MBP-RB3$^{1-330}$	88457

Data from dose-effect studies were analysed using the KaleidaGraph software package (Synergy software). Using these data I determined the values of IC_{50} for the inhibition of PDE isoenzymes by GST- and MBP-fusion proteins. The IC_{50} value is the concentration of the inhibitory fusion protein that produces 50% of the maximum inhibition attainable. The IC_{50} values were calculated by fitting the data to an equation of the form

$$v = V-\{(V[I])/([I]+IC_{50})\}$$

where v = PDE activity, V = PDE activity in the absence of an inhibitory GST or MBP-fusion protein, [I] = micromolar concentration of inhibitory fusion protein.

2.16.1 The effect of Lyn SH3-GST on the inhibition of RB3 by GST-RB3$^{1-330}$

The effect of Lyn SH3-GST on the inhibition of rpde6 (RNPDE4A5) by GST-RB3$^{1-330}$ was determined using a modification of the protocol described in section 2.16 above. Lyn SH3-GST was expressed in *E coli* and affinity purified on glutathione Sepharose beads (see section 2.7.2). Cytosolic rpde6 was bound to Lyn SH3-GST using the pull down method described in section 2.17. A sample (400µg) of the purified Lyn SH3-GST bound to glutathione beads was incubated with a sample (240 EU) of cytosolic rpde6

from transfected COS-7 cells. The beads were washed three times with ice-cold complete KHEM buffer and complexes of rpde6 bound to Lyn SH3-GST were eluted into a total volume of 300µl of glutathione elution buffer over a period of 45min. Assuming that all the Lyn SH3-GST was eluted (i.e. 400µg ≡ 11.6nM) the final concentration of Lyn SH3-GST in this eluate can be estimated to be 38.6µM

Samples of this glutathione eluate containing rpde6 bound to Lyn SH3-GST were mixed 1:1 (v/v) with purified GST-RB3$^{1-330}$ or GST diluted in 20mM Tris-HCl, pH8.0. These mixtures were incubated on ice for 1h. Samples of these mixtures (50µl) were then assayed for PDE activity, beginning with the addition of 50µl 2µM 8-[^{3}H]-cAMP. The final concentration of Lyn SH3-GST in these assays was therefore ~9.6µM. As a control, the activity of samples of cytosolic rpde6, diluted in glutathione elution buffer, were determined in the presence or absence of GST-RB3$^{1-330}$ or GST. The activity of rpde6 ± Lyn SH3-GST added to the assay was within the linear range (see section 2.15.3) in the absence of GST or GST-RB3$^{1-330}$. The final concentration of GST-RB3$^{1-330}$ or GST in the assay was 1µM.

2.17 Pull down/binding assay with GST-fusion proteins

This was performed using a modification of a procedure described previously (O' Connell et al., 1996). GST-fusion proteins were purified on glutathione Sepharose beads using the batch method (section 2.7.2.1). Volumes of 50% glutathione Sepharose slurry containing 200µg of immobilised fusion protein were made up to 200µl with a 50% slurry of PBS-washed beads. The beads were then pelleted and the supernatants were discarded. The pellets were resuspended in the high-speed supernatant (S) fraction from COS-7 transiently transfected with rpde6, containing 100 EU of PDE activity. The immobilised fusion protein and cytosol were incubated for 30min at 4°C end-over-end. The beads were then collected by centrifugation for 5s at 13,000g and the supernatant was retained. The beads were held on ice and washed 3 times with 400µl complete KHEM buffer (see Table 2.11, section 2.11) over a 15min period. The original supernatant and washes were pooled to form unbound fraction and aliquots were taken for PDE assay and western blotting. Bound PDE was eluted from the beads by incubating 3 times in 100µl elution buffer (10mM glutathione, 50mM Tris-HCl, pH8.0), at 4°C for 15min. The eluted fractions were pooled and aliquots were taken for PDE assay and western blotting.

2.17.1 Determination of percentage binding

The percentage binding of PDE4 species to GST fusion proteins was determined from both the PDE enzyme activity and immunoreactivity in the bound and unbound fractions obtained as described above.

2.17.1.1 Percentage binding determined from PDE enzyme activity

The total PDE activity in the bound (EU_{BOUND}) and unbound ($EU_{UNBOUND}$) fractions was determined using the PDE assay. The percentage of the PDE4 species that was 'pulled down' by the GST-fusions under the experimental conditions described (section 2.17) was calculated as follows:

$$\% \text{ binding} = 100\% \times [EU_{BOUND} / (EU_{BOUND} + EU_{UNBOUND})].$$

2.17.1.2 Percentage binding determined from PDE immunoreactivity

A range of sample volumes (e.g. 5, 10, 15, 20 and 25µl) for the bound and unbound fractions were separated by SDS-PAGE (section 2.9) and transferred onto nitrocellulose. The nitrocellulose membranes were immunoblotted using a primary antibody specific the PDE4 species of interest. The membranes were then developed by ECL and exposed to X-ray film (section 2.10). The net intensities of the bands corresponding to the protein of interest were determined by densiometry using the Kodak 1D image analysis software. For both fractions, the net intensity values were plotted against the fraction volume originally loaded on the SDS-PAGE gel to yield linear graphs. The gradients of these graphs gave values for the intensity units per µl as a measure of the immunoreactivity in the bound and unbound fractions (see Figure 2.2, section 2.12). The total immunoreactivity values for the bound and unbound fractions were used to calculate the percentage binding of the PDE4 species to the GST fusions.

CHAPTER 3

Determination of the PDE4 splice variants expressed in mouse 3T3-F442A preadipocyte cells using the reverse transcription polymerase chain reaction (RT-PCR)

3.Determination of the PDE4 splice variants expressed in mouse 3T3-F442A preadipocyte cells using the reverse transcription polymerase chain reaction (RT-PCR)

CHAPTER 3 INTRODUCTION

In this chapter I describe my contribution to a collaborative project examining the role of PDE4 in the growth hormone (GH) promoted differentiation of 3T3 F442A preadipocyte cells to adipocytes. In section 3.1 I give the background to this project and I describe the initial observations showing that GH activates PDE4 in the 3T3 F442A cells. In section 3.2 I present my RT-PCR and sequence analyses of the PDE4 isoenzymes expressed by these cells. Dr S. MacKenzie showed that GH caused an increase in the activity of PDE4A immunoprecipitated with anti-PDE4A antiserum in a PI3-kinase- and p70S6 kinase-dependent manner (MacKenzie et al., 1998). Having shown that PDE4A5 is the sole PDE4A splice variant expressed in these cells (section 3.2.1), I go on to show that the level of the PDE4A transcript is not affected by GH treatment (section 3.3). This result suggested that GH does not increase PDE4A activity by upregulating PDE4A5 transcription, but rather via an affect on translation or a post-translational modification. Following this result, Dr MacKenzie showed that GH treatment caused an upward band shift of the PDE4A5 isoenzyme on SDS-PAGE that was concomitant with PDE4A activation (section 3.4.1). Depletion of PDE4A5 with specific antisense oligodeoxynucleotides enhanced the GH-dependent differentiation of these cells (section 3.4.1). These results suggested that GH-dependent activation of PDE4A5, via PI3-kinase and p70S6 kinase, might serve as a brake on the process of differentiation. In section 3.4.3 I discuss the implications of these findings and future perspectives.

3.1 A model system for studying the role of PDE4 in cell differentiation

As discussed in the Introduction chapter, (section 1.4), there are now at least 17 different PDE4 isoenzymes identified in mammals. These show different characteristics of targeting and regulation in cells that are determined largely by their unique NH_2-terminal regions. It has been proposed that the diverse responses of cells to signals that act via cAMP may partly depend on the specific combination of PDE isoenzymes that different cells express. Therefore, a major aim in the study of the PDE4 isoenzyme family is to assign

specific physiological roles for individual splice variants in cAMP signalling (Houslay and Milligan, 1997).

To this end we require model cell systems where we can analyse the role of defined, endogenously expressed PDE isoenzymes on measurable cAMP-dependent processes *in vivo*. The differentiation of certain strains of mouse-derived 3T3 fibroblast cells to adipocytes is one example of a model system for study. These cell lines permit the study of adipocyte differentiation in culture.

For some time it has been known that the non-specific phosphodiesterase inhibitor, IBMX, promoted the differentiation of 3T3 preadipocyte cell lines to mature adipocytes (Russell and Ho, 1976). In 1985 Elks and Manganiello (Elks and Manganiello, 1985) showed that Ro 20-1724, now known to be a PDE4 specific inhibitor (Houslay et al., 1998), promoted 3T3-L1 adipocyte differentiation as effectively as IBMX. The PDE3 selective inhibitor, cilostamide, however, had no such effect. These results suggested that an increase in the intracellular concentration of cAMP, caused by inhibition of PDE4 activity (but not by inhibition of PDE3), promoted the differentiation of preadipocytes to adipocytes. However, it should be pointed out that the effect of cAMP on preadipocyte differentiation is complex and stage-dependent (Yarwood et al., 1998). Therefore, in the past, different groups have reported positive (Elks and Manganiello, 1985), negative (Spiegelman and Green, 1981) and neutral (Wang et al., 1992) effects of cAMP on differentiation. Currently it is thought that preadipocytes go through a 'priming' stage prior to a final progression to differentiation. Increased cAMP levels appear to be needed to allow the final differentiation stage (see below).

3.1.1 The effect of growth hormone (GH) on the differentiation of 3T3 F442A preadipocyte cells to adipocytes

The presence of growth hormone (GH) is essential for the differentiation of 3T3 cells to adipocytes (Xu et al., 1995; Zezulak and Green, 1986). GH is a major regulator of cell growth and metabolism. It is known to have a positive regulatory effect on the differentiation of a range of cells lines, including myoblasts (Ewton and Florini, 1980), liver cells (Norstedt and Palmiter, 1984) and bone cells [osteoblasts (Kassem et al., 1998) and osteoclasts (Nishiyama et al., 1996)]. The mechanism of action of GH has been extensively studied in the 3T3 F442A cell line (Smit et al., 1996; Xu et al., 1995; Yarwood et al., 1998; Yarwood et al., 1999). A dual effector theory has been proposed for the GH-

dependent differentiation of preadipocytes (Yarwood et al., 1998; Zezulak and Green, 1986). Initially, GH treatment of the preadipocytes, over a two-day period, provokes the formation of a pool of cells that are primed for differentiation. When given the appropriate signal, e.g. insulin, IGF-1 or EGF, these cells progress to a fully differentiated state where they exhibit the biochemical and morphological characteristics of mature adipocytes (Bjorntorp et al., 1980; Yarwood et al., 1998; Zezulak and Green, 1986). In the absence of this second signal the cells fail to differentiate.

GH is known to activate a number of signalling pathways as shown in Figure 3.1. However, the precise GH signalling pathways that regulate 3T3 F442A differentiation remain to be determined. A key event following the binding of GH to its plasma membrane-associated receptor (GHR) is the dimerisation of this receptor and the recruitment, dimerisation and activation of the Janus family cytoplasmic tyrosine kinase, JAK2. This event leads to the activation of a number of signalling pathways including the phosphoinositide-3 kinase (PI3-kinase) pathway, the PKC pathway and possibly the raf-MEK-ERK pathway (see Figure 3.1) (Argetsinger and Carter-Su, 1996). There is evidence to suggest that activated JAK2 recruits and activates the SH2- and SH2+SH3 domain-containing proteins, SHC and Grb2 respectively (Argetsinger and Carter-Su, 1996; VanderKuur et al., 1995). This event may lead to the activation of the raf-MEK-ERK pathway via Sos and ras as shown in Figure 3.1, although the GH-dependent activation of the ras, raf and MEK components of this pathway has not been shown to date. In this regard it should also be noted that in 3T3 F442A cells the GH-dependent activation of ERK by requires specific isoforms of PKC (MacKenzie et al., 1997) (Anderson, 1992). Activation of JAK2 GH has also been shown to lead to the activation of the cytoplasmic transcription factors STATs (signal transducers and activators of transcription) (Smit et al., 1996). Once activated, STATs translocate to the nucleus where they bind to specific enhancer elements and activate the transcription of a number of genes including those encoding the detoxifying hydroxylase cytochrome P450, the transcription factor c-fos and the serine protease inhibitor 2.1 (spi 2.1) (Argetsinger and Carter-Su, 1996).

Given that the PDE inhibitors, particularly the PDE4 inhibitors, promoted differentiation we wished to ascertain if GH served to acutely regulate the PDE activity in these cells. If this should prove to be the case, we wished to determine whether PDE had any role in the manner whereby GH regulates differentiation. Intriguing, a post-doctoral investigator in our laboratory, Dr S. MacKenzie, showed that GH treatment of 3T3 F442A

preadipocytes produced a rapid (maximal at ~20-30min), transient increase in the rolipram-inhibited PDE4 activity [see ref. (MacKenzie et al., 1998)]. It was further shown that activation of PDE4 by GH in these cells resulted in a decrease in the intracellular concentration of cAMP. The latter was shown to be the case (MacKenzie et al., 1998). Furthermore, rolipram inhibition of PDE4 activity ablated this drop in cAMP levels and served to potentiate the differentiation of these preadipocytes (MacKenzie et al., 1998). Therefore, whilst GH is necessary to prime cells for differentiation, it might also serve as a brake on the differentiation process by increasing PDE4 activity.

In order to understand this process more fully, it was necessary to define the PDE4 splice variants that are expressed in 3T3 F442A cells. This would allow the identification of the precise PDE4 splice variant(s) involved in the GH-stimulated response. Unfortunately, splice variant-specific antibodies are not available for the majority of individual isoforms that differ at their NH_2-termini. However, PDE4 specific antibodies are available that allow the detection of members of the four separate subfamilies 4A, 4B, 4C and 4D (see Introduction, section 1.4). These were raised against the extreme COOH-terminal regions that are shared by all the splice variants derived from a single gene. It is thus possible to get some idea of the isoforms present by running cell lysate on SDS-PAGE, immunoblotting with subfamily specific antisera and determining their size relative to recombinant standards. However, no such standards are available for murine enzymes and rat and human splice variants can migrate differently. Therefore, in order to identify the PDE4 splice variants expressed by 3T3 F442A cells it was imperative to use RT-PCR as a diagnostic probe (see section 3.2 below). Dr MacKenzie verified the results of my RT-PCR analyses by using the western blotting strategy described above. This type of strategy has been successfully used by our laboratory in a number of studies (Bolger et al., 1997; Erdogan and Houslay, 1997; Huston et al., 1997; Kostic et al., 1997). An additional advantage of the RT-PCR approach is that the PCR fragments amplified using this method can be used to obtain sequence information for the 5' ends of the splice variant mRNAs. This can be used to design antisense oligodeoxynucleotides to block the expression of specific isoforms and thus determine their function in GH-dependent differentiation of adipocytes.

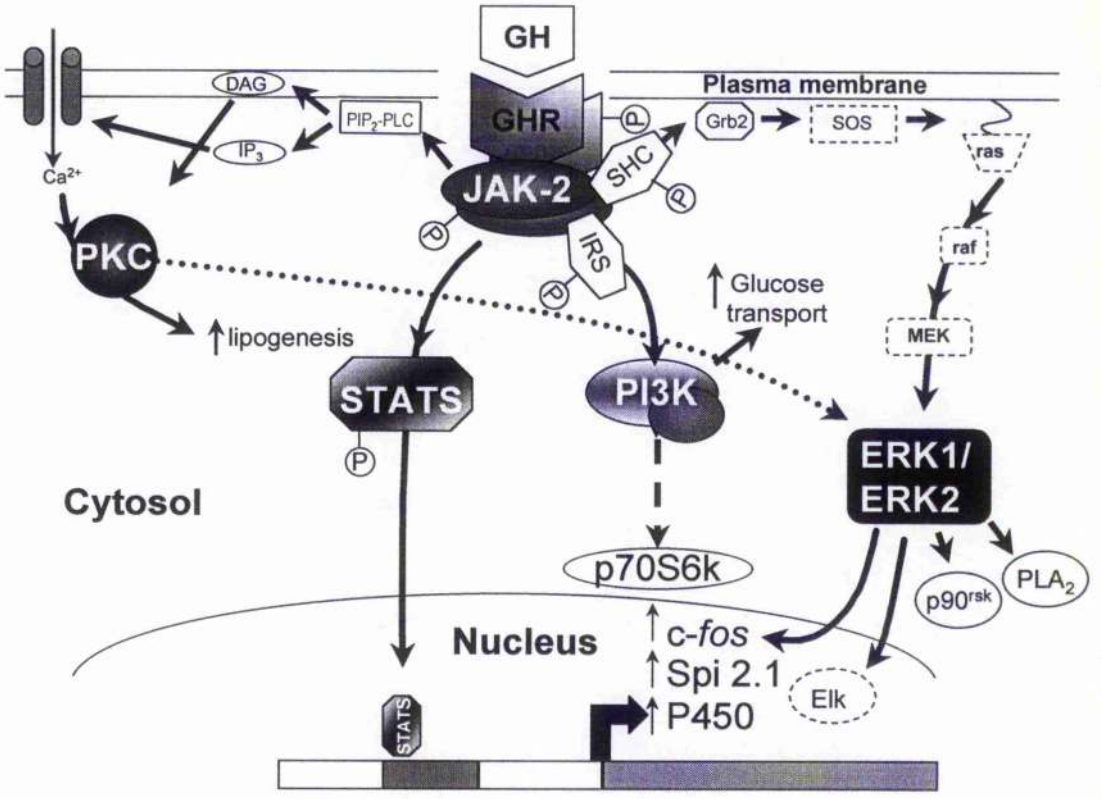

Figure 3.1 Signalling downstream of the growth hormone receptor

GHR dimerises upon binding GH and this complex recruits, homodimerises and activates JAK2 cytoplasmic tyrosyl kinase. JAK2 phosphorylates itself and GHR, which leads to the recruitment and phosphorylation of the IRS1 and Shc. IRS1 in turn recruits and activates PI3-kinase, which activates the proteins involved in glucose transport and p70S6 kinase via a pathway which may involve PDK1 and PKB. Phosphorylated Shc recruits and activates Grb2, which may lead to the activation of the Raf-MEK-ERK pathway, although in 3T3 F442A cells the GH-dependent activation ERK requires specific isoforms of PKC. Activated ERKs phosphorylate and regulate a number of proteins including phospholipase A_2 (PLA_2), protein kinases (e.g. p90rsk) and transcription factors (e.g. c-fos and Elk). Activated JAK2 can also phosphorylate and activate the STAT cytoplasmic transcription factors and protein kinase C (PKC) via the phospholipase C pathway.

In the above figure proteins given a broken outline have not yet been shown to be activated by GH stimulation. A circled P denotes proteins that are tyrosyl phosphorylated by JAK2. This figure is based on the one shown in (Argetsinger and Carter-Su, 1996).

3.2 Screening of 3T3 F442A preadipocyte cells for the expression of PDE4 splice variants using RT-PCR

Reverse-transcription PCR (RT-PCR) has been used in a number of studies to define the PDE mRNA transcripts that are expressed by various cells or tissues (Bolger et al., 1997; Engels et al., 1994; Huston et al., 1997; Kostic et al., 1997; Spence et al., 1997; Spence et al., 1995). This technique requires the extraction of total RNA from the cell. This is then reverse-transcribed to make cDNA. PCR reactions are carried out on this cDNA to detect the presence of mRNA transcripts for the various isoenzymes using isoenzyme-specific primer pairs. The successful amplification of the appropriate part of the cDNA encoding a PDE4 splice variant indicates the expression of the mRNA for this isoenzyme in 3T3 F442A cells. The advantages of this technique are that it is simple, the components of the reaction are easily prepared and the reactions themselves are quick (Scotland et al., 1998).

As discussed in section 1.4, the process of 5' alternative RNA splicing in PDE4 primary transcripts involves the fusion of upstream exons, that encode the unique NH_2-terminal domains of PDE4 isoenzymes, with downstream exons that encode UCR1, UCR2 and the catalytic unit. The downstream exons that encode the catalytic unit and portions of UCR2 are found in all splice variants. Therefore, RT-PCR primer pairs that anneal to sequences within these exons will detect any of the splice variants for a particular gene and are thus referred to as generic primers. Detection of specific splice variants requires the use of 5' (sense) primers that anneal to sequences within the regions that encode the unique NH_2-terminal splice domains. I have used a range of RT-PCR primer pairs to screen 3T3 F442A cells for the mRNA transcripts for all the known PDE4 splice variants. The results for each of the four PDE4 genes (PDE4A-D) are presented separately in the sections below (sections 3.2.1 to 3.2.4).

3.2.1 RT-PCR analysis of PDE4A splice variants and detection of the murine PDE4A5 transcript

The 3T3 F442A preadipocytes are a mouse cell line. At the start of this study no sequence information was available on murine PDE4 isoenzymes. Therefore, the primer

pairs were designed using rat or human sequence data. This is acceptable, as a comparison of the nucleotide sequences for rat PDE4 isoenzymes with their human counterparts indicates that there is high sequence conservation between species (Houslay et al., 1998).

RNA was extracted from unstimulated 3T3 F442A preadipocytes and reverse-transcribed to make cDNA, using reverse transcriptase in combination with a poly (dT) oligodeoxynucleotide (ODN) primer (see Methods chapter, section 2.6.4). This primer initiates reverse transcription from the poly A tail found at the COOH-terminal end of mature mRNAs. The resultant cDNA was used in a set of PCR reactions to detect either any PDE4A isoenzyme (generic PDE4A) or one of the three known rat PDE4A splice variants: -RNPDE4A1 (RD1), RNPDE4A5 (rpde6), and RNPDE4A6 (rpde39). All PCR reactions were carried out as described in the Methods chapter, section 2.6.5. The ODN primer pairs used and the PCR reaction conditions are shown in Table 3.2. As positive controls, identical PCR reactions were carried out using plasmids encoding the appropriate PDE4A splice variants (see legend for Figure 3.3). The annealing positions for the primers used are shown in Figure 3.2. Samples of the PCR reaction products were separated by agarose gel electrophoresis and the DNA bands were then stained with ethidium bromide and visualised with UV light.

The results for the RT-PCR screen for PDE4A splice variants are shown in Figure 3.3. The bands corresponding to the fragments obtained for the positive control reactions (using plasmid template) are shown on the left-hand side of this figure. Note that no bands were observed for the no-template negative control reactions (data not shown). The bands obtained using 3T3 F442A cDNA are shown on the right-hand side of the figure. Positive results were obtained for the PCR reactions used to detect generic PDE4A and the splice variant PDE4A5. No fragment bands of the appropriate size were obtained for the splice variants PDE4A1 or PDE4A6.

The bands obtained must be of the correct molecular weight in order to exclude the possibility that the primers have detected pre-mRNA or the wrong splice variant. The 'observed' molecular weights of the PCR fragments were calculated from their distances of migration relative to the molecular weight markers (see Methods chapter, section 2.6.5). There is a close correspondence between the predicted and observed molecular weights (MW) in base pairs (bp) for the generic PDE4A band (see Table 3.1, below). However, the observed molecular weights of the bands obtained in the PDE4A5 PCR reactions (positive control and 3T3 F442A cDNA template) were higher than predicted. In order to verify that

the fragment obtained in 3T3 F442A cDNA reaction did correspond to the mouse homologue of PDE4A5, it was sequenced as described in section 3.2.1.1.

Table 3.1 Comparison of the predicted and observed molecular weights (in bp) for the bands obtained in the PCR screen for PDE4A splice variants.

PDE4A species	Predicted MW (bp)	Observed MW (bp)*	
		Positive control (plasmid template)	3T3 F442A cDNA template
PDE4A (generic)	233	244.2 ± 1.4	252.6 ± 2.8
PDE4A5	825	872.8 ± 26	924.7 ± 42

*means of at least three separate experiments ± SE

Western blot analyses ((MacKenzie et al., 1998) and Dr MacKenzie-personal communication) failed to identify immunoreactive species that co-migrated with RD1 (79kDa) and rpde39 (98kDa). However a band was present that co-migrated with rat rpde6 (RNPDE4A5) at 109kDa. Thus, the RT-PCR results would indicate that this species is indeed the murine homologue of RNPDE4A5.

The tissue distribution of both RNPDE4A1 and RNPDE4A6 appears to be rather restricted. Thus, RNPDE4A1 has only ever been detected in the brain, whereas RNPDE4A6 expression appears to be confined to the testes (Bolger et al., 1996) and hepatocytes (Houslay lab- unpublished). However, RNPDE4A5 and its human homologue HSPDE4A4 appear to have a wider distribution in tissues, being found in both brain (McPhee et al., 1995), thymocytes (ElBawab et al., 1997), Jurkat T-cells (Seybold et al., 1998), pheochromocytoma (PC12) cells and U937 human monocytes (MacKenzie and Houslay, 2000).

Table 3.2 Table showing PDE4A RT-PCR primers used and conditions

PDE4A Species	Primer S=Sense, A= Antisense			Nucleotide fragment amplified	Frag. Size (bp)	Cycle conditions		
						D	A	E
PDE 4A (generic) M26715	S	GR28[a]	GCGGGACCT(A/G) CTGAAGAAAT TCC	459-651*	233	94°C 1min	57°C 2min	72°C 3min
	A	GR29[a]	CAGGGTG(A/G)TC CACATCGTGG					
PDE4A1 M26715	S	GR37[a,b]	TTCTTCTCCG AGACCTGCTC CAAGC	16-387	372	94°C 1min	52°C 2min	72°C 3min
	A	GR36[a,b]	CAGGCCCCAT TTGCTCAAGT TCTCC					
PDE4A5 L27057	S	GR43	TCCTTCCACG GCACCGGTAC C	265-1089	825	94°C 1min	62°C 80sec	72°C 1min
	A	GR36	CAGGCCCCAT TTGCTCAAGT TCTCC					
PDE4A6 L36467	S	GR20[a]	GCCCACACAG GCTTGGTGAT TTATCC	-178-37	215	94°C 1min	62°C 80sec	72°C 1min
	A	GR21[a]	ATATTCGAGG CAGTGTCAGC CTCTTGC					

In the above table the sequences of the sense (5') and antisense (3') RT-PCR oligodeoxynucleotide (ODN) primers are shown alongside the PDE4A transcript (splice variant or generic transcript) that they detect. The GenBank accession numbers for the sequences of the rat PDE4A splice variants used to design the primer sets are given in the first column. The temperatures and hold times for the denaturation (D), annealing (A) and elongation (E) stages of the PCR cycle are shown. All PCR reactions were carried out in a total volume of 25µl as described in the Methods chapter, section 2.6.5. The number of cycles carried out in each case was 40. The nucleotide fragments amplified and their sizes in base pairs (bp) are also given for each primer pair where negative positions refer to nucleotides upstream of the translation start codon. The specificity of these primer pairs was verified by screening them against a library of PDE4 cDNAs.

a =(Kostic et al., 1997), b = (Sullivan et al., 1998). * = fragment of cDNA corresponding to RNPDE4A1 amplified

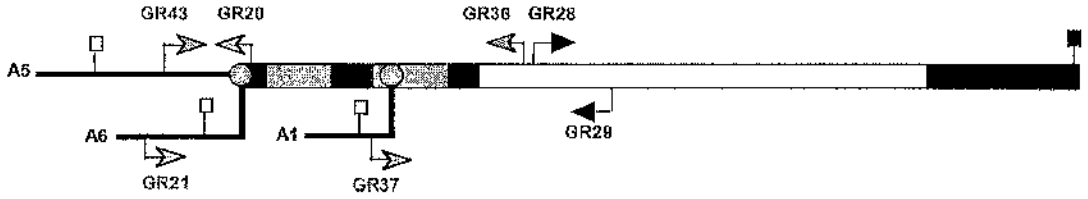

Figure 3.2 Figure showing the annealing positions of RT-PCR primers used to probe PDE4A splice variants identified in rat.

This diagram shows the annealing positions for the RT-PCR primers on the cDNA obtained by reverse-transcription of the mRNA transcripts for the three known rat PDE4A splice variants, RNPDE4A1, RNPDE4A5 and RNPDE4A6. The positions of the ATG initiator methionine codons are marked with white squares, whereas the termination codons are marked with black squares. Grey and white bars mark the positions of the upstream conserved regions (UCR1 and UCR2) and the catalytic unit,respectively. Black bars represent the unique NH_2-terminal splice domains and grey circles mark the splice junctions. The annealing positions for the splice variant-specific ODN primers are indicated with grey arrows. Black arrows show the position of primers used for the detection of the generic PDE4A mRNA transcript. Note that the sense primer (GR21) for the detection of PDE4A6 cDNA anneals to a position on the cDNA that is upstream of the start codon of the corresponding mRNA transcript.

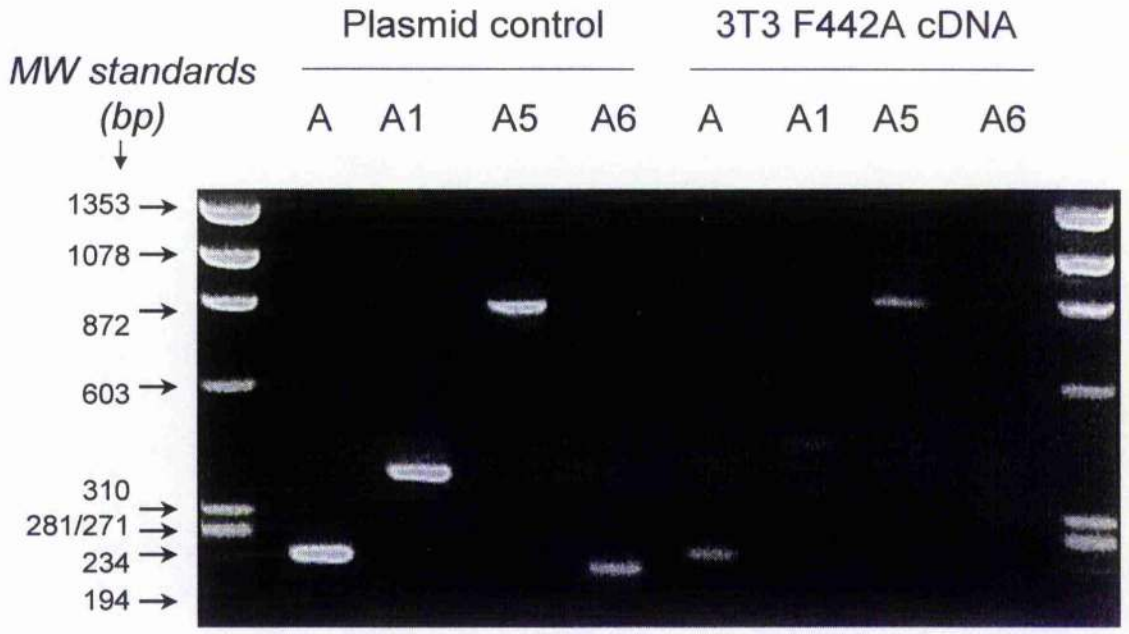

Figure 3.3 RT-PCR analysis of PDE4A splice variants expressed in 3T3 F442A mouse preadipocyte cells.

RNA was extracted from 3T3 F442A mouse preadipocyte cells and used as a template for first strand cDNA synthesis as described in the Methods chapter, section 2.6.1. The cDNA that was produced was used as a template in PCR reactions using generic primers for the detection of all PDE4A splice variants (A) or the splice variant specific primers for the detection of PDE4A1 (A1), PDE4A5 (A5) and PDE4A6 (A6). As a positive control, the same sets of primers were used in PCR reactions where plasmids containing the appropriate clones were used as a template. The positive control plasmids used were pSVL-RD1 (for PDE4A and PDE4A1), pSV-SPORT-rpde6 (for PDE4A5) and pcDNA-rpde39 (for PDE4A6). The results for the positive control reactions are shown in the left-hand four lanes, whereas the results obtained using 3T3 F442A cDNA as a template are shown in the right-hand four lanes. The molecular weight standards (in bp) are shown on the left. The predicted amplified product sizes are PDE4A (generic) = 233 bp, PDE4A1 = 372 bp, PDE4A5 = 825 bp and PDE4A6 = 215 bp.

3.2.1.1 Sequencing of the PDE4A5 amplified fragment

In order to confirm that the fragment amplified in the above RT-PCR screen was indeed mouse PDE4A5, this fragment was 'TA' cloned and sequenced as described in detail in the Methods chapter, 2.6.6. This nucleotide sequence has been deposited in GenBank (accession number AF038895).

An alignment of the new nucleotide sequences obtained for mouse PDE4A5 with the corresponding sequences from rat PDE4A5 and the human homologue (HSPDE4A4) is shown in Figure 3.4. The new mouse nucleotide sequence determined as a result of this analysis (excluding the primer sequences at each end of the insert) corresponds to nucleotides 286 to 1064 of rat PDE4A5 and nucleotides 286-1106 in human PDE4A4. Figure 3.5 shows an alignment of the predicted amino acid sequences for this region in the mouse, rat and human homologues. As illustrated in Figure 3.5 the region sequenced encompasses the COOH-terminal seven amino acid residues of the unique NH_2-terminus of PDE4A5, the upstream conserved regions UCR1 and UCR2 and the first 37 amino acid residues of the catalytic unit as defined by Houslay et al (Houslay et al., 1998). Figure 3.4 and Figure 3.5 both show the high sequence conservation between rat and mouse PDE4A5. The nucleotide sequences of rat and mouse PDE4A5 are 79% identical. However, 73% of these mutations are silent so that the predicted amino acid sequences show 94% identity. This high conservation suggests that the NH_2-terminal non-catalytic region plays an essential role in the regulation or function of PDE4A5.

As expected, the mouse sequence shows more similarity to the rat sequence than the human sequence (Figure 3.5). The mouse and rat forms of PDE4A5 lack a 5-residue insert found at the COOH-terminus of the unique NH_2-terminal splice domain of the human homologue HSPDE4A4. Moreover, mouse PDE4A5, like rat PDE4A5, lacks the proline-rich insert found in the LR2 region of the human homologue, PDE4A4 (amino acids 313-320). This proline-rich insert in HSPDE4A4 is proposed to act as a molecular switch that mediates the interconversion of high and low rolipram affinity conformations that can be operated with appropriate SH3 domain-containing proteins (Huston et al., 1996; McPhee et al., 1999). My sequence analysis suggests that the kinetic properties of mouse PDE4A5 (MMPDE4A5) will reflect rat PDE4A5 rather than the human homologue, HSPDE4A4. However, it should be noted that apart from the insert regions, the MMPDE4A5 and HSPDE4A4 sequences show 89.7% identity at the amino acid level.

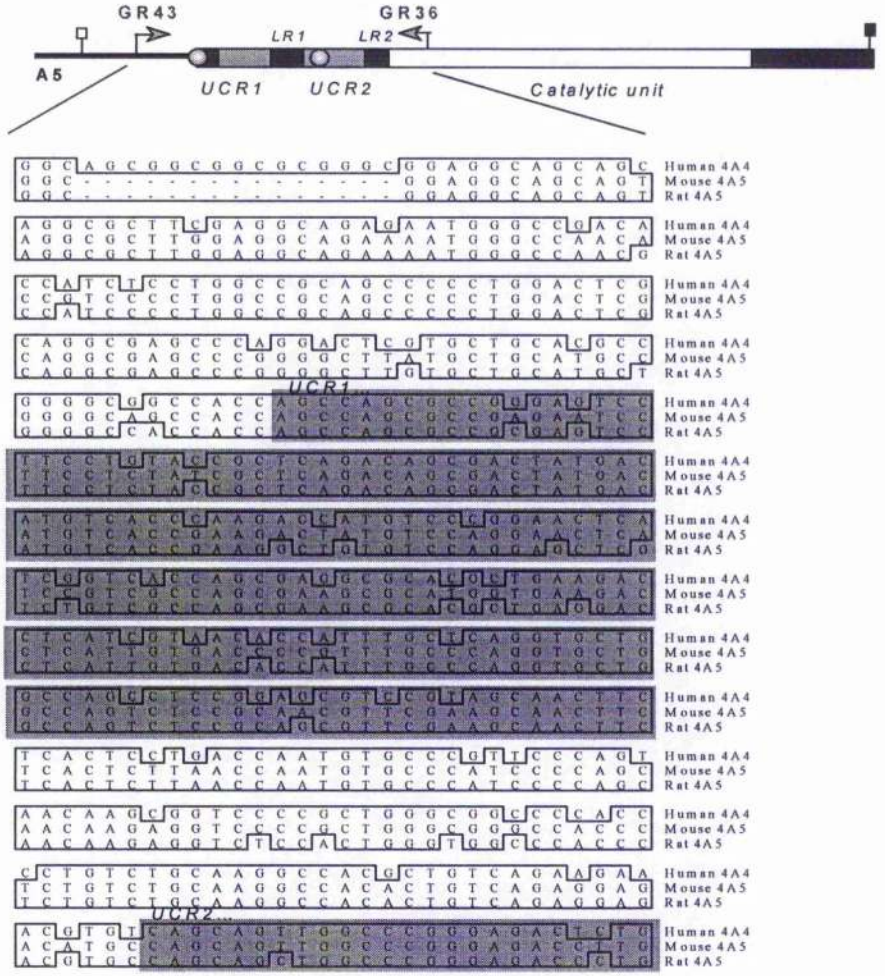

Figure 3.4 Alignment of the nucleotide sequences for mouse and rat PDE4A5 (nucleotides 286 to 1064) and human PDE4A4 (nucleotides 286-1106).

This figure shows the nucleotide sequence of the fragment amplified with PDE4A5-specific primers using 3T3 F442A cDNA as a template. The primer sequences at both ends of the PCR fragments have been excluded. The mouse nucleotide sequence has been aligned with the corresponding rat and human sequences; nucleotides 286 to 1064 in RNPDE4A5 and nucleotides 286 to 1106 in human HSPDE4A4. The bases that match the mouse sequence are boxed. The regions encoding the upstream conserved regions UCR1 and UCR2 and part of the catalytic unit are shaded. The GenBank accession numbers for the mouse, human and rat sequences are AF038895, L20956 and L27057, respectively. The key for the upper diagram in this figure is the same as that described in the legend for Figure 3.2. This alignment was performed using the Clustal method (Higgins and Sharp, 1988) within the DNA Star programme (Lasergene).

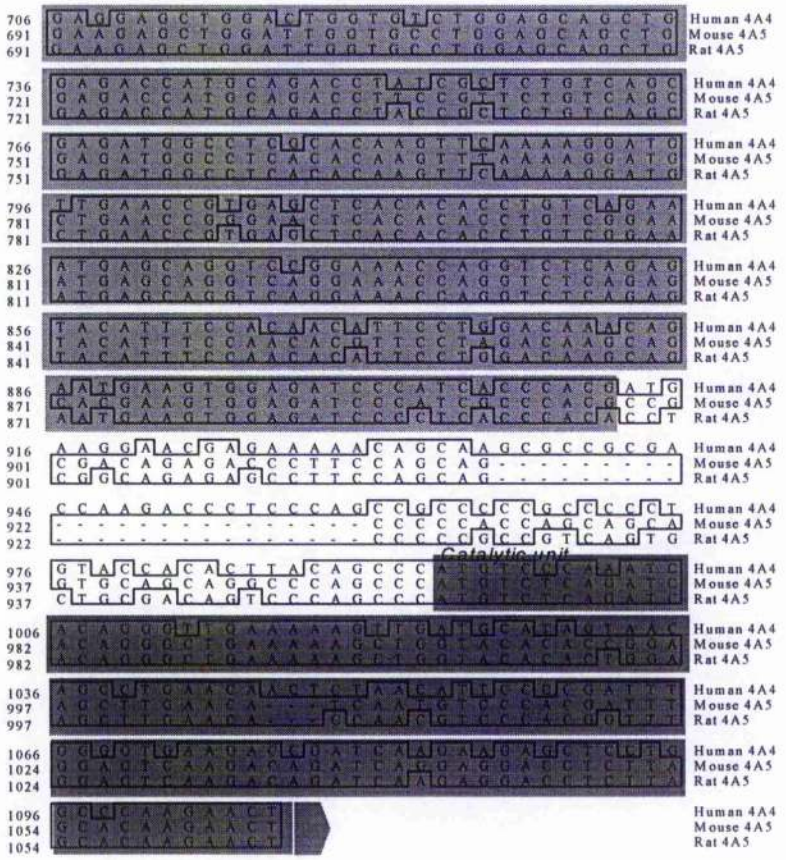

Figure 3.4 continued

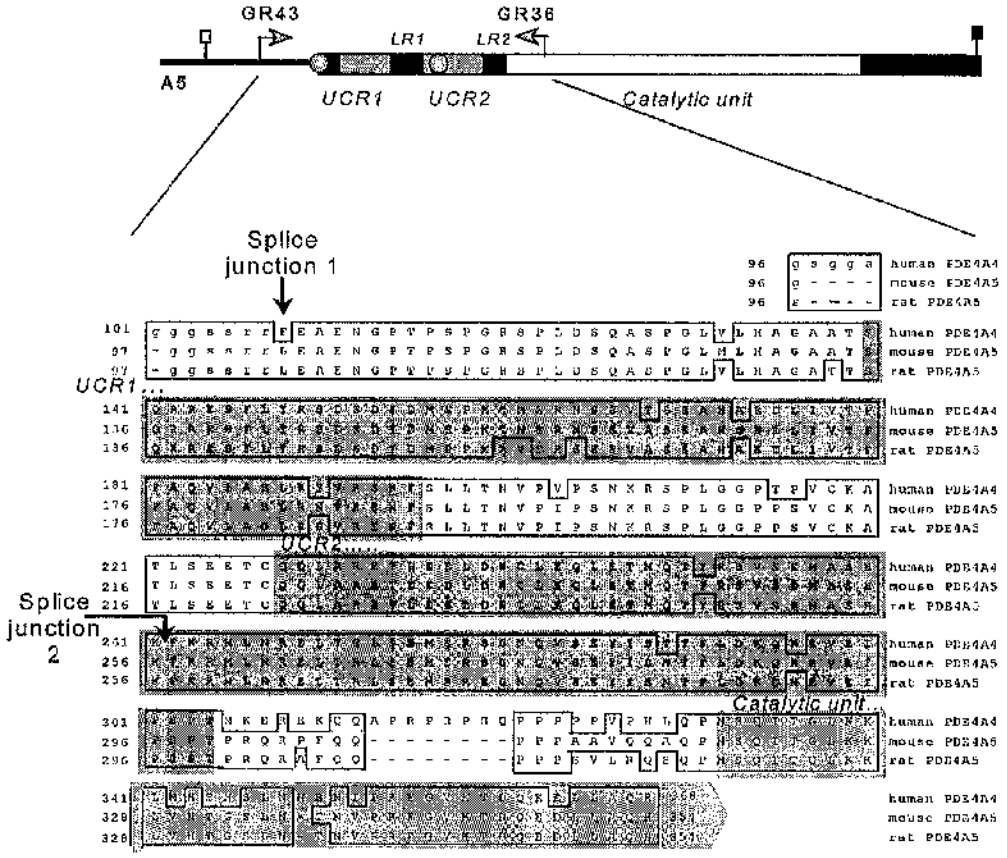

Figure 3.5 Alignment of the predicted amino acid sequence for mouse and rat PDE4A5 (amino acids 96-354) and human PDE4A4 (amino acids 96-368)

In this alignment the residues that match the mouse sequence are boxed. The region of mouse PDE4A5 cDNA that was amplified and sequenced encompasses the COOH-terminal seven amino acid residues of the unique NH_2-terminus of PDE4A5 (lower case letters), UCR1 and UCR2 (both shaded), and the first 37 amino acids of the catalytic unit (shaded). The points at which the sequences of PDE4A6 and PDE4A1 diverge from PDE4A5 are marked as splice junctions 1 and 2,respectively. The GenBank accession numbers for the mouse, human and rat sequences are AF038895, L20956 and L27057 respectively. The key for the upper diagram in this figure is the same as that described in the legend for Figure 3.2. This alignment was performed using the Clustal method (Higgins and Sharp, 1988) within the DNA Star programme (Lasergene).

3.2.2 RT-PCR analysis of PDE4B splice variants and detection of the murine PDE4B2 transcript

The 3T3 F442A cDNA was used in a PCR screen for PDE4B splice variants. There are three splice variants that have been cloned from rats and humans, PDE4B1, PDE4B2 and PDE4B3. The primer pairs and the PCR reaction conditions used for the detection of these PDE4B splice variants are shown in Table 3.4. The annealing positions for the ODN primers on the cDNA corresponding to the three alternative mRNA transcripts are shown in Figure 3.6. As positive controls, identical PCR reactions were carried out using plasmids encoding the appropriate PDE4B splice variants. Samples of the PCR reaction products were separated by agarose gel electrophoresis and visualised as before. The results from the RT-PCR analysis of 3T3 F442A cells are shown on the right of Figure 3.7 next to the results for the positive control reactions, shown on the left. Again, no bands were observed for the no-template, negative control reactions (data not shown).

This PCR screen detected the presence of transcripts for PDE4B (generic) and the splice variant PDE4B2. The bands obtained using 3T3 F442A cDNA as a template co-migrated with the bands obtained in the corresponding positive control reactions. There is a reasonably close correspondence between the predicted and observed molecular weights (MW) for these fragments as shown below in Table 3.3.

Table 3.3 Comparison of the predicted and observed molecular weights (in bp) for the PDE4B2 amplified PCR fragment.

PDE4B species	Predicted MW (bp)	Observed MW (bp)*	
		Positive control (plasmid template)	3T3 F442A cDNA template
PDE4B (generic)	786	787.8 ± 26	826.6 ± 26
PDE4B2	679	676.2 ± 5.6	732.9 ± 18

* means of at least three separate experiments ± SE

No bands were observed using the ODN primers specific for the 'long' PDE4B splice variants PDE4B1 and PDE4B3 (see Figure 3.6). Therefore, the short form PDE4B2 appears to be the only PDE4B splice variant expressed by mouse 3T3 F442A preadipocytes. This result supports western blot analysis done using a PDE4B-specific COOH-terminal polyclonal antibody as primary reagent (MacKenzie et al., 1998). This showed the presence of a single immunoreactive band that co-migrated with recombinant HSPDE4B2 (human).

Table 3.4 Table showing PDE4B RT-PCR primers used and conditions

	Primer S=Sense, A= Antisense			Nucleotide fragment amplified	Frag. Size (bp)	Cycle conditions		
						D	A	E
PDE4B (generic) J04563	S	GR30	CAGCTCATGA CCCAGATAAG TGG	907-1692*	786	94°C 1min	55°C 2min	72°C 3min
	A	GR31	GTCTGCACA(A/G) TGTACCATGT TGCG					
PDE 4B (long form) J04563	S	GR3	AAACCTTCAC GGAGCACCGA ACAAGAGG	561-1067*	507	94°C 1min	58°C 80sec	72°C 70sec
	A	GR4	GCCACGTTGA AGATGTTAAG GCCCCATT					
PDE 4B2 L27059	S	GR17	TTGGTAGATC ACTGACACCT CATCCCG	-116-551	667	94°C 1min	58°C 80sec	72°C 70sec
	A	GR4	GCCACGTTGA AGATGTTAAG GCCCCATT					
PDE 4B3 U85048	S	4123	CTCCACGCAG TTCACCAAGG AAC	137-734	598	95°C 1 min	63°C 2min	72°C 3min
	A	4122	TGTGTCAGCT CCCCGTTCAG C					

The sequences of the sense (5') and antisense (3') RT-PCR ODN primers for the detection of PDE4B transcripts are shown. The primer sets for the detection of PDE4B (generic), PDE4B2 or PDE4B (long forms) were designed using sequence information for rat splice variants (Kostic et al., 1997). The PDE4B3-specific primers were designed using the sequence of the human splice variant HSPDE4B3 (Huston et al., 1997). The GenBank accession numbers for the sequences of the rat and human PDE4B splice variants used to design the primer sets are given in the first column. The number of cycles carried out in each case was again 40.

*Nucleotide fragment amplified in RNPDE4B1

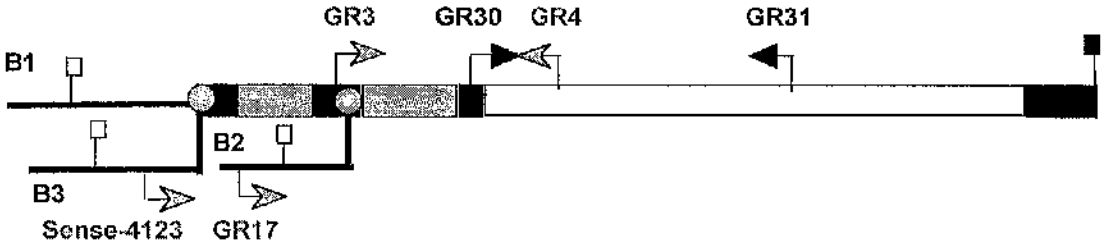

Figure 3.6 Figure showing the annealing positions of RT-PCR primers used to probe PDE4B splice variants identified in rats and humans

This diagram shows the annealing positions for the RT-PCR primers on the cDNA obtained by reverse-transcription of the mRNA transcripts for the three known PDE4B splice variants, PDE4B1, PDE4B2 and PDE4B3. Note that the sense primer (GR17) for the detection of PDE4B3 cDNA anneals to a position on the cDNA that is upstream of the start codon. The key for this figure is the same as that described in the legend for Figure 3.2.

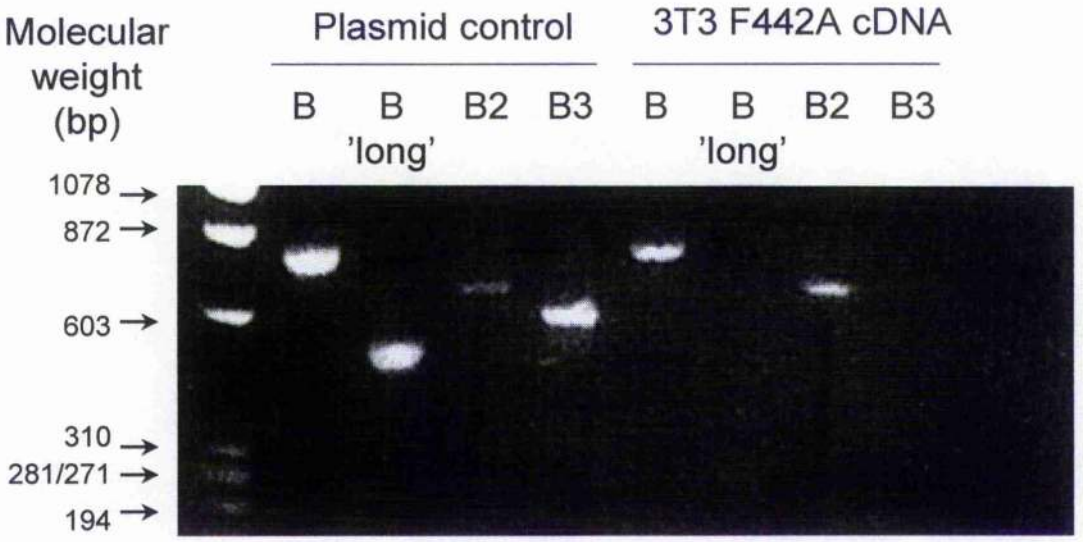

Figure 3.7 RT-PCR analysis of PDE4B splice variants expressed in 3T3 F442A mouse preadipocyte cells.

The cDNA produced from total RNA extracted from 3T3 F442A cells was used as a template in an RT-PCR screen for PDE4B mRNA transcripts. The primers used were either generic primers for the detection of all PDE4B splice variants (B), long PDE4B specific primers (B 'long') for the detection of PDE4B1+PDE4B3 or splice variant specific primers for the detection of PDE4B2 (B2) or PDE4B3 (B3). The positive control templates used were pDPD (RNPDE4B1) for PDE4B and long-PDE4B, mouse brain cDNA for PDE4B2 and pdeos41 (HSPDE4B3) for PDE4B3. Samples (9ul) of the positive control reaction products and the 3T3 F442A cDNA template reaction products were separated by agarose (2%) gel electrophoresis, stained with ethidium bromide and visualised with a UV transilluminator. The results for the positive control reactions are shown in the left-hand four lanes, whereas the results obtained using 3T3 F442A cDNA as a template are shown in the right-hand four lanes. The molecular weight standards (in bp) are shown on the left. The predicted sizes of the amplified fragments are PDE4B (generic) = 786, PDE4B1 = 507, PDE4B2 = 667 and PDE4B3 = 598.

3.2.2.1 Sequencing of the PDE4B2 amplified fragment

In order to confirm that the fragment amplified in the above RT-PCR screen was indeed mouse PDE4B2, this fragment was again 'TA' cloned and sequenced as described in the Methods chapter, section 2.6.6. Note that the 5' sense primer used to identify PDE4B2 (GR17) anneals to a region on the cDNA template that is upstream of the translation start codon. Therefore, a portion of the mouse nucleotide sequence at the 5' end corresponds to a non-coding sequence.

An alignment of the new nucleotide sequences obtained for mouse PDE4B2 (excluding the primer sequences at each end of the insert) with the corresponding sequences from rat and human PDE4B2 is shown in Figure 3.8. The sizes of the nucleotide sequence fragments that are encompassed by the PDE4B2-specific primer pair (GR17+GR4) differed in mouse, rat and human. In mouse PDE4B2 this region, excluding the primer sequences at each end, extended from nucleotides –95 to 524 (total length = 619 bases). This aligns with nucleotides –89 to 524 (613 bases) of RNPDE4B2 and nucleotides -107 to 524 (631 bases) in HSPDE4B2. The differences in the lengths of the sequence are due to insertions and deletions in the non-coding region of the PDE4B2 mRNA (see Figure 3.8).

An alignment of the predicted amino acid sequence for the coding region of the amplified fragment for mouse PDE4B2 with the corresponding sequences from rat and human is shown in Figure 3.9. This region covers the first 174 amino acids of PDE4B2 and includes the whole of UCR2 and the first 42 amino acids of the catalytic unit. As shown in Figure 3.6, PDE4B2 is a short splice variant and therefore lacks UCR1.

Figure 3.8 and Figure 3.9 both show the high sequence conservation between rat human and mouse PDE4B2. Of the 9 nucleotide differences noted between the mouse and human PDE4B2, 7 of these mutation were silent, producing no change in the predicted amino acid sequence. The predicted amino acid sequence of the mouse PDE4B2 is 98.9% identical to the rat sequence and 93.1% identical to the human sequence. All of the amino acid differences between the mouse, rat and human sequences occur within the unique NH_2-terminal splice domain of PDE4B2.

This result confirms that mouse 3T3 F442A cells do express a mouse homologue of PDE4B2. This result again demonstrates the high conservation of sequence between equivalent PDE4 isoenzymes from different species.

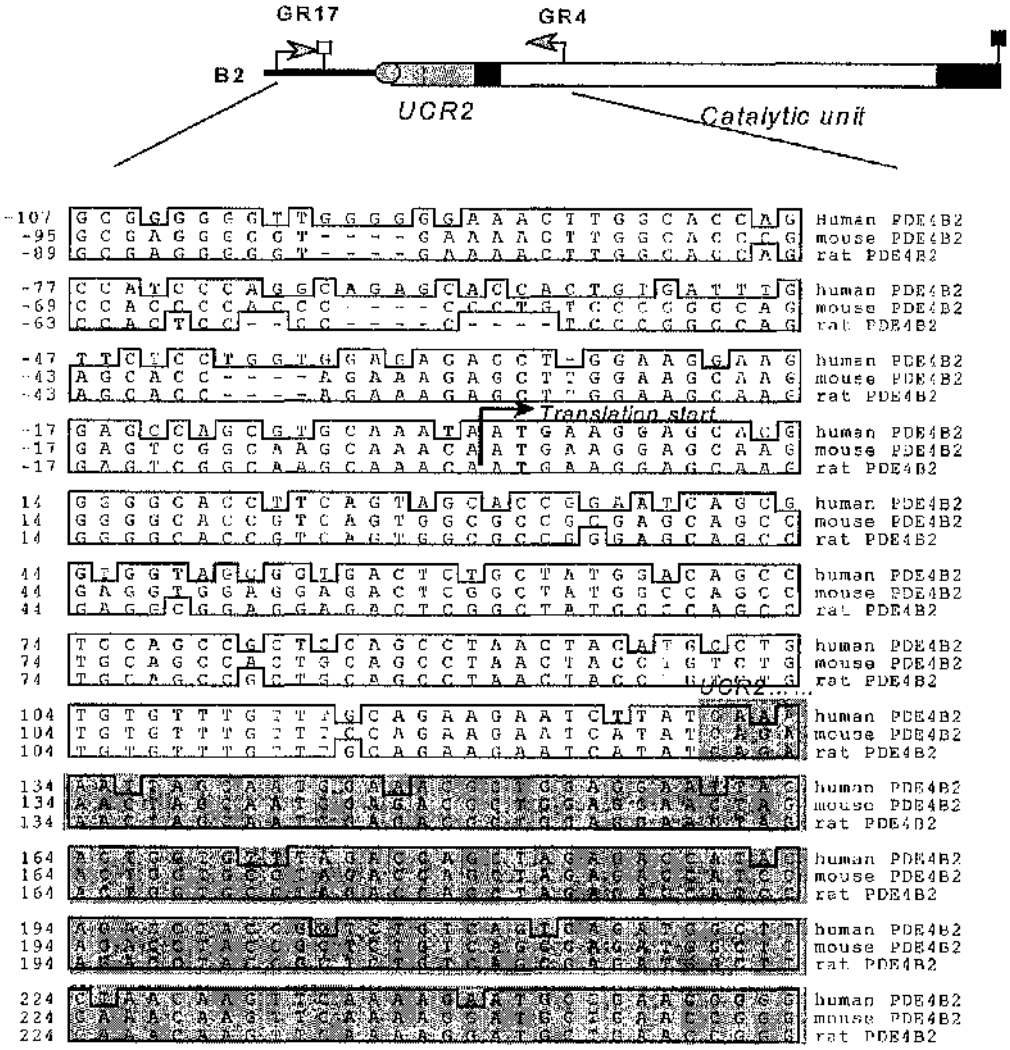

Figure 3.8 Alignment of the nucleotide sequences for mouse, rat and human PDE4B2
This figure shows the nucleotide sequence of the fragment amplified with PDE4B2-specific primers using 3T3 F442A cDNA as a template. The primer sequences at both ends of the PCR fragments have been excluded. The mouse nucleotide sequence has been aligned with the corresponding rat (GenBank accession number L27058) and human (GenBank accession number L20971) sequences. The bases that match the mouse sequence are boxed. The regions corresponding to UCR2 and part of the catalytic unit are shaded. The numbers on the left refer to the nucleotide position. This alignment was performed using the Clustal method (Higgins and Sharp, 1988) within the DNA Star programme (Lasergene).

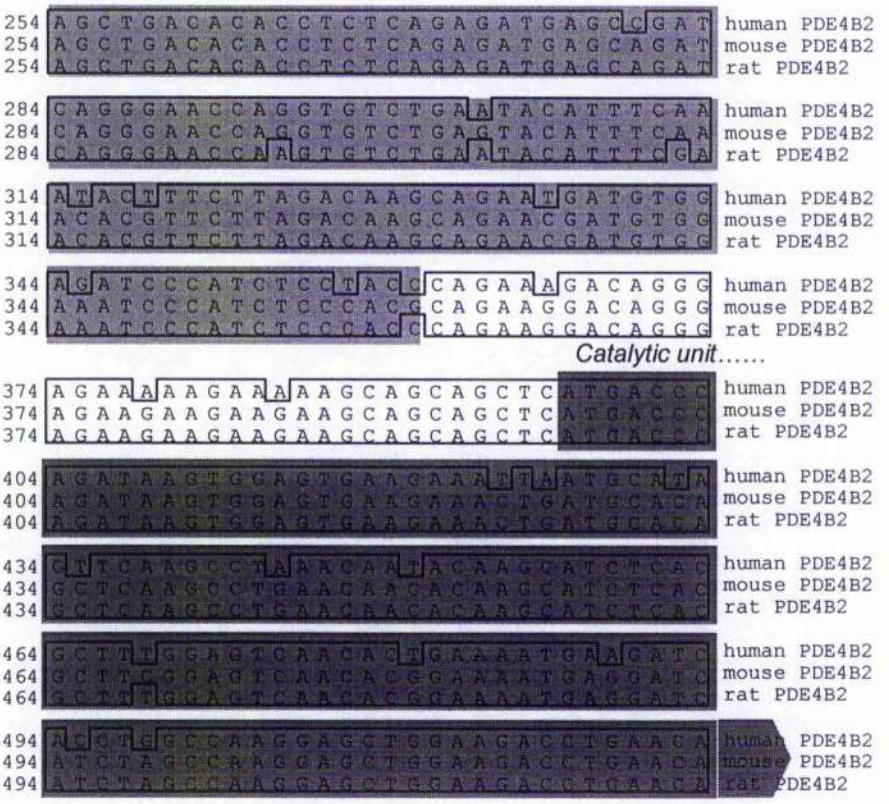

Figure 3.8 continued.

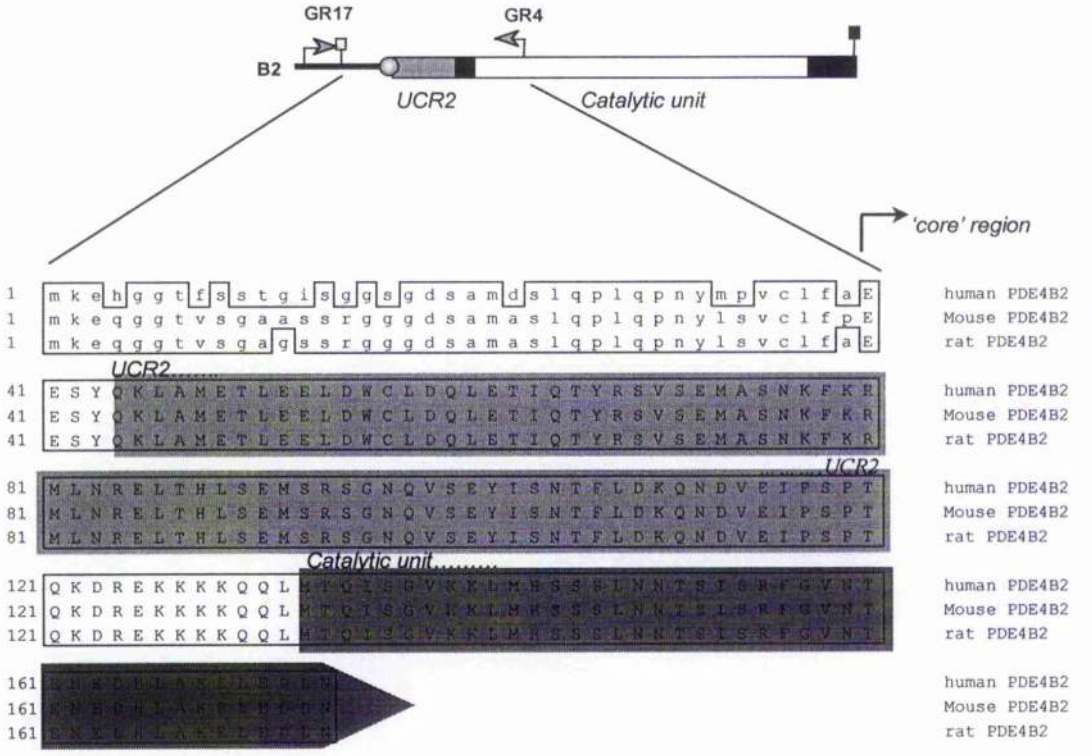

Figure 3.9 Alignment of the predicted amino acid sequence for mouse, human and rat PDE4B2 (amino acids 1-174)

The predicted amino acid sequence of the amplified region of mouse PDE4B2 is shown aligned with the corresponding rat (GenBank accession number L27058) and human (GenBank accession number L20971) PDE4B2 sequences. Amino acid residues that match the mouse sequence are boxed. Upstream conserved region 2 (UCR2) and the first 42 amino acid residues of the catalytic unit are shaded. This alignment was performed using the Clustal method (Higgins and Sharp, 1988) within the DNA Star programme (Lasergene).

3.2.3 RT-PCR analysis of PDE4C

The splicing of the PDE4C mRNA is more complex than that for PDE4A, B and D. At the present time, seven human PDE4C clones have been isolated (Bolger et al., 1993; Obernolte et al., 1997; Owens et al., 1997) although PDE4C5-7 may be cloning artefacts (Sullivan et al., 1999). The mRNAs that have been shown to encode naturally occurring HSPDE4C splice variants (HSPDE4C1-HSPDE4C4) are shown in Figure 3.10. At the time at which this study was carried out, only one PDE4C splice variant, PDE4C1, had been cloned from rat and human. Therefore, the primers used in this study were designed against rat PDE4C1 (rpde36) (Bolger et al., 1994). The sequences and PCR conditions for these primers are shown in Table 3.6. The annealing positions of these primers on cDNA complementary to the rat and human PDE4C mRNA transcripts are shown in Figure 3.10. This diagram shows that this primer pair will detect all the known PDE4C splice variants.

This primer pair was used on 3T3 F442A cDNA. As a positive control, an identical PCR reaction was carried out using a plasmid encoding rpde36 (RNPDE4C1, (Bolger et al., 1994)). Samples of the PCR reaction products were separated by agarose gel electrophoresis and visualised as before. The results from this RT-PCR analysis are shown in Figure 3.11. Again, no band was observed for the no-template negative control reaction (data not shown).

This PCR screen detected the presence of a DNA sequence complementary to a PDE4C transcript in 3T3 F442A cDNA. The band obtained co-migrated with the band obtained in the corresponding positive control reaction. There is a close correspondence between the predicted and observed molecular weight (MW) for this fragment as shown below in Table 3.5.

Table 3.5 Comparison of the predicted and observed molecular weights (in bp) for the PDE4C amplified PCR fragment.

PDE4C species	Predicted MW (bp)	Observed MW (bp)*	
		Positive control (plasmid template)	3T3 F442A cDNA template
PDE4C1	390	378.9 ± 2.2	379.7 ± 2.8

* means of at least three separate experiments ± SE

We can therefore conclude from this result that 3T3 F442A preadipocytes do express a PDE4C splice variant. This result was supported and extended by western blot analysis using a PDE4C-specific COOH-terminal polyclonal antibody as primary reagent (MacKenzie et al., 1998). This showed an immunoreactive band that co-migrated with a recombinant HSPDE4C2 standard (Owens et al., 1997). It was therefore concluded that 3T3 F442A cells express a mouse homologue of PDE4C2.

Table 3.6 Table showing PDE4C RT-PCR primers used and conditions

	Primer S=Sense, A= Antisense			Nucleotide fragment amplified	Frag. Size (bp)	Cycle conditions		
						D	A	E
PDE 4C L27061	S	GS32	CCATGGCCCA GATCACTGGG CTG	857-1246	390	94°C 1 min	58°C 80sec	72°C 70sec
	A	GS31	RGTCHGTGAA VACAGCVTCC ARDGC					

R = (A or G); *V* = (A, C, or G); *D* = (A, G, or T) and H = (A, C or T). The GenBank accession number for the sequence of rpde36 (RNPDE4C1) used to design these ODN primers is given. The number of cycles carried out was again 40.

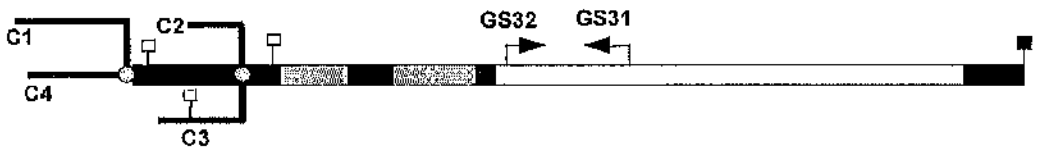

Figure 3.10 Figure showing annealing position of RT-PCR primers used to probe PDE4C

This diagram shows the annealing positions for the RT-PCR primers on the cDNA obtained by reverse-transcription of the mRNA transcripts for the four known human PDE4C splice variants. The key is the same as that described in the legend for Figure 3.2. Note that the translated regions of the mRNAs encoding the splice variants PDE4C1 and PDE4C4 are identical, because the nucleotide sequences of these mRNAs diverge immediately upstream of the initiator methionine codon. Note also that the unique NH_2-terminal splice domain of HSPDE4C2 contains stop codons in all three reading frames. Therefore, translation of HSPDE4C2 starts at a methionine that is downstream of the splice junction.

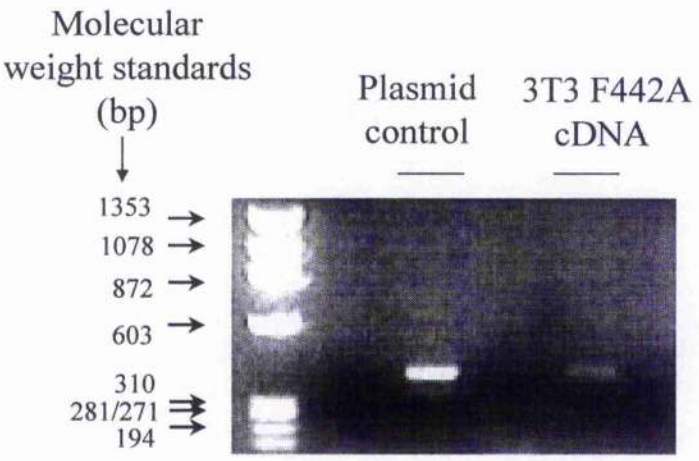

Figure 3.11 RT-PCR analysis of PDE4C expressed in mouse 3T3 F442A preadipocyte cells.

3T3 F442A cDNA was used as a template in RT-PCR reaction for PDE4C. The primers used detected the presence of the mRNA transcripts for any of the four naturally occurring PDE4C splice variants (PDE4C1- PDE4C4). The positive control template used was pRPDE36 (RNPDE4C1). Samples (9ul) of the positive control reaction products and the 3T3 F442A cDNA template reaction products were separated by agarose (2%) gel electrophoresis, stained with ethidium bromide and visualised with a UV transilluminator. The molecular weight standards (in bp) are shown on the left. The predicted size of the amplified fragment is 390bp.

3.2.4 RT-PCR analysis of PDE4D splice variants and detection of the transcripts for murine PDE4D3, PDE4D4 and PDE4D5

The 3T3 F442A cDNA was again used in a PCR screen for PDE4D splice variants. There are five splice variants that have been cloned from rats and humans, PDE4D1-5. The primer pairs and the PCR reaction conditions used for the detection of these three PDE4D splice variants are shown in Table 3.7.

Note that a single pair of primers was used for the detection of both PDE4D1 and PDE4D2. As explained in the legend for Figure 3.12, PDE4D2 mRNA is obtained from PDE4D1 by deletion of an 86 nucleotide section, downstream of the PDE4D1 start codon (ATG). The primers GR8 and GR6 that anneal to either side of this deletion point, can detect both PDE4D1 and PDE4D2. The size of the amplified fragment obtained indicates whether the PDE4D1 or PDE4D2 transcript is expressed.

3.2.4.1 Design of PDE4D3-specific oligonucleotide primers

At the time when this study was carried out no PDE4D3-specific primer pair was available. Only a 'long form' PDE4D-specific 5' primer existed, GR5 (Kostic et al., 1997), which annealed to a sequence found between the first and second splice junctions (see Figure 3.12). Therefore, I designed a new PDE4D3-specific primer, AP4 (Table 3.7) that would anneal to a section of the unique NH_2-terminal splice region of PDE4D3. Mouse PDE4D3 has not yet been cloned. Therefore, the new primer was designed using sequences for rat and human forms of PDE4D3.

A number of factors relevant to the design of ODN primers were taken into consideration. Internal complementarity within the primer sequence, which might result in the formation of secondary structures, was avoided. The overall codon degeneracy of the annealing site for the primer was kept as low as possible in order to minimise the possibility of mutations between species. This is because inter-species mutations are more likely in regions of high degeneracy, where more silent mutations can occur, which do not cause deleterious changes in the amino acid sequence of the protein. The primer was designed so that its melting temperature would be in the 60-65°C range of the potential 3' PDE4D antisense primers GR35, GR6 and SE13 with which it could be used (see Table 3.7). The AP4 + GR6 primer pair combination gave the strongest signal in pilot

experiments using a plasmid control template (HSPDE4D3) and this combination was chosen for future studies.

Table 3.7 Table showing PDE4D RT-PCR primers used and conditions

PDE4A Species	Primer S=Sense, A= Antisense			Nucleotide fragment Amplified	Frag Size (bp)	Cycle conditions		
						D	A	E
PDE 4D (generic) M25342	S	GR43[a]	CC(C/T)(C/T)TGACTG TTATCATGCA CACC	583-844	262	94°C 1 min	50°C 80sec	72°C 70sec
	A	GR35[a]	GATC(C/T)ACATC ATGTATTGCA CTGGC					
PDE 4D1 M25342	S	GR8	ACGTCAAGCT GGAGCATCTC GGC	-85-313	398	94°C 1 min	58°C 80sec	72°C 70sec
	A	GR6	CCTGGTTGCC AGACCGACTC ATTTCA					
PDE4D2 M25349	S	GR8	ACGTCAAGCT GGACCATCTC GGC	-233-79	312	94°C 1 min	58°C 80sec	72°C 70sec
	A	GR6	CCTGGTTGCC AGACCGACTC ATTTCA					
PDE 4D3 L20970	S	AP4	ATTTTCCGTT CAGAAGGCAT TCCTGG	17-577	561	94°C 1 min	50°C 80sec	72°C 70sec
	A	GR6	CCTGGTTGCC AGACCGACTC ATTTCA					
PDE 4D4 L20969	S	SE10[a,b]	AGCGCTACCT GTACTGTC	338-922	585	94°C 1 min	52°C 70sec	72°C 100sec
	A	SE13[a,b]	ACTTGTTGGA GGCCATCTCA C					
PDE 4D5 AF012073	S	2779	CTGTTGCAGC ATGAGAAGTC C	109-793	685	94°C 1 min	52°C 70sec	72°C 100sec
	A	GR6	CCTGGTTGCC AGACCGACTC ATTTCA					

The ODN primers labelled GR-number were designed by Dr. G. Rena using the sequences for the rat homologues of the appropriate splice variants. The primers SE10, SE13 and 2779 were designed by Dr S. Erdogan using the sequences for human homologues of the appropriate splice variants. The PCR reaction conditions are presented as they were in Table 3.2 for the PDE4A-specific RT-PCR primers. The GenBank accession numbers for the sequences of the rat and human PDE4D splice variants detected by the primer sets are given in the first column. The number of cycles carried out in each case was again 40.
a = (Kostic et al., 1997), b = (Bolger et al., 1997)

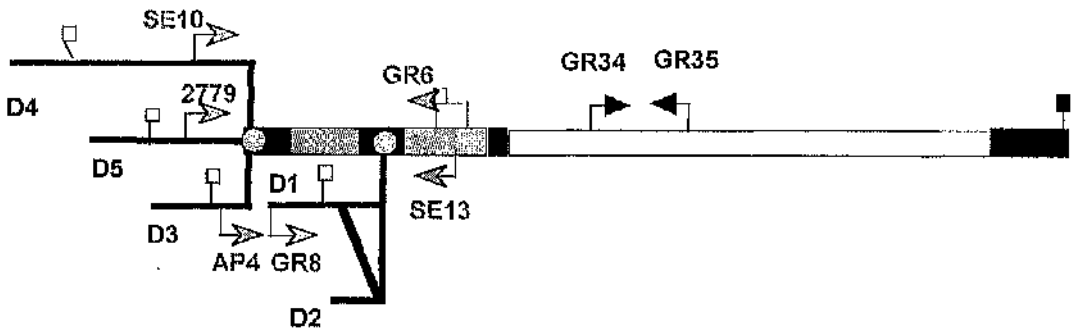

Figure 3.12 Figure showing the annealing positions of RT-PCR primers used to probe PDE4D splice variants

This diagram shows the annealing positions for the RT-PCR primers on the cDNA obtained by reverse-transcription of the mRNA transcripts for the five known PDE4D splice variants, PDE4D1 (D1) to PDE4D5 (D5). The key used is the same as that described in the legend for Figure 3.2. Note that a single primer pair (GR8 + GR6) is used for the detection of both PDE4D1 and PDE4D2. PDE4D2 mRNA is obtained from PDE4D1 mRNA by deletion of an 86 nucleotide section, downstream of the start codon (ATG). This results in a switch to a different reading frame, which prevents the expression of a functional PDE. Instead, translation of PDE4D2 is initiated from an ATG in the middle of UCR2. GR8 and GR6 anneal to positions on either side of the deletion point. The size of the amplified fragment obtained indicates whether the PDE4D1 or PDE4D2 transcript is present, as shown in Table 3.7.

3.2.4.2 Results for the RT-PCR analysis of PDE4D splice variants expressed in 3T3 F442A cells

As positive controls, identical PCR reactions were carried out using plasmids encoding the appropriate PDE4D splice variants. Samples of the PCR reaction products were separated by agarose gel electrophoresis and visualised as before. The results from the RT-PCR analysis of 3T3 F442A cells are shown on the right of Figure 3.13 next to the results for the positive control reactions, shown on the left. Again, no bands were observed for the no-template negative control reactions (data not shown).

Fragments of the expected sizes were obtained using 3T3 F442A cDNA for generic PDE4D and the splice variants PDE4D3, PDE4D4 and PDE4D5. The bands obtained using 3T3 F442A cDNA co-migrated with the bands obtained in the corresponding positive control reactions. There is a close correspondence between the predicted and observed molecular weights (MW) for these fragments as shown below in Table 3.8.

Table 3.8 Comparison of the predicted and observed molecular weights (in bp) for the PDE4D amplified PCR fragments.

PDE4D species	Predicted MW (bp)	Observed MW (bp)*	
		Positive control (plasmid template)	3T3 F442A cDNA template
PDE4D (generic)	262	268.0 ± 4.3	274.9 ± 6.2
PDE4D3	561	573.4 ± 8.9	587.9 ± 17
PDE4D4	585	634.0 ± 9.7	611.7 ± 3.3
PDE4D5	685	706.8 ± 23	700.8 ± 21

* means of at least three separate experiments ± SE.

The above result was supported by western blot analysis using a PDE4D-specific COOH-terminal polyclonal antibody as primary reagent (MacKenzie et al., 1998). This showed two immunoreactive bands that co-migrated with recombinant HSPDE4D3 and HSPDE4D5 (data not shown). From these independent analyses it was concluded that 3T3 F442A cells express mouse homologues of PDE4D3 and PDE4D5.

No immunoreactive band co-migrating with the PDE4D4 standard (at 119 kDa) was observed on the immunoblot of the 3T3 F442A cell lysate (MacKenzie et al., 1998), even though RT-PCR analysis *did* detect a transcript for this splice variant (see Figure 3.13). It should be noted that western blotting analyses have a window of sensitivity. It may be that the level of PDE4D4 expression was below the limit of detection of the antibody used. It is possible that the expression of PDE4D4 is specifically regulated at the level of

translation. Examples of this phenomenon of translational regulation include the iron (Fe)-dependent regulation of the mammalian Fe storage protein, ferritin (Walden et al., 1988; Walden and Thach, 1986) and the proteins of the Surf Clam oocyte before and after fertilisation (Rosenthal et al., 1980). In the former case, the translation of ferritin is inhibited by an Fe-binding protein which binds to the 5' untranslated region of the ferritin mRNA. Upon binding soluble Fe atoms, this protein is released, which allows the translation of ferritin. Translational regulation of protein expression allows rapid control of protein concentrations, without turnover of mRNA. In resting 3T3 F442A cells the expression of PDE4D4 could be inhibited at the level of translation. Certain signals or conditions might release PDE4D4 mRNA from this inhibition, which would allow a sudden increase in PDE4D4 activity. The above result for PDE4D4 underlines the need to back up the results of RT-PCR screening, which detect the transcripts for specific proteins, with western blot analysis, which detects the actual proteins themselves.

In conclusion, western blot analysis suggests PDE4D4 is not expressed in resting 3T3 F442A cells or that it is expressed at a much lower level than PDE4D3 and PDE4D5. Therefore, PDE4D3 and PDE4D5 are the major species present in 3T3 F442A cells.

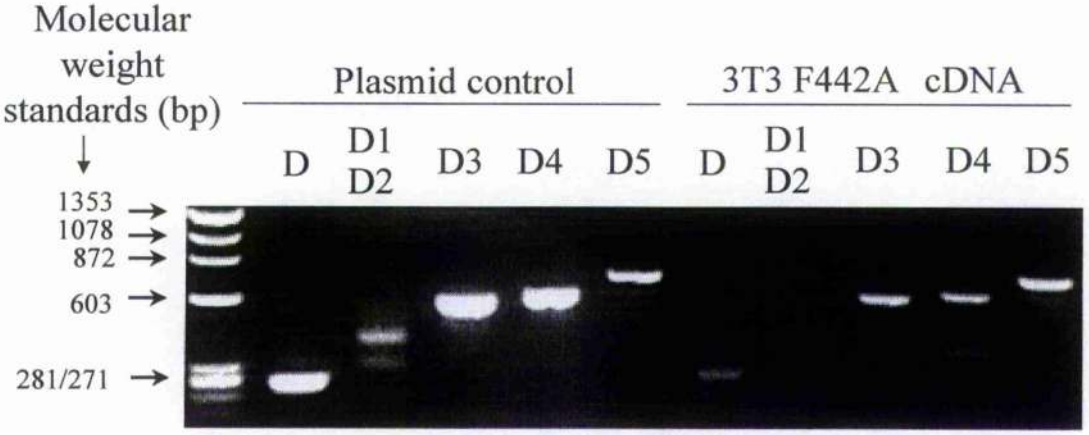

Figure 3.13 RT-PCR analysis of PDE4D splice variants expressed in 3T3 F442A mouse preadipocyte cells.

The cDNA produced from total RNA extracted from 3T3 F44A cells was used as a template in an RT-PCR screen for PDE4D mRNA transcripts. The primers used were either generic primers for the detection of all PDE4D splice variants (D), or splice variant specific primers for the detection of PDE4D1 and PDE4D2 (D1/D2), PDE4D3 (D3), PDE4D4 (D4) or PDE4D5. The positive control templates used were pPDE79 for PDE4D, mouse brain cDNA for PDE4D1 and PDE4D2, pPDE43 for PDE4D3, pPDE39 for PDE4D4 and pPDE79 for PDE4D5. Samples (9ul) of the positive control reaction products and the 3T3 F442A cDNA template reaction products were separated by agarose (2%) gel electrophoresis, stained with ethidium bromide and visualised with a UV transilluminator. The molecular weight standards (in bp) are shown on the left. Amplified product sizes were PDE4D (generic) =262bp, PDE4D1= 398bp, PDE4D2 = 312bp, PDE4D3 = 561bp, PDE4D4 = 585bp and PDE4D5 = 681bp.

3.2.4.3 Sequencing of the PDE4D5 amplified fragment (nucleotides 109-309)

As further verification of the above RT-PCR and western blotting results, the correct identity of the PDE4D5 PCR fragment was checked by sequencing as described in the Methods chapter, section 2.6.7. The nucleotide sequence that was obtained was deposited in GenBank (accession number AF038896). In Figure 3.14 this mouse nucleotide sequence has been aligned with the equivalent sequence from human PDE4D5 (HSPDE4D5) and the nucleotide sequence of (rat) RNPDE4D3 (Bolger et al., 1994) downstream of the first splice junction (RNPDE4D5 has not yet been cloned).

The mouse PDE4D5 nucleotide sequence is 93.2% identical to the human sequence and 95.8% identical to the rat sequence. All the nucleotide mutations are silent, so the predicted amino acid sequence is 100% identical to both the human PDE4D5 sequence and the available rat PDE4D sequence downstream of the first splice junction. This region of the amino acid sequence is shown in Figure 3.15.

This result confirms that mouse 3T3 F442A cells do express a mouse homologue of PDE4D5. The 100 percent conservation of sequence across the mouse, rat and human species suggests that this NH_2–terminal region of PDE4D5 may perform one or many essential functions and any change to its structure cannot be tolerated. We already know that amino acids 22-77 of PDE4D5, upstream of the region sequenced here, are essential for binding to scaffold protein RACK1 (Yarwood et al., 1999) (see Introduction chapter, section 1.8.5).

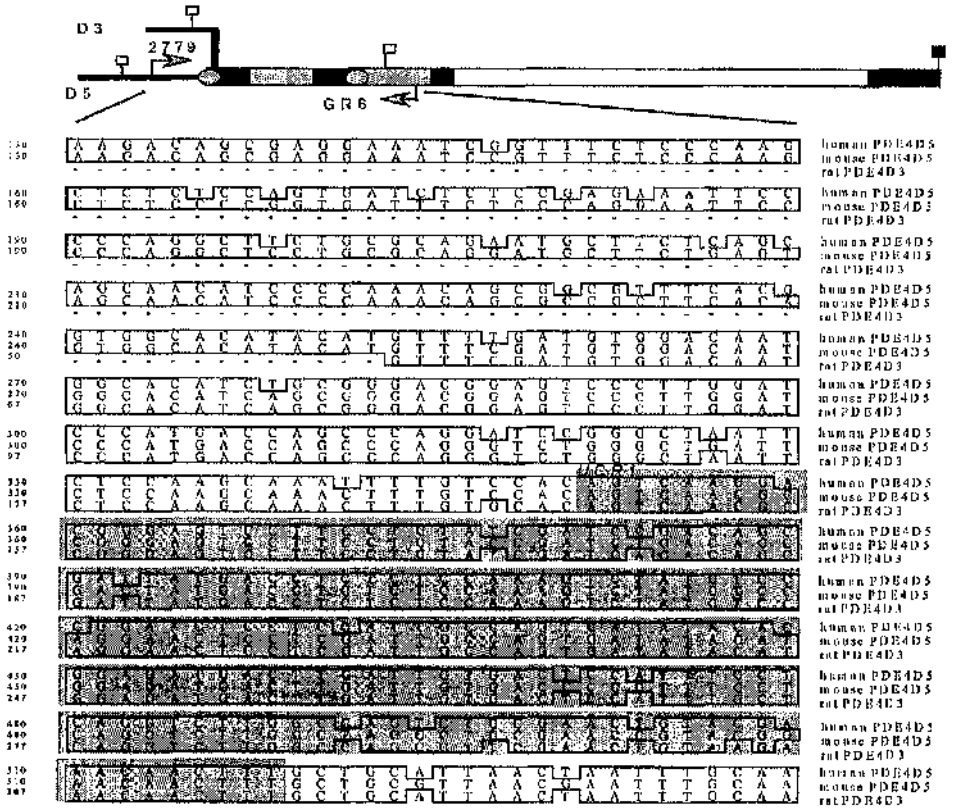

Figure 3.14 Alignment of the nucleotide sequence for mouse and human PDE4D5 and rat PDE4D3

This figure shows the nucleotide sequence of the fragment amplified with PDE4D5-specific primers using mouse 3T3 F442A preadipocyte cDNA as a template. The ODN primer sequences at both ends of the PCR fragments have been excluded. The mouse nucleotide sequence (GenBank accession number AF038896) has been aligned with the corresponding human PDE4D5 sequence (nucleotides 130-757, GenBank accession number AFO12073) and the rat PDE4D3 sequence downstream of the first splice junction (nucleotides 67-554, GenBank accession number L27059). Bases that match the mouse sequence are boxed. The sections of nucleotide sequence corresponding to the regions encoding UCR1 and part of UCR2 are shaded. The domain structure for the splice variants PDE4D3 and PDE4D5 is shown at the top of the diagram. This alignment was performed using the Clustal method (Higgins and Sharp, 1988) within the DNA Star programme (Lasergene).

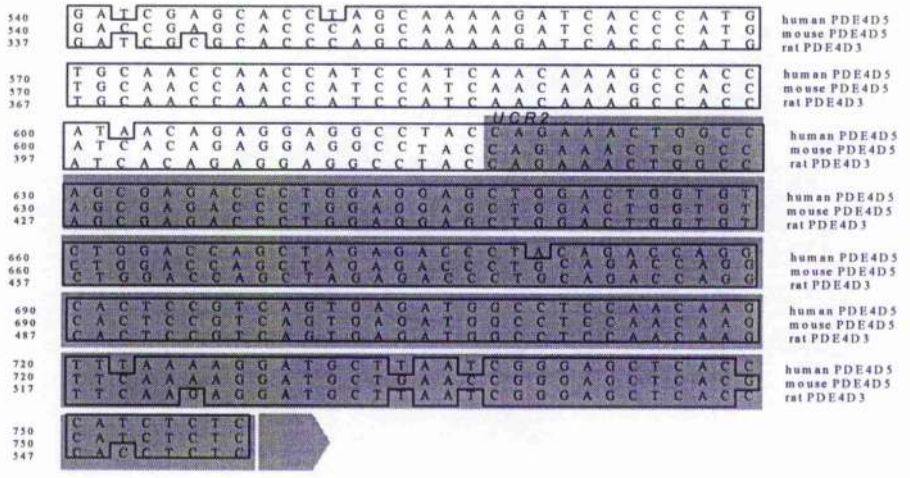

Figure 3.14 continued

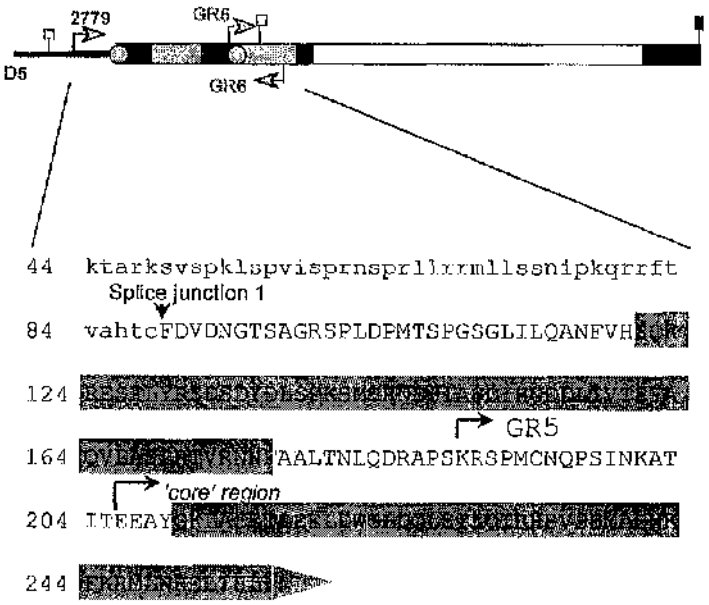

Figure 3.15 Predicted amino acid sequence for mouse PDE4D5 (amino acids 44-255) The GenBank accession number for this sequence is AF038895. The key for this figure is the same as that described in the legend for Figure 3.2. This alignment was performed using the Clustal method (Higgins and Sharp, 1988) within the DNA Star programme (Lasergene).

3.2.5 Conclusions from RT-PCR screen of 3T3-F442A cells

From the above studies we can conclude that 3T3 F442A cells express the mouse homologues of PDE4A5, PDE4B2, PDE4D3, PDE4D5 and a PDE4C splice variant that is probably PDE4C2 as deduced from western blotting studies (MacKenzie et al., 1998). Therefore, 3T3 F442A cells are unusual in that they express splice variants from all four PDE4 genes A, B, C and D (Houslay et al., 1998; Muller et al., 1996). Although generic PDE4C has been detected in a few tissues, including brain, lung and kidney (Engels et al., 1994; Houslay et al., 1998; Muller et al., 1996), the above study provides the first description of an endogenous PDE4C species using RT-PCR, western blotting and activity analyses [see above and (MacKenzie et al., 1998)].

Sequence analysis showed that the mouse homologue of PDE4A5 is more closely related to rat form (RNPDE4A5) than the human form in that it lacks the proline rich-insert present in the LR2 region of the latter. The sequence data for the mouse homologues of PDE4A5, PDE4B2 and PDE4D5 showed that the PDE4 splice variants are well conserved between rats, humans and mice.

3.3 PMA, GH and wortmannin do not effect the levels of the generic PDE4A transcript in 3T3 F442A preadipocytes

As discussed in the introduction to this chapter, one of the initial observations in this study, reported by Dr MacKenzie, was a rapid (maximal at ~20-30min), transient increase in PDE4 activity caused by GH (MacKenzie et al., 1998). It was then shown that GH increased the PDE4A activity immunoprecipitated from the 3T3 F442A cells using anti-PDE4A COOH-terminal antisera to immunopurify and analyse PDE4 selectively. PDE4A accounted for almost half (47 ± 5%) of the PDE4 activity in these cells. My results for the RT-PCR screen for PDE4A splice variants (Figure 3.3) and western blotting results (MacKenzie et al., 1998) suggested that PDE4A5 was the sole PDE4A splice variant expressed in 3T3 F442A preadipocytes. Therefore, it appeared that GH specifically caused an increase in PDE4A5 activity.

Studies were carried out in order to determine the signalling pathway by which GH activates PDE4A5 activity. Early on in these investigations it was thought that protein kinase C (PKC) might be involved as this is activated downstream of the growth hormone receptor (see Figure 3.1, section 3.1.1). Another signalling protein, that is activated as a

result GH stimulation, is phosphoinositide-3 kinase (PI3-kinase, see Figure 3.1). Dr MacKenzie showed that the PI3-kinase inhibitors, wortmannin and LY 294002, blocked the activation of PDE4A5 by GH. To corroborate this result, Dr MacKenzie showed that transfection of a dominant negative form of PI3-kinase (Δ p85 PI3-kinase) also ablated GH activation of PDE4A5. Therefore, it was concluded that GH activated PDE4A in a PI3-kinase dependent manner.

It was originally thought that GH might increase PDE4A activity by upregulating gene transcription, in a manner similar to the affect of TSH on PDE4D1 and PDE4D2 levels in thyroid FRTL-5 cells (see Introduction chapter, section 1.6) (Conti et al., 1995; Sette et al., 1994; Swinnen et al., 1991). I used RT-PCR to investigate whether the PI3-kinase-dependent increase in PDE4A5 activity in 3T3 F442A cells was due to an increase in PDE4A transcription. I used the same technique to investigate whether the PKC activator, phorbol 12-myristate 13-acetate (PMA), would affect PDE4A transcription. The 3T3 F442A cells were stimulated with GH (25nM) or PMA (25nM) in the presence and absence of wortmannin (2nM) for 30min before being harvested. These concentrations and incubation times were known to be optimal for the desired effects of these biochemical agents, described above. Equal amounts of RNA from these stimulated cells and control cells were used as templates for first strand cDNA synthesis reactions. In order to compare the levels of generic PDE4A transcript in control and treated cells, equal amounts of the resultant cDNA were employed as templates in a PCR reaction using the PDE4A-specific primers (GR28 and GR29) used in the experiment presented in Figure 3.3, section 3.2.1. The conditions used for this PCR reaction are as shown in Table 3.2, section 3.2.1. As an internal control, ODN primers specific for the ubiquitously expressed β-actin (SE14 + SE15) were included in this PCR reaction. Equal volumes of the PCR reaction products were separated on a 2% agarose gel and the bands were visualised by ethidium bromide staining and UV-transillumination. The levels of the PDE4A transcripts in the differently treated cells were assessed on the basis of the intensities of the PDE4A bands relative to the β-actin bands. The results are shown in Figure 3.16.

No changes in the level of the PDE4A transcript, relative to the β-actin transcript, were observed when 3T3 F442A preadipocytes were treated with GH, PMA or wortmannin. This suggests that GH does not cause an increase in PDE4A5 activity by increasing the rate of transcription. The results also indicated that the PI3-kinase inhibitor wortmannin and the PKC activator, PMA had no effect on the PDE4A transcript levels.

Therefore, we can conclude that wortmannin does not ablate GH activation of PDE4A through an effect on transcription. It was also later shown that the PKC inhibitor, chelerythrine chloride, had no effect on GH stimulation of PDE4A5 activity, suggesting that PKC is not involved in this pathway.

In agreement with these results, the transcriptional inhibitor, actinomycin D, failed to prevent GH from stimulating PDE4A5 activity (MacKenzie et al., 1998). The rapid (maximal at 10-20min) activation of PDE4A5 with GH is not consistent with an effect on transcription. In addition, western blotting analysis showed no change in PDE4A5 protein levels with GH (MacKenzie et al., 1998). These results suggest that GH activates PDE4A5 via a post-translational modification. The lack of an effect on transcription suggests that STATs (signal transducers and activators of transcription; see section 3.1.1 and Figure 3.1) are not directly involved in the activation of PDE4A5.

Figure 3.16 The intracellular level of the PDE4A transcript in 3T3 F442A cells is unaffected by GH, PMA or wortmannin treatment

As described in the Methods chapter, (section 2.1.4.1) confluent, serum starved 3T3 F442A preadipocyte cells were incubated for 30min with either GH (25nM) or PMA (25nM) in the presence or absence of 2nM wortmannin, or were left untreated (C = result for untreated control cells). Immediately after this treatment, RNA was extracted, purified and used as a template for first strand cDNA synthesis as described in section 2.5 of the Methods. Equal amounts of the resultant cDNA were employed in a PCR reaction that contained a primer pair for the detection of the PDE4A generic transcript and a primer pair specific for the β-actin transcript as an internal control. The PDE4A-specific primers were also used on mouse testicular cDNA (T) and RD1 cDNA (pSVL-RD1) as positive controls. 9ul samples of the PCR reaction products were separated on a 2% agarose gel containing 0.5μg/ml ethidium bromide and visualised by UV transillumination. The generic primer pairs used to detect PDE4A transcripts amplified a fragment of 233bp, whereas the β-actin internal control primers amplified a fragment of 466bp. The β-actin internal control primers had the following sequences SE14 (sense) = CATCGTCACC AACTGGGACG AC, SE15 (antisense) = CGTGGCCATC TCTTGCTCGA AG. The above result is typical for this experiment which was carried out three times.

CHAPTER 3 CONCLUSIONS

3.4 Discussion and conclusions

In sections 3.4.1 and 3.4.2 below I describe the final results of this collaborative study. In section 3.4.3 I discuss the implications of my results and offer suggestions for future work.

3.4.1 GH activation of PDE4A5 serves as a brake on the process of differentiation

At the start of this study it was noted that inhibition of PDE4 activity with rolipram potentiated GH-induced differentiation of 3T3 F442A preadipocytes (see section 3.1.1) by approximately two-fold (MacKenzie et al., 1998). Dr MacKenzie went on to show that specific ablation of PDE4A5, by antisense treatment, also promoted differentiation. This was done using an ODN primer designed to block the translation of PDE4A5 by binding to the first 18 nucleotides of the translated region of the PDE4A5 mRNA transcript. Treatment of 3T3 F442A cells with this ODN primer potentiated GH-induced differentiation, measured using the glycerol-3-phosphate dehydrogenase (GPDH) assay. These results suggest that the specific activation of PDE4A5 by GH acts as a brake on differentiation. The positive effect of PDE4A5 inhibition on 3T3 F442A differentiation was almost equivalent to the effect of total PDE4 inhibition with rolipram (MacKenzie et al., 1998).

As discussed in section 3.1.1, a dual effector theory has been proposed for GH-promoted differentiation of 3T3 F442A preadipocytes (Yarwood et al., 1998; Zezulak and Green, 1986) in which GH-primed preadipocytes require a secondary signal such as insulin or IGF-1 to progress to the fully differentiated state. The results of the above study suggest a model where GH holds 3T3 F442A cells in a primed state through the use of PDE4A5 activation. The secondary signals may act by blocking or inhibiting the pathway that transduces the GH-dependent activation of PDE4A5 or they may directly inhibit PDE4A5, to release the brake and allow full differentiation to progress. Alternatively, they may activate other signalling pathways that override the effect of PDE4A5 activation.

The 3T3 F442A preadipocytes have been shown to express PDE3 activity at levels equal to or greater than PDE4 (MacKenzie et al., 1998). Furthermore, the PDE3 specific

inhibitor, cilostamide, partially ablated the GH-dependent drop in intracellular cyclic AMP levels (MacKenzie et al., 1998). However, PDE3 inhibition did not potentiate GH-dependent preadipocyte differentiation. This result is further evidence that PDEs regulate distinct pools of cAMP within cells that control separate processes (see Introduction chapter, section 1.2.1).

3.4.2 GH activates PDE4A5 via JAK2, PI3-kinase and p70S6 kinase

As mentioned above, GH-stimulation of 3T3 F442A cells causes a PI3-kinase-dependent increase in PDE4A5 activity. My RT-PCR analyses and Dr MacKenzie's western blot analyses showed that this activation was not the result of an increase in PDE4A5 expression. However, Dr MacKenzie showed that GH-stimulation of PDE4A5 activity was accompanied by an upward band-shift for this protein on SDS-PAGE [see ref. (MacKenzie et al., 1998)]. This implied that the activation of PDE4A5 by GH might be the result of a post-translational modification, such as a phosphorylation. The PI3-kinase inhibitors, wortmannin and LY 294002 and transfection of the dominant negative form of PI3-kinase (Δ p85 PI3-kinase) blocked this band-shift. Having established the above, Dr S. Mackenzie and Dr S. Yarwood went on to identify the other components of the signalling pathway that mediated GH-dependent activation of PDE4A5 (MacKenzie et al., 1998).

A number of groups have shown that PI3-kinase activates p70S6 kinase (see Figure 3.1, section 3.1.1) (Han et al., 1995; Proud, 1996; Weng et al., 1995). This activation is not direct, but is believed to be mediated by a protein called FRAP (FKBP12-rapamycin associated protein). The fungal macrolide rapamycin prevents activation by FRAP of p70S6 kinase (Brown et al., 1995). Rapamycin blocked both the band-shift and the activation of PDE4A5 by GH (MacKenzie et al., 1998). Rapamycin also blocked the GH-dependent increase in the intracellular concentration of cAMP. In addition, transfection of a constitutively active mutant form of p70S6 kinase into 3T3 F442A cells gave rise to GH-independent activation of PDE4A5. These results suggest that activated p70S6 kinase activates PDE4A5 *in vivo*. This activation is not necessarily direct.

It was further shown that JAK2 was an intermediate kinase in the GH-dependent activation of PDE4A5. Antisense ODN primers, that specifically blocked the expression of JAK2, ablated GH-dependent stimulation of PDE4A5 activity (MacKenzie et al., 1998). The conclusions of this study are that GH activates PDE4A5 in 3T3 F442A cells via JAK2,

PI3-kinase and a p70S6 kinase. This pathway is illustrated in Figure 3.17. Specific activation of PDE4A5 in this way inhibits the process of differentiation.

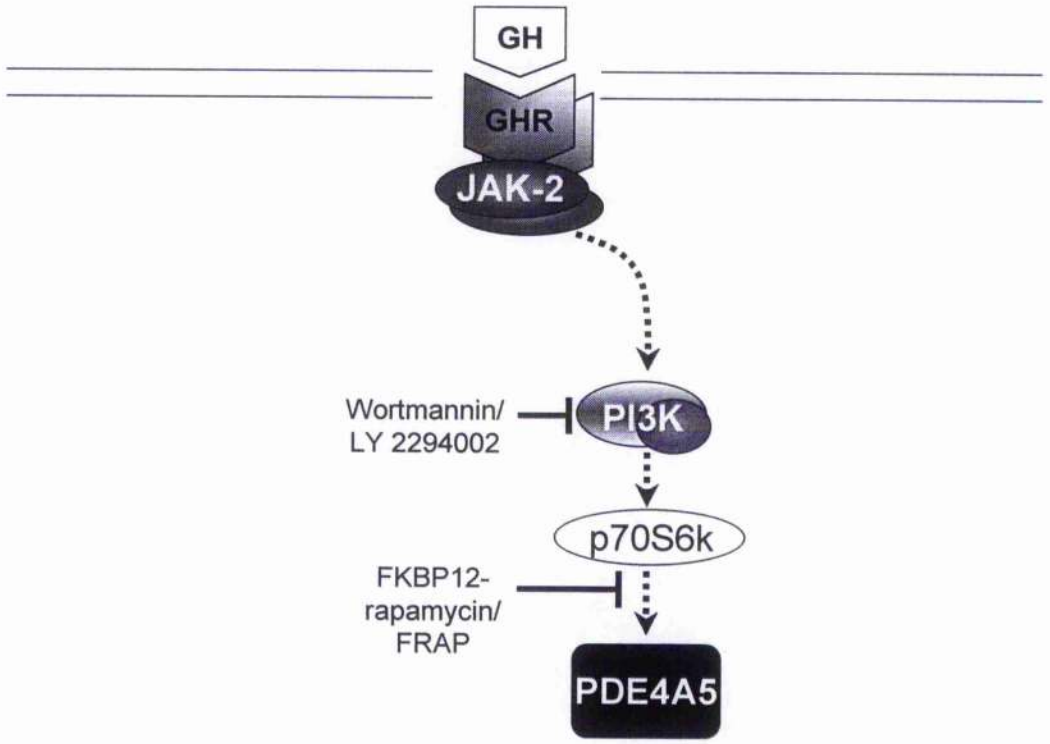

Figure 3.17 GH stimulates PDE4A5 via JAK2, PI3-kinase and p70S6 kinase. Activation of PDE4A5 by growth hormone has a negative effect on 3T3 F442A preadipocyte differentiation. The signalling pathway that has been established for the activation of PDE4A5 by GH in 3T3 F442A cells is illustrated. The dotted lines indicate that each of the activation steps in this pathway may occur through unidentified intermediary proteins. The points of action of the inhibitors used in this study are shown. The fungal macrolide rapamycin blocks the activation of p70S6 kinase by acting on FRAP (FKBP12-rapamycin associated protein). As discussed in chapter 5, section 5.2.2, rapamycin associates with the immunophilin protein FKBP12. Rapamycin-FKBP12 complexes associate with FRAP and this prevents activation by FRAP of p70S6 kinase (Brown et al., 1995). It is possible that other signalling pathways may act via FRAP to regulate the GH-dependent activation PDE4A5.

3.4.3 Final conclusion and future work

My RT-PCR analysis showed that 3T3 F442A cells express a number of splice variants (PDE4B2, PDE4C, PDE4D3 and PDE4D5) in addition to PDE4A5. Unlike PDE4A5, these other splice variants do not appear to be involved in the negative effect of GH on 3T3 F442A differentiation. This is because PDE4A5 inhibition with antisense and total PDE4 inhibition with rolipram both potentiated GH-dependent differentiation to equivalent degrees. These results suggest that different PDE4 splice variants have distinct roles in 3T3 F442A preadipocytes as opposed to interchangeable functions that merely increase the redundancy of the PDE system. The other splice variants may be targeted to different locations within the cell where they control different intracellular pools of cAMP and different cAMP-dependent processes. An aim for future studies will be to define the roles for the other PDE4 splice variants in 3T3 F442A intracellular signalling.

We still need to establish the exact post-translational modification (e.g. phosphorylation event) that causes the upward band-shift for PDE4A5 on SDS-PAGE that is concomitant with PDE4A5 activation downstream of p70S6 kinase. This may uncover other mechanisms for controlling PDE4A5 activity and hence 3T3 F442A differentiation. In addition, it would also be interesting to assess whether similar mechanisms for the control of differentiation occur in other cells where PDE4A5 is specifically expressed.

The post-translational modification of PDE4A5 may directly cause activation of this enzyme via a change in the conformation of its active site that facilitates the catalytic process. Alternatively, the post-translational modification may disrupt the interaction of PDE4A5 with an inhibitory protein. Either process may cause a change in the subcellular location of PDE4A5. Therefore, it would be interesting to use immunofluorescence confocal microscopy to analyse the intracellular distribution of PDE4A5 before and after treatment of 3T3 F442A preadipocytes with GH. If GH did cause a change in PDE4A5 localisation within the cells it would be of further interest to know the effect of rapamycin (which inhibits p70S6 kinase) on this change. It would also be interesting to know whether the activation status of PDE4A5 and any change in its subcellular distribution were maintained in differentiated adipocytes.

CHAPTER 4

Studies on the association of PDE4 amino-terminal regions with the membrane fraction of COS-7 cells

4. Studies on the association of PDE4 amino-terminal regions with the membrane fraction of COS-7 cells

CHAPTER 4 INTRODUCTION

In this chapter I investigate the intracellular targeting of PDE4 splice variants, via their unique NH_2-terminal regions. I have expressed the NH_2-terminal regions of the rat PDE4A isoenzymes RNPDE4A1 (RD1) and RNPDE4A5 (rpde6) as fusions to the COOH-terminus of the soluble enzyme glutathione-*S*-transferase (GST) and I have tested the ability of these constructs to interact with the P2-membrane fraction of COS-7 cells. In section 4.2 I demonstrate that the NH_2-terminal 100 amino acids of RD1 confer P2-membrane association on GST and that this association is disrupted by the non-ionic detergent Triton X-100. In section 4.3.2 I use GST constructs to show that just the NH_2-terminal domain of rpde6 can associate with the membrane fraction and that the region between Gly108 and Lys256 is sufficient for this association. In section 4.4 I examine the association of these PDE4 NH_2-termini-GST fusions with heat-treated P2-membrane fraction. These studies suggest that the NH_2-terminal regions of RD1 and rpde6 interact with distinct components of the P2-membrane fraction with different thermal stabilities. In section 4.5 I discuss the above findings, and the potential use of GST-fusion proteins in further studies on PDE4 targeting and protein-protein interactions.

4.1 The NH_2-terminal splice domains of rpde6 and RD1 isoenzymes determine their intracellular targeting

As discussed in the introduction (section 1.8) the NH_2-terminal regions of PDE4 splice variants are involved in intracellular targeting (Houslay et al., 1997; Houslay, 1996; Houslay et al., 1998). Studies have shown that the PDE4 splice variants within a particular subfamily, which differ only at their unique NH_2-termini, show distinct modes of targeting in cells (Bolger et al., 1997; Huston et al., 1997). For instance, immunofluorescence analyses showed that the rat PDE4A splice variant, RD1 (RNPDE4A1) associated with the plasma membrane and intracellular vesicles of transfected COS-7 cells (Shakur et al., 1995), whereas rpde6 (RNPDE4A5) associated with the cytoskeleton, particularly in the perinuclear region (Huston et al., 2000). An NH_2-terminal truncate Met^{26}RD1, which consisted of just the rat PDE4A core unit, had a diffuse cytosolic distribution in transfected COS-7 cells. This suggested that removal the unique NH_2-terminal regions abolished the association of PDE4A splice variants with the membrane and cytoskeleton. It has further been shown rpde6 can bind to the SH3 domains of Src-family tyrosyl kinases in contrast to

the other long PDE4A splice variant rpde39 (RNPDE4A6) (O' Connell et al., 1996). This suggests that splice variants are targeted to specific proteins by their unique NH_2-terminal splice domains. The identification of these targeting proteins is a major research aim.

Differences were also observed between the splice variants in terms of their distribution between the P1 (low-speed pellet), P2 (high-speed pellet) and S (cytosolic) subcellular fractions of transfected COS-7 cells (see Methods chapter, section 2.11 for the definition of these fractions). Furthermore, the splice variants that associate with the particulate fractions differ in terms of the resistance of these associations to disruption with salt and detergent. For example, the association of both rpde6 and rpde39 (RNPDE4A6) with the P2-pellet fraction was resistant to high salt concentrations (NaCl) and the non-ionic detergent Triton X-100 (Bolger et al., 1996; McPhee et al., 1995). This suggested that these splice variants associate with components of the cytoskeleton (Jackson et al., 1994; Slusarewicz et al., 1994). RD1, in contrast, was dissociated from the P2-pellet fraction by Triton X-100 treatment, which suggested an interaction with a membrane protein or lipid (McPhee et al., 1995). The PDE4B and PDE4D splice variants also show marked differences in their ability to interact with the particulate fractions and the susceptibility of these interactions to Triton X-100 and high NaCl concentrations. These observations again suggest that the different unique NH_2-terminal splice domains interact with different intracellular components.

One unanswered question is whether the targeting sequences of PDE4 enzymes are contained completely within their unique NH_2-termini or whether sequences within the NH_2-termini combine with sequences within the core region to form binding surface for interaction with the relevant targeting proteins. The ability of the unique NH_2-termini to target PDE4 isoenzymes can be tested by expressing these domains separately as fusions to essentially 'soluble' proteins that do not associate with the P1 or P2 particulate fractions. This strategy was used successfully by Scotland and Houslay to show that the NH_2-terminal 25 amino acid splice domains of RD1 conferred membrane (high speed pellet) association on the soluble bacterial enzyme CAT (Scotland and Houslay, 1995) (see section 1.8.1).

In this chapter an alternative strategy was used where PDE4 NH_2-terminal regions were expressed as fusions to the soluble protein glutathione-*S*-transferase (GST) from *Schistosoma japonicum* (Smith and Johnson, 1988). This protein has a self-contained globular structure (Lim et al., 1994). The COOH-terminus of GST is on the outside of the structure and peptides fused to this end are likely to be exposed for interaction with their

target proteins or lipids. The GST tag also provides a means for the detection of these fusion proteins using anti-GST antibodies. GST-fusions have been used by a number of groups to define the membrane association domains of various proteins. For instance, Wang et al showed that the PH domain (as opposed to the Dbl-homology domain) of the metastasis-inducing Tiam-1 protein mediated the binding of this protein to brain membranes (Wang et al., 1997). Similarly, Plant et al used GST-fusions to show that the C2 domain of the ubiquitin protein ligase Nedd-4 was sufficient to mediate the Ca^{2+}-dependent association of this protein with cellular membranes (Plant et al., 1997).

4.2 The NH_2-terminal region of RNPDE4A1 (RD1) confers P2-membrane fraction association on the normally soluble GST

I began by investigating whether the NH_2-terminal region of RD1 could confer membrane (high-speed pellet) fraction association on GST. COS-7 cell membranes were used as this was the original cell line used to characterise both rpde6 and RD1 (McPhee et al., 1995; Shakur et al., 1993; Shakur et al., 1995). A plasmid (pGS31) was prepared that expressed the NH_2-terminal 100 amino acids region of RD1 as a fusion to the COOH-terminus of GST. The structure of this GST-$RD1^{1-100}$ construct is illustrated in Figure 4.1. The first 100 amino acids of RD1 includes the unique 25 amino acid splice domain, the second half of UCR2 and a segment of the core region up to the first 4 amino acids of the catalytic unit.

4.2.1 Purification of GST-$RD1^{1-100}$

This fusion protein was purified using the column purification method and eluted with glutathione buffer as described in the Methods chapter (section 2.7.2). The purified preparation was analysed by SDS-PAGE and Coomassie staining (see Figure 4.2). GST alone was similarly over-expressed, purified and analysed by SDS-PAGE (see Chapter 5, section 5.4, Figure 5.9). The observed molecular weight for GST-$RD1^{1-100}$ (38.1 ± 1.0kDa, [mean ± SE, n=3]), was close to its actual molecular weight calculated from its sequence (39.0kDa). In addition to the bands corresponding to the full-length fusion proteins, there were a number of lower molecular weight bands in the ~25-32kDa range. These bands may be the result of the proteolytic degradation of the RD1 section of this fusion protein. Only a few of these bands ran below the observed molecular weight for the GST tag (~27kDa), which is relatively resistant to proteolytic degradation (Harris, 1998).

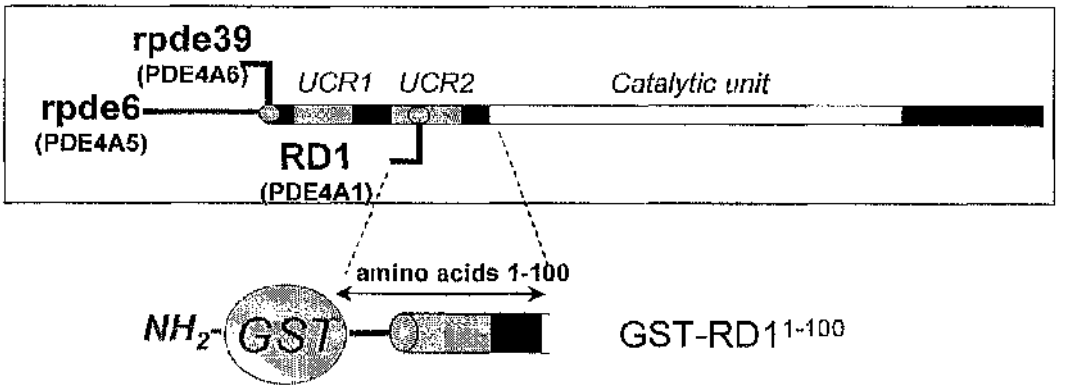

Figure 4.1 GST-RD1$^{1-100}$ fusion protein

This figure illustrates the NH_2-terminal region of RD1 expressed as a fusion to the COOH-terminus of GST (GST-RD1$^{1-100}$). The other rat PDE4A splice variants, rpde6 and rpde39, are also shown in this diagram. The unique NH_2-terminal splice domains are indicated by the thinner black lines. The circles represent the positions of the splice junctions. Grey and white rectangles represent the UCR and catalytic regions, respectively.

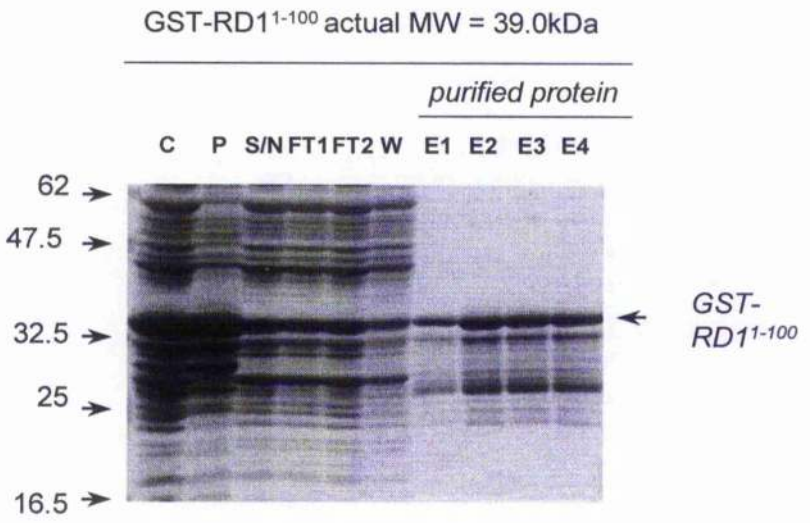

Figure 4.2 Over-expression and purification of GST-RD1$^{1-100}$

Samples (≤60µg protein) from different stages of the glutathione Sepharose column purification process (see section 2.7.2.2) were separated by SDS-PAGE (10%[w/v] acrylamide) and stained with Coomassie blue. *C* = crude bacterial lysate; *P* = pellet and *S/N* = supernatant after sonication and centrifugation; *FT1/FT2* = Flow through 1 and 2 after passing the sonicated supernatant through the column twice. *W* = complete PBS wash. *E1-4*= elutions with glutathione buffer. The observed molecular weight of full-length GST-RD1$^{1-100}$ on SDS-PAGE was 38.1 ± 1.0 (mean ± SE, n=3), which corresponds closely with its calculated molecular weight of 39.0kDa.

4.2.2 Binding of GST-RD1$^{1-100}$ to P2-membrane fraction of COS-7 cells.

Purified GST-RD1$^{1-100}$ and GST (control) were incubated with the P2-pellet fraction of untransfected COS-7 cells. This P2-pellet fraction was obtained by high-speed (100,000*g*) centrifugation of the supernatant obtained from a low speed (1000*g*) centrifugation of cell homogenate [as described in the Methods, section 2.11 and in (Shakur et al., 1995)]. The P2-pellet fraction contains plasma membrane, Golgi, ER and lysosomal membranes and cytoskeletal components (Jung and Moroi, 1988; Scotland et al., 1998). Therefore, from now on this fraction will be referred to as the P2-membrane fraction.

After incubation with GST-fusion protein, the P2-membrane mixtures were subjected to high-speed centrifugation as described above to obtain membrane pellets and supernatants (*S1*), containing unbound fusion protein. The membrane pellets were then washed by resuspension in complete KHEM buffer with or without the non-ionic detergent Triton X-100 (1% v/v). The mixtures were then centrifuged again at high-speed to obtain membrane pellet (*P*) and supernatant (*S2*) fractions. Samples of the pellet and supernatant fractions were then separated by SDS-PAGE and immunoblotted with anti-GST antisera as the primary reagent.

As shown in Figure 4.3, full-length GST-RD1$^{1-100}$ does indeed become associated with the P2-membrane fraction of COS-7 cells: a single immunoreactive band was observed in the bound fraction (*P*, lane 1) after washing with KHEM. This band co-migrated with an immunoreactive band in the unbound fraction (*S1*) running at the expected molecular weight for GST-RD1$^{1-100}$ (~39kDa). This association was resistant to washing with the KHEM buffer as no immunoreactive band was observed in the resultant supernatant (*S2*) from this wash. In contrast, GST did not appear to associate with the membrane pellet (*P*, lane 7) under these conditions, but was present in excess in the unbound fraction (*S1*, lane 8). Therefore, the NH_2-terminal 100 amino acids of RD1 appear to confer membrane association on the normally soluble GST.

My results on the membrane association of GST-RD1$^{1-100}$ agree with the findings of Scotland and Houslay who showed that the NH_2-terminal 25 amino acid splice domain of RD1 conferred membrane association on CAT (Scotland and Houslay, 1995). However, in this CAT construct the RD1 splice domain was fused to the NH_2-terminus of CAT. In contrast, in the GST-RD1$^{1-100}$ construct used in my experiments, the 100 amino acid NH_2-terminal region of RD1 was fused to the COOH-terminus of GST (see Figure 4.1).

Therefore, I have shown that the NH_2-terminus of the RD1 splice domain does not have to be free for this region to associate with the membrane fraction. This is significant, as it suggests that the RD1 splice domain does not interact with the membrane via the direct, transmembrane insertion of its extreme NH_2-terminus into the lipid bilayer, as the NH_2-terminal GST tag would prevent this. However, if the NH_2-terminal splice domain can bend to form a hairpin structure, hydrophobic sequences within this domain could be presented in a way that allows their interaction with the membrane bilayer (discussed below).

Figure 4.3 also shows that the association of GST-RD1$^{1-100}$ with the P2-membrane fraction is disrupted by non-ionic detergent. After just one wash with 1% Triton X-100, GST-RD1$^{1-100}$ appears in the supernatant (*S2*, lane 6) in contrast to the supernatant obtained after washing with KHEM buffer alone (*S2*, lane 3). In addition, the amount of GST-RD1$^{1-100}$ associated with membrane pellet after washing with Triton X-100 is clearly less than that associated with the membrane pellet after washing with complete KHEM. These results suggest that the association of RD1 with P2-membrane fraction is predominantly mediated by hydrophobic (and not electrostatic) interactions. This agrees with studies showing the dissociation of both RD1 (Shakur et al., 1995) and an RD1 (1-100 amino acid)-CAT construct (Scotland and Houslay, 1995) from the particulate fraction of transfected COS cells in the presence of low concentrations of this non-ionic detergent. This observation did not answer the question of whether RD1 interacts with a membrane lipid or protein, as both interactions could be mediated by weak hydrophobic forces.

In an attempt to answer the latter question, an analysis of the structure of this NH_2-terminal splice domain has been carried out by ^{1}H-NMR (Smith et al., 1996) (see Introduction, section 1.8.1). Smith et al showed that this splice domain consists of two helical regions separated by a hinge. The first helical region, Leu3-Cys11, is amphipathic in nature, and contains the polar residues Asp5, Cys8, Glu9, Thr10, and Cys11. The second of these helical regions, Pro14-Lys24 contains a compact unit of hydrophobic residues, Pro14-Trp20, shown to be necessary for membrane association (Smith et al., 1996). The overall structure of the RD1 NH_2-terminal splice domain suggests that it could form a hairpin conformation that could present the hydrophobic region for an interaction with the membrane bilayer. This agrees with my finding that the membrane association of the RD1 NH_2-terminal region was not prevented by an NH_2-terminal GST tag (see above).

As shown in Figure 4.3, the unbound fractions (*S1*, lanes 2 and 5) contain a number of immunoreactive bands that run below the band corresponding to full-length GST-RD1^{1-}

^{100} (main ones indicated with arrowheads). These bands probably represent the products of the proteolytic degradation of GST-RD1$^{1-100}$. The fact that these bands are immunoreactive suggests that they represent COOH-terminal truncates of GST-RD1$^{1-100}$, where the NH_2-terminal domain of RD1 has been partially removed (see schematic diagram of GST-RD1$^{1-100}$ in Figure 4.1). The bands at ~29kDa (lower arrowhead) are just above the molecular weight of GST (*SI*, lanes 8 and 11), which suggest that the RD1 100 amino acid NH_2-terminal region has been almost entirely removed. As Figure 4.3 shows, these degradation products do not associate with the P2-membrane fraction (*P*, lanes 1 and 4). Therefore, this suggests that the disruption of the RD1 NH_2-terminus prevents the membrane association of GST-RD1$^{1-100}$.

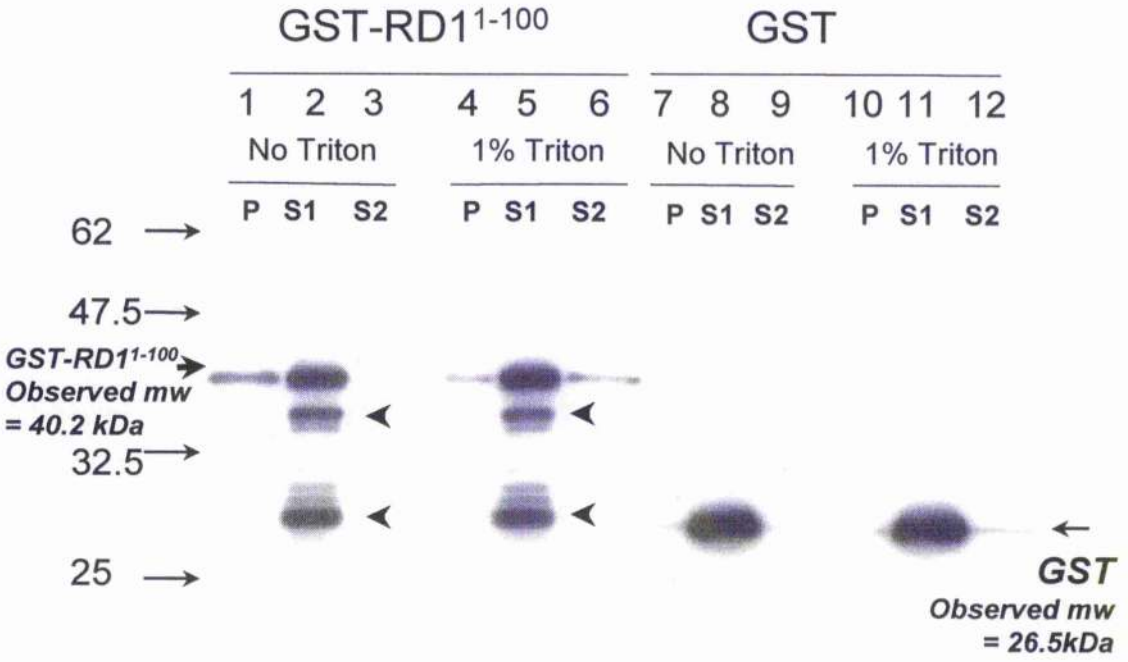

Figure 4.3 The NH_2-terminal 100 amino acids of RD1 confer P2-membrane association on the normally soluble GST.

Samples (200μg) of the P2-membrane fraction of COS-7 cells were completely resuspended in 200μl complete KHEM buffer containing either purified GST-RD1$^{1-100}$ or purified GST (50μg/ml) and incubated on ice for 1h. After incubation these mixtures were subjected to centrifugation at 100,000*g* for 30min. The unbound fractions (*S1*) from this first centrifugation step were retained. The pellets were then washed once by resuspension in complete KHEM buffer with or without 1% Triton X-100. These mixtures were then centrifuged before to yield a second supernatant fraction (*S2*). All three fractions, *S1*, *P* and *S2* were resolved by SDS-PAGE [10% (w/v) acrylamide], transferred onto nitrocellulose and immunoblotted with anti-GST antisera as primary reagent (see Methods chapter, section 2.10, Table 2.10 for the details of this antibody). Arrowheads indicate the products of GST-RD1$^{1-100}$ proteolytic degradation.

The molecular weight standards (in kDa) are shown on the left. The molecular weight of GST-RD1$^{1-100}$ predicted from its amino acid sequence is 39.0 kDa.

4.3 The NH_2-terminal region of rpde6 confers P2-membrane fraction association on the normally soluble GST

As discussed above, studies have suggested that the NH_2-terminal region of rpde6 (RNPDE4A5) is responsible for the intracellular targeting of rpde6 and its association with the particulate fractions of COS-7 cells. This hypothesis had not been tested directly. Therefore, I expressed the entire 256 amino acid NH_2-terminal region of rpde6 as a fusion to GST. I then tested this construct for association with the P2-membrane fraction of COS-7 cells. The precise location of the membrane-targeting region within the NH_2-terminus of rpde6 was investigated further by expressing the region Leu103-Lys256 as a fusion to GST. This is the region of NH_2-terminus of rpde6 that is shared with the other long rat PDE4A splice variant, rpde39 (RNPDE4A6).

4.3.1 Purification of GST-rpde6$^{1-256}$ and GST-rpde6$^{103-256}$

A schematic diagram of the constructs GST-rpde6$^{1-256}$ and GST-rpde6$^{103-256}$ is shown in Figure 4.4. These GST-fusions were over-expressed and purified as described in the Methods (section 2.7.2). Samples taken at various stages of the purification process were analysed by SDS-PAGE and Coomassie staining (Figure 4.5). The observed molecular weights for GST-rpde6$^{1-256}$ (56.2 ± 1.7) and GST-rpde6$^{103-256}$ (46.6 ± 0.5) were close to their actual molecular weights calculated from their sequences (55.4kDa and 44.0kDa,respectively). In the purification of GST-rpde6$^{1-256}$ a number of molecular weight bands were observed particularly in the 27-34kDa range which are probably the products of the proteolytic degradation of GST-rpde6$^{1-256}$.

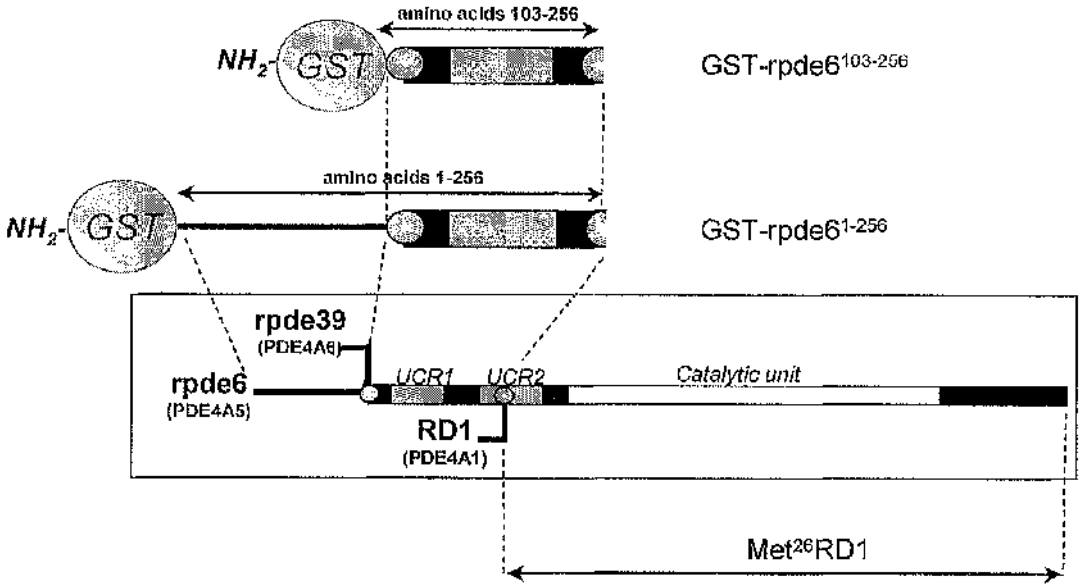

Figure 4.4 GST-rpde6$^{1-256}$ and GST-rpde6$^{103-256}$ fusion proteins

This figure illustrates the NH_2-terminal regions of rpde6 (RNPDE4A5) that were expressed as fusions to the COOH-terminus of GST. GST-rpde6$^{1-256}$ contains the entire NH_2-terminus to the core region. GST-rpde6$^{103-256}$ contains the part of the NH_2-terminus of rpde6, from the first to the second splice junction, that is shared with rpde39 (RNPDE4A6). The key to this diagram is the same as that used in Figure 4.1.

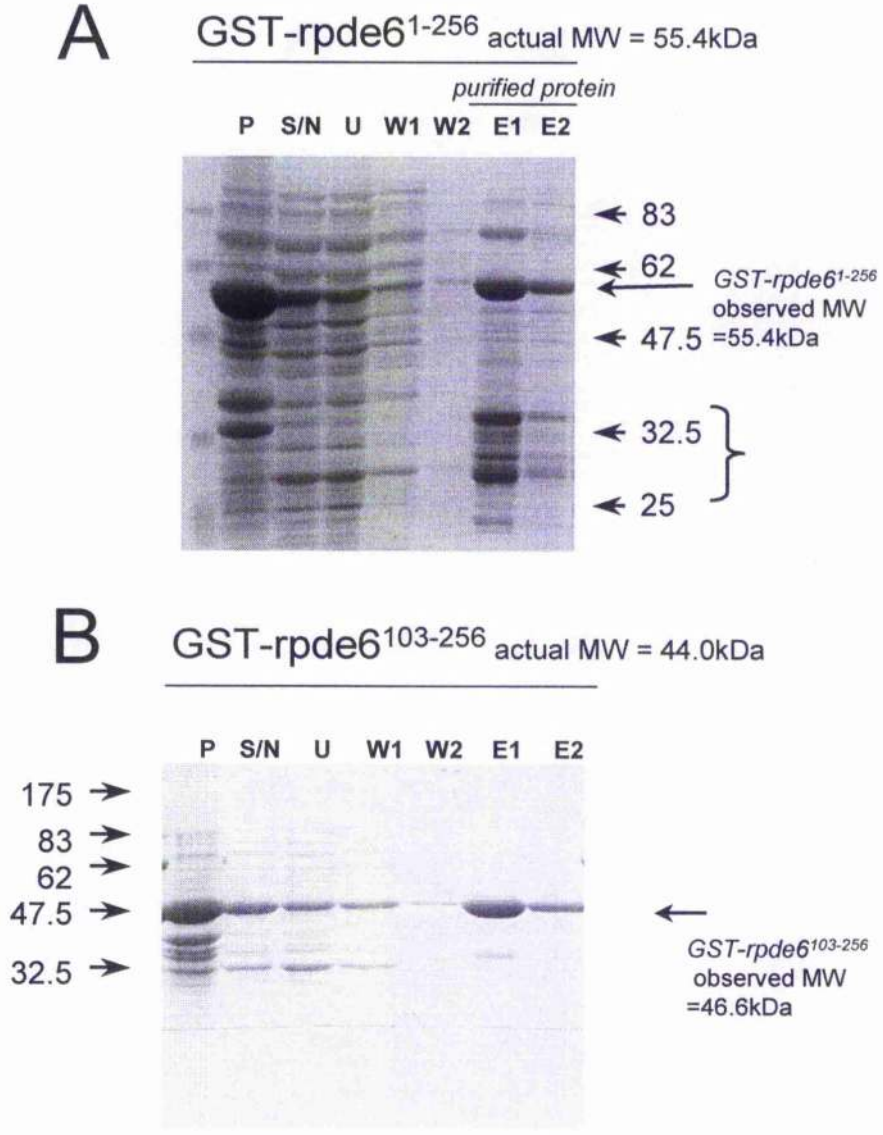

Figure 4.5 Purification of GST-rpde6$^{1-256}$ and GST-rpde6$^{103-256}$

The fusion proteins GST-rpde6$^{1-256}$ and GST-rpde6$^{103-256}$ were routinely over-expressed and purified on glutathione Sepharose using the 'batch' methods (see section 2.7.2). Samples (≤60μg) were separated by SDS-PAGE and visualised by staining with Coomassie. *C*= crude bacteria, *P*= sonicated pellet, *S/N*= sonicated supernatant, *U*= supernatant containing unbound protein after incubation with glutathione Sepharose beads. *W*= PBS wash , E1-2= elutions with glutathione buffer. Curly brackets indicate possible proteolytic degradation products (See discussion on the purification of [GST-RD1$^{1-100}$ (section 4.2.1)].

4.3.2 Binding of GST-rpde6$^{1-256}$ and GST-rpde6$^{103-256}$ to P2-membrane fraction of COS-7 cells

These constructs were tested for association with the P2-membrane fraction using the same method that was used for GST-RD1$^{1-100}$ in the previous section. Samples of purified GST-rpde6$^{1-256}$ and GST-rpde6$^{103-256}$ were incubated with samples of the P2-membrane fraction of COS-7 cells. The P2-pellets were washed several times with complete KHEM buffer. They were then separated by SDS-PAGE, transferred onto nitrocellulose and immunoblotted using anti-GST as primary reagent (Figure 4.6). Samples of each of the purified proteins were run alongside the appropriate pellets to confirm that the immunoreactive proteins in the bound fraction ran at the correct molecular weight. The lanes for the bound fractions (*B*) in Figure 4.6 show that both GST-rpde6$^{103-256}$ and GST-rpde6$^{1-256}$ associated with the P2-membrane fraction. The association of these two GST fusions was resistant to repeated washing with KHEM. In contrast GST showed no association after just one wash with KHEM buffer (see Figure 4.3, *P*, lane 7). The immunoreactive bands for GST-rpde6$^{103-256}$ and GST-rpde6$^{1-256}$ in the bound fractions (*B*) co-migrated with purified protein standards (*Sta*) at observed molecular weights of 46.6 ± 0.5 and 56.2 ± 1.7 respectively (mean ± SE, n=3).

Therefore, these results indicate that the NH_2-terminus of rpde6 can target the normally cytosolic GST to the high-speed P2-membrane fraction of COS-7 cells. Furthermore, these results suggest that the region from residues Leu103 to Lys256 in rpde6 is sufficient for membrane association and that the unique NH_2-terminal splice region and the core region are not necessary for this association. Unfortunately, studies on the membrane association of the unique NH_2-terminal splice domain of rpde6 were prevented by the susceptibility of the GST-rpde6$^{1-94}$ construct to proteolytic degradation.

Intriguingly, the 103-256 region of rpde6 contains UCR1, which is shared by all long PDE4 splice variants. It should be noted that all the long forms that have been analysed so far associate with the particulate fractions, P1 and P2, of transfected COS-7 cells, to varying degrees (Bolger et al., 1997; Bolger et al., 1996; Huston et al., 1997). In addition to the UCR1 region, there is a ~25 amino acid region upstream of UCR1, extending from Gly108-Ala132 in rpde6, that is moderately conserved in a number of long forms (see Figure 4.7) (Houslay et al., 1998). Either or both of these regions may contain targeting motifs for association with P2-membrane proteins.

Interestingly, studies have shown that a deletion mutant of rpde6 (Δp7 rpde6), which lacks the NH_2-terminus to the start of UCR2 (Ser218 in Figure 4.7), associated with the P2-membrane fraction of transfected COS-7 cells (Beard and Houslay, unpublished). However, Met^{26}RD1, which was truncated to the RD1 splice junction, half way through UCR2 (see Figure 4.1), was completely soluble. These results suggested that a motif within the NH_2-terminal half of UCR2 (amino acids 218-256) was sufficient for P2-membrane fraction association.

However, this theory is not supported by the lack of particulate fraction association shown by the short splice variant HSPDE4D1 (Bolger et al., 1997) and human PDE4A truncated species HSPDE4A4C (h6.1) which have complete UCR2 regions (McPhee et al., 1999). The conformations of these particular splice domains may hide the proposed UCR2 membrane-association domains. Alternatively, other sequences upstream of the NH_2-terminal half of UCR2 mediate the P2-membrane fraction association.

It has previously been shown that the association of rpde6 with the high-speed P2 pellet fraction of COS-7 cells is resistant to washing with a combination of high salt concentrations and Triton X-100 (McPhee et al., 1995). The Triton X-100-insoluble high-speed pellet represents the cytoskeletal fraction. (El Benna et al., 1999; Jung and Moroi, 1988; Perrot-Applanat et al., 1992; Yan et al., 1995). Therefore, these results suggest that rpde6 interacts with a component of the cytoskeletal fraction of transfected COS-7 cells. If the region between amino acid residues 103 and 256 in rpde6 is responsible for P2-membrane fraction association it is possible that this region associates with a cytoskeletal protein. However, BLAST analysis of this region, using the SWISPROT database, did not reveal any significant sequence similarities with other proteins, except with other PDE4 splice variants. Therefore, this does not give us any insight into the nature of the interacting protein.

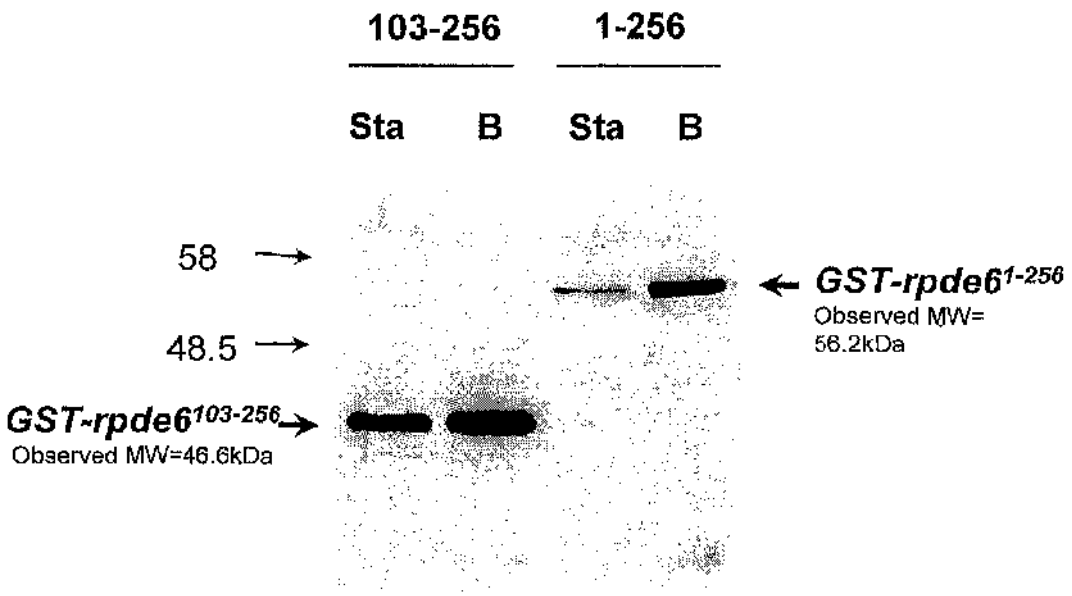

Figure 4.6 The NH_2-terminal 256 amino acids of rpde6 confer P2-membrane association on the normally soluble GST.

Samples of the P2-membrane fraction of COS-7 cells were resuspended to a concentration of 1mg/ml protein and incubated with purified GST-rpde6$^{1-256}$, or GST-rpde6$^{103-256}$ (50µg/ml) as described in the legend for Figure 4.3. After incubation, the P2-membrane pellets were recovered by centrifugation and washed three times in complete KHEM buffer (see Methods, section 2.13). The pellet fractions (*B*) were then resolved by SDS-PAGE [10% (w/v) acrylamide], transferred onto nitrocellulose and immunoblotted with anti-GST antisera as primary reagent (see Methods chapter, section 2.10, Table 2.10). As a positive control, samples of the purified GST-fusion proteins (*Sta*) were separated alongside the bound fractions.

The molecular weight markers (in kDa) are shown on the left. GST-rpde6$^{1-256}$ and GST-rpde6$^{103-256}$ have calculated molecular weights of 57.3 and 46kDa respectively.

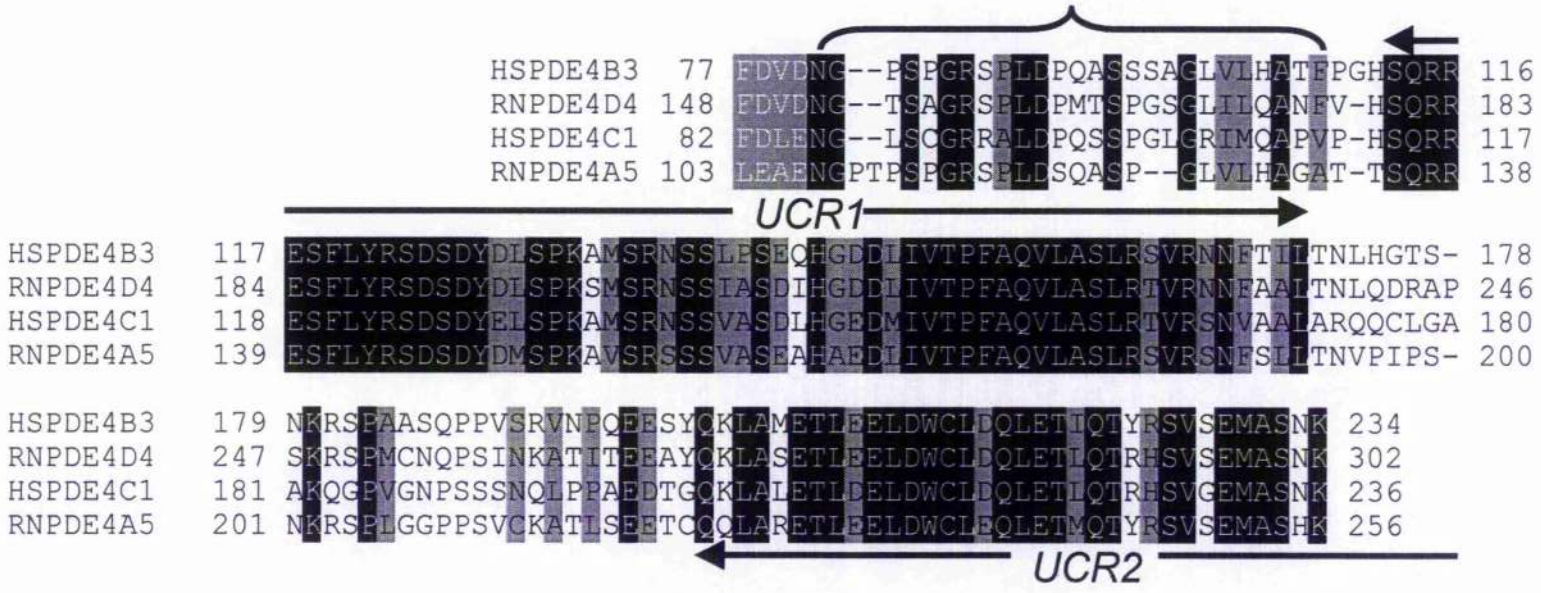

Figure 4.7 Alignment of amino acids 103-256 of rpde6 (RNPDE4A5) with the corresponding regions of other long PDE4 splice variants

The putative membrane association region of rpde6 (amino acids 103-256) was aligned with the corresponding regions from other long PDE4 isoenzymes. This region encompasses all of UCR1 and the NH_2-terminal half of UCR2. This region also contains a stretch of ~25 amino acids (curly bracket), upstream of UCR1, that is reasonably well conserved between long PDE4 splice variants. Totally conserved residues are shaded in black whereas partially conserved residues (i.e. hydrophobic, acidic, basic) are shaded in grey. The GenBank accession numbers for these splice variants are RNPDE4A5, L27057; HSPDE4B3, U85048; HSPDE4C1, Z46632; RNPDE4D4, AF031373.

4.4 The NH_2-terminal regions of rpde6 and RD1 interact with components of the P2-membrane fraction that exhibit different thermostabilities.

The thermal-stabilities of the components of the P2 fraction that interact with the NH_2-terminal regions of rpde6 and RD1 were investigated. This was does in order to gain further insight into the nature of these targeting components, which could be lipids or proteins. Therefore samples of the P2-membrane fraction were treated at 50°C for varying periods of time. This temperature was chosen as a being suitable for the denaturation of proteins as it had previously been shown to completely inactivate RD1 catalytic activity over a period of 30min (Shakur et al., 1993). The heat-treated P2 samples were incubated with the fusions GST-rpde6$^{1-256}$ and GST-RD1$^{1-100}$ as described above (sections 4.2.2 and 4.3.2). The P2-pellets were then washed several times prior to separation by SDS-PAGE and immunoblotting with anti-GST antisera in order to determine the relative amounts of fusion protein bound to each of the samples.

As shown in Figure 4.8 heat-treatment of the P2 fraction caused a marked decrease in the association of GST-rpde6$^{1-256}$. This suggested that the component(s) of the P2-membrane fraction that associated with GST-rpde6$^{1-256}$ were denatured at 50°C. Quantitative analysis of the western blots by densitometry indicated that the half-life of denaturation of these component(s) was ~23min (see Figure 4.9). The above results support the hypothesis that the NH_2-terminus of rpde6 associates with the P2-membrane fraction by interacting with one or a number of proteins that are susceptible to thermal denaturation.

In contrast, Figure 4.8 and Figure 4.9 show that no general decrease was observed in the association of GST-RD1$^{1-100}$, even after incubation of the P2-membranes at 50°C for 2h. This suggests that RD1 interacts with a relatively thermostable component of the P2-membrane fraction, possibly a lipid.

Panel *B* in Figure 4.8 provides further evidence that the NH_2-terminus of rpde6 is essential for membrane association. On this immunoblot, a sample of the purified preparation of GST-rpde6$^{1-256}$ had been run for comparison (*Sta*). The 25-33kDa immunoreactive bands probably represent truncates of GST-rpde6$^{1-256}$ where the rpde6 section of GST-rpde6$^{1-256}$ has been degraded by bacterial proteases during the purification process. It should be noted that in contrast to the full-length GST-rpde6$^{1-256}$, which runs at ~56kDa, the 25-33kDa degradation products do not bind to the P2-membrane fraction. Therefore, this further confirms that an intact rpde6 NH_2-terminal region is necessary for P2-pellet association.

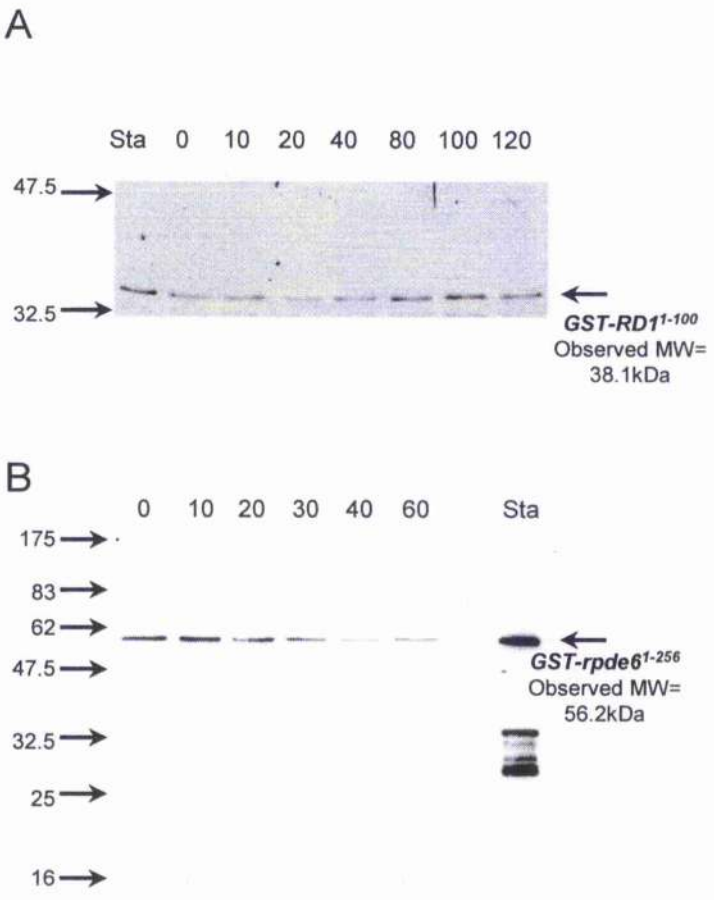

Figure 4.8 Heat treatment of the P2-membrane fraction reduces the binding of GST-rpde6$^{1-256}$ but not GST-RD1$^{1-100}$.

Equal samples (200μg) of the COS-7 cell P2-membrane fraction were resuspended in complete KHEM buffer and incubated at 50°C for the indicated periods of time (in mins). The P2 fractions were then pelleted by centrifugation (100,000*g*, 30min, 4°C) and resuspended in 50μg/ml of either *A* GST-RD1$^{1-100}$ or *B* GST-rpde6$^{1-256}$ as described in the legend for Figure 4.3. After incubation for 1h on ice, the pellets were washed 3 times in complete KHEM buffer prior to separation by SDS-PAGE [10% (w/v) acrylamide] and transferred onto nitrocellulose. The relative amounts of GST-fusion protein associated with the membrane samples were analysed by immunoblotting with anti-GST antisera as primary reagent. In panel *B* purified GST-rpde6$^{1-256}$ (*Sta*) was also immunoblotted for comparison.

GST-rpde6$^{1-256}$ and GST-RD1$^{1-100}$ have calculated molecular weights of 55.4 and 39.0kDa respectively.

These results are typical of an experiment repeated three times for GST-rpde6$^{1-256}$ and twice for GST-RD1$^{1-100}$.

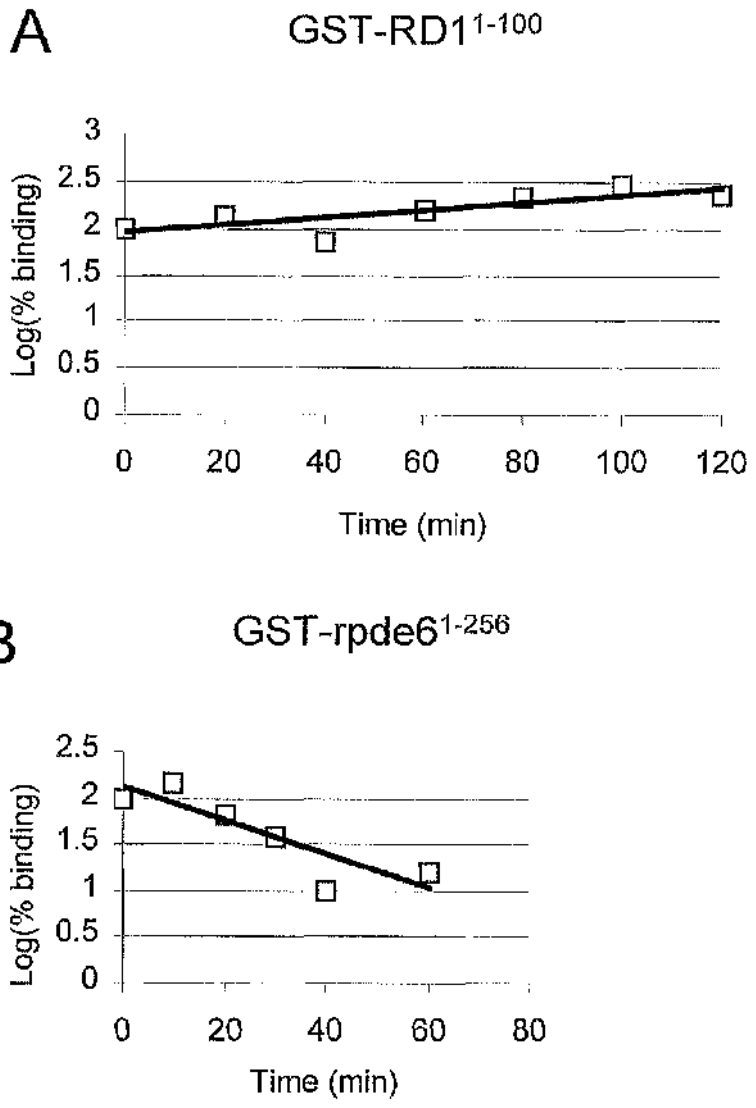

Figure 4.9 Quantitative analysis of the association of GST-rpde6$^{1-256}$ and GST-RD1$^{1-100}$ with heat (50°C) treated P2-membrane fraction

Immunoblots as shown in Figure 4.8 were scanned and analysed using Kodak imaging software. The net intensities of the immunoreactive bands were used to calculate the relative association of *A* GST-RD1$^{1-100}$ and *B* GST-rpde6$^{1-256}$ with the 50°C-treated P2-membranes. The binding values were expressed as a percentage of the association with untreated P2-membranes. The plots shown are of Log (% association) against incubation time. The half-life of denaturation for the targeting component that binds to GST-rpde6$^{1-256}$ was calculated as the treatment time that gave 50% association (NB. Log [50%] = 1.7). These results are typical of an experiment repeated three times for GST-rpde6$^{1-256}$ and twice for GST-RD1$^{1-100}$.

4.5 Discussion and conclusions

This study has shown that fusions of the NH_2-terminal regions of PDE4 splice variants to GST can be used as tools for analysing potential high speed P2-membrane association domains. The advantages of this method are that the GST fusion proteins can be prepared and purified easily and these constructs can be readily detected using anti-GST antisera. In this way different regions of PDE4 splice variants can be assessed for membrane-association in isolation from the rest of the protein. Using this method, both the NH_2-terminal 100 amino acids of RD1 and amino acids 103-256 within the NH_2-terminal region of rpde6 were shown to be sufficient for P2-membrane association.

A potential disadvantage of using GST-PDE4 fusion proteins to assess membrane binding was the susceptibility of the PDE4 parts of these fusions to degradation by bacterial proteases. However, the proteolytic degradation products of GST-RD1$^{1-100}$ and GST-rpde6$^{1-256}$ failed to associate with the P2-membrane fraction in contrast to the full-length fusion proteins. This provided further evidence that the NH_2-terminal domains of rpde6 and RD1 were necessary for P2-membrane fraction association. Therefore, in this case the presence of proteolytic degradation products was an advantage.

The NH_2-terminus of RD1 was able to associate with the P2-membrane fraction even though it was fused to the COOH-terminus of GST. Therefore, this result suggested that the RD1 NH_2-terminus does not have to be free to mediate P2-membrane fraction association.

The region Leu103- Lys256 within the NH_2-terminal region of rpde6 (RNPDE4A5) is shared with the other long rat PDE4 splice variant rpde39 (RNPDE4A6). Both these splice variants interact with P2-membrane fraction in a manner resistant to detergent and high [NaCl]. The results of my study suggest that the 103-256 region mediates interaction with the P2-membrane fraction, rather that the unique NH_2-terminal regions of rpde6 and rpde39. It should be noted that the unique NH_2-terminal splice domain of rpde6 contains the putative SH3-domain binding motifs that are believed to mediate the interaction of rpde6 with the SH3 domains of Src-family tyrosyl kinases (O' Connell et al., 1996). Therefore, rpde6 may form a complex with both a membrane-fraction targeting protein via region 103-256 and an SH3-domain containing protein via its unique NH_2-terminal splice domain.

This chapter has also shown that the analysis of the binding of these GST fusion proteins with heat-treated P2-membrane fractions could be used to assess the relative thermostabilities of the P2-membrane components that interact with the PDE4 isoforms in question. This method provides a means for determining the half-life of denaturation of the unknown targeting components. A 50°C treatment of the P2-membrane fraction had no effect on the association of GST-RD1$^{1-100}$ but reduced the binding of GST-rpde6$^{1-256}$. This implied that the NH_2-terminus of RD1 interacted with thermostable component(s) of the P2-membrane fraction. In contrast the component(s) that interacted with the NH_2-terminus of rpde6 were denatured at 50°C with a half-life of 23min.

The thermostable nature of the targeting component that binds to RD1 suggests that it might be a lipid. However, rather than having a uniform association with all cellular membranes, RD1 has a specific subcellular distribution pattern, which differs according to the cell type. In follicular thyroid carcinoma cells RD1 was observed to associate mainly with the Golgi apparatus (Pooley et al., 1997). This was also observed in COS-7 cells, but in the latter cell type a major fraction of RD1 was found to be associated with punctate vesicular structures (Shakur et al., 1995). If the target for RD1 interaction is a lipid, this lipid must have a non-uniform distribution within cellular membranes. Evidence has accumulated for the existence of lipid microdomains in cells (Brown and London, 1998). For instance lateral clusters of lipid cholesterol and sphingolipids called rafts have been shown to occur. These form specific associations with integral membrane proteins such as the IgE receptor in mast cells (Holowka et al., 2000) and the T-cell receptor in T-lymphocytes (Janes et al., 1999) and they affect downstream signalling from these receptors. It is possible that RD1 specifically interacts with a similar type of lipid microdomain. An alternative explanation for my results is that RD1 is interacting with a thermostable protein.

The thermal-denaturation of the P2-membrane fraction component that interacts with GST-rpde6$^{1-256}$ agrees with the subcellular fractionation studies and immunofluorescence microscopy studies that suggest that rpde6 is targeted to a cytoskeletal protein (Huston et al., 2000). Components of the cytoskeleton are known to be present in the P2-membrane fraction (El Benna et al., 1999; Jung and Moroi, 1988; Perrot-Applanat et al., 1992; Yan et al., 1995).

4.5.1 Suggestions for future work

The next step in this investigation is to identify the precise molecular components within the P2-membrane fraction that interact with these PDE4 splice variants. In the search for protein-interaction partners, a major problem that needs to be addressed is the insoluble nature of the P2-membrane fraction. Note that the interaction of rpde6 with the P2-membrane fraction is resistant to solubilisation with Triton X-100 detergent and high [NaCl]. Therefore, the affinity purification of interacting proteins in the P2-fraction using GST-PDE4 (NH_2-termini) fusion proteins bound to a glutathione Sepharose column cannot be performed as this method relies on there being a soluble fraction that can be passed through the column.

However, these GST-fusions could be used to probe the P2-membrane fraction by far-western blotting (Joyal et al., 1997; Tibbs et al., 1998). In this method, the proteins in the P2-membrane fraction could be separated by SDS-PAGE and transferred onto nitrocellulose. The nitrocellulose filters could then be incubated with the purified GST-PDE4 (NH_2-termini) fusion proteins as a primary probe. The filters could then be probed with anti-GST antisera followed by secondary antibody, and developed by ECL as usual. Alternatively, radiolabelled GST fusions could be used to probe the filters which could then be developed by autoradiography (Bregman et al., 1989). The signals obtained would then reveal the molecular weights of potential binding partners, as estimated from the distance of migration of the bands on the SDS-PAGE gel (Carr and Scott, 1992; Joyal et al., 1997; Scott and Gurnett, 1998). Used in conjunction with other techniques such as expression library screening and yeast-2-hybrid analysis, this information could be used to determine the precise identity of the interaction partners for these PDE4 splice variants in the P2-membrane fraction.

The identification of these binding partners and the interaction domains on the PDE4 splice variants may lead the way to drugs that disrupt the targeting and function of specific PDE4 isoenzymes that are only expressed in certain tissues. Such drugs would hopefully have very specific actions, with minimal side effects.

CHAPTER 5

The immunophilin-like protein RB3 interacts with and inhibits the PDE4 cyclic AMP-specific phosphodiesterase rpde6 (RNPDE4A5)

5. The immunophilin-like protein RB3 interacts with and inhibits the PDE4 cyclic AMP-specific phosphodiesterase rpde6 (RNPDE4A5)

CHAPTER 5 INTRODUCTION

In this chapter I have characterised the interaction between the rat PDE4 isoenzyme RNPDE4A5 (rpde6) and a novel immunophilin-like protein, RB3. RB3 was originally identified as a protein binding partner of rpde6 by Prof. Graeme Bolger (University of Utah) who used the yeast two-hybrid system to screen a rat brain cDNA library using rpde6 as a bait. In section 5.1 I have briefly described the results of this yeast-2-hybrid analysis carried out by Prof G. Bolger. In section 5.2 I have analysed the sequence and domain structure of RB3 and have reviewed work that has been published on the human and mouse homologues of this protein. In sections 5.3 to 5.13 I have described my analysis of the interaction between rpde6 and RB3. I have mapped the sites of contact on both proteins and determined the effect of RB3 on the catalytic activity of rpde6, which points towards a regulatory role for RB3 *in vivo*. In section 5.13 I have also investigated whether rpde6 interacts with FKBP52, a protein that shares homologous domains with RB3. I end the chapter in section 5.15 by discussing the implications of the rpde6:RB3 interaction on the regulation and function of rpde6 *in vivo*. For simplicity, the original name rpde6 is used rather than RNPDE4A5 throughout this chapter.

5.1 Yeast-2-hybrid analysis of rpde6

The PDE4 cyclic AMP specific phosphodiesterase isoenzyme rpde6 (RNPDE4A5) was originally cloned from a rat brain cDNA library (Bolger et al., 1994). This long form PDE4A splice variant is expressed in the cortex, hypothalamus and striatum of the brain (McPhee et al., 1995). However, as mentioned in the Introduction, section 1.8.2, the expression of rpde6 is not limited to the CNS. Recombinant rpde6 has been extensively characterised in transfected COS-7 cells in terms of its subcellular distribution, inhibition by rolipram and kinetic properties (McPhee et al., 1995). As discussed in chapter 3, the endogenous murine form of this splice variant is specifically activated by growth hormone in mouse 3T3 F442A preadipocytes (MacKenzie et al., 1998). The unique extreme NH_2-

terminal splice domain of rpde6 contains three proline-rich putative SH3 domain binding sites and confers on rpde6 the ability to interact with the SH3 domains of Src family tyrosyl kinases (O' Connell et al., 1996). To gain a greater understanding of the intracellular targeting and regulation of this splice variant, a search was made for potential protein-protein interaction partners using the yeast two-hybrid system.

As rpde6 was originally cloned from brain, it was logical to use a rat brain cDNA library in a yeast two-hybrid screen for proteins that interact with rpde6. Prof. Bolger cloned the full open reading frame of rpde6 into the *Not*1 site of pLEXAN to generate a plasmid which encodes a fusion between rpde6 and the DNA binding domain of *Escherichia coli* LexA protein (Bolger, 1998; Yarwood et al., 1999). The rat brain cDNA library that was used was cloned into the vector pGADGH that expresses proteins as fusions with the activation domain of the *Saccharomyces cerevisiae* protein GAL4. Screens of this library, using the LexA-rpde6 construct, were performed in *S. cerevisiae* strain L40 (Bolger, 1998). Positive clones were initially selected for growth in the absence of histidine and then transferred to patches and assayed for *LacZ* activity using a filter β-galactosidase assay.

5.1.1 Yeast two-hybrid analysis identified the rat homologue of ARA9/XAP2 as a protein binding partner for rpde6

The cDNA clone that was isolated using rpde6 in yeast two-hybrid screen was the rat homologue of the human protein ARA9/XAP2 (Carver and Bradfield, 1997; Kuzhandaivelu et al., 1996) and the mouse protein AIP (Ma and Whitlock, 1997). The function and characteristics of ARA9/XAP2 are discussed below in section 5.2. In this thesis, I shall refer to this rat homologue of ARA9/XAP2 by the original name of the clone, RB3 (rat brain No. 3). The predicted amino acid sequences of rat RB3 and its human and murine homologues are shown in Figure 5.1. As shown, this protein is highly conserved between species.

Using the yeast two-hybrid system, no interaction was observed between RB3 and a large variety of control baits expressed as LexA fusions (Prof. Graeme Bolger, personal communication). This panel of control baits included lamin, several kinases (including casein kinase II, ras and raf), protein phosphatases and transcription factors. The negative results from these controls suggests that the rpde6:RB3 interaction is specific. They also

demonstrate that RB3 does not exhibit intrinsic transactivation activity, i.e. it does not combine directly with the DNA binding domain, LexA, to initiate *LacZ* transcription. In addition, Prof. Bolger observed no interaction between the rpde6 bait and the above control proteins expressed as GAL4 fusions.

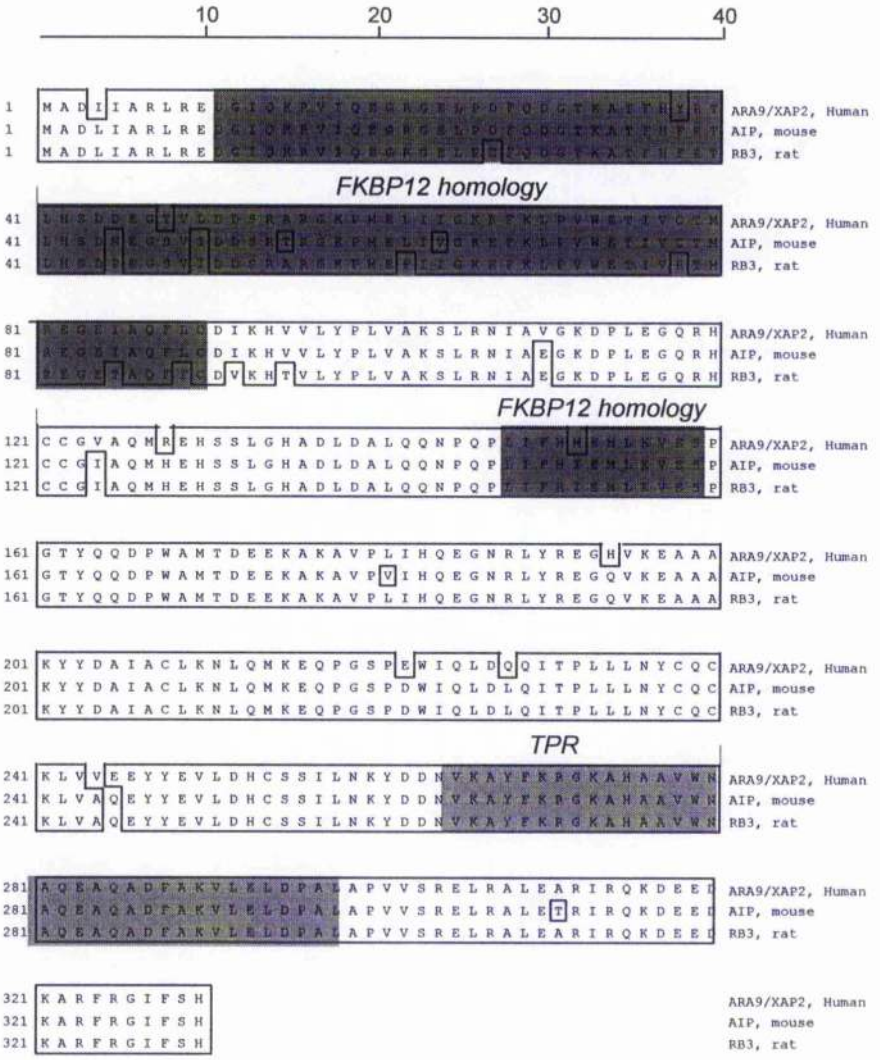

Figure 5.1 Alignment of ARA9/XAP2, AIP and RB3

This figure shows an alignment of the predicted amino acid sequences of human ARA9/XAP2 (GenBank accession No. U78521), mouse AIP (GenBank accession No. U85489) and rat RB3 cloned by Prof. Graeme Bolger (University of Utah). These homologues are highly conserved between species. The regions of homology (Asp11-Cys90 and Leu148-Ser159) with the immunophilin FKBP12, first observed by Carver and Bradfield (Carver and Bradfield, 1997), are shaded in dark grey. The TPR domain between Val265 and Leu298 is indicated by a lighter shade of grey. Amino acid numbering is shown to the left.

5.2 Characteristics of ARA9/XAP2

Several studies suggest that the expression of RB3 is not confined to the brain. The human form of RB3, ARA9 (aryl hydrocarbon receptor associated protein 9) and the mouse form of RB3, AIP (aryl hydrocarbon receptor interacting protein), were both isolated using the yeast two-hybrid system to search for proteins that interacted with the aryl hydrocarbon receptor (AhR) (Carver and Bradfield, 1997; Ma and Whitlock, 1997). The ARA9 protein was isolated from a human B-cell line cDNA library (Carver and Bradfield, 1997), whereas AIP was isolated from a mouse hepatoma cell line cDNA library (hepa1c1c7) (Ma and Whitlock, 1997). The aryl hydrocarbon receptor (AhR) is a ligand-activated transcription factor that regulates the transcription of the enzymes of xenobiotic metabolism such as cytochrome P4501A1. The function of the aryl hydrocarbon receptor is discussed below in section 5.2.1

Kuzhandaivelu et al independently discovered ARA9, using the yeast two-hybrid system, as a protein that interacts with the hepatitis B virus transcriptional activator protein X (Kuzhandaivelu et al., 1996). This group named the isolated protein XAP2 (X-associated protein 2). XAP2 appears to have a negative effect on transcriptional activation mediated by X. Another group, Meyer and Perdew, independently discovered ARA9/XAP2 as a protein that co-immunoprecipitates with AhR in COS1 cells. They subsequently cloned the simian (African green monkey) homologue of ARA9/XAP2 from COS-1 cells (Meyer et al., 1998).

As in shown in Figure 5.1, the human, mouse and rat forms of ARA9/XAP2 are all highly homologous. The human and simian forms of ARA9/XAP2 are identical. The human and mouse homologues of ARA9/XAP2 are all cytosolic proteins of around 38kDa (Carver and Bradfield, 1997; Kuzhandaivelu et al., 1996; Ma and Whitlock, 1997; Meyer et al., 1998). Northern blot analysis shows that they are ubiquitously expressed in a wide number of cell lines and tissues (Carver and Bradfield, 1997; Kuzhandaivelu et al., 1996; Meyer et al., 1998). Western blotting analysis by Meyer et al with anti-ARA9/XAP2 antibodies identified the highest levels of the ARA9/XAP2 in the mouse spleen and thymus (Meyer et al., 1998).

5.2.1 Interaction of ARA9/XAP2 with the aryl hydrocarbon receptor (AhR) and heat shock protein 90

Several independent studies have shown that ARA9/XAP2 forms a complex with AhR and the molecular chaperone heat shock protein 90 (hsp90). ARA9/XAP2 and AhR can be co-immunoprecipitated with anti-AhR antisera or anti-ARA9/XAP2 antisera (Carver and Bradfield, 1997; Ma and Whitlock, 1997; Meyer et al., 1998). Similarly, ARA9/XAP2 and hsp90 can be co-immunoprecipitated with anti-ARA9/XAP2 or anti-hsp90 antisera (Carver and Bradfield, 1997; Ma and Whitlock, 1997). There is some uncertainty over whether the presence of AhR is required for an interaction between hsp90 and ARA9/XAP2. Ma and Whitlock showed that hsp90 and AIP (the murine homologue of ARA9/XAP2) could be co-immunoprecipitated in the absence of AhR (Ma and Whitlock, 1997). However, Carver and Bradfield conversely showed that the presence of AhR was necessary for a ARA9/XAP2:hsp90 interaction (Carver and Bradfield, 1997).

As mention above, AhR is a cytoplasmic ligand-activated transcription factor, expressed in a wide range of cells. The ligands that bind to and activate AhR are polycyclic halogenated aromatic hydrocarbons (PAHs) that include the environmental toxin 2,3,7,8-tetrachlorodibenzo-*p*-dioxin (TCDD) (Schmidt and Bradfield, 1996). In the liver, ligand binding and activation of AhR results in the induction of the gene encoding cytochrome P4501A1 that oxygenates PAHs (Ma and Whitlock, 1997; Schmidt and Bradfield, 1996). Therefore, AhR appears to be a major player in mediating response of the cell to environmental pollutants.

The current model for the mode of action of AhR is as follows. In the cytoplasm, prior to ligand binding, AhR is found in a complex with a dimer of the heat shock protein 90 and a ~43kDa protein which is probably ARA9/XAP2 (Carver and Bradfield, 1997). Upon ligand binding to AhR a complex of AhR with the hsp90 dimer translocates to the nucleus where AhR dissociates from the hsp90 dimer and becomes associated with the ARNT (aryl hydrocarbon receptor nuclear translocator) (Carver and Bradfield, 1997; Meyer et al., 1998). It is not known whether ARA9/XAP2 also translocates to the nucleus. This AhR:ARNT heterodimer binds dioxin response elements (DREs) within the promoter regions of genes such as *CYP1A1* and regulates their transcription.

This model for signalling via AhR is strikingly similar to the model for signalling via steroid hormone receptors such as the glucocorticoid receptor, GR (Barnes, 1997) and the progesterone receptor, PR. These receptors mediate the effects of steroid hormones on

the transcription of specific sets of genes within cells. GR forms associations that are similar to those suggested for AhR (Silverstein et al., 1997). In the absence of glucocorticoid, cytoplasmic GR is complexed with an hsp90 homodimer and an immunophilin protein, such as FKBP52 or Cyp40 (Barnes, 1997; Carver and Bradfield, 1997). In the presence of glucocorticoid GR translocates to the nucleus and the hsp90 homodimer dissociates. Within the nucleus the GRs then dimerise. The GR homodimers associate with the glucocorticoid response elements (GREs) within the promoter regions of specific genes where they can activate or inhibit gene transcription. The models for steroid and aryl hydrocarbon receptor signalling are illustrated in Figure 5.2.

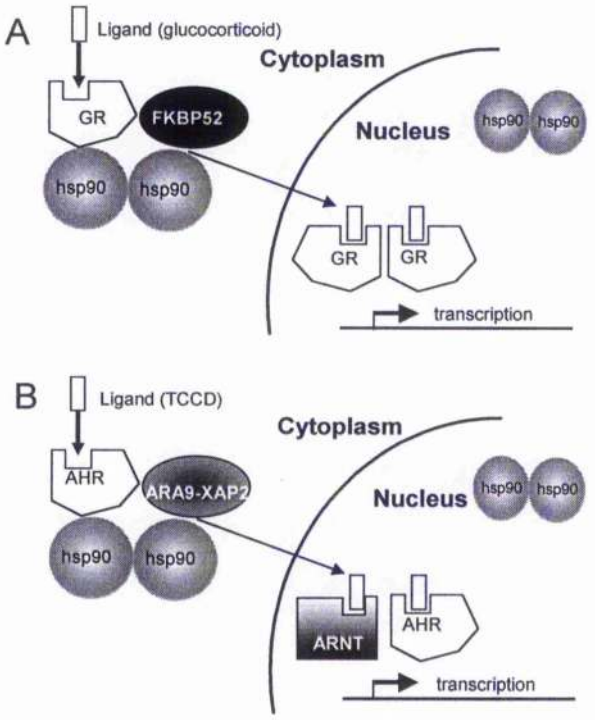

Figure 5.2 Proposed model for steroid hormone signalling.

The proposed models for glucocorticoid receptor (GR in *A*) and aryl hydrocarbon receptor (AhR in *B*) signalling are similar. In both models a ligand (either glucocorticoid or TCCD) binds to the receptor which causes the receptor-hsp90 complex to translocate to the nucleus. Once inside the nucleus hsp90 dissociates and the activated GR homodimerises or the activated AhR heterodimerises with ARNT. These complexes then bind to their cognate enhancer elements to regulate the transcription of specific sets of genes. hsp90 is essential for the function of GR and AhR (Carver and Bradfield, 1997). In GR signalling, hsp90 association increases hormone binding capacity whereas hsp90 dissociation is associated with increased DNA binding capacity (McGuire et al., 1994). The role of the immunophilin (FKBP52) component of the cytosolic GR complex maybe to target the GR complex to specific locations within the cell (Owens-Grillo et al., 1996).

5.2.2 RB3 shows homology to the FKBP-immunophilin family of proteins

The predicted amino acid sequence of RB3 is homologous to the FKBP-family of immunophilin proteins. Table 5.1 shows the results of BLAST search of the SWISSPROT protein sequence database (National Centre for Biotechnology Information) using the RB3 sequence. BLAST analysis shows that the proteins most similar to RB3 are mostly homologues of the FK506 binding proteins, FKBP52 and FKBP51. An alignment of the amino acid sequences of RB3 and FKBP52 is shown in Figure 5.3.

FKBPs form part of the immunophilin family. This family of proteins bind to the immunosuppressant fungal macrolides FK506, rapamycin, and cyclosporin A. The immunophilin family is divided into two main sub-families in eukaryotes: FK506 binding proteins (FKBP) and cyclophilins (Cyp). The cyclophilins bind cyclosporin A and range in size from about 20kDa (CypA, CypB, CypC and CypD) to 40kDa (Cyp40). FKBPs bind FK506 and rapamycin and are named according to their molecular weights, which range from 12 to 52kDa. Members of the FKBP subfamily include FKBP12, FKBP12.6, FKBP13, FKBP25, FKBP51 and FKBP52. Despite having similar functions in cells, cyclophilins and FKBPs have different 3 dimensional structures and their sequences do not align.

Immunophilins are found to be conserved throughout a wide range of organisms including plants and prokaryotes (Kay, 1996; Marks, 1996). Both families exhibit an enzyme activity known as peptidyl prolyl *cis-trans* isomerase activity (otherwise known as PPIase or rotamase activity). In FKBP proteins the PPIase active site is located in the FKBP homology region. PPIase enzymes catalyse the rotation of the C-N bond on the NH_2-terminal side of proline residues in proteins (Kay, 1996). This suggests that immunophilins might regulate protein folding in the cell (Fruman et al., 1994) although this has not been demonstrated *in vivo*. The PPIase activity of immunophilins is inhibited by the immunosuppressant drugs they bind. The amino acid residues in FKBP12 that interact with FK506 are also components of the PPIase active site (Michnick et al., 1991; Van Duyne et al., 1991). As yet, no physiological function has been defined for the PPIase activity of FK506 binding proteins in cells (Fruman et al., 1994; Kay, 1996; Marks, 1996).

The immunosuppressant compounds FK506, rapamycin and cyclosporin A, that bind immunophilins, have been used to prevent tissue rejection following organ transplantation (Marks, 1996). One mechanism for immunosuppression has been

established for FK506 and cyclosporin A. The immunophilin:drug complexes FKBP12:FK506, CypA:CsA and CypB:CsA have been shown to bind to and inhibit the Ca^{2+} and calmodulin-dependent protein phosphatase calcineurin (otherwise known as protein phosphatase 2B) (Liu et al., 1991). Inhibition of calcineurin prevents the dephosphorylation of the nuclear factor of activated T-cells (NF-AT). This prevents the translocation of NF-AT to the nucleus where it activates a number of immune response genes including the gene for the cytokine IL-2 (Fruman et al., 1994). This mechanism is illustrated in Figure 5.4. Therefore, immunophilin:drug complexes are directly involved in immunosuppression.

As mentioned above (section 5.2.1), immunophilin proteins such as FKBP52 (Czar et al., 1994), FKBP51 (Nair et al., 1997) and Cyp40 (Owens-Grillo et al., 1996) form complexes with steroid hormone receptors *in vivo*. A model has been proposed where these immunophilins are involved in the targeting and movement of these complexes to specific regions within the cell (Owens-Grillo et al., 1996; Pratt et al., 1999). For instance, FKBP52 is found in the both the cytoplasm (~20%) and the nucleus (~80%). Cytoplasmic FKBP52 has been localised to microtubules (Czar et al., 1994; Owens-Grillo et al., 1996; Perrot-Applanat et al., 1995) which suggests that it may be associated with the trafficking machinery of the cell. In addition, the distribution of nuclear FKBP52 overlaps that of the steroid receptor, GR (Czar et al., 1994). These observations provide circumstantial evidence that FKBP52 is involved in the cytoplasmic-nuclear trafficking of GR.

The similarity between RB3 and FKBP52 suggests that RB3 may play a role in AhR signalling analogous to FKBP52 in GR signalling. Ma and Whitlock suggest that the mouse homologue of RB3, AIP, may be involved in the nuclear targeting of AhR although their is no evidence that AIP translocates to the nucleus at any stage (Ma and Whitlock, 1997).

Table 5.1 The first 8 closest homologues of RB3 ranked in order of their similarity to the RB3 sequence

Homologue	Species[a]	Similarity Score (bits)	Expect (E) value[b]
FKBP52	Rabbit (*Oryctolagus coniculus*)	72	1×10^{-12}
FKBP52	Human (*Homo sapiens*)	71	4×10^{-12}
70kDa PPIase	Wheat (*Triticum aestivum*)	68	2×10^{-11}
FKBP52	Mouse (*Mus musculus*)	62	1×10^{-9}
FKBP51	Human (*Homo sapiens*)	62	2×10^{-9}
FKBP51	Mouse (*Mus musculus*)	59	9×10^{-9}
Cyp40	Cattle (*Bos taurus*)	45	4×10^{-4}
TOM70, mitochondrial protein transporter	Yeast (*Saccharomyces cerevisiae*)	44	4×10^{-4}

(a) Note that the human, mouse and simian homologues of RB3 have been omitted from the list.

(b) The E value is a measure of statistical significance

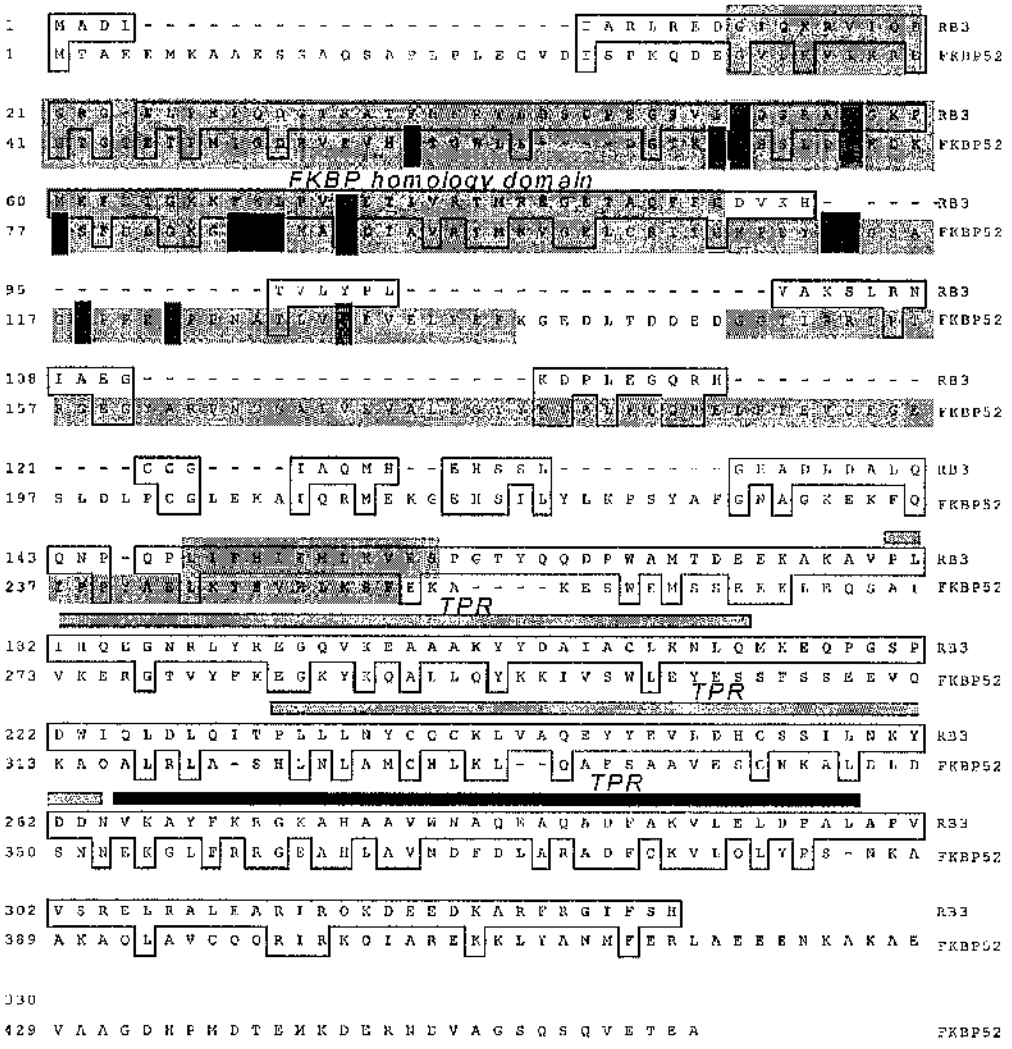

Figure 5.3 Sequence alignment of FKBP52 and RB3

This figure shows an alignment of rat RB3 with rat FKBP52 (GenBank accession No. P27124). The amino acid residue positions are shown on the left. Amino acid residues in FKBP52 that are identical to those in RB3 are boxed. The regions homologous to the FKBP-domain consensus are shaded in light grey. Residues shaded in darker grey are components of the FK506 binding site (Van Duyne et al., 1991). These residues are also components of the PPIase active site (Kay, 1996). The TPR region shared between FKBP52 and RB3 (Val265 to Leu298 in RB3) is overlined with a black bar. The other two TPR domains of FKBP52 are overlined with grey bars.

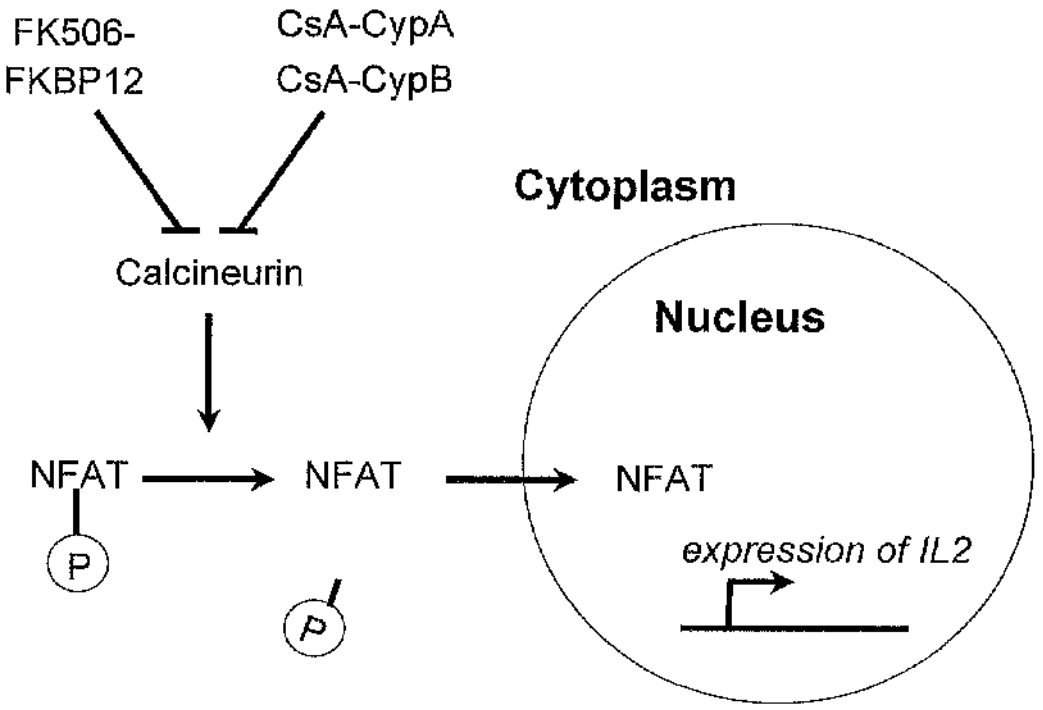

Figure 5.4 One mechanism for the immunosuppressive actions of FK506 and cyclosporin A (CsA)

The immunophilin:drug complexes FKBP12:FK506, CypA:CsA and CypB:CsA bind to and inhibit the Ca^{2+}/ CaM-dependent protein phosphatase calcineurin, which prevents the dephosphorylation of the nuclear factor of activated T-cells (NF-AT). Phosphorylated NF-AT is unable to enter the nucleus. Inhibition of calcineurin by FKBP12 or CsA therefore prevents the NF-AT-dependent regulation of a number of immune response genes, including the gene for IL-2.

5.2.3 Analysis of the predicted amino acid sequence of RB3

Figure 5.5 shows a schematic comparison of the domain structure of RB3 with its closest relative FKBP52. Note that an amino acid sequence alignment of these two proteins was shown in Figure 5.3 in the previous section. FKBP52 and RB3 share a number of structural features, which are discussed in the sections below. Most notably, both FKBP52 and RB3 have FKBP homology domains found towards their NH_2-termini and TPR repeats in their COOH-terminal regions.

5.2.3.1 The FKBP homology domain

FK506 binding proteins contain domains, called FKBP domains. The FKBP domain consensus was generated from a comparison of 30 protein sequences from eukaryotes and prokaryotes (Kay, 1996). Two or three copies of this domain are found in certain family members. FKBP12 essentially consists of one FKBP-domain. In Figure 5.5 black rectangles indicate regions homologous to FKBP12 in FKBP52 and RB3. RB3 has two regions of similarity to FKBP12, (amino acids 11-90 and 148-159) whereas FKBP52 appears to contain two complete FKBP domains (amino acids 32-137 and 148-252) (see also Figure 5.3). In FKBP proteins these FKBP homology domains contain the PPIase active site which binds to FK506. The 14 residues identified as components of the FK506 binding/PPIase site (Kay, 1996; Van Duyne et al., 1991) in FKBP52 have been highlighted in grey in Figure 5.3. An alignment of FKBP52 with RB3 suggests that only 3 out of the 14 component residues are conserved in RB3. A similar alignment of RB3 with FKBP12 indicates that only 5 of the 14 FK506 binding residues are conserved in RB3 (Carver et al., 1998). These results suggest that RB3 may not bind FK506 or have PPIase activity.

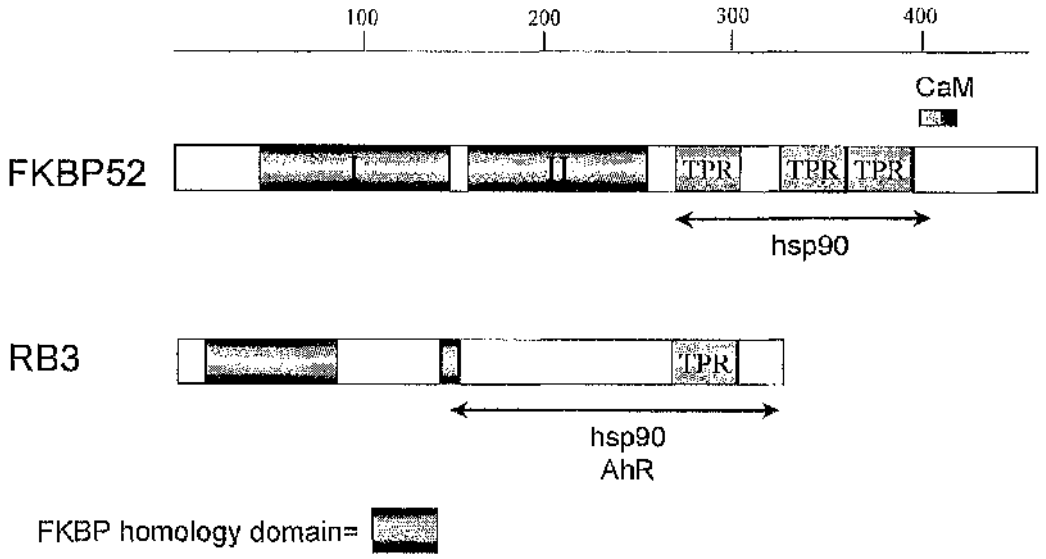

Figure 5.5 Domain structure of RB3 and FKBP52

This figure shows a schematic representation of the domain structures of RB3 and its closest homologue, FKBP52. Black blocks indicate regions of homology to the FKBP domain consensus (Kay, 1996). The grey blocks indicate the positions of the TPR motifs and double-headed arrows mark out the regions that have so far been shown to be necessary for interaction with hsp90 (and AhR in the case of RB3). A scale indicating the number of amino acid residues is shown at the top of the diagram. No attempt has been made here to align the schematic structures of these two proteins.

5.2.3.2 The TPR domain and interaction with hsp90

The closest relative of RB3, FKBP52 has been shown to contain three tetratricopeptide repeats (TPRs) in its COOH-terminal region. As discussed in the Introduction (section 1.11.4) these are 34 amino acid regions that are found in wide range of proteins (Goebl and Yanagida, 1991; Hirano et al., 1990; Lamb et al., 1995; Sikorski et al., 1990). TPR domains are believed to be involved in protein-protein interactions (Lamb et al., 1995). The consensus sequence, generated from a comparison of TPR repeats from five different proteins, is shown in Figure 5.6. Note that the consensus sequence is highly degenerate (Goebl and Yanagida, 1991).

The groups that cloned the RB3 human form, ARA9/XAP2 (Carver and Bradfield), and the RB3 mouse form, AIP (Ma and Whitlock) suggest that RB3 contains 3 TPR repeats (Carver and Bradfield, 1997; Ma and Whitlock, 1997). However, only one of these TPR motifs between amino acids 265 and 298 closely matches the consensus (see Figure 5.6). This is the only TPR identified by Meyer et al who cloned the simian homologue of RB3 (XAP2) from COS-1 cells (Meyer et al., 1998). An alignment of this region of RB3 with the TPR consensus is shown in Figure 5.6.

Note that Ma et al and Carver et al disagree on the location of the other two TPR regions. Ma and Whitlock state the positions as amino acids 118-152 (TPR1) and amino acids 205-239 (TPR2) (Ma and Whitlock, 1997). Carver and Bradfield state the positions as amino acids 182-215 (TPR1) and amino acids 234-268 (TPR2) (Carver and Bradfield, 1997). However, in all these regions the similarity of these sequences to the TPR consensus is only very slight. Therefore, for the remainder of this chapter, I shall work on the assumption that RB3 contains only one TPR motif located between amino acids 265 and 298 (see Figure 5.5). As shown by Meyer et al, this third TPR is very similar to the third TPR domain of FKBP52 (see Figure 5.3) (Meyer et al., 1998).

In addition to FKBP52, TPR domains containing three repeats have been identified in the FKBP proteins FKBP51 (Young et al., 1998), FKBP52 (Callebaut et al., 1992) and Cyp40 (Ratajczak and Carrello, 1996). These TPR domains have been shown to mediate interaction with the molecular chaperone hsp90 (Carrello et al., 1999; Nair et al., 1997; Owens-Grillo et al., 1996; Peattie et al., 1992; Perrot-Applanat et al., 1995; Prodromou et al., 1999). Deletion mapping studies in all three immunophilins have shown that the TPR region is required for interaction with the molecular chaperone hsp90 (see Figure 5.5).

Carver and coworkers showed that the COOH-terminal half of ARA9/XAP2, from amino acids 154 to 330, which contains the TPR motif, interacts with AhR and hsp90 *in vitro*. This result points to a possible role for this single TPR motif in an interaction with hsp90. However, more recently, Meyer and Perdew have shown that deletion of the COOH-terminus downstream of the TPR motif (amino acids 299-330) abolishes association with hsp90. Therefore it appears that the TPR motif may be necessary, but not sufficient, for interaction with hsp90. Carver and coworkers also showed that this region of ARA9/XAP2 mediates interaction with AhR as well (Carver et al., 1998) (see Figure 5.5).

5.2.3.3 Interaction of RB3 with calcineurin

As discussed earlier, FKBP12-FK506 can bind to and inhibit the protein phosphatase calcineurin. A number of other immunophilin-drug complexes can also associate with calcineurin including FKBP51-FK520 (Baughman et al., 1995) and cyclophilin-CsA (Liu et al., 1991). The possibility that RB3 interacts with calcineurin is discussed later in this chapter (section 5.7.3).

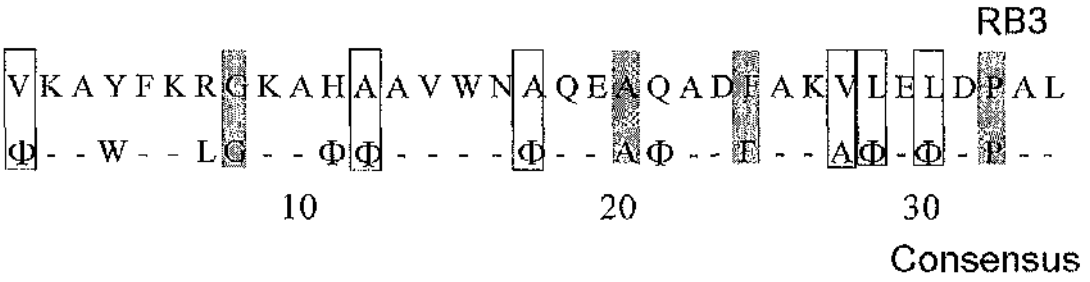

Figure 5.6 Alignment the TPR motif of RB3 with the consensus

The top line shows the sequence of the TPR domain of RB3 from Val265 to Leu298. The bottom line shows the consensus TPR sequence derived from alignments of TPR domains from CDC27, CDC23, CDC16, SSN6 and SKI3 (Das et al., 1998; Lamb et al., 1995). RB3 residues that match the consensus residues precisely are shaded in grey. Residues that are similar in terms of their hydrophobicity are boxed. Φ = hydrophobic residue

5.3 Characterisation of the interaction between RB3 and rpde6

It is widely recognised that the yeast two-hybrid system is prone to false positives. Even though a number of controls were carried out to test the specificity of the rpde6:RB3 interaction in yeast (section 5.1.1 above) it is important use alternative methods to confirm and extend results from these yeast two-hybrid analyses.

I used a GST fusion system to analyse the interaction between RB3 and rpde6 expressed in COS-7 cells. Initially I examined whether purified full-length RB3, fused to GST and immobilised on glutathione Sepharose beads, could 'pull down' rpde6 from the cytosolic fraction of rpde6-transfected COS-7 cells. The approach I have used here is similar to the one successfully used to demonstrate an interaction between the SH3 domains of Src family tyrosyl kinases and rpde6 (O' Connell et al., 1996; Scotland et al., 1998).

COS-7 cells were used to express rpde6 as these allow high levels of expression of transiently transfected PDE4 isoenzymes and they exhibit very low levels of endogenous PDE activity (Scotland et al., 1998). In my hands, the cytosolic fraction from rpde6 transfected COS-7 cell typically exhibited a PDE activity of 0.75-1.05nmol (cAMP)/min/mg protein. Cytosolic fractions from mock transfected COS-7 cells always exhibited an activity <5% of the activity from rpde6 transfected COS-7 cells.

An insert for the coding region of RB3 was cloned into the *Not1* site of a pGEX-5X-3 vector by Prof. Bolger. In *E.coli* this construct (GST-RB3$^{1-330}$) expresses full length RB3 fused to the COOH-terminal end of GST. I over-expressed and purified GST-RB3$^{1-330}$ and GST in *E. coli* as described in the methods (section 2.7). In order to assess the purity of these preparations, samples of the purified GST-RB3$^{1-330}$ and GST were separated on an SDS-PAGE gel (12%[w/v] acrylamide) and visualised by Coomassie blue staining. As shown in Figure 5.9 bands of the correct predicted molecular weights for GST-RB3$^{1-330}$ (65kDa) and GST (27kDa) were observed in the appropriate lanes. Bands corresponding to proteolytic degradation products or contaminating bacterial proteins were not observed in these lanes.

I then incubated purified GST-RB3$^{1-330}$ bound to glutathione Sepharose beads with cytosol from rpde6-transfected COS-7 cells diluted in complete KHEM buffer. GST was

used in the same manner as a control. I then washed the beads with complete KHEM buffer and eluted the bound protein with glutathione buffer (see Methods chapter, section 2.17). This process was repeated for GST as a control. Samples of the bound fractions (eluted protein) and the unbound fractions (washes) were separated by SDS-PAGE, transferred onto nitrocellulose and immunoblotted for PDE4A.

As shown in Figure 5.7, rpde6 becomes associated with GST-RB3$^{1-330}$ immobilised on glutathione Sepharose beads. An immunoreactive band running at 108 ± 3kDa (mean ± S.E., n = 3), which corresponds closely with the published observed molecular weight for rpde6 of 109kDa (McPhee et al., 1995), was observed in the bound fraction for GST-RB3$^{1-330}$. This association of GST-RB3$^{1-330}$ with rpde6 appeared to be specific; only an extremely faint band was observed in the bound fraction for GST. Therefore, the presence of RB3 was absolutely necessary for binding of rpde6 to occur. This result was the first demonstration of an interaction between rpde6 and RB3 *in vitro*. It strongly suggested that the rpde6:RB3 interaction was not an artefact of the yeast two-hybrid system.

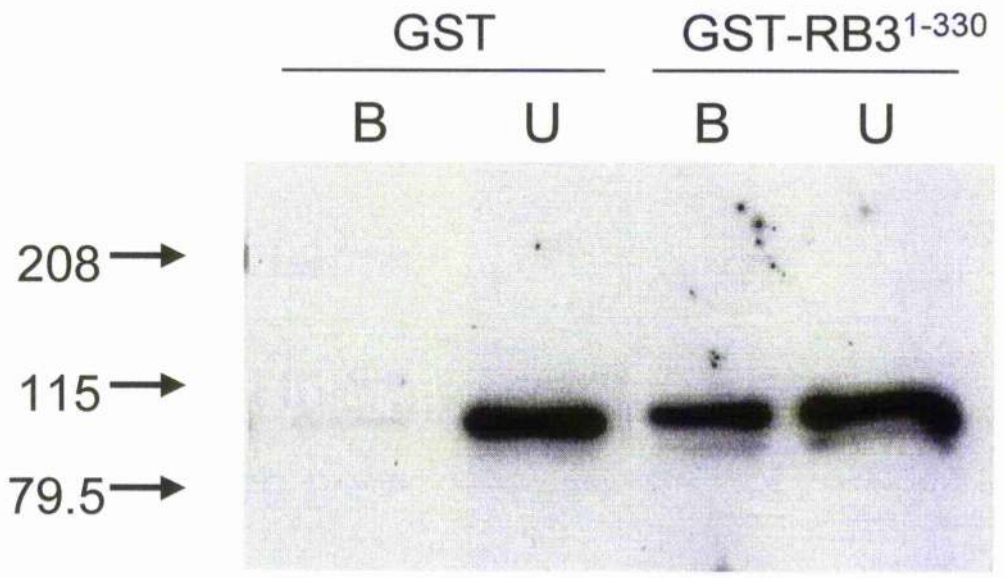

Figure 5.7 Cytosolic rpde6 from transfected COS-7 cells binds to RB3 *in vitro*.
A pull down assay was carried out to assess the binding of rpde6 to RB3 *in vitro* as described in the Methods chapter (see section 2.17). Samples of cytosol, containing 100 EU of PDE activity, from COS-7 cells transiently transfected with a plasmid encoding rpde6 (pSV.SPORT-rpde6) were incubated for 30min with 200µg of GST-RB3$^{1-330}$ or GST (control) bound to glutathione Sepharose beads. The beads were pelleted by centrifugation and washed with 3 x 400µl complete KHEM buffer by resuspension and centrifugation. The supernatants were retained and pooled to produce an unbound fraction. Bound protein was eluted with 3 x 100µl 10mM glutathione, 50mM Tris-HCl pH 8.0. Samples of the bound (B) fraction (20µl) and the unbound (U) fraction (4µl) were then separated on an SDS-PAGE gel (10% [w/v] acrylamide). The separated proteins were transferred onto nitrocellulose and probed for rpde6 using anti-PDE4A polyclonal antibody as primary reagent. The standard molecular weights in kDa are shown on the left. This result is typical of an experiment carried out three times.

5.4 Locating the binding region for rpde6 on RB3

As mentioned above in section 5.2.3, RB3 contains regions of similarity to FKBP12 in its NH_2-terminal half and a TPR motif in its COOH-terminal half. Having demonstrated that an interaction occurs between RB3 and rpde6 under the conditions of the above pull down assay I went on to determine which region of RB3 is responsible for this interaction.

Constructs encoding GST fusions of the NH_2-terminal half of RB3 (GST-RB3$^{1-169}$) or the COOH-terminal half of RB3 (GST-RB3$^{170-330}$) fused to the COOH terminus GST were prepared by Prof. Bolger in pGEX-5X-3 (the regions fused to GST are illustrated in Figure 5.8). I over-expressed and purified GST-RB3$^{1-169}$ and GST-RB3$^{170-330}$ in *E. coli* as described in the methods (section 2.7). Samples of the GST-RB3$^{1-169}$ and GST-RB3$^{170-330}$ were separated on an SDS-PAGE gel (10%[w/v] acrylamide) and visualised by Coomassie blue staining. As shown in Figure 5.9, bands close to the predicted molecular weights for GST-RB3$^{1-169}$ (47kDa) and GST-RB3$^{170-330}$ (46kDa) were observed in the appropriate lanes. No proteolytic degradation products or contaminant bacterial proteins were observed in these preparations.

A comparison of the binding of rpde6 to the three GST-RB3 fusions, GST-RB3$^{1-169}$ (NH_2-terminal half), GST-RB3$^{170-330}$ (COOH-terminal half), GST-RB3$^{1-330}$ (full length) and GST was made using the pull down assay method described in the previous section (5.3) and the Methods (section 2.17). Samples (200μg) of the GST-fusion proteins or GST were immobilised on glutathione Sepharose beads and were incubated with cytosolic rpde6 (100 EU) for 30min at 4°C. The beads were then pelleted and washed several times with complete KHEM buffer. The supernatant and washes were retained and pooled to produce an unbound fraction. Bound protein was eluted with glutathione buffer. To determine the percentage binding of rpde6 to the various GST-RB3 fusions, samples of the bound and unbound fractions were assayed for PDE activity.

The results presented in Figure 5.10 again showed that rpde6 specifically associated with a GST-fusion of full length RB3 (GST-RB3$^{1-330}$) and that essentially no association was seen with GST. In addition rpde6 associates with a GST fusion of the COOH-terminal half of RB3 (GST-RB3$^{170-330}$). In contrast to this, negligible binding was observed between rpde6 and the NH_2-terminal half of rpde6 fused to GST (GST-RB3$^{1-169}$). The results suggest that regions within the COOH-terminal half of RB3 may mediate association with rpde6.

The above results for the percentage binding of rpde6 to the three GST-RB3 fusions, presented in Figure 5.10, were determined on the basis of rpde6 enzyme activity in the bound and unbound fractions. To confirm these results the percentage binding was determined on the basis of rpde6 immunoreactivity in these fractions. Samples of the bound and unbound fractions from the above pull down assay were separated by SDS-PAGE, transferred onto nitrocellulose and immunoblotted with anti-PDE4A polyclonal antibody. The amount of rpde6 in the bound and unbound fractions was determined from the density of the bands obtained. The results obtained for this immunoblot analysis are presented in Figure 5.11. These results reflected the results obtained from the analysis of PDE activity in the bound and unbound fractions (Figure 5.10). They again showed significant association of rpde6 with full length RB3 (GST-RB3$^{1-330}$) and the COOH-terminal half of RB3 (GST-RB3$^{170-330}$) negligible association with GST-RB3$^{1-169}$ and no association with GST.

This result is again shown in a representative immunoblot for the binding of rpde6 to the NH_2- and COOH-terminal halves of RB3 (see Figure 5.12). This again shows the COOH-terminal half of RB3 (amino acids 170-330) pulls down cytosolic rpde6 whereas the NH_2-terminal half (amino acids 1-169) does not. We can therefore hypothesise that RB3 associates with rpde6 via its COOH-terminal half.

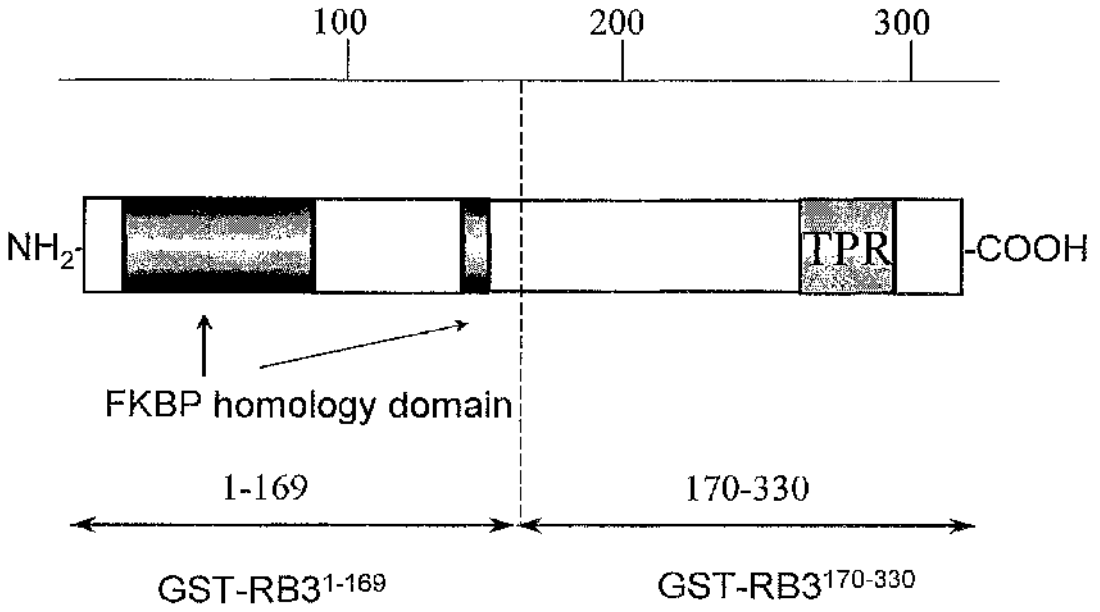

Figure 5.8 GST-fusions of the NH_2- and COOH-terminal halves of RB3

To assess which region of RB3 interacts with rpde6, constructs encoding the NH_2- or COOH-terminal halves of RB3 fused to GST were prepared in pGEX-5X-3. As described in section 5.2.3, the NH_2-terminal portion (amino acids 1-169) contains the region homologous to the FKBP domain. The COOH-terminal region (amino acids 170-330) contains a TPR motif. These GST-fusions were used in pull down experiments to test for interaction with rpde6.

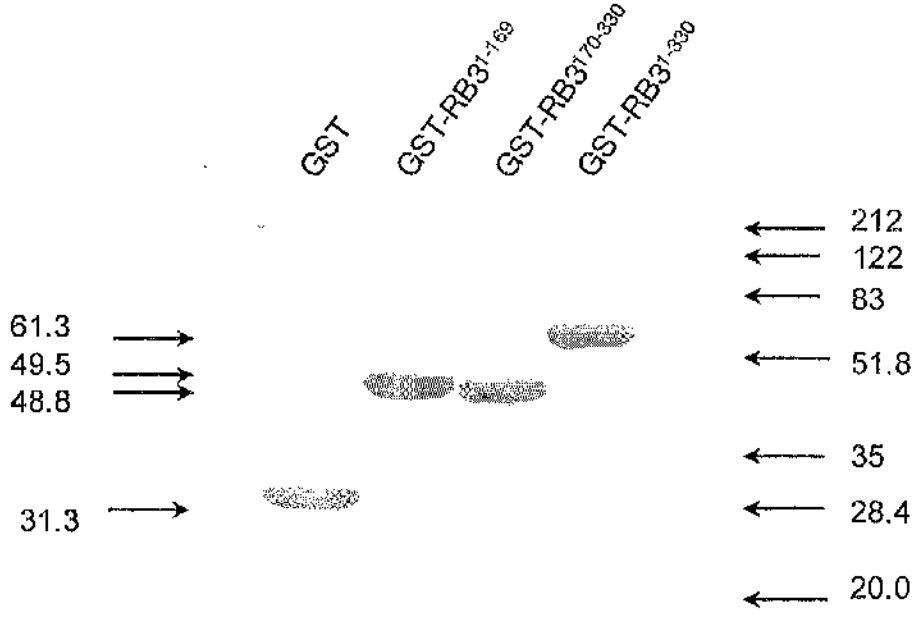

Figure 5.9 Purification of GST, GST-RB3$^{1-330}$, GST-RB3$^{1-169}$ and GST-RB3$^{170-330}$. GST fusions of full length RB3 (amino acids 1-330) and the NH_2- and COOH-terminal halves of RB3 were over-expressed in *E. coli* and purified as described in the methods (see section 2.7). Samples (10μg) of the GST fusions were separated on an SDS-PAGE gel (10% [w/v] acrylamide). The observed molecular weights (in kDa) of these GST-fusion proteins (shown on the left) corresponded closely with their actual molecular weights, which were as follows: GST, 27.4kDa; GST-RB3$^{1-169}$, 46.6kDa; GST-RB3$^{170-330}$, 45.9kDa and GST-RB3$^{1-330}$, 65.0kDa.

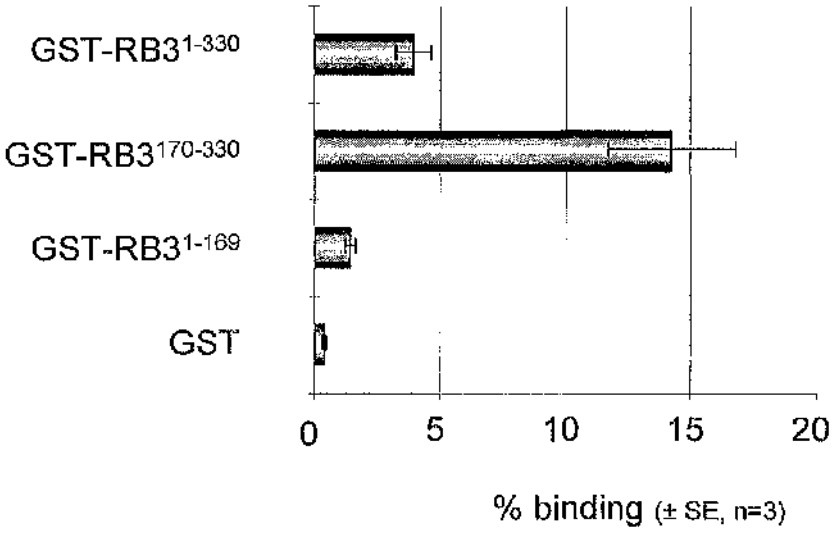

Figure 5.10 GST-RB3$^{170-330}$ but not GST-RB3$^{1-169}$ pulls down rpde6: (PDE activity data)

This chart shows the relative binding of the rpde6 to the following GST fusions: GST-RB3$^{1-169}$ (NH_2-terminal half of RB3, amino acids 1-169), GST-RB3$^{170-330}$ (COOH-terminal half of RB3, amino acids 170-330), GST-RB3$^{1-330}$ (full length RB3, amino acids 1-330) and GST alone. Samples of cytosolic (S fraction) rpde6 from transiently transfected COS-7 cells, containing 100EU PDE activity, were incubated with 200µg samples of the above fusion proteins immobilised on glutathione Sepharose beads for 30min at 4°C as described in the Methods chapter, section 2.17. The beads were pelleted and washed with ice-cold complete KHEM buffer and the resultant supernatants were combined to form an unbound fraction. Bound protein was eluted with 10mM glutathione, 50mM Tris pH 8.0. The total PDE activity in the bound (EU_{BOUND}) and unbound ($EU_{UNBOUND}$) fractions was determined using the PDE assay. The percentage of rpde6 that was 'pulled down' by the GST-fusions under the experimental conditions described was calculated as follows:

% binding = 100% x [EU_{BOUND} / (EU_{BOUND}+ $EU_{UNBOUND}$)].

The percentage binding values are shown as the means of three experiments ± S.E.

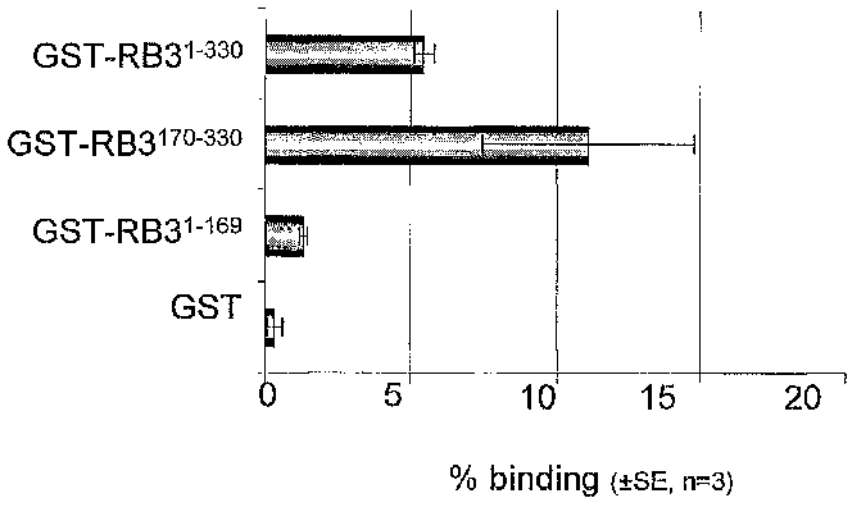

Figure 5.11 GST-RB3$^{170-330}$ but not GST-RB3$^{1-169}$ pulls down rpde6: (quantitative western blot analysis)

The % binding of rpde6 to GST-RB3 fusions was re-assessed by measuring rpde6 immunoreactivity in the bound and unbound fraction from the pull down assay described in the legend for Figure 5.10. Samples of the bound and unbound fractions were run on an SDS-PAGE gel, transferred onto nitrocellulose and immunoblotted for RB3. The immunoblots were scanned and the net densities of the rpde6 immunoreactive bands were plotted against the sample volume run for both the bound and unbound fractions. This was used to calculate the % binding of rpde6 to the GST-fusions. This procedure is described in detail in the Methods chapter, section 2.17.1. The % binding values are the means of three experiments ± S.E.

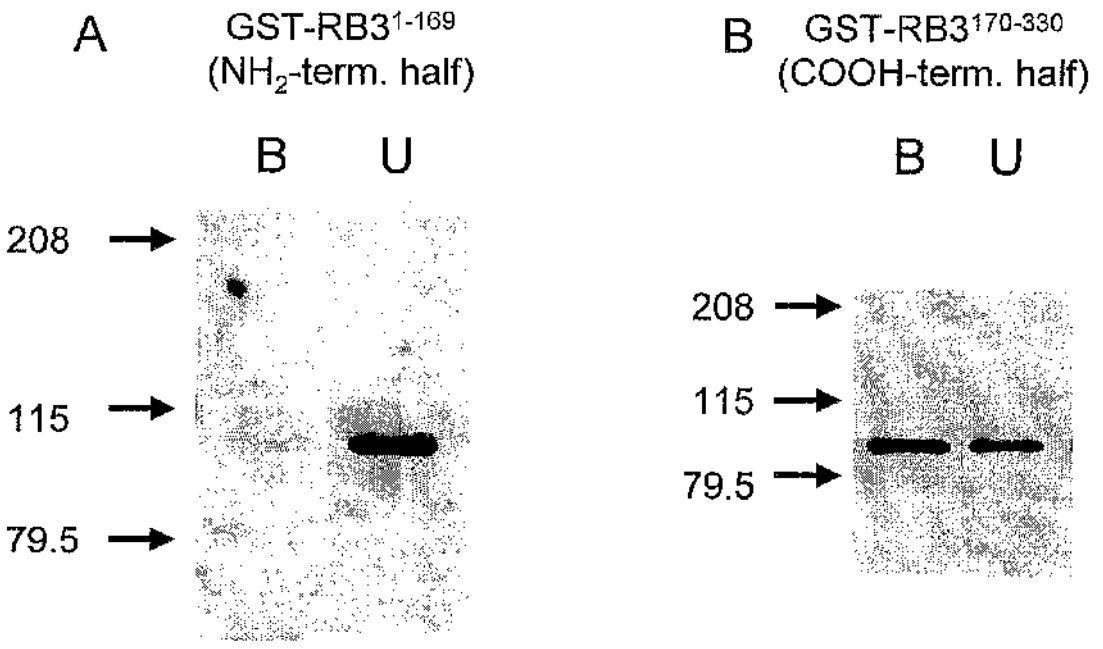

Figure 5.12 Western blot analysis of the association of GST-RB3$^{1-330}$, GST-RB3$^{1-169}$, GST-RB3$^{170-330}$ and GST with rpde6

A pull down assay was carried out as described in the legend for Figure 5.10. 8µl volumes of the bound fractions (*B*) and 3.2µl volumes of the unbound (*U*) fractions were separated by SDS-PAGE and immunoblotted with anti-PDE4A antiserum as primary reagent to assess the association of rpde6 with either the NH_2- or COOH-terminal halves of RB3 expressed as GST-fusions. The positions of the molecular weight standards (in kDa) are shown to the left of the immunoblots. This result is typical of an experiment carried out three times.

5.4.1 The COOH-terminal half of RB3 (amino acids 170-330) binds to rpde6 *in vitro*.

The results shown above suggest that a binding site for rpde6 exists within the COOH-terminal half of rpde6. This is intriguing as the COOH-terminal halves of the human and mouse homologues of RB3 (ARA9/XAP2 and AIP respectively) have been shown to mediate association with both hsp90 and AhR (see section 5.2.3.2) (Carver et al., 1998; Meyer and Perdew, 1999). This region also contains the TPR motif (Figure 5.8) between amino acids 265 and 298. As mentioned in section 5.2.3.2 the TPR domains within the COOH-terminal regions of FKBP52 (Radanyi et al., 1994) and Cyp40 (Ratajczak and Carrello, 1996) have also been shown to mediate interaction with hsp90. Therefore, the TPR domain of RB3 may mediate interaction with both hsp90 and rpde6.

The NH_2-terminal half of RB3, which contains regions of homology to the FKBP12, does not appear to be involved in binding rpde6. However, this finding does not exclude a role for this NH_2-terminal region in regulating the interaction of RB3 with rpde6. Post-translational modifications or protein-protein interactions in either the NH_2- or COOH-terminal halves of RB3 may increase or decrease the accessibility of the rpde6 binding site or its affinity for rpde6. Indeed, RB3 may adopt two or more interchangeable conformations *in vivo* that have varying affinities for rpde6. In this way, the factors that influence the conformational state of RB3 may regulate the intracellular targeting or activity of rpde6.

5.4.2 Time course for the association of rpde6 with GST-RB3$^{170-330}$.

The time course for the interaction of the COOH-terminal half of RB3 with rpde6 was established. This was done to determine the optimal incubation time for studies on the interaction between rpde6 and RB3 *in vitro*. Equal samples of cytosolic rpde6 from transfected COS-7 cells were incubated with equal amounts of purified GST-RB3$^{170-330}$ bound to glutathione Sepharose beads. The percentage binding was determined for each time point. The results are shown in Figure 5.13.

Rapid binding of rpde6 to GST-RB3$^{170-330}$ was observed. Maximum binding appeared to occur within ~8min at 4°C. This is similar to the time course observed for the interaction of rpde6 with the SH3 domain of Src kinase in which maximum binding is achieved after ~5min (O' Connell et al., 1996).

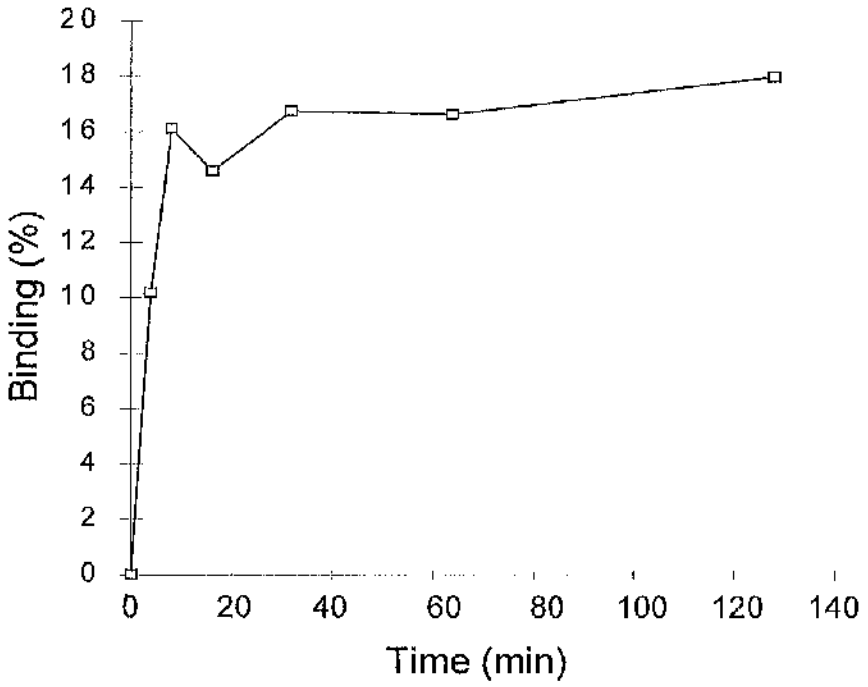

Figure 5.13 Time course for the binding of rpde6 to GST-RB3$^{170-330}$.
Samples of cytosolic rpde6 (containing 100EU PDE activity) were incubated at 4°C with 200μg samples of GST-RB3$^{170-330}$ bound to glutathione Sepharose beads for the times shown. Incubation was terminated by pelleting the beads at ~13,000*g* for 5s. The supernatants were removed and the beads were washed 3 times with complete KHEM buffer. Bound protein was eluted with 10mM glutathione, 50mM Tris-HCl, pH 8.0. Percentage binding was determined by comparing the total PDE activity in the bound and unbound fractions (see the legend for Figure 5.10, section 5.4) and plotted against time (n = 1).

5.5 Comparison of the subcellular distributions of RB3 and rpde6 in transfected COS-7 cells

An important aspect of the PDE4 isoenzymes is their specific targeting to different compartments within the cell (see Introduction chapter, sections 1.8). The various patterns of intracellular targeting are conferred on PDE4 splice variants by their unique NH_2-terminal splice domains. The subcellular distributions of a number of PDE4 isoenzymes, including rpde6, have been determined in transiently transfected COS-7 cells. (Houslay et al., 1998) (see Introduction section 1.4). Immunofluorescence analysis indicated that rpde6 was distributed throughout the cytoplasm (Huston et al., 2000). The pattern of immunofluorescence was not diffuse, but was localised to specific structures. The immunofluorescence signal intensified near the nucleus and the cell periphery suggesting an association with the perinuclear and cortical cytoskeleton. No nuclear staining was observed (Huston et al., 2000). The distribution of rpde6 was also analysed by simple cellular fractionation in both transfected COS-7 cells and brain. In both cases, rpde6 was distributed between the particulate (P1 and P2) and the soluble cytosolic (S) fractions (McPhee et al., 1995).

PDE4 isoenzymes may form different protein-protein interactions and adopt different conformations in different subcellular compartments. The most notable example of this is HSPDE4A4B (pde46) (McPhee et al., 1999) which appears to switch from a low to a high affinity state for rolipram inhibition when it becomes associated with a component of the particulate fraction of COS-7 cells (see Introduction chapter, 1.8.3). rpde6 also exhibits slightly different kinetic properties in the particulate and soluble fractions of COS-7 cells. The conformational state of rpde6 may affect its interaction with RB3. For this reason it is important to define the subcellular compartment(s) where the rpde6:RB3 interaction occurs. I therefore analysed the subcellular distribution of RB3 in transfected COS-7 cells. A necessary tool for this analysis was a primary antibody specific for RB3. Therefore, I generated anti-RB3 antisera in rabbits as described in the section below.

5.5.1 Generation of anti-RB3 antisera

Antisera were raised against purified GST-RB3$^{1-330}$ in two New Zealand White rabbits (574 and 575) as described in Methods section 2.13. To test the antisera produced,

COS-7 cells were transfected with plasmid expressing RB3 (pcDNARB3VSV). Samples of whole cell lysate from these cells (or untransfected COS-7s) were separated by SDS-PAGE and transferred onto nitrocellulose. The nitrocellulose filters were then immunoblotted with the antisera (574 and 575) as primary reagent (see Methods chapter, section 2.10). The antisera were diluted 1:1000.

Figure 5.14 shows that the rabbits had raised antibodies to RB3 just 20 days after the first injection with GST-RB3$^{1-330}$. The antisera detected a band at 41.2 ± 0.1 (mean ± S.E.) which is close the predicted molecular weight for RB3 of 37.7 kDa. The slight discrepancy between the observed and expected molecular weights was partly due to the fact that the plasmid used in these transfections (pcDNARB3VSV) expressed RB3 with an 11 residue epitope tag (vsv tag) (Soldati and Perriard, 1991), which would produce a slight increase in the molecular weight. Note that this band was only detected in the lanes containing lysate from COS-7 cells transfected with plasmid expressing RB3 (pcDNARB3VSV). No band was detected in lanes containing an equivalent amount of protein from untransfected COS-7 cells. This strongly suggests that these two antisera specifically detect RB3. The specificity of these antisera appears to be good; few background bands were observed on the blots.

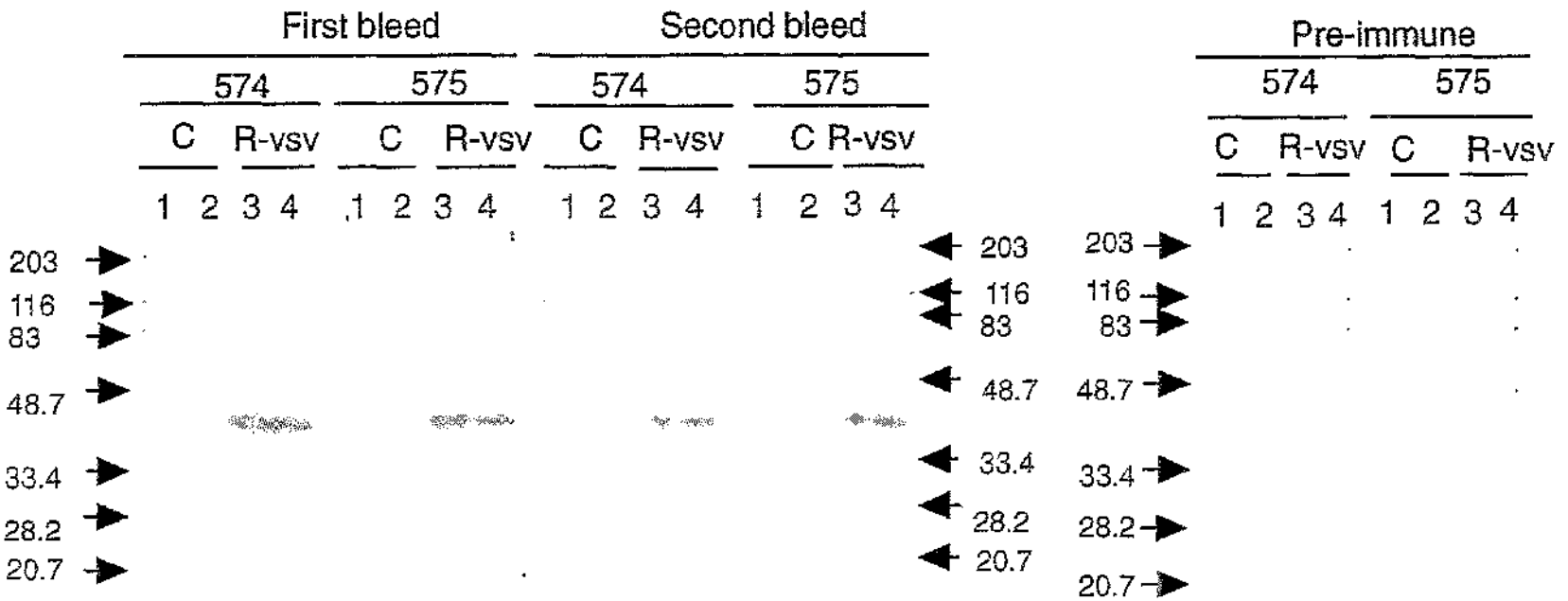

Figure 5.14 Testing of anti-RB3 polyclonal antibody

Samples (10μg or 50μg) of the high speed supernatant fraction from COS-7 cells transfected with a plasmid expressing vsv tagged RB3 (R-vsv) or untransfected COS-7 lysates (C) were separated by SDS-PAGE (10% [w/v] acrylamide). The proteins were then transferred onto nitrocellulose. The filters were probed for 2h at room temperature with samples of the first bleed and second bleed from rabbits 574 and 575 diluted 1:1000 in 137mM NaCl, 20mM Tris-HCl pH 8.0 plus 1% skimmed milk (See Methods chapter, sections 2.10 and 2.13). Pre-immune serum taken from both rabbits prior to antigen injection was use as a control. After the primary antibody step, the filters were then washed and probed with HRP-conjugated anti-rabbit IgG antibody diluted 1:10,000. The filters were then washed and developed by ECL as described in section 2.10.

5.5.2 Subcellular distribution of RB3 in transfected COS-7 cell

The anti-RB3 antisera generated as described above were used to determine the subcellular distribution of RB3 in transfected COS-7 cells. COS-7 cells were transfected with a plasmid expressing untagged full length RB3 (pcDNARB3) provided by Prof. Bolger. The cells were homogenised and separated into low speed (P1) and high-speed (P2) particulate fractions and a cytosolic (S) fraction as described in the Methods chapter (section 2.11). The volumes of these fractions were normalised and samples were immunoblotted for RB3 to determine the relative amounts of immunoreactive protein in each fraction. The apparent molecular weight on SDS-PAGE of the untagged RB3 used in the above experiments was 39.3 ± 0.6 kDa (mean ± S.E., n=4). This is close to calculated molecular weight of RB3, which is 37.7 kDa.

The above method for subcellular distribution analysis has been used routinely to assess the subcellular distribution of a number of PDE4 isoenzymes including rpde6 (Bolger et al., 1997; Huston et al., 1997; Lobban, 1994; McPhee et al., 1995; Shakur et al., 1995). The results of the analysis for RB3 are shown in Figure 5.15 and Figure 5.16. Data for the subcellular distribution of rpde6 in transfected COS-7 cells from (McPhee et al., 1999) are also presented in Figure 5.15 (b) for comparison.

Although both rpde6 and RB3 have major components in the cytosolic fraction of transfected COS-7, their subcellular distributions differ (Figure 5.15 and Figure 5.16). Whereas ~28% of rpde6 immunoreactivity was associated with the P2-particulate fraction (McPhee et al., 1999) almost no RB3 was P2-associated. However, portions of both rpde6 and RB3 are present in the P1 low speed pellet fraction of transfected COS-7 cells. The rpde6:RB3 interaction differs from the RACK1:PDE4D5 interaction (described in the Introduction, section 1.8.5) where RACK1 and PDE4D5 show very similar patterns of distribution between the subfractions of transfected COS-7 cells (Yarwood et al., 1999). The results suggest that endogenous RB3 does not mediate the association of rpde6 with the P2 pellet fraction but may be involved in targeting rpde6 to the P1 pellet fraction.

Interestingly, the subcellular distribution of RB3 is similar to that of a human truncated PDE4A species HSPDE4A4C (h6.1) (Huston et al., 1996; McPhee et al., 1999). Like RB3, h6.1 was largely cytosolic, but showed ~15-20% association with the low speed (P1) pellet and no association with the high speed pellet (P2) in transfected COS-7 cells. Intriguingly, immunofluorescence analysis of the subcellular distribution of h6.1 by laser

scanning confocal microscopy, showed that it had a non-random distribution throughout the cytosol, with pronounced labelling of the perinuclear cytoskeleton (Huston et al., 1996). Therefore, this result shows that although fractionation studies suggest that RB3 is largely cytosolic, RB3 may actually localise mainly to specific subcellular structures in intact cells. During subcellular fractionation analysis, the interaction of RB3 with these structures may be disrupted to release soluble RB3 that appears in the cytosolic (S) fraction. The advantage of immunofluorescence analysis is that, in this method, the cells are not ruptured, but are instead fixed to microscope slides and stained with the appropriate primary antibody followed by an appropriate secondary antibody, tagged with a fluorescent marker. Therefore, this technique is more likely to preserve the protein-protein associations that exist *in vivo*. This indirect immunofluorescence analysis also can be used to analyse the co-localisation of two different proteins such as rpde6 and RB3.

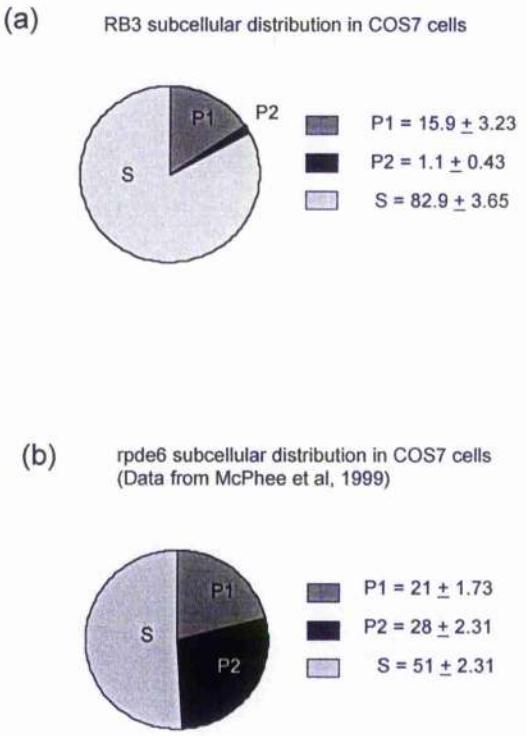

Figure 5.15 Calculated distribution of RB3 immunoreactivity in the subcellular fractions of transfected COS-7 cells

(a) COS-7 cells were transiently transfected with pcDNARB3 prepared by Prof. Bolger, University of Utah. The transfected cells were homogenised and fractionated to produce a low-speed pellet (P1), a high-speed pellet (P2) and a high-speed supernatant (S) as described in section 2.11.2. The volumes of these fractions were normalised and samples of varying volumes were separated on a 12% (w/v) SDS-PAGE gel and immunoblotted for RB3 using the anti-RB3 antiserum 574 (see section 2.10) as the primary antibody. The relative densities of the immunoreactive bands corresponding to RB3 were plotted against sample volume. The slopes obtained were used to calculate the distribution of RB3 immunoreactivity in the P1, P2 and S fractions. This procedure is described in detail in section 2.12.

(b) The subcellular distribution of rpde6 in transiently transfected COS-7 cells as determined by McPhee et al, using the method described above, (McPhee et al., 1999) is shown for comparison.

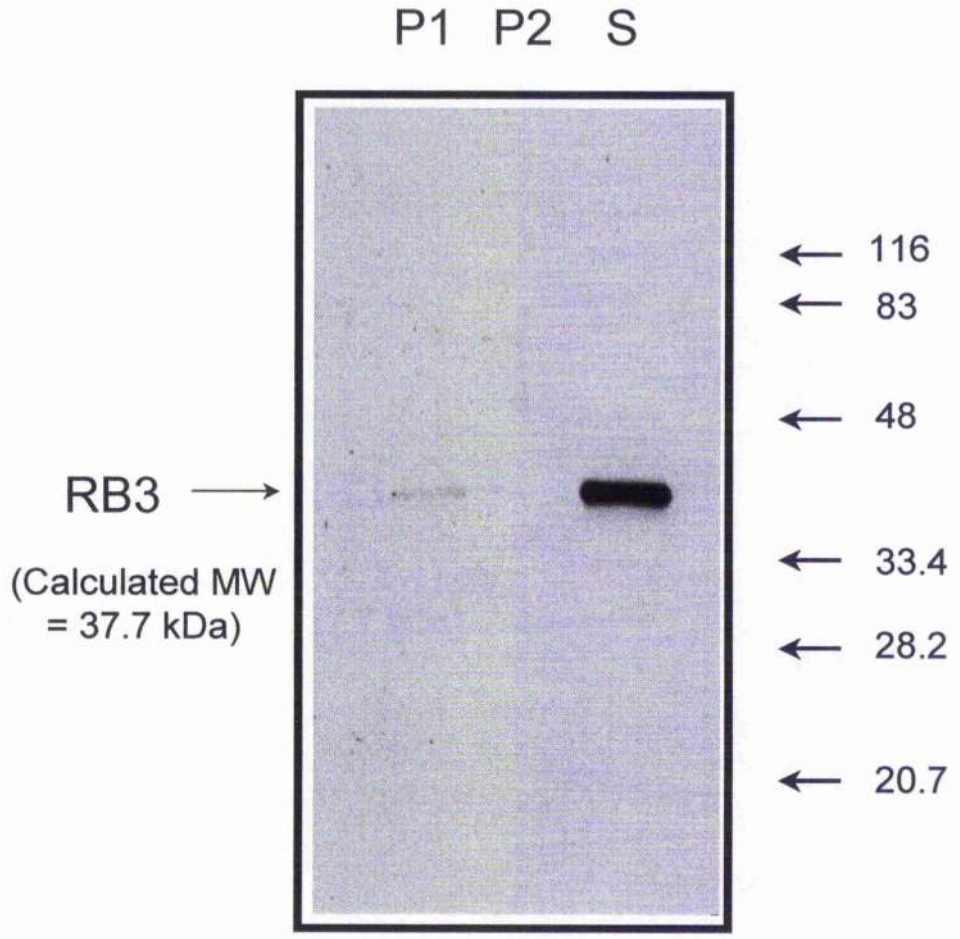

Figure 5.16 Subcellular distribution of RB3 in transfected COS-7 cells

This figure shows a representative immunoblot for the subcellular distribution of RB3 in transfected COS-7 cells. Equal volumes of the fractions P1, P2 and S from RB3 transfected COS-7 cells were separated by 12% SDS-PAGE and immunoblotted for RB3. This result is typical for this experiment which was repeated three times.

5.5.3 Subcellular distribution of ARA9/XAP2 in other cells

The above result for the subcellular distribution of RB3 disagrees slightly with the results obtained for the subcellular distributions of the human and mouse homologues of RB3 in the cells where they are expressed endogenously. Kuzhandaivelu et al showed that human homologue, ARA9/XAP2, is present in the cytosolic but not the nuclear fraction of HeLa cells and Ma et al showed the same result for the mouse homologue of AIP in mouse hepatoma (hepa1c1c7) cells (Kuzhandaivelu et al., 1996; Ma and Whitlock, 1997). Both groups defined the 'nuclear fraction' as the pellet obtained by centrifuging cell homogenate at a low speed. This fraction is comparable to the low-speed pellet (P1) obtained by our fractionation procedure where I observe ~15% of total RB3 immunoreactivity. Leaving aside the possibility that RB3 is incorrectly targeted in transiently transfected COS-7 cells as opposed to native cells, my result suggests that RB3 may indeed have a role in targeting proteins to the nucleus. This role has been suggested for both the mouse homologue AIP (Ma and Whitlock, 1997) and FKBP52 (Owens-Grillo et al., 1996; Pratt et al., 1999).

5.6 The anti-RB3 polyclonal antibody detects the presence of RB3 in MOLT3 monocytes, B-cells, Jurkat T-cells, U937 cells and HEK293 cells

An investigation into the functional significance of the rpde6:RB3 interaction would be aided by the availability of a cell line that expresses RB3 endogenously. Therefore, the anti-RB3 polyclonal antibody generated above was used to screen a number of cell lines for the expression of RB3. Given that RB3 is highly conserved between species, (see Figure 5.1), we would expect the anti-RB3 polyclonal antibody used above to be able to detect the human and mouse forms of RB3 (ARA9/XAP2 and AIP respectively). A number of immune system cell lines were included in this screen, in response to the observation by Meyer et al of high levels of AIP expression in mouse thymus and spleen (Meyer et al., 1998). All cells were homogenised in 0.5% Triton X-100 and samples of the whole cell lysates, containing equal amounts of protein, were separated by SDS-PAGE (12% [w/v] acrylamide), transferred onto nitrocellulose and immunoblotted for RB3. Whole cell lysate from COS-7 cells transfected with RB3 was used as a positive control.

An immunoreactive band that co-migrates with RB3 is observed in lanes corresponding to T-lymphoblastic MOLT-3 cells, U937 human monocytes, B-cells, Jurkat T-cells and human embryonic kidney (HEK) 293 cells (see Figure 5.17). These cell lines

represent potential model systems for the study of RB3 function *in vivo*, although RB3 expression appears to be relatively low in U937 cells. In addition, U937 monocytes (MacKenzie and Houslay, 2000) and Jurkat T-cells (Seybold et al., 1998) have been shown to express the human homologue of rpde6 (HSPDE4A4B, pde46). Therefore, an *in vivo* interaction between ARA9/XAP2 and the human homologue of rpde6 may occur in these cells. MOLT-3 monocytes (Hayon et al., 1999) and B-cells (Hewitt et al., 1997) have not yet been screened for PDE4 isoenzymes.

Intriguingly, my anti-RB3 antibody detected the expression of a slightly larger protein in COS-1 and COS-7 cells. This may represent a larger relative of RB3 that is preferentially expressed in COS cells, or a post-translationally modified form of RB3. A number of other immunoreactive bands are observed in the 55-83kDA range and these may represent high molecular weight immunophilins with structural similarities to RB3. A band at ~56kDa (marked with an arrow) is frequently observed. This may correspond to RB3's closest relative, FKBP52, which runs at approximately this molecular weight (Czar et al., 1994).

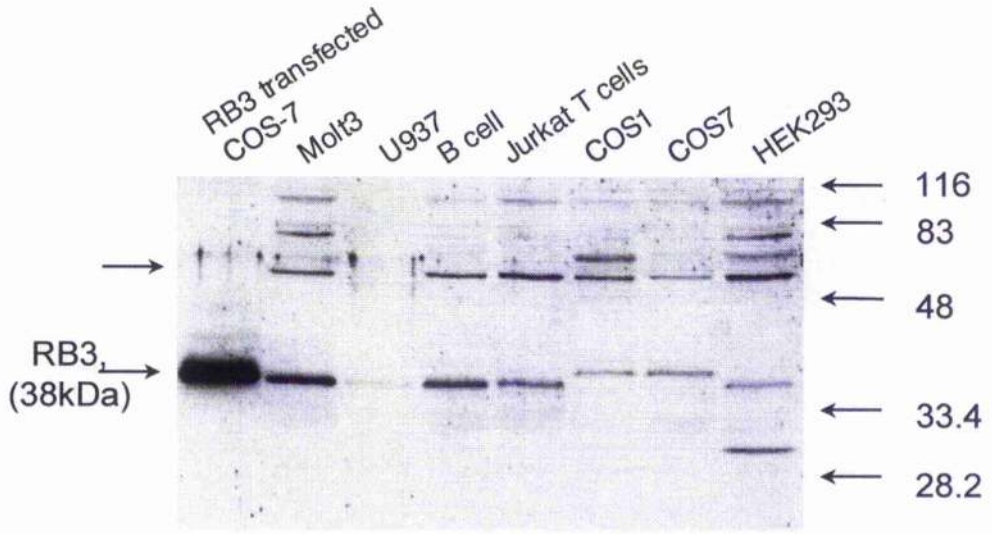

Figure 5.17 Western blot analysis of various cell lines for the presence of RB3
Homogenates from various cell lines were analysed by immunoblotting for the expression of endogenous RB3. The homogenates were prepared as described in the Methods chapter (section 2.11). Briefly, confluent adherent cells (COS-7 cells, COS-1 cells and HEK293) were washed twice with ice cold incomplete KHEM buffer and then scraped into complete KHEM buffer (+ 1mM DTT and protease inhibitors) containing 0.5% Triton-X-100. Suspended cells (MOLT3 monocytes, U937 and B-cells) were centrifuged and washed twice with ice cold KHEM buffer before being resuspended in ice cold complete KHEM buffer containing 0.5% Triton-X-100. All cell lines were homogenised, Bradford assayed for protein and mixed with Laemmli buffer. These mixtures were then boiled for 3min and samples containing 100μg of protein were separated by SDS-PAGE (12% [w/v] acrylamide gel). A sample of the S fraction from COS-7 cells transfected with RB3 (pcDNA RB3) was run on the same gel as a positive control. The separated proteins were transferred onto nitrocellulose and probed with anti-GST-RB3 antibody (antibody 574, see Table 2.10). The molecular weight standards (in kDa) are shown on the left. The position of the RB3 immunoreactive band is marked with an arrow. The arrow above this, at around 56kDa, indicates a band that may correspond to FKBP52.

5.7 RB3 interaction inhibits the activity of cytosolic rpde6

An important step towards understanding the functional significance of the rpde6:RB3 interaction is to determine whether RB3 affects the catalytic activity of rpde6 *in vitro*. If an effect was observed this would imply a direct role for RB3 in the regulation of PDE4 function and cAMP signalling. No effect would imply that RB3 might have a role in tethering rpde6 to other signalling proteins, or in targeting rpde6 to specific locations within the cell, without altering its catalytic activity. In this role, RB3 would be analogous to an adaptor protein or targeting subunit (Hubbard and Cohen, 1993).

5.7.1 Inhibition of rpde6 activity with GST-RB3$^{1-330}$

To assess the effect of RB3 on rpde6 activity, cytosol from rpde6 transfected COS-7 cells was incubated with increasing concentrations of purified GST-RB3$^{1-330}$. To do this, GST-RB3$^{1-330}$ was purified as described in the Methods chapter (section 2.7) and dialysed into Tris buffer (20mM Tris-HCl, pH 8.0). The fusion protein was then diluted to the appropriate molar concentrations with Tris buffer. Equal amounts of cytosolic rpde6, diluted in complete KHEM buffer and containing ~1 EU of PDE activity (in the absence of GST-fusion protein), were combined with varying concentrations of GST-fusion protein, incubated on ice for 1h, and then assayed for PDE activity as described in the Methods chapter, section 2.16. The time course presented in Figure 5.13 suggests that 1h is a sufficient time for the rpde6:RB3 interaction to reach saturation.

As shown in Figure 5.18, GST-RB3$^{1-330}$ inhibited rpde6 activity in a dose-dependent manner. A 1μM concentration of GST-RB3$^{1-330}$ achieved a maximum ~60% inhibition of the activity measured in the absence of GST-RB3$^{1-330}$. An identical concentration of GST had no effect on rpde6 activity. Therefore, the RB3 part of GST-RB3$^{1-330}$ was absolutely required for this inhibition. The concentration of GST-RB3$^{1-330}$ that produced a half-maximal inhibition of rpde6 (IC_{50}), was 0.22 ± 0.04 μM (mean value from three separate dose-response curves ± S.E.). Assuming that this IC_{50} value reflects the dissociation constant (K_d), this result suggests that RB3 associates with rpde6 with a submicromolar binding affinity.

RB3 could not completely inhibit rpde6 activity. Concentrations of GST-RB3$^{1-330}$ higher than 1μM did not inhibit more than ~60% of total rpde6 activity (data not shown). This suggests that RB3 is a non-competitive inhibitor, i.e. RB3 does not block the access of

cAMP to the active site on rpde6, but instead binds to another site, causing a conformational change that impairs the catalytic process.

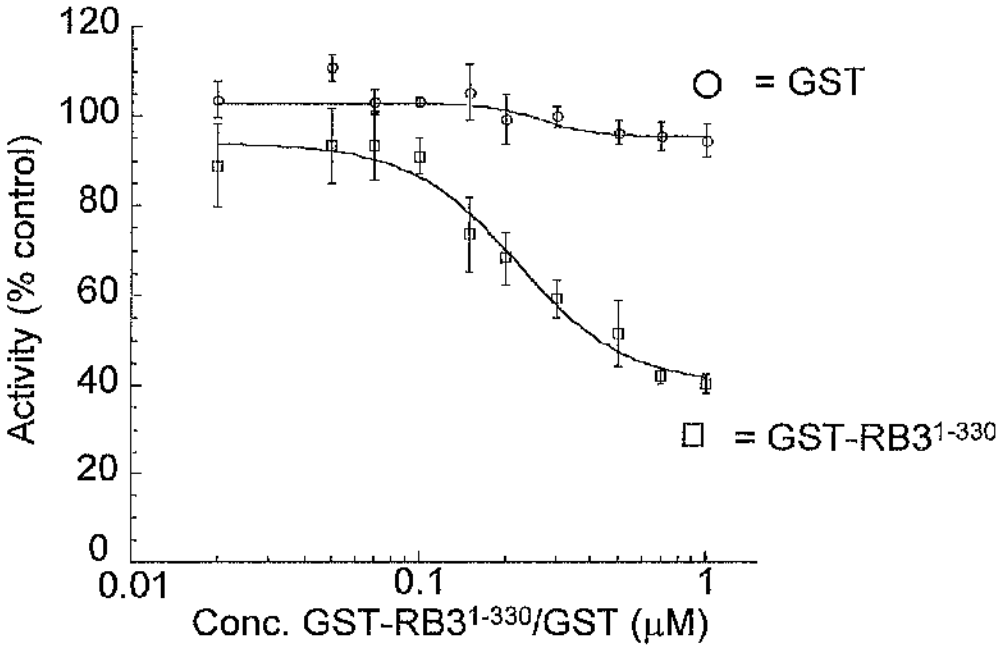

Figure 5.18 GST-RB3$^{1-330}$ inhibits cytosolic rpde6 from transfected COS-7 cells
This figure shows the dose-dependent inhibition by GST-RB3$^{1-330}$, of soluble, cytosolic rpde6. This experiment was carried out as described in the Methods chapter, section 2.16. Equal samples of the cytosolic (S) fraction of rpde6 transfected COS-7 cells diluted in complete KHEM buffer were mixed with increasing concentrations of GST-RB3$^{1-330}$ (□) or GST (O) diluted in 20mM Tris-HCl pH 8.0. Molar concentrations of GST-RB3$^{1-330}$ and GST were determined on the basis of their calculated molecular weights. After incubating on ice for 1h, the mixtures were assayed for PDE activity as described in the Methods chapter. The PDE activities are expressed as a percentage of the control activity in the absence of GST-fusion protein and are the means of three experiments ± S. E.

5.7.2 Inhibition of rpde6 with MBP-RB3$^{1-330}$

To confirm that this inhibitory effect was not peculiar to a GST fusion of RB3, I assessed the effect of a maltose binding protein (MBP) fusion of RB3 on rpde6 activity. A pMAL plasmid (pcDNARB3) expressing MBP fused to the amino terminus of full length RB3 (MBP-RB3$^{1-330}$) was generated by Prof. Bolger. I expressed and purified both MBP-RB3$^{1-330}$ and MBP (from the plasmid pMALc2) on amylose beads as described in the Methods chapter (section 2.7.2). The purified proteins were eluted with maltose buffer and dialysed into 20mM Tris pH8.0. Samples were analysed by SDS-PAGE and Coomassie blue staining (see Figure 5.19).

The effect of MBP-RB3$^{1-330}$ on rpde6 activity was determined as described for GST-RB3$^{1-330}$ i.e., equal samples of cytosolic rpde6 in complete KHEM buffer were mixed with a range of concentrations of MBP-RB3$^{1-330}$, diluted in 20mM Tris pH8.0. These mixtures were then assayed for PDE activity. The results are shown in Figure 5.20.

The MBP-RB3$^{1-330}$ fusion also inhibited rpde6 activity, the maximum inhibition being 40-45%. Note that a small inhibitory effect is also observed for MBP, although only at concentrations ≥ 0.5μM. The IC_{50} (see above) for inhibition with MBP-RB3$^{1-330}$ was 0.11 ± 0.01 μM which is very similar to the IC_{50} value obtained for GST-RB3$^{1-330}$ (see section 5.7.1). Therefore, RB3 expressed in two different fusion constructs consistently causes inhibition of rpde6 *in vitro*. The submicromolar (~0.1-0.2μM) IC_{50} values obtained in both experiments may suggest that the rpde6:RB3 interaction has a submicromolar dissociation constant (K_d).

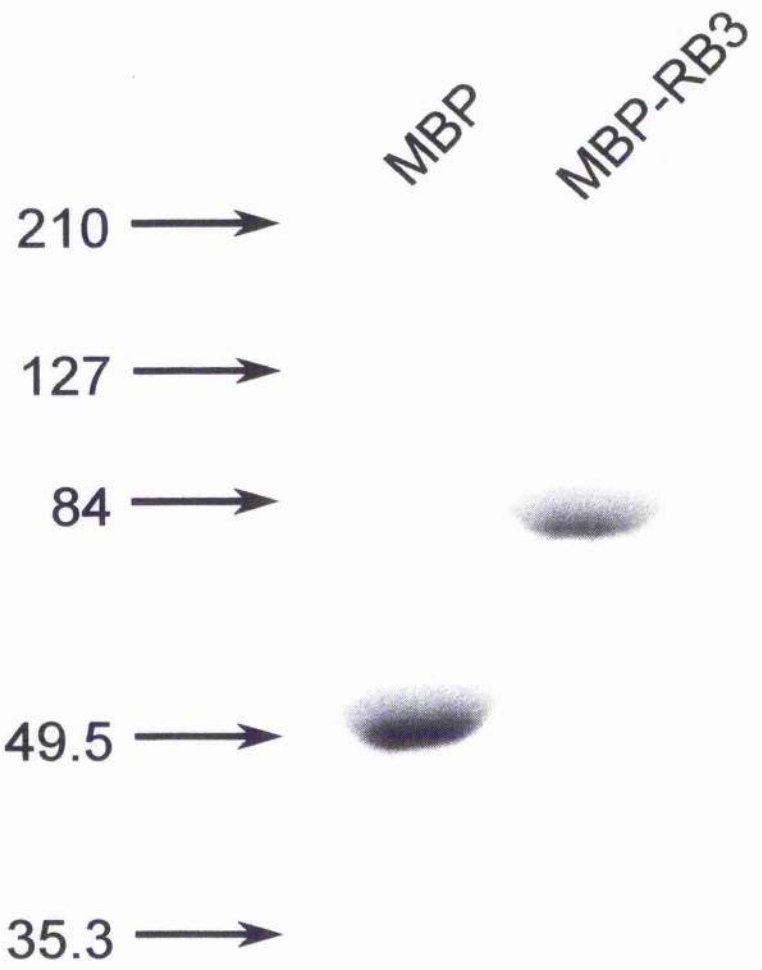

Figure 5.19 Purification of MBP-RB3$^{1-330}$ and MBP

A fusion of RB3 to the COOH-terminus of MBP (MBP-RB3$^{1-330}$) and MBP alone were over-expressed in *E.coli* and purified on amylose beads as described in the Methods chapter (section 2.7.2). The purified proteins were eluted with 10mM maltose in PBS and dialysed into 20mM Tris, pH8.0. 10μg samples were analysed by SDS-PAGE (12% [w/v] acrylamide) and Coomassie blue staining. The molecular weight standards (Biorad) are shown on the left of the figure. The actual molecular weights (from their sequences) of MBP-RB3$^{1-300}$ (88.5kDa) and MBP (50.8kDa) corresponded closely with their observed molecular weights of 88.7kDa and 53.7kDa respectively.

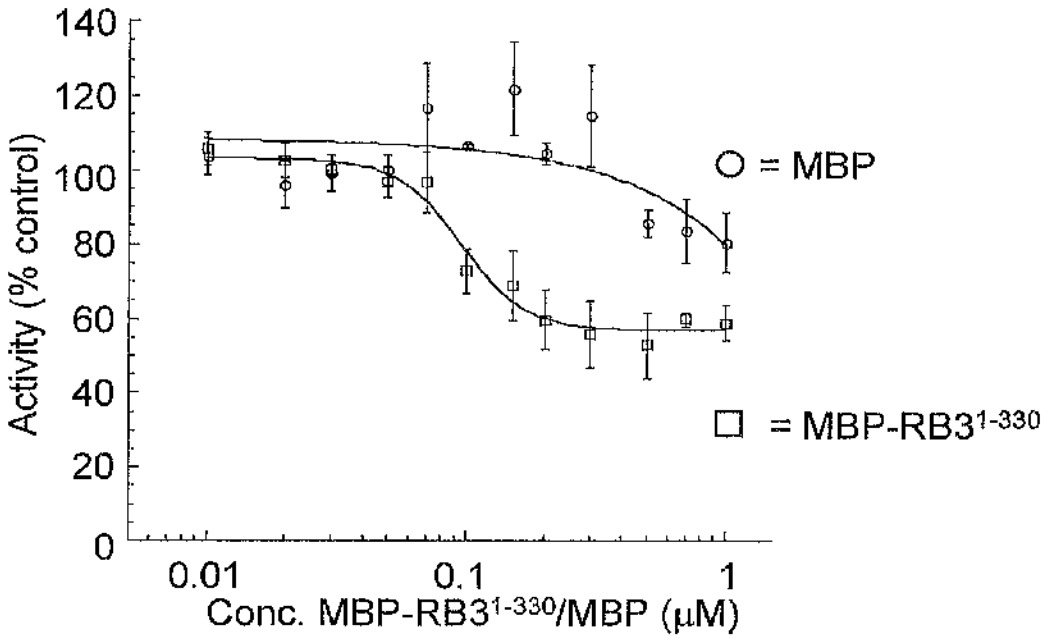

Figure 5.20 MBP-RB3$^{1-330}$ inhibits cytosolic rpde6 from transfected COS-7 cells

This figure shows the dose-dependent inhibition, by MBP-RB3$^{1-330}$, of soluble, cytosolic rpde6 from transfected COS-7 cells. The effects of both MBP-RB3$^{1-330}$ (□) and MBP (O) on rpde6 activity are shown. This experiment was carried out as described for GST-RB3$^{1-330}$ in the legend for Figure 5.18 and the Methods chapter (section 2.16). The PDE activities are expressed as a percentage of the control activity measured in the absence of MBP-fusion protein and are the means of three experiments ± S. E.

5.7.3 The presence of FK506 and rapamycin does not affect the inhibition of rpde6 by RB3

As discussed in section 5.2.3.1, RB3 contains regions of similarity to FKBP-homology domain I of FKBP52 and also FKBP12 which essentially consists of one FKBP-homology domain. The FKBP homology domains of FK506-binding proteins contain the PPIase active site, which catalyses the *cis-trans* isomerisation of peptide bonds on the amino terminal side of proline residues. PPIase activity is also found in the cyclophilins. The immunosuppressant drugs FK506, rapamycin and cyclosporin A bind to and inhibit the PPIase active sites of immunophilins. Several studies have implicated PPIase activity in the regulation of protein function. For example, the cyclophilin Cyp40 inhibits the DNA binding capacity of the oncogenic transcription factor c-Myb. This negative regulation of c-Myb is dependent on the PPIase activity of Cyp40 (Leverson and Ness, 1998). Another example is the prolyl isomerase Pin1. The PPIase of this protein is required for it to restore the function of the protein tau, which binds to microtubules and promotes microtubule assembly (Lu et al., 1999).

The presence of proline rich motifs within the unique NH_2-terminus of rpde6 suggested that a PPIase active site within RB3 might be responsible for its inhibitory effect on rpde6. To test this hypothesis, the inhibitory effect of GST-RB3$^{1-330}$ on rpde6 was assessed in the presence of the PPIase inhibitors FK506 and rapamycin. These inhibitors were incubated with GST-RB3$^{1-330}$ at 4°C for 1h prior to the addition of rpde6. The assay was then carried out as described in section 5.7.1 and the Methods chapter, section 2.16. Samples of GST-RB3$^{1-330}$/immunosuppressant mixture were mixed with cytosolic rpde6 from transfected COS-7 cells. These mixtures were then incubated for a further 1h on ice and assayed for PDE activity. The final concentrations of FK506 and rapamycin used in this assay were 1μM and 10nM respectively. These were chosen on the basis of their published affinities (K_is) for various FKBP proteins as shown Table 5.2 below.

Table 5.2 Affinities of FK506 and rapamycin for various FKBP proteins.

FKBP protein	K_i FK506 (nM)	K_i Rapamycin (nM)	Reference
FKBP12	0.6 1 1.7 -	0.25 - - 0.2	(Park et al., 1992) (Bram et al., 1993) (Harrison and Stein, 1990) (Bierer et al., 1990)
FKBP13	55	-	(Bram et al., 1993)
FKBP25	160 180	0.9 -	(Galat et al., 1992) (Bram et al., 1993)
FKBP52	10	8	(Peattie et al., 1992)

For E = enzyme, I = inhibitor and EI= enzyme/inhibitor complex Ki= [E][I]/[EI]

The effect of 1μM GST-RB3$^{1-330}$ (or GST) on rpde6 activity in the presence of 1μM FK506 or 10nM rapamycin was determined. Figure 5.21 showed that neither 10nM rapamycin nor 1μM FK506 significantly affected the inhibitory effect of RB3 on rpde6 activity. The presence of these concentrations of drugs produced no change the dose-response curve for inhibition of rpde6 by GST-RB3$^{1-330}$ (n=1, data not shown). One can infer from these results that the interaction between rpde6 and RB3 is unaffected by the presence of FK506 or rapamycin.

These results imply regulation of PDE activity is not involved in the mechanism of immunosuppression of either FK506 or rapamycin. In addition to these results, Carver and coworkers failed to detect the binding of ^{3}H-FK506 to ARA9/XAP2. These results are perhaps unsurprising given that an alignment between RB3 and FKBP52 shows that only 3 of the 14 residues involved in FK506 binding are completely conserved in RB3 (Kay, 1996; Van Duyne et al., 1991) (see Figure 5.3). Therefore it is probable that RB3 lacks both FK506/rapamycin binding capacity and PPIase activity. This further suggests that RB3, unlike FKBP12, does not interact with calcineurin. A composite surface including components of both FK506 and the FKBP12 is believed to be necessary for a strong interaction with calcineurin (Aldape et al., 1992; Futer et al., 1995). As RB3 does not appear to bind to FK506 this presumably rules out an interaction with calcineurin.

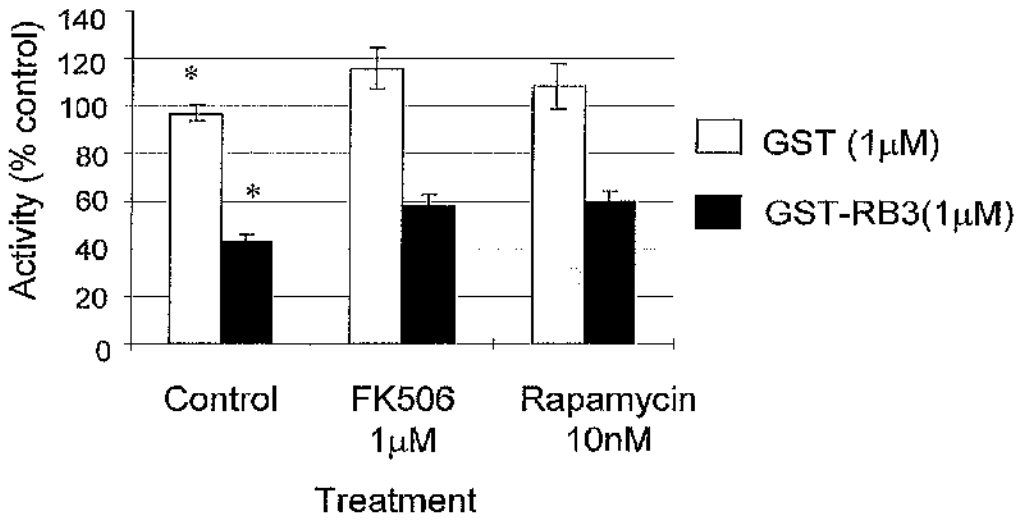

Figure 5.21 rpde6 is inhibited by RB3 in the presence of 1μM FK506 and 10nM rapamycin

GST or GST-RB3$^{1-330}$ (4μM) were incubated with 4μM FK506 or 40nM rapamycin on ice for 1h at 4°C. 25μl samples of this mixture were incubated with 25μl samples of COS-7 cell expressed rpde6, diluted in complete KHEM buffer, for a further 1h at 4°C and then assayed for PDE activity by the addition of 1μM 8-[^{3}H]-labelled cAMP. The final concentrations in the assay were therefore GST-RB3$^{1-330}$ = 1μM, FK506 = 1μM, rapamycin = 10nM. The activities are presented as a percentage of the control activity determined in the absence of GST-fusion protein.

*These results were presented previously in Figure 5.18 and are shown here for comparison.

5.7.4 Cytosolic rpde6 is inhibited by interaction with the COOH-terminal half of RB3 (amino acids 170-330)

In section 5.4 I showed that the COOH terminal half of RB3 (amino acids 170-330) is sufficient for interaction with rpde6. However, another region of RB3 may be required for rpde6 inhibition. Therefore, the effects of the NH_2- and COOH- terminal halves of RB3 (illustrated in Figure 5.8) on rpde6 activity were determined. Equal samples of rpde6 from transfected COS-7 cells were incubated with increasing concentrations of GST-$RB3^{1-169}$ and GST-$RB3^{170-330}$ using the method described above for GST-$RB3^{1-330}$ (section 5.7.1). The PDE activity in these samples was then determined.

As shown in Figure 5.22, the COOH terminal half of RB3 expressed as a GST fusion (GST-$RB3^{170-330}$) inhibited rpde6 with the similar potency to the full length RB3 (GST-$RB3^{1-330}$). Absolutely no inhibition was observed with the NH_2-terminal half of RB3 expressed as a GST-fusion (GST-$RB3^{1-169}$). The maximum inhibition of rpde6 (~50%) was achieved with 1μM GST-$RB3^{170-330}$. The concentration of GST-$RB3^{170-330}$ that produced an inhibition of rpde6 that was 50% of the maximum inhibition (IC_{50}) was 0.31 ± 0.06 μM (mean value from three separate dose-response curves ± S.E.), which is close to the value of 0.22 ± 0.04 μM obtained for GST-$RB3^{1-330}$ (see section 5.7.1). Therefore, the COOH-terminal half of RB3 appears to be able to mediate both the binding and inhibition of rpde6. Note that within the COOH-terminal 161 amino acid residues of RB3, separate sequences may mediate binding and inhibition. These results suggest that regions of sequence similarity to FKBP12 within the NH_2-terminal half of RB3 do not appear to be involved in either binding or inhibition.

As discussed in section 5.2.3.2, this COOH terminal region (amino acids 170-330) interacts with hsp90 and AhR and contains a TPR motif (Carver et al., 1998; Meyer and Perdew, 1999). No specific function has yet been assigned to the NH_2-terminal half of RB3. As discussed above (section 5.4.1), the NH_2-terminus of RB3 may introduce a mechanism of regulation whereby changes to its phosphorylation status or protein-protein interactions affect the inhibitory binding of the COOH-terminal half to rpde6.

Another example of enzyme inhibition mediated by a TPR-containing protein is the inhibition of hsp90 ATPase activity by Sti1 (Prodromou et al., 1999). Sti1 causes 100% inhibition of hsp90 ATPase activity by directly contacting and obstructing the active site. In contrast the ~50% inhibition observed with GST-$RB3^{170-330}$ suggests that RB3 inhibits

rpde6 allosterically, causing a conformational change that reduces its catalytic efficiency without completely abolishing activity or blocking the active site.

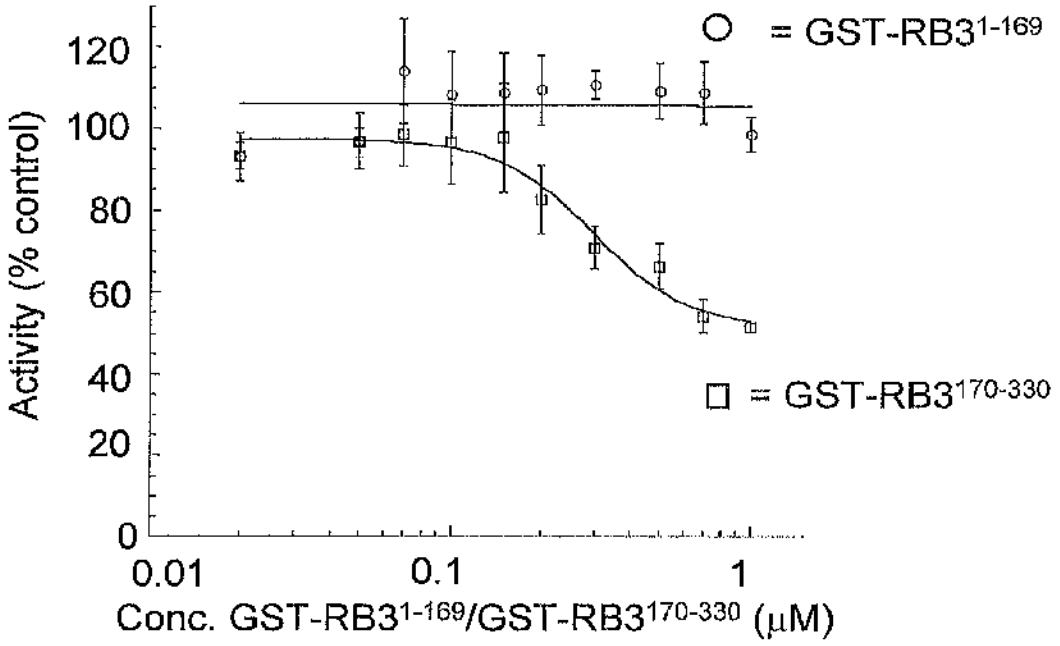

Figure 5.22 GST-RB3$^{170-330}$ but not GST-RB3$^{1-169}$ inhibits cytosolic rpde6

This figure shows the dose-dependent inhibition, by GST-RB3$^{170-330}$ but not by GST-RB3$^{1-169}$ of soluble cytosolic rpde6. Samples of the cytosolic (S) fraction of rpde6 transfected COS-7 cell fractions diluted in complete KHEM buffer were mixed with increasing molar concentrations of GST-RB3$^{170-330}$ (□) or GST-RB3$^{1-169}$ (O) diluted in 20mM Tris-HCl, pH8.0 as described in the Methods chapter, section 2.16. After incubating on ice for 1h the mixtures were assayed for PDE activity. The activities are expressed as a percentage of the control activity in the absence of GST-fusion protein and are the means of three experiments ± S.E.

5.8 Particulate rpde6 is resistant to inhibition by GST-RB3$^{1-330}$ and GST-RB3$^{170-330}$

Full length RB3 and the COOH-terminal half of RB3 (RB3$^{170-330}$), which contains the TPR motif and excludes the NH_2-terminal FKBP homology region, have both been shown to inhibit cytosolic rpde6 (section 5.7). However, rpde6 activity is not only found in the cytosolic fraction (~51%), but is also distributed between the P1 low-speed pellet fraction (~21%) and P2 high-speed pellet fraction (~28%) of both brain and transiently transfected COS-7 cells (McPhee et al., 1995; McPhee et al., 1999). Furthermore, the association of rpde6 with a combined particulate/membrane fraction (P1 and P2) is resistant to disruption with high salt concentrations (2M NaCl) and/or detergent treatment (1% Triton X-100) (McPhee et al., 1995). This suggests that rpde6 may bind to cytoskeletal structures associated with these fractions that are not disrupted with detergent and/or salt (Jackson et al., 1994) (Slusarewicz et al., 1994). Any interaction with peripheral or integral membrane protein or membrane lipids would be disrupted by such treatments (McPhee et al., 1995). As discussed in section 5.5.2 (Figure 5.15) RB3 is also found in the P1 pellet fraction (~16%) and the cytosolic fraction (~83%) of transfected COS-7 cells whilst being absent from the P2 pellet fraction.

An outstanding question was whether P1 and/or P2 pellet-associated rpde6 were susceptible to binding/inhibition by RB3 in a manner similar to cytosolic rpde6. Therefore, the activity of P1 and P2 pellet-associated rpde6 was assessed in the presence of increasing concentrations of purified GST-fusions of either full length RB3 (GST-RB3$^{1-330}$) or the TPR-containing COOH-terminal half of RB3 (GST-RB3$^{170-330}$). I used the assay procedure described above in section 5.7 and in the Methods chapter, section 2.16. COS-7 cells were transfected with rpde6, homogenised and fractionated to obtain the P1 and P2 pellet fractions as described in the Methods chapter, section 2.11. These pellet fractions were resuspended in complete KHEM buffer. Equal samples of these resuspended pellet fractions, containing ~1 EU of PDE activity in the absence of GST-fusion protein, were incubated on ice for 1h with increasing concentrations of either GST-RB3$^{1-330}$, GST-RB3$^{170-330}$ (COOH-terminal half), GST-RB3$^{1-169}$ (NH_2-terminal half) or GST. The samples were then assayed for PDE activity as described in the Methods chapter, section 2.15.

As shown in Figure 5.23, GST-RB3$^{1-330}$ (full length RB3) did not cause inhibition of P1 pellet-associated rpde6 at concentrations up to 3μM. In contrast, soluble cytosolic rpde6 was dose-dependently inhibited over this range (Figure 5.18, section 5.7.1). The

NH_2-terminal half of RB3 (GST-$RB3^{1-169}$), which has been shown not to inhibit cytosolic rpde6, also did not cause inhibition of P1 pellet-associated rpde6. Therefore, association of rpde6 with the P1 low speed pellet fraction appeared to block the inhibitory effect of RB3 that is observed using cytosolic rpde6.

A similar result was observed with the P2 (high-speed pellet fraction)-associated rpde6 shown in Figure 5.24. Thus, neither GST-$RB3^{1-330}$ (full length RB3) nor GST-$RB3^{170-330}$ (COOH-terminal half of RB3) caused inhibition of P2 pellet-associated rpde6 in contrast to the inhibition achieved using soluble cytosolic rpde6. Therefore, association of rpde6 with both particulate fractions (P1 and P2) appears to prevent the inhibitory effect of RB3.

Note that in these assays, the pellet fractions were resuspended in complete KHEM buffer in the absence of detergent or high salt concentrations. This treatment would have left many of the multi-protein complexes intact, including those of the cytoskeleton. These data suggest that particulate fraction-associated rpde6 is protected from RB3 inhibition, perhaps by interaction with other proteins. Indeed, it has been suggested that SH3 domain containing proteins, such as fodrin and cortactin, may anchor rpde6 to the cytoskeleton and hence the particulate fraction of cells (see Introduction, section 1.8.2) (Houslay et al., 1997; Houslay, 1996; Houslay et al., 1998). One possibility is that, in the particulate fractions, access of RB3 to rpde6 may be blocked by SH3 domain containing proteins. Alternatively, these proteins may block the ability of RB3 to alter the conformation of rpde6 so as to affect its activity.

Of course, given that both RB3 and rpde6 are present in P1 pellet fraction it is possible that P1 pellet-associated rpde6 is actually in a complex with endogenous RB3 (and possibly other proteins) in which it is inhibited. If that is so, we would expect the activity of the P1 pellet fraction rpde6 to be less than that of cytosolic rpde6. Indeed, the activity of the combined particulate fraction (P1 + P2) rpde6 was shown to be ~67% (McPhee et al., 1995) of that obtained for cytosolic rpde6.

RB3 may be involved in targeting rpde6 to the P1 fraction. However, the submicromolar affinity of the rpde6:RB3 interaction, estimated from inhibition studies (section 5.7) may not be high enough for RB3 to mediate the targeting of rpde6 to the P1 fraction by itself. Both RB3 and rpde6 may bind with high affinity to other unidentified protein binding partners. These interactions need not necessarily exclude the association of

rpde6 and RB3 in the P1-pellet. Indeed, these other interaction partners may facilitate the binding of rpde6 to endogenous COS-7 RB3 in the P1 pellet.

In conclusion, the above results suggest that P1 and P2 pellet-associated rpde6 is resistant to inhibition with both GST-RB3$^{1-330}$ and GST-RB3$^{170-330}$ in contrast to soluble RB3, which is inhibited by both. The unidentified protein(s) that interact with rpde6 in the particulate fraction may sterically block the access of exogenous RB3 or force rpde6 to adopt a conformation in which it is inhibited. In the P1 pellet fraction the interacting protein may be endogenous RB3 itself. The possibility that the GST tag prevents the access of RB3 to the particulate fraction rpde6 in this assay cannot be excluded.

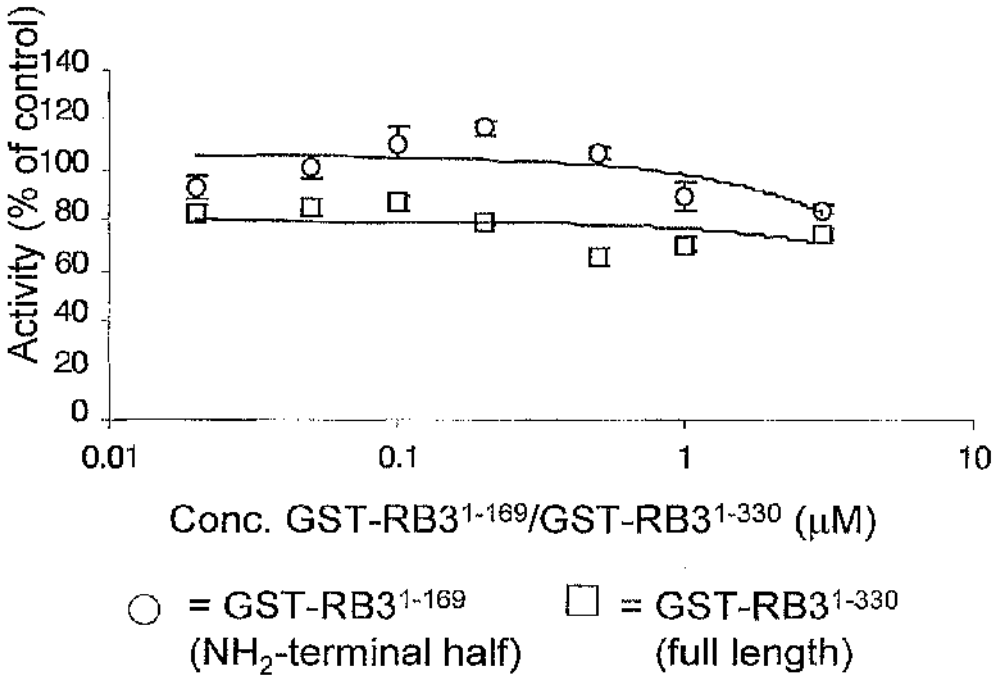

Figure 5.23 P1 pellet fraction rpde6 is resistant to inhibition by full length RB3
This graph shows the effect of increasing concentrations of GST-RB3$^{1-330}$ (full length) or GST-RB3$^{1-169}$ (NH_2-terminal half of RB3) on the activity of low speed pellet (P1) fraction-associated rpde6. Samples of the P1-pellet fraction of rpde6-transfected COS-7 cells, diluted in complete KHEM buffer, were mixed with increasing molar concentrations of GST-RB3$^{1-330}$ (□) or GST-RB3$^{1-169}$ (O) diluted in 20mM Tris-HCl pH8.0. After incubating for 1h on ice the mixtures were assayed for PDE activity as described in the Methods chapter, section 2.15. The activities are expressed as a percentage of the control activity in the absence of GST-fusion protein and are the means of three experiments ± S. E.

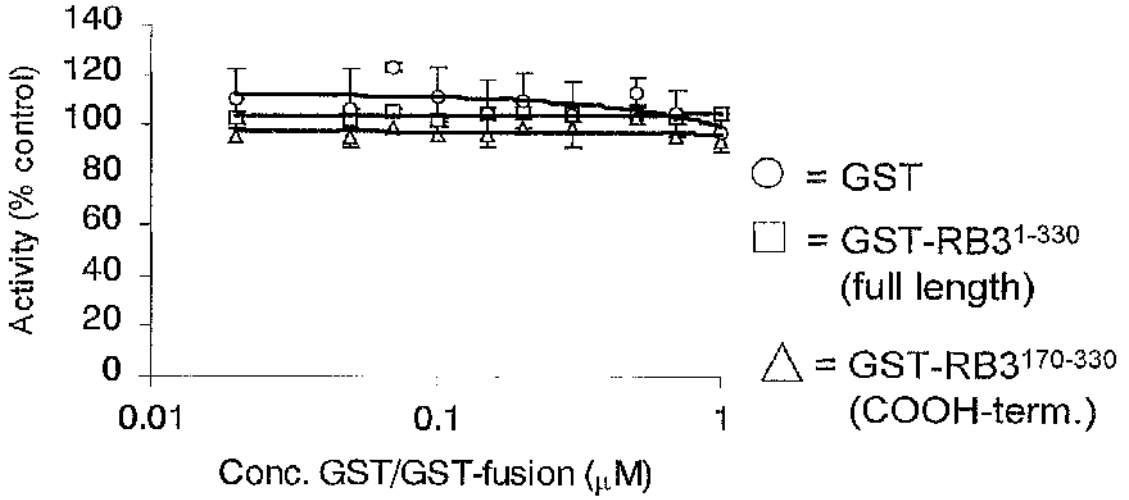

Figure 5.24 P2-fraction rpde6 is resistant to inhibition by both full length RB3 and the COOH-terminal half of RB3 ($RB3^{170-330}$)

This graph shows the effect of increasing concentrations of GST-$RB3^{1-330}$ (full length), GST-$RB3^{170-330}$ (COOH-terminal half of RB3) and GST on the activity of high-speed pellet (P2) fraction associated rpde6. Samples of the membrane (P2) fraction of rpde6 transfected COS-7 cells, diluted in complete KHEM buffer, were mixed with increasing concentrations of GST-$RB3^{1-330}$ (□), GST-$RB3^{170-330}$ (Δ) or GST (O) diluted in 20mM Tris-HCl pH 8. After incubating for 1h on ice the mixtures were assayed for PDE activity as described in the Methods chapter, section 2.15. The activities are expressed as a percentage of the control activity in the absence of GST or GST-fusion protein and are the means of three experiments ± S. E.

5.9 Lyn-SH3 competes with RB3 for interaction with rpde6

It has been shown previously that the unique NH_2-terminal splice domain of rpde6 contains three proline-rich putative SH3 domain binding motifs each with the minimal consensus PxxP (Alexandropoulos, 1995; O' Connell et al., 1996; Pawson, 1995) (see Introduction chapter, section 1.8.2). In addition, this 102 amino acid splice domain confers on rpde6 the ability to interact with the SH3 domains of a number of Src family tyrosyl kinases, expressed as GST fusions (O' Connell et al., 1996). Particularly strong interactions were observed between rpde6 and the SH3 domains of Src, Lyn and Fyn (O' Connell et al., 1996). As discussed in the previous section, SH3 domain-containing proteins may mediate the interaction of rpde6 with the particulate fractions. These interactions may protect particulate rpde6 from inhibition by soluble RB3. I investigated whether the interaction of soluble cytosolic rpde6 with Lyn SH3 would block the inhibitory binding of RB3. Note that O'Connell et al showed that interaction with Lyn SH3-GST does not alter rpde6 activity (O' Connell et al., 1996).

The effect of 1μM GST-$RB3^{1-330}$ on rpde6 activity in the presence of Lyn SH3-GST was assessed. The experimental system I used is detailed in the Methods chapter, section 2.16.1. A GST fusion of the SH3 domain of Lyn [see (McPhee et al., 1999; O' Connell et al., 1996)], was expressed in *E coli* and affinity purified on glutathione Sepharose beads (see section 2.7.2). In order to bind rpde6 to Lyn SH3, a sample (400μg) of the purified Lyn SH3-GST bound to glutathione beads was incubated with a sample (240EU) of cytosolic rpde6 from transfected COS-7 cells. The beads were washed with complete KHEM buffer and complexes of rpde6 bound to Lyn SH3-GST were eluted with glutathione elution buffer.

Samples of the glutathione eluate containing rpde6 bound to Lyn SH3-GST were mixed 1:1 (v/v) with purified GST-$RB3^{1-330}$ or GST diluted in 20mM Tris-HCl, pH8.0. These mixtures were incubated on ice for 1h prior to an assay for PDE activity. As a control, the activity of samples of cytosolic rpde6, diluted in glutathione elution buffer, were determined in the presence or absence of GST-$RB3^{1-330}$ or GST. The activity of rpde6 ± Lyn SH3-GST added to the assay was within the linear range (i.e. the amount of rpde6 added to the assay would consume no more than 10% of the cAMP substrate in the absence of GST or GST-$RB3^{1-330}$). The final concentration of GST-$RB3^{1-330}$ or GST in the assay was 1μM.

The results in Figure 5.25 show that the association of Lyn-SH3 with rpde6 severely reduced the inhibitory effect of RB3 on rpde6 activity. GST-RB3$^{1-330}$ produced only ~20% inhibition of Lyn SH3-associated rpde6 in contrast to the ~45% inhibition observed in the absence of GST-RB3$^{1-330}$ (see Figure 5.18). This result suggests that Lyn SH3-GST does indeed alter the functional interaction of RB3 with rpde6.

It may be that Lyn-SH3 and RB3 bind, in a competitive and mutually exclusive manner, to overlapping or topologically adjacent sites on rpde6. Alternatively, Lyn SH3 binding may affect the conformation of rpde6 such that RB3 binding is now unable to cause inhibition. The latter suggestion is feasible as we already know that SH3 binding to the LR2 region of HSPDE4A4B (the human homologue of rpde6) can cause conformational changes in the catalytic unit (McPhee et al., 1999). The slight inhibition that is observed in the presence of Lyn SH3-GST suggests that some RB3 can successfully compete with Lyn SH3 for interaction with rpde6. It should be noted that some dissociation of the rpde6/Lyn SH3-GST complex may have occurred after it had been eluted with glutathione.

On the assumption that all the Lyn SH3-GST was eluted after binding of rpde6, the final concentration of Lyn SH3-GST in this assay was estimated to be 8-10μM (see Methods chapter, section 2.16.1). Lyn SH3-GST is thus in considerable excess over the 1μM GST-RB3$^{1-330}$ in this assay. Therefore, we cannot use these results to draw conclusions on the relative affinities of Lyn SH3 and RB3 for rpde6. However, we can conclude that when Lyn SH3-GST is present in excess, it hinders RB3-mediated inhibition of rpde6. This result lends support to the suggestion that P2-particulate fraction associated rpde6 may be protected from RB3-mediated inhibition by interaction with other proteins.

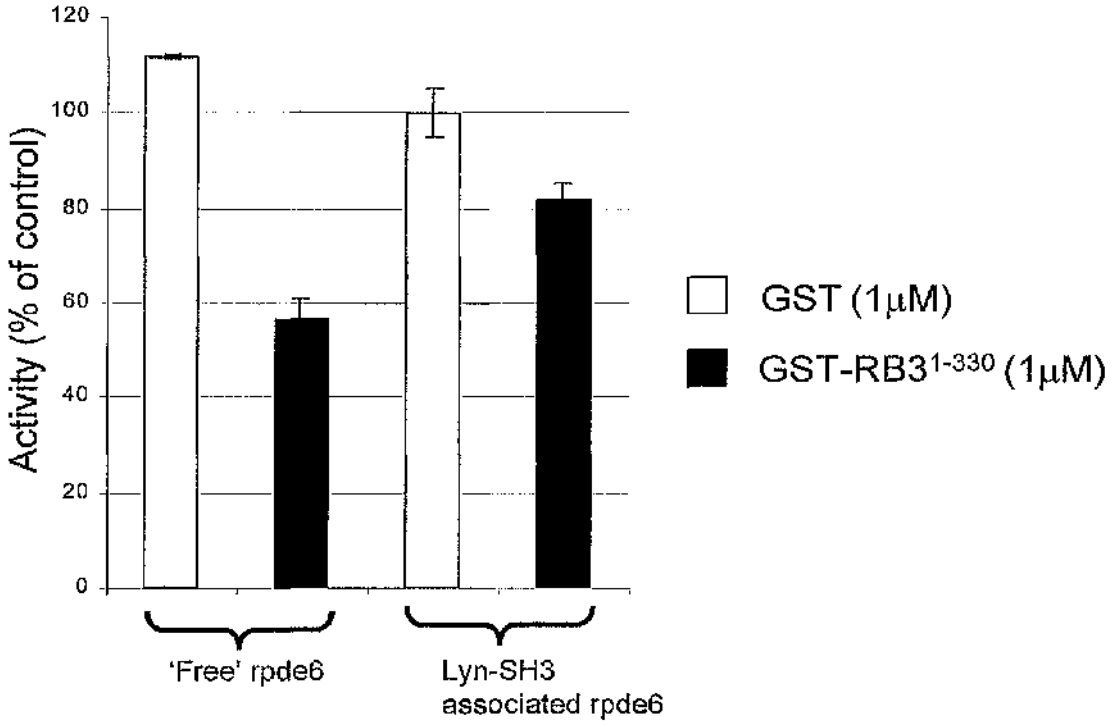

Figure 5.25 Lyn SH3-associated rpde6 is resistant to RB3 inhibition

The cytosolic fraction of COS-7 cells expressing rpde6 was incubated with a fusion of the SH3 domain of Lyn tyrosyl kinase immobilised as a GST fusion protein on glutathione Sepharose beads. After washing the beads, complexes of rpde6 bound to Lyn SH3-GST were eluted with 10mM glutathione, 50mM Tris pH 8.0. 25μl samples of the eluate ('Lyn SH3 associated rpde6') were added to 25μl samples of 4μM GST-RB3$^{1-330}$ or 4μM GST diluted in 20mM Tris pH 8.0. After incubating on ice for 1h, PDE activity was measured in the presence of 1μM 8-[^{3}H] cyclic AMP as described in the Methods chapter (section 2.15). As a control, cytosolic rpde6 ('free' rpde6), diluted in glutathione elution buffer, was PDE assayed in the presence or absence of GST-RB3$^{1-330}$ or GST. The concentration of both GST and GST-RB3$^{1-330}$ in the final reaction mixture was 1μM. The activities are expressed as percentages of the control activity determined for Lyn SH3-associated rpde6 in the absence of GST-RB3$^{1-330}$ or GST. The values are the means of 3 experiments ± S.E.

5.10 Δp1 rpde6 (Δ2-10 rpde6) is inhibited by RB3

For several years it has been appreciated that the unique NH_2-terminal splice domains of PDE4 isoenzymes have a profound effect on the kinetic properties of the catalytic unit. Therefore, proteins that regulate PDE activity may act by binding to these NH_2-terminal splice domains. In order to understand the mechanism for RB3 inhibition of rpde6, NH_2-terminal deletions of rpde6 were prepared (by Dr Grant Scotland, University of Glasgow). I tested one of these, Δp1 rpde6, for inhibition by RB3. Δp1 rpde6 lacks the first 9 amino acids of rpde6 after the initiator methionine (see Figure 5.28, section 5.11, below). Interestingly this region contains one of the 3 putative SH3 domain binding motifs (O' Connell et al., 1996). In addition, Ser8 in this region is within a putative phosphorylation site for PKC ($S^8E^9R^{10}$) (see Table 5.3, section 5.11.3.2, below).

As shown in Figure 5.26 and Figure 5.27, GST-$RB3^{1-330}$ and GST-$RB3^{170-330}$ both caused dose-dependent inhibition of Δp1 rpde6. 1μM GST-$RB3^{1-330}$ caused a maximum inhibition of around 45-50%. Slightly less marked inhibition (~40%) was effected by an equivalent concentration of GST-$RB3^{170-330}$. The IC_{50} for GST-$RB3^{1-330}$ inhibition of Δp1 rpde6 was 0.18 ± 0.05μM (mean ± S.E., n = 3). The IC_{50} for GST-$RB3^{170-330}$ inhibition was 0.20μM (n = 1).Both of these IC_{50} values correspond well with the equivalent values obtained for inhibition full-length rpde6 (see Figure 5.18 and Figure 5.22). Therefore, we can conclude Δp1 retains the structural features that are required for inhibition by RB3. These results suggest that RB3 interaction occurs at site downstream of Arg10.

Studies by Beard et al have shown that the association Δp1 rpde6 with Lyn SH3 is severely reduced is comparison with full-length rpde6 (Beard and Houslay, unpublished). As shown in the previous section, the presence of Lyn SH3 partially blocks the inhibition of full-length rpde6 by RB3. Therefore, it would be interesting to see whether the presence of Lyn SH3 also affects the inhibition of Δp1 rpde6 by RB3.

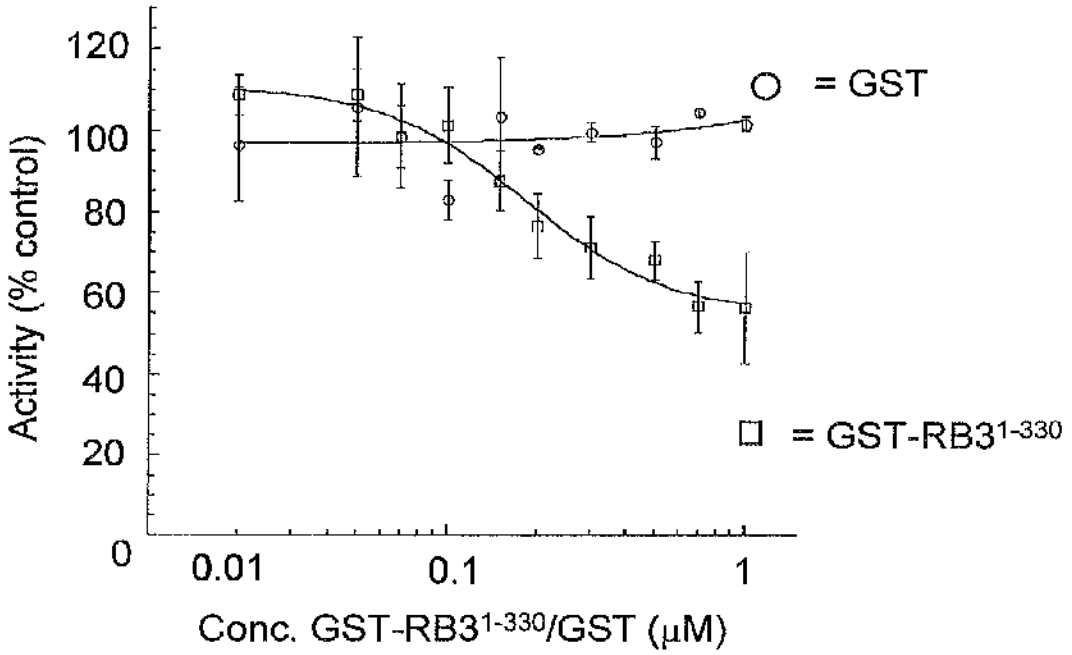

Figure 5.26 Δp1 rpde6 is inhibited by GST-RB3$^{1-330}$.

The effect of GST-RB3$^{1-330}$ (□) or GST (O) on the activity of soluble Δp1 rpde6 is shown. Equal samples of the cytosolic fraction of COS-7 cells transfected with the NH_2-terminal rpde6 deletion mutant Δp1 rpde6 (Δ2-10 rpde6), were diluted in complete KHEM buffer and incubated for 1h on ice with increasing concentrations of either GST-RB3$^{1-330}$ or GST diluted in 20mM Tris-HCl pH 8.0. These mixtures were then assayed for PDE activity. The activity is expressed a percentage of the control activity (~1EU), measured in the absence of GST-fusion protein or GST. The values for the GST-RB3$^{1-330}$ (□) and GST (O) curves are the means of 3 and 2 experiments, respectively ± S.E.

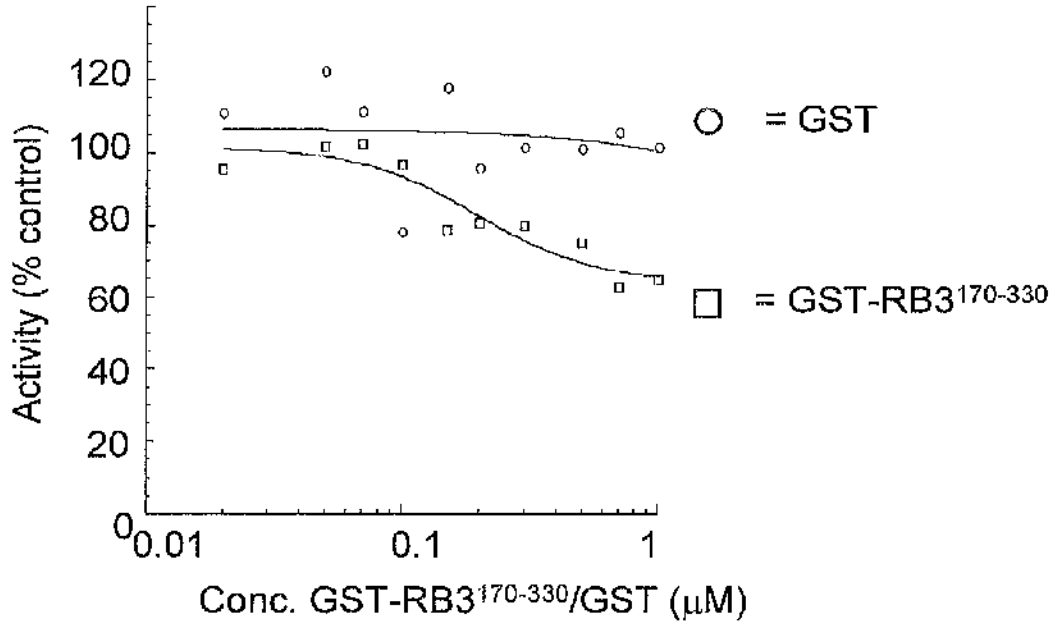

Figure 5.27 Δp1 rpde6 is inhibited by GST-RB3$^{170-330}$.

The effect of GST-RB3$^{1-330}$ (□) or GST (O) on the activity of soluble Δp1 rpde6 (Δ2-10 rpde6) is shown (n = 1). The experiment was carried out as described in the legend for Figure 5.26. The activity is expressed as a percentage of the control activity (~1 EU), measured in the absence of GST-fusion protein or GST.

5.11 Locating the binding region on rpde6 for RB3

Locating the acceptor site(s) for RB3 on rpde6 will provide us with an insight into the mechanism of RB3 inhibition. An important question is whether the acceptor site is within a conserved region (UCR1, UCR2 or catalytic unit) or a region unique to rpde6. Answering this question will allow us to predict whether other PDE4 splice variants in addition to rpde6 are regulated by RB3.

I have screened a series of NH_2-terminal truncations of rpde6, (prepared by Dr. G. Scotland and Dr. M. Beard), for interaction with RB3 (see Figure 5.28). These NH_2-terminal truncations were engineered using the expression vector pSV-SPORT-rpde6 in which rpde6 expression is under the control of an SV40 promoter. These deletions were truncated at various significant positions within the NH_2-terminus of rpde6. Δp1 was generated by removal of the sequence containing the first putative SH3 domain binding motif. Δp4 was made by truncating to the first splice junction, where rpde6 and rpde39 diverge (see Figure 5.28, panel A). Δp5 represents rpde6 downstream of the start of UCR1. In Δp6, rpde6 is truncated to the beginning of linker region 2 (LR2), whereas Δp7 was generated by truncation to 5 amino acid residues before the start of UCR2. Met^{26}RD1 represents the core region of rat PDE4A downstream of the splice junction for RD1, in the centre of UCR2 (Figure 5.28, panel A). The deletion mutant Δp6-loop Δp7 is equivalent to Δp6 rpde6 with the region from the start of UCR2 to the second splice junction removed.

GST-$RB3^{170\text{-}330}$ was used in a pull down assay to test the above rpde6 truncates for interaction with RB3. The plasmids expressing the above deletion mutants were each transiently transfected into COS-7 cells. Samples of cytosol from these transfected cells, containing 100EU of PDE activity, were incubated with samples of GST-$RB3^{170\text{-}330}$ (or GST) on glutathione Sepharose beads at 4°C for 30min. The time course obtained for the binding of rpde6 to GST-$RB3^{170\text{-}330}$ suggested that this was sufficient time for interactions to occur to completion (see Figure 5.13, section 5.4.2). The beads were then isolated by centrifugation and washed with complete KHEM buffer. Bound protein was eluted with glutathione buffer. The percentage binding of the rpde6 deletion mutants to GST-$RB3^{170\text{-}330}$ was determined from the total PDE activity in the bound and unbound fraction, as described previously (see section 5.4). The results are shown in Figure 5.29.

The rpde6 truncates Δp1 to Δp7 showed significant association with GST-$RB3^{170\text{-}330}$. However, in contrast, very little association was observed between Met^{26}RD1 and

GST-RB3$^{170-330}$. No association was observed between any of the deletion mutants and GST (Figure 5.29). These results, obtained from following PDE activity, were supported by an analysis of the immunoreactive protein in the bound and unbound fractions (Figure 5.30). This was monitored as described above in section 5.4. Samples of the bound and unbound fraction were separated by SDS-PAGE, transferred onto nitrocellulose and immunoblotted with anti-PDE4A polyclonal antibody as primary reagent. The percentage binding values of the various NH_2-terminal deletions to GST-RB3$^{170-330}$ were calculated from the densities of the immunoreactive bands obtained. Again, the deletion mutants Δp1 to Δp7 showed significant binding in contrast to Met^{26}RD1 which showed very little binding.

These results led us to conclude that a 42 amino acid residue region from the start of UCR2 (Ser218) to the RD1 splice junction (Arg259) in the middle of UCR2, is necessary for interaction with RB3. In support of this hypothesis, removal of this region from Δp6 rpde6, to create the mutant Δp6-loop-Δp7, abolished binding to GST-RB3$^{170-330}$.

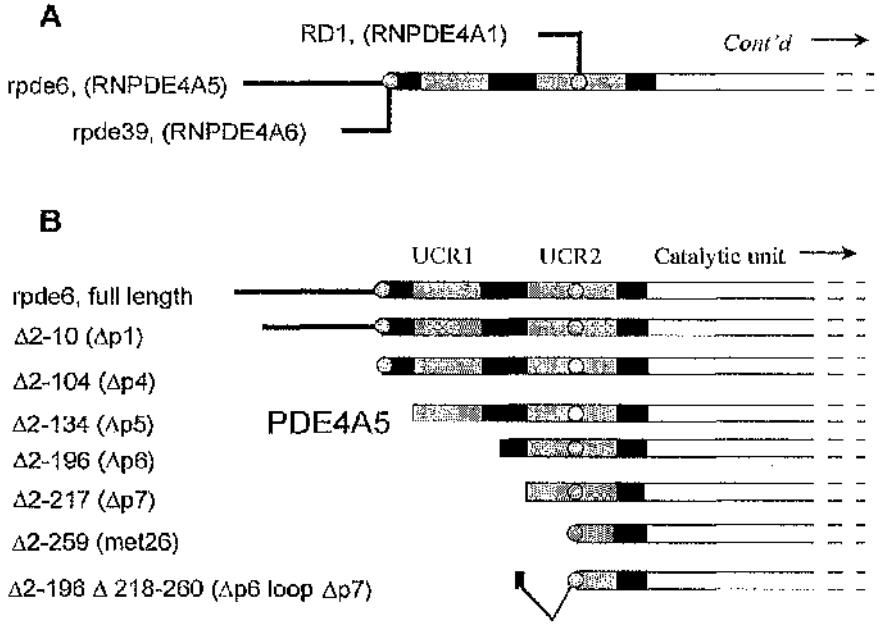

Figure 5.28 NH_2-terminal truncates of rpde6 used to determine the RB3 binding domain.

Panel A shows a schematic representation of rpde6 in relation to the other PDE4A splice variants, rpde39 (RNPDE4A6) and RD1 (RNPDE4A1). The unique NH_2-terminal splice domains are shown as black lines. The two splice junctions are marked with grey circles. Upstream conserved regions are shown as grey bars, the catalytic unit is indicated with a white bar. Panel B shows the range of rpde6 NH_2-terminal deletion mutants used to map the binding site for RB3. The names of the NH_2-terminal truncates (in parentheses) and the amino acid residues deleted, are shown on the left. Plasmids expressing deletion mutants Δp1-Δp7 were generated by mutagenesis of the cDNA for full-length rpde6 in pSVL, by Dr G. Scotland, University of Glasgow. Δp6 loop Δp7 is equivalent to Δp6 rpde6 with the first half of UCR2 deleted and was generated by Dr M. Beard. Met^{26}RD1 was engineered in pSV-SPORT by our group previously (Shakur et al., 1993). For all truncates except Met^{26}RD1, the initiator methionine for full-length rpde6 was retained. Excluding this methionine, the start sites for the various truncation mutants were as follows: Δp1= Ser11, Δp4= Leu103, Δp5= Ser135, Δp6= Pro197, Δp7= Ser218. The start site for Met^{26}RD1 is at Met260 in rpde6.

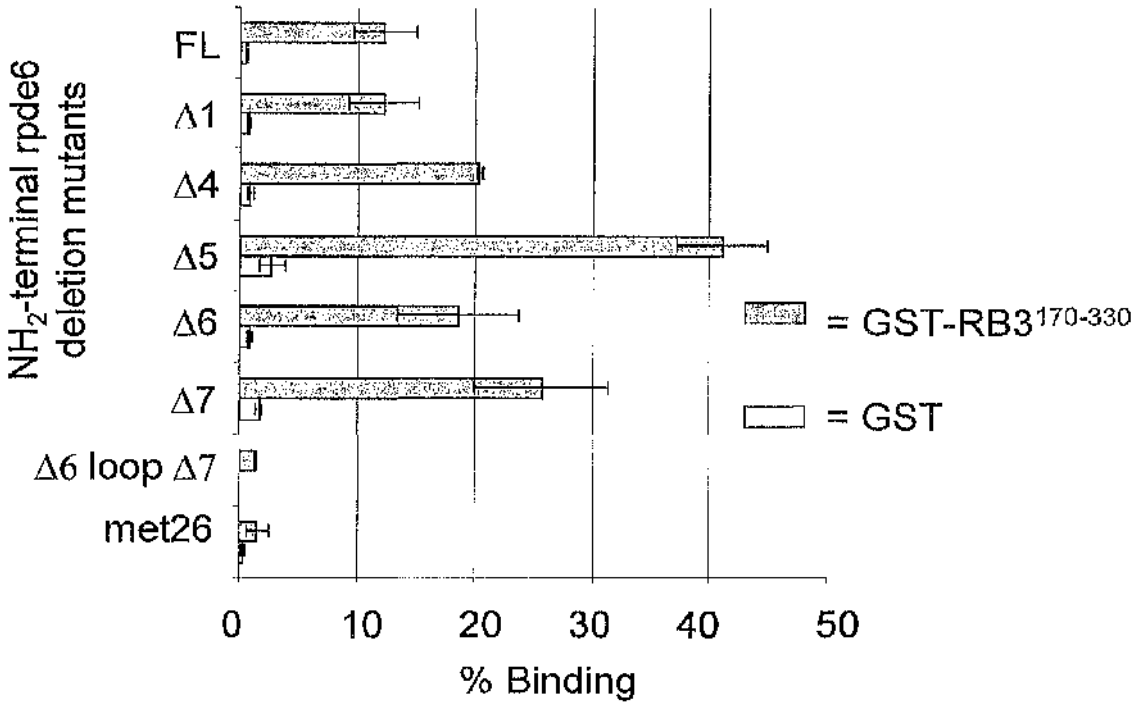

Figure 5.29 Association of rpde6 NH_2-terminal deletion mutants with the COOH-terminal half of RB3 (GST-RB3$^{170-330}$) (PDE activity data)

This chart shows the relative binding of rpde6 NH_2-terminal deletion mutants to the GST-RB3$^{170-330}$ (COOH-terminal half of RB3, amino acids 170-330) and GST alone. COS-7 cells were transiently transfected with the NH_2-deletions illustrated in Figure 5.28. Samples of the cytosolic (S) fractions from these cells were incubated with purified GST-RB3$^{170-330}$ or GST bound to glutathione Sepharose beads. The beads were then washed with complete KHEM buffer and bound protein was eluted with 10mM glutathione, 50mM Tris pH 8.0. The total PDE activity in the bound (EU_{BOUND}) and unbound ($EU_{UNBOUND}$) fractions was determined using the PDE assay. The percentage of rpde6 that was 'pulled down' by the GST-fusions under the experimental conditions described was calculated as follows: % binding = 100% x [EU_{BOUND} / (EU_{BOUND}+ $EU_{UNBOUND}$)]. The percentage binding values are shown as mean of three experiments ± standard error. The pull down assay protocol is described in detail in section 2.17. FL= full-length rpde6.

*No control data was obtained for the association of Δp6 loop Δp7 with GST.

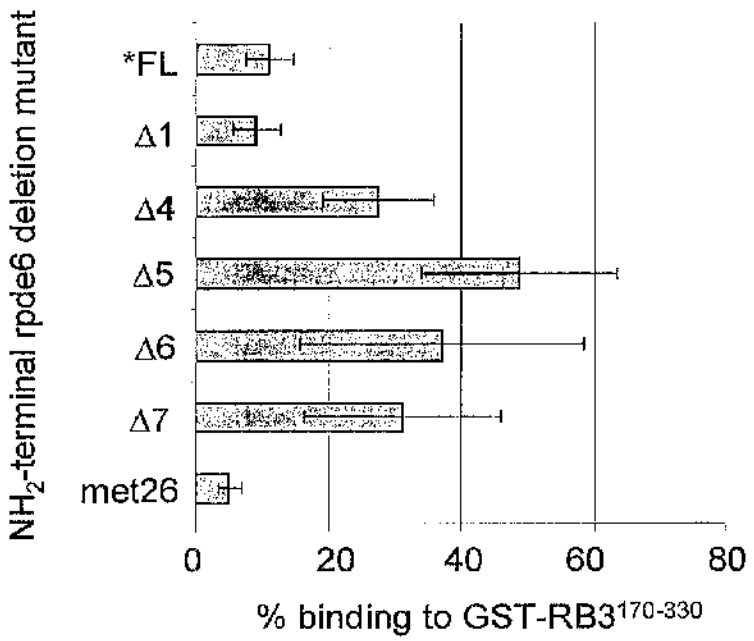

Figure 5.30 Analysis of the binding of rpde6 NH_2-terminal deletion mutants to the COOH-terminal half of RB3 (GST-RB3$^{170-330}$) by western blotting

The % binding of the NH_2-terminal rpde6 deletion mutants (illustrated in Figure 5.28) to the COOH-terminal half of RB3 (GST-RB3$^{170-330}$) was re-assessed by measuring PDE4A immunoreactivity in the bound and unbound fraction from the pull down assay described in the legend for Figure 5.29. Samples of the bound and unbound fractions were separated by SDS-PAGE and immunoblotted for RB3. The % binding was calculated from the relative densities of the immunoreactive bands for the bound and unbound fractions. This procedure is described in detail in the Methods chapter, section 2.17.1. The % binding values are the means of three experiments ± S.E. FL= full-length rpde6.

5.11.1 NH_2-terminal deletions of rpde6 bind to RB3 with greater affinity than the full length rpde6

The percentage binding values obtained above give a rough indication of the relative binding affinities of the rpde6 NH_2-terminal deletion mutants to GST-RB3$^{170-330}$. Comparison of the percentage binding values obtained for the deletion mutants, determined from PDE activity and immunoreactivity measurements, suggests truncation of the NH_2-terminus up to Ser218 increases the affinity of the interaction of rpde6 with the COOH-terminal half of RB3. Analysis of both PDE activity and immunoreactivity suggested that the percentage binding was highest for Δp5 rpde6; ~40-50% binding was observed for Δp5 in contrast to ~10-15% binding observed for full-length rpde6 (see Figure 5.29 and Figure 5.30 above). The binding values for Δp6 (~20-35%) and Δp7 (~25-30%) were also significantly higher than that of the full-length rpde6. Therefore it appears that sequences upstream of the start of Δp5 (start of UCR1, see Figure 5.28) do not enhance the binding of rpde6 to RB3.

It seems that removal of sequences in rpde6 that are not involved in binding RB3 may increase the affinity of the interaction. Therefore the sequences upstream of the RB3 binding site in rpde6 may impede its interaction with RB3, possibly by steric hindrance. Post-translational modifications or protein-protein interaction that alter the conformation of rpde6, may change the accessibility of the binding sites and, in this way, regulate the rpde6:RB3 interaction.

It should be noted that a more reliable assessment of the binding affinities of rpde6 deletion mutants to GST-RB3$^{170-330}$ requires an ELISA binding assay or BIAcore procedure using purified rpde6 deletion mutants in addition to purified GST-RB3$^{170-330}$ at known concentrations (Nieba et al., 1996).

5.11.2 Sequence analysis of the RB3 binding domain

The above results suggest that the region from the start of UCR2 to the RD1 (RNPDE4A1) splice junction contains a sequence required for interaction with RB3 (see Figure 5.31 below). As mentioned in the Introduction chapter, section 1.4, the RD1 splice variant is unusual in that its splice junction is located near the middle of UCR2. The splice junction for the known short forms of PDE4B and PDE4D are located at the beginning of UCR2 (see Introduction, section 1.4). Therefore, the RB3 interaction site is highly conserved in nearly all PDE4 isoenzymes including the short forms PDE4B2 and PDE4D1.

However, the unique NH_2-terminal splice domains of these isoenzymes will affect the accessibility of this binding site. Therefore, not all of these isoenzymes may associate with RB3.

This region of UCR2 is necessary, but possibly not sufficient for interaction with RB3. Regions downstream of the RD1 splice junction may also be necessary for interaction with RB3. In order to define fully the RB3 binding region, a series of COOH-terminal truncations of rpde6 will have to be tested for association with RB3. These could be expressed as GST-fusion proteins for use in pull down assays using cytosolic COS-7 cell expressed RB3. The residues in rpde6 involved in binding RB3 may be spread out in the amino acid sequence but topologically adjacent in the 3D structure.

Both the putative SH3 domain binding motifs in the rpde6 (O' Connell et al., 1996) and the RACK1 binding site in PDE4D5 (Yarwood et al., 1999) are located in the unique NH_2-termini of these PDE4 isoenzymes. In contrast, the region defined above as necessary for RB3 interaction site is relatively close to the catalytic unit. This may explain why RB3 affected rpde6 activity, whereas RACK1 or SH3 domain interactions do not affect PDE activity (O' Connell et al., 1996; Yarwood et al., 1999).

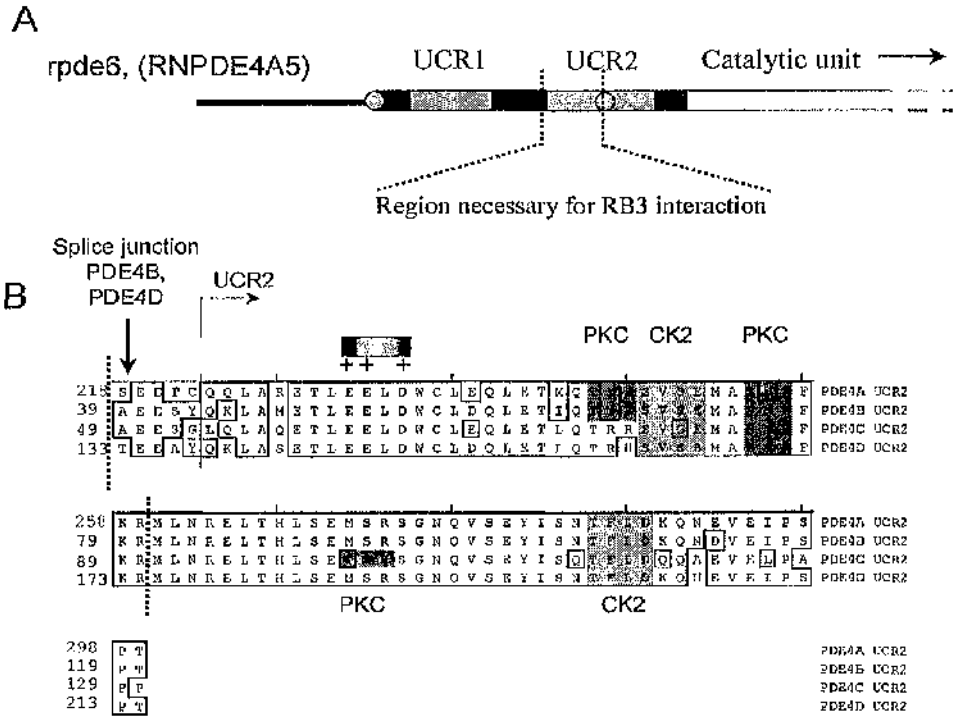

Figure 5.31 Alignment of rat UCR2 sequences.

This figure shows an alignment of the UCR2 regions from PDE4A, PDE4B, PDE4C and PDE4D. The numbers to the left of the sequences refer to the amino acid positions in the splice variants RNPDE4A5 (rpde6; GenBank accession No. L27057), RNPDE4B2 (GenBank accession No. L27058), RNPDE4C1 (GenBank accession No. L27061) and RNPDE4D3 (GenBank accession No. UO9497). Residues that match the consensus sequence for this region are boxed. The region in rpde6 necessary for interaction with RB3 is contained between the vertical dashed lines. Note that this region actually starts 5 amino acid residues before the NH_2-terminal start of UCR2. The UCR2 regions were analysed for the presence of putative phosphorylation sites using MotifFinder (http://www.motif.genome.ad.jp). Shaded boxes indicate the positions of putative phosphorylation sites for protein kinase C and casein kinase 2.

5.11.3 Key amino acid residues within the RB3 interaction domain

Analysis using yeast two-hybrid and *in vitro* binding studies in PDE4D3 has shown that UCR1 and UCR2 interact with each other (Beard et al., 2000). This interaction was blocked by alanine substitution of the acidic residues Glu146, Glu147 and Asp149 within the NH_2-terminal half of UCR2. The positions of the equivalent residues in rpde6 are Glu231, Glu232 and Asp234 and these residues are marked '+' in panel B of Figure 5.31 above. The UCR1:UCR2 interaction was also abolished by mutation of two positively charged amino acids to alanine, (Arg98 and Arg101 in PDE4D3), found towards the COOH-terminal end of UCR1 (Beard et al., 2000). Significantly, mutation of Ser54 (in PDE4D3) to Asp at the NH_2-terminal end of UCR1 also disrupted the interaction. This Asp substitution mimics phosphorylation of Ser54 by PKA. A model was thus proposed, where UCR1:UCR2 interactions are determined by electrostatic interactions that are disrupted by PKA phosphorylation at Ser54.

Clearly, interaction of RB3 with the amino terminal half of UCR2 could potentially disrupt the UCR1:UCR2 interaction, which may in turn affect the structure and activity of the catalytic region. This may explain the observed inhibitory effect of RB3 on rpde6 activity.

5.11.3.1 Does the first half of UCR2 contain a TPR domain acceptor site?

As discussed in the introduction to this chapter (section 5.2.3.2), the immunophilins FKBP52 and Cyp40 and the immunophilin-related protein, ARA9/XAP2 (human homologue of RB3), all interact with hsp90 via their COOH-terminal regions. In both FKBP52 and Cyp40, the hsp90-interaction region has been mapped to their three-repeat TPR domains (Barent et al., 1998; Radanyi et al., 1994; Ratajczak and Carrello, 1996). This suggests that the single TPR repeat of ARA9/XAP2 may be involved in binding hsp90. As TPR domains are believed to mediate a wide range of protein-protein interactions (Lamb et al., 1995) the TPR motif of RB3 may also mediate interaction with rpde6.

It would be extremely useful to know the nature of the TPR domain acceptor site on hsp90 as this might help identify the precise residues in rpde6 that interact with RB3. Hartl and co-workers have shown that the COOH-terminal 104 amino acid region of hsp90α mediates interaction with several TPR domain containing proteins (Young et al., 1998).

Similarly, Carrello et al have mapped the acceptor site for a number of TPR proteins to the COOH-terminal 124 amino acids of hsp90β (Carrello et al., 1999). In addition, Carrello et al showed that the sequence EEVD, at the COOH-terminus of hsp90β, is absolutely necessary for interaction with Cyp40. This EEVD microdomain is also found in the COOH-terminus of heat shock cognate protein 70 (Hsc70) where it has been shown to mediate interactions with TPR domain-containing proteins (Liu et al., 1999).

Interestingly, in rpde6 a similar sequence, $E^{231}E^{232}L^{233}D^{234}$ is found in the NH_2-terminal half of UCR2, the region shown to be necessary for interaction with RB3. These residues are conserved in all members of the PDE4 gene family (see Figure 5.31 above). Therefore, it is possible that this microdomain may mediate interaction with TPR motif in the COOH-terminal half of RB3. As discussed in the above section, the glutamate pair and the aspartate residue in this motif are also essential for the intramolecular interaction between UCR1 and UCR2. The TPR domain of RB3 may compete with UCR1 for interaction with these residues.

Of further interest is work by Russell et al who showed that the conserved, positively charged residues, Lys97 and Arg101, in the third TPR motif of protein phosphatase 5 (PP5), were essential for hsp90 interaction (Russell et al., 1999). These residues are found at similar positions in the TPR motif of RB3, (Lys266 and Arg271) (see Figure 5.6, section 5.2.3.2). Russell et al conjectured that these residues might interact electrostatically with the EEVD motif. In addressing this question, Russell et al also showed that alanine substitution the glutamate pair in this microdomain significantly diminished, but did not eliminate binding of PP5, suggesting the existence of additional binding residues in hsp90 (Russell et al., 1999). By analogy, rpde6:RB3 complex formation may depend on electrostatic interactions between Lys266 and Arg271of the RB3 TPR motif and a number of acidic residues, including those in the EELD motif in the NH_2-terminal half of UCR2.

It should be noted that, unlike the EELD motif of rpde6, the EEVD motifs of both hsp90 and hsp70 are found at their extreme COOH-termini, which might be a necessity for interaction with TPR domains. However, the possibility that the EELD motif of rpde6 forms part of a TPR acceptor site is worthy of further investigation.

5.11.3.2 Putative phosphorylation sites within the RB3 interaction region

Many protein-protein interactions are affected by phosphorylation. For instance, SH2 domains only interact with sequences containing a phosphorylated tyrosine.

Conversely, as discussed below, phosphorylation of FKBP52 by casein kinase 2 disrupts interaction with hsp90 (Miyata et al., 1997). Therefore, in attempting to understand the regulation of the rpde6:RB3 interaction it is useful to locate the putative phosphorylation sites with the RB3 interaction region on rpde6 and the COOH-terminal half of RB3.

Figure 5.31, panel B shows the putative phosphorylation sites within the entire UCR2 region of rat PDE4A (PDE4A UCR2) and their conservation in other PDE4 genes. As shown in this figure, in rpde6 (a PDE4A splice variant) the region necessary for RB3 interaction (enclosed by vertical dotted lines) contains three putative phosphorylation sites; two for protein kinase C and one for casein kinase 2. In addition, the COOH-terminal half of UCR2 contains another phosphorylation site for casein kinase 2 as shown in Figure 5.31. As mentioned in the beginning of section 5.11.2, the RB3 interaction region may extend downstream of Met260. Phosphorylation of one or more of the putative sites within the RB3 interaction region may prevent or enhance the interaction between rpde6 and RB3. The consensus sequences for these phosphorylation sites are shown in Table 5.3, below.

Table 5.3 Consensus phosphorylation sites for protein kinase C and casein kinase 2

Kinase	Consensus phosphorylation site
Casein kinase 2 (CK2)	[ST]-X-X-[DE]
Protein kinase C (PKC)	[ST]-X-[RK]

In the above table the positions the amino acid residues are represented by letters separated by dashes (X= any amino acid). Letters contained within square brackets represent the amino acid residues that can occupy that position in the phosphorylation motif. Note that PKC and CK2 are serine/threonine protein kinases.

As mentioned above, the protein-protein interactions of RB3's closest relative, FKBP52, are regulated by phosphorylation. CK2-dependent phosphorylation of FKBP52 disrupts hsp90 binding (Miyata et al., 1997) which has been mapped to the COOH-terminal TPR domain (Radanyi et al., 1994). Although the authors identified Thr143 as being a major substrate for CK2, other sites in FKBP52 may be CK2 phosphorylated, preventing interaction with hsp90. RB3 contains four putative CK2 sites and two PKC sites. The effect of CK2 or PKC phosphorylation on the interaction between RB3 and rpde6 is worthy of future investigation.

5.12 Effect of PMA and forskolin/IBMX stimulation on the rpde6:RB3 interaction.

As mention above, the RB3 interaction domain contains two putative PKC sites. This suggested that PKC phosphorylation of this region might affect the interaction of rpde6 with RB3. In addition, a number of PDE4 isoenzymes are activated or inhibited by ERK2 (MAP kinase) phosphorylation of a conserved site near the COOH-terminus of the catalytic unit (Hoffmann et al., 1999; MacKenzie et al., 2000). ERK2 phosphorylation of rpde6 may also prevent or enhance the inhibitory binding of RB3. ERK2 is activated in a PKC dependent manner (MacKenzie et al., 1997). Therefore, to assess the effect of PKC on the rpde6:RB3 interaction, COS-7 cells transfected with rpde6 were stimulated with phorbol 12-myristate 13-acetate (PMA). PMA mimics the second messenger diacylglycerol (DAG) which binds to and activates PKC. COS-7 cells transfected with rpde6 were stimulated for 5 min with 100nM PMA. This treatment is known to produce an optimal ERK2-dependent inhibition of PDE4D3 activity (Baillie, MacKenzie and Houslay, unpublished). Cytosolic rpde6 from these cells was then tested for inhibition by GST-RB3$^{1-330}$.

Protein kinase A (PKA) has been shown to activate the PDE4D3 isoenzyme by phosphorylation of Ser54 at the NH_2-terminal end of UCR1 (Hoffmann et al., 1998; Sette and Conti, 1996). This serine is conserved in all 'long' PDE4 isoenzymes. As mentioned above, in section 5.11.3, phosphorylation at Ser54 of UCR1 disrupts interaction between UCR1 and UCR2 (Beard et al., 2000). Alteration in the conformation of the UCR1:UCR2 domain may affect interaction with RB3. To examine this, rpde6 transfected COS-7 cells were stimulated with a combination of 100μM forskolin and 100μM IBMX for 20min to elevate intracellular cAMP levels and activate PKA. Such treatment is known to cause an optimal phosphorylation of HSPDE4D3 (MacKenzie, Baillie and Houslay, unpublished). Cytosolic rpde6 from PKA stimulated cells was tested for interaction with RB3, by assessing inhibition with GST-RB3$^{1-330}$.

The effect of PMA or IBMX/forskolin treatment on rpde6 inhibition by GST-RB3$^{1-330}$ is shown in Figure 5.32. As shown in this figure, such treatments have no significant effect on the ~40-50% inhibition observed in the presence of 1μM GST-RB3$^{1-330}$. The conditions used were known to activate PKA, PKC and ERK2 (downstream of PKC) (MacKenzie et al., 1997) to a sufficient level for phosphorylation of PDE4D3 (Baillie et al,

unpublished work). Either none of these kinases phosphorylate rpde6 (PDE4A5) or phosphorylation does not alter the conformation or electrostatic properties of rpde6 in a way that prevents interaction with RB3.

As mentioned in section 5.11.3.2, the region on rpde6 necessary for interaction with RB3 contains a putative CK2 phosphorylation site. The signalling pathways that regulate CK2 are unknown (Miyata et al., 1997). Therefore, the above experiment does not exclude the possibility that CK2 may regulate the rpde6:RB3 interaction.

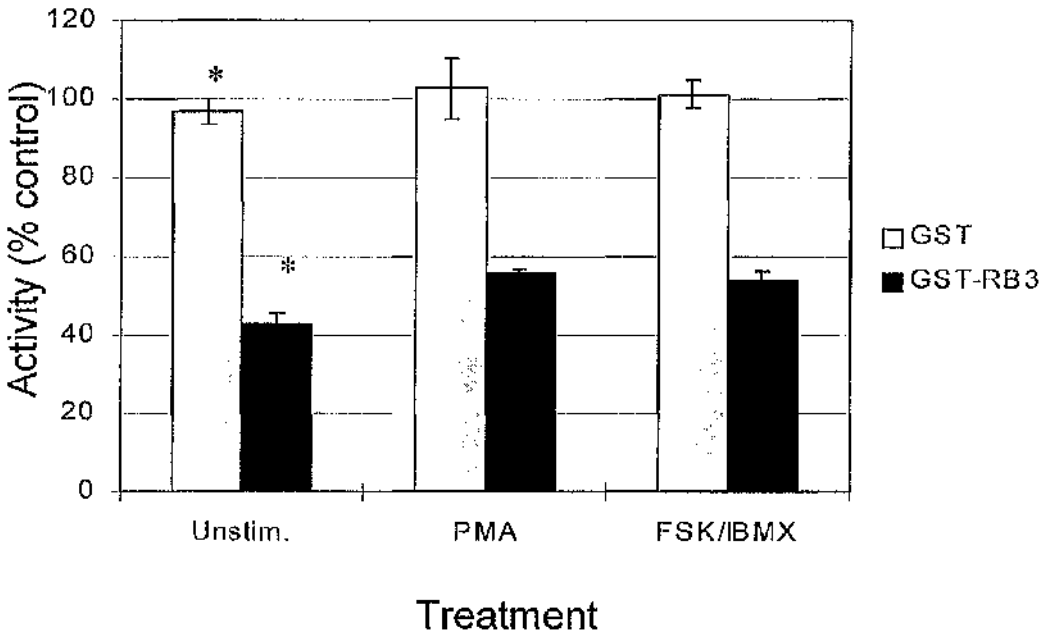

Figure 5.32 GST-RB3$^{1-330}$ inhibition of cytosolic rpde6 from transiently transfected COS-7 cells stimulated with either PMA or forskolin /IBMX.

COS-7 cells were transfected with rpde6 and stimulated with either 100nM PMA for 5min or 100μM IBMX for 20min followed by 100μM forskolin for a further 20min. Samples of the cytosolic (S) fraction from these cells were incubated with GST or GST-RB3$^{1-330}$ (final assay concentration = 1μM) for 1h on ice prior to PDE assay with 1μM 8-[^{3}H]-cAMP. The activity values are expressed as a percentage of the control activity in the absence of GST-fusion protein. The values are the means of three experiments ± S.E.

*= these data were shown previously in Figure 5.18, section 5.7.1 and are shown again here for comparison.

5.13 Interaction of rpde6 with FKBP52

In terms of understanding the regulation and targeting of rpde6 it is important to establish whether the rpde6:RB3 interaction is specific, or whether rpde6 can interact with other proteins that are similar to RB3. It should be noted that RB3 might not be the 'real' binding partner for rpde6 *in vivo*. Although RB3 was pulled out in a screen of a rat brain cDNA library, rpde6 (PDE4A5) is expressed in a number of cell lines including rat thymocytes (ElBawab et al., 1997) and 3T3 preadipocytes (MacKenzie et al., 1998). The 'real' rpde6 interaction partner may only be expressed in tissues other than the brain and may not have been present in the rat brain cDNA library. Therefore, a screen of brain cDNA may have pulled out RB3 because it bore the closest structural similarity to the 'real' interaction partner. In addition, earlier studies showed that the COOH-terminal half of RB3, which contains a TPR motif, appears to be responsible for interacting with (section 5.4.1) and inhibiting (section 5.7.4) rpde6. No direct role has been found for the NH_2-terminal half of RB3 in these functions. Therefore, the yeast two-hybrid analysis may have pulled out RB3 because its COOH-terminal half contains regions that are similar in sequence or structure to regions of the native interaction partner. An important feature of the COOH-terminal half of RB3 is the presence of a TPR motif in its COOH-terminal region. It may be the case that rpde6 does not exclusively bind to RB3, but instead binds to one or a number of other TPR domain-containing proteins.

Although yeast two-hybrid analyses cannot confirm that RB3 is the 'true' binding partner for rpde6, this does not lessen the importance of studying the rpde6:RB3 interaction. At a minimum, RB3 may provide a paradigm for one type of interaction that rpde6 undergoes. At a maximum, RB3 may be one of a number of TPR proteins that interact with rpde6.

We would expect a potential protein-protein interaction partner to have a similar subcellular distribution to rpde6. Therefore, in order to facilitate the search for potential binding partners, a list of TPR proteins, whose subcellular distribution patterns have been studied, was compiled (Table 5.4). Many of the TPR domain proteins listed in Table 5.4 are involved in cell cycle control (cdc16, cdc23 and cdc27) or transcriptional repression (SSN6 or nuc2+) and are therefore localised to nucleus or the mitotic spindle during mitosis (Lamb et al., 1995; Sikorski et al., 1990). These proteins are unlikely to interact with rpde6 *in vivo* as immunofluorescence studies using confocal microscopy suggest that the rpde6 is excluded from the nucleus (Huston et al., 2000). Other TPR proteins are

involved in protein import into the mitochondria (Yano et al., 1998) or the peroxisome (Terlecky et al., 1995) and are exclusively targeted to these organelles. This makes them unlikely candidates as protein-protein interaction partners for rpde6, which does not associate with these organelles.

More likely candidates include cyclophilin 40 (Cyp40) whose TPR domain containing COOH-terminus shares sequence similarity with the COOH-terminus of RB3 (see Table 5.1, section 5.2.2) This protein has a speckled distribution in the cytoplasm of rat pulmonary endothelial cells (see Table 5.4) (Owens-Grillo et al., 1996). However, Russell et al has recently suggested that the TPR containing protein phosphatase 5 (PP5), is predominately cytosolic in HeLa cells (Russell et al., 1999) (Table 5.4). This protein may therefore occupy the appropriate compartments for interaction with rpde6. Interestingly, rapsyn (Ponting and Phillips, 1996) is an interesting example of a TPR protein that is involved in organising the cytoskeleton at the postsynaptic density. A similar protein may mediate the observed targeting of rpde6 to structures that resemble the cytoskeleton in transfected COS-7 cells (Huston et al., 2000).

As shown in section 5.2.2, FKBP52 is homologous to RB3. Like RB3, FKBP52 contains a TPR domain in its COOH-terminal region and an FKBP homology domain in its NH_2-terminal region. It is possible that FKBP52 also interacts with rpde6. Analysis by immunofluorescence microscopy shows that FKBP52 is targeted to both the nucleus and the cytoplasm (Owens-Grillo et al., 1996). Cytoplasmic FKBP52 is localised to a cytoskeletal network and this pattern is reminiscent of the subcellular distribution of rpde6, observed in transfected COS-7 cells (Huston et al., 2000). This suggests that FKBP52 and rpde6 may occupy the same intracellular compartments. In order to test whether FKBP52 could bind to and regulate rpde6, I assessed the effect of FKBP52 on rpde6 enzyme activity.

Table 5.4 Subcellular distribution of TPR domain containing proteins

Only TPR domains for which subcellular distribution has been studied are listed in the table below.

TPR protein	No. TPRs	Function	Subcellular distribution		Refs.
			Cell	Subcellular distribution	
Cdc16, cdc23, cdc27,	9-10	Mitosis- part of Anaphase promoting complex (APC)	*S. cerevisiae* HeLa	Localises to spindle/centrosome during mitosis	(Goebl and Yanagida, 1991) (Lamb et al., 1995) (Sikorski et al., 1990)
Cut9+ nuc2+	10	Mitosis	*S. pombe*	Nucleus (nuclear scaffold)	(Goebl and Yanagida, 1991) (Hirano et al., 1990)
PRP6	9	Splicing	*S. cerevisiae*	Nucleus	(Goebl and Yanagida, 1991)
SKI3, Ssn6	8 10	Transcription	*S. cerevisiae*	Nucleus	(Goebl and Yanagida, 1991)
FKBP52	3	FK506 binding protein	Rat pulmonary endothelial COS7 MDCK GT1 (mouse neuronal cells)	80% localised to the nucleus (not nucleoli) 20% cytoplasm Cytoplasmic FKBP52 is found associated with microtubules	(Owens-Grillo et al., 1996) (Perrot-Applanat et al., 1995) (Czar et al., 1994)
ARA9/ AIP/ XAP2	1	Form complex with the Aryl hydrocarbon receptor and hsp90	Mouse hepatoma cells:hepa1c1c7 HeLa cells	Cytoplasm	(Kuzhandaivelu et al., 1996; Ma and Whitlock, 1997)
Cyp40	3	Cyclophilin	Rat pulmonary endothelial	Punctate bodies in cytoplasm Nucleoli	(Owens-Grillo et al., 1996)
PAS8p, PAS10p, PXR1	7	Protein import-peroxisomes	*Pichia pastoris* (methylotrophic yeast)	Peroxisomes	(Lamb et al., 1995) (Terlecky et al., 1995)
MAS70, Tom20, HTOM34p	7	Protein import-mitochondrial	Rat pulmonary endothelial cells, Transiently transfected COS7 cells	Outer mitochondrial membrane	(Owens-Grillo et al., 1996) (Yano et al., 1998)

Table 5.4 ***continued***

TPR protein	No. TPRs	Function	Subcellular distribution		Refs.
			Cell	Subcellular distribution	
P67 phox (NADPH oxidase subunit)	4	Superoxide (O_2^-) generation	Phagocytes	Cytoplasm (translocates to membrane when activated)	(Ponting, 1996)
Rapsyn	8	Molecular linker between AChR and dystrophin-dystroglycan Organises postsynaptic cytoskeleton	*Torpedo californica*	Postsynaptic membranes	(Ponting and Phillips, 1996)
PP5	3	Protein phosphatase	COS1 cells HeLa cells HeLa cells L929	Mitotic spindle apparatus during metaphase Nucleus Cytoplasm Cytoplasm	(Carrello et al., 1999; Ollendorff and Donoghue, 1997) (Chen et al., 1994) (Russell et al., 1999)
O-linked GlcNAc transferase	13	*O*-linked glycosylation of proteins in the cytoplasm and nucleus	*C. elegans* embryonic cells CHO cells Transfected HEK293 cells	Nucleus and perinuclear region Nucleus and cytoplasm	(Lubas et al., 1997) (Kreppel et al., 1997)

5.13.1 FKBP52 inhibits rpde6

The effect of soluble recombinant FKBP52 on rpde6 activity was assessed in a manner similar to that for RB3 (see section 5.7). I obtained, from Prof. G. Bolger, a plasmid encoding a GST-fusion of full length FKBP52. The effect of increasing concentrations of this purified GST-FKBP52 on the activity of cytosolic rpde6 from transfected COS-7 cells was determined as described previously in this chapter (section 5.7). I thus over-expressed this protein in *E. coli* and purified it on glutathione Sepharose beads. FKBP52 is a relatively large protein of the kind that often purify poorly when expressed as GST fusions (Harris, 1998). Therefore I used the modifications for the over-expression and purification procedure set out in section 2.7.3. Note that even with these modifications I was unable to purify usable amounts of a GST-fusion of another high molecular weight immunophilin, Cyp40. Therefore, I was unable to test Cyp40 for interaction with rpde6 using the pull down assay procedure.

After purifying the GST-FKBP52 on glutathione Sepharose beads, the protein was eluted with glutathione buffer and dialysed into 20mM Tris pH 8.0. Samples were analysed by SDS-PAGE and Coomassie blue staining. A typical gel is shown in Figure 5.33. A band [74.1± 3.2 kDa, (mean ± SE, n=4)] of approximately the predicted molecular weight (79kDa) was obtained for GST-FKBP52. However, a strong lower molecular weight band just below the 50.7 kDa marker was obtained that may represent a proteolytic degradation product.

The effects of GST-FKBP52 on COS-7 cell expressed rpde6 activity were determined. This fusion protein was then diluted to the appropriate molar concentrations with Tris buffer. Equal amounts of cytosolic rpde6, diluted in complete KHEM buffer and containing ~1 EU of PDE activity (in the absence of GST-fusion protein), were combined with varying concentrations of GST-fusion protein, incubated on ice for 1h, and then assayed for PDE activity as described in the Methods chapter, section 2.16.

Interestingly, GST-FKBP52 produced a significant inhibition of rpde6 activity (see Figure 5.34). This inhibition was as marked as the inhibition of cytosolic rpde6 with GST-RB3$^{1-330}$ (see Figure 5.18, section 5.7.1). A maximal inhibition (~55% of the control activity) was achieved at a GST-FKBP52 concentration of 1μM. The IC_{50} for GST-FKBP52 inhibition of rpde6 was 0.16 ± 0.07μM (mean value from three separate dose-response curves ± S.E.), which is comparable to the IC_{50} of 0.22 ± 0.04μM obtained for

GST-RB3$^{1-330}$. It should be noted, however, that if the fraction of the FKBP52 fusion protein that was degraded was inactive, then the IC_{50} would be lower. Further studies are needed using fusion protein purified to remove this degradation product in order to define the true IC_{50} value.

Therefore, RB3 may not be unique in its ability to interact with and inhibit rpde6. The above result suggests that a number of different TPR protein may be capable of binding to rpde6 in a way that restricts its catalytic function. The TPR proteins with which rpde6 interacts may vary from cell to cell. This may be a means for the tissue-specific regulation and targeting of rpde6. The above result shows that in order to understand the regulation, targeting and function of rpde6 we need investigate other proteins, apart from RB3.

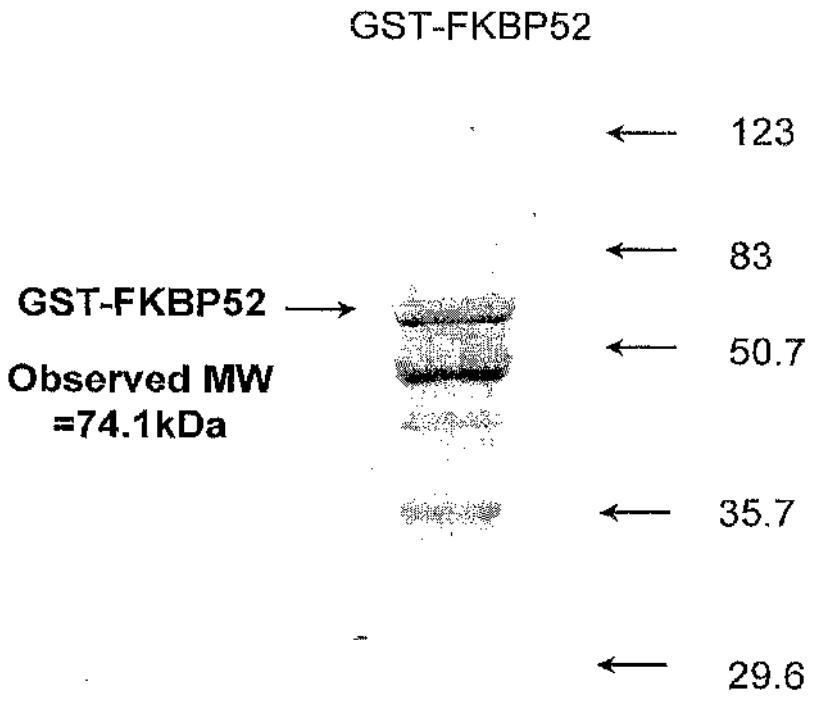

Figure 5.33 Purification of GST-FKBP52

A GST-fusion of full length FKBP52 was over-expressed in *E. coli* (BL21 DE3) and purified using the modified method detailed in section 2.7.3. A 10μg sample of purified GST-FKBP52 was separated on an 8% SDS-PAGE gel. The proteins were visualised by Coomassie staining. The positions of the molecular weight markers (Biorad broad range) are shown on the right. The predicted molecular weight for GST-FKBP52 is 78.9kDa.

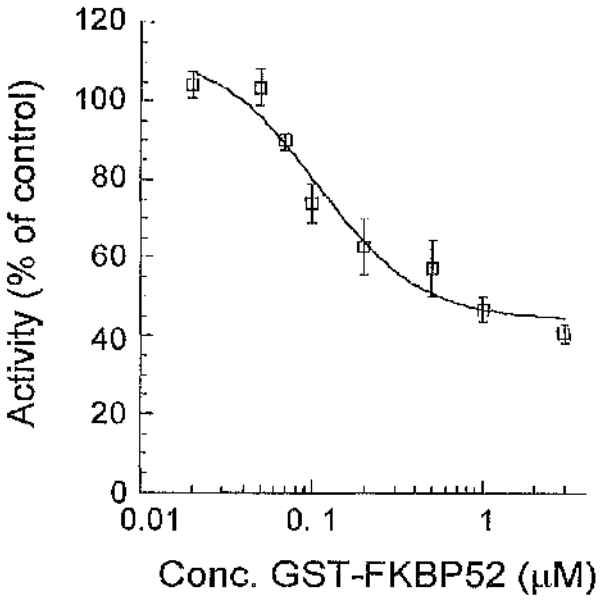

Figure 5.34 FKBP52 inhibits rpde6

This figure shows the inhibition of soluble cytosolic rpde6 by GST-FKBP52. Samples of the cytosolic (S) fraction of rpde6 transfected COS-7 cell fractions diluted in cKHEM were mixed with varying concentrations of purified GST-FKBP52 diluted in 20mM Tris-HCl pH 8.0. After incubating on ice for 1h, the mixtures were assayed for PDE activity by the addition of 1μM 8-[^{3}H] labelled cAMP. The concentration on the x-axis refers to the final concentration of GST-FKBP52 in the assay (after the addition of 8-[^{3}H] cAMP). Molar concentrations of GST-FKBP52 were determined on the basis of calculated molecular weights as described in the Methods chapter (section 2.16). The activities are expressed as a percentage of the control activity in the absence of GST-fusion protein (means ± S.E, n = 3).

5.14 Does hsp90 mediate or inhibit the rpde6:RB3 interaction?

As discussed in section 5.2.3.2, hsp90 interacts with ARA9/XAP2 (human form of rat RB3) *in vivo*. There is some controversy as to whether the presence of the aryl hydrocarbon receptor (AhR) is required for this interaction. Ma and Whitlock were able to co-immunoprecipitate hsp90 and AIP (the mouse homologue of ARA9/XAP2) in AhR-deficient mouse hepatoma cells (Ma and Whitlock, 1997). However, Carver and Bradfield were unable to co-immunoprecipitate *in vitro* translated ARA9/XAP2 and hsp90 in the absence of AhR (Carver and Bradfield, 1997). The latter finding suggests that ARA9/XAP2 and hsp90 only interact in a complex that includes AhR.

Regardless of whether AhR is necessary for complex formation between ARA9/XAP2 and hsp90, two groups have independently shown that the COOH-terminus of ARA9/XAP2 is essential for this interaction. Carver and co-workers showed that amino acids 154-330 of ARA9/XAP2 were sufficient for an interaction with hsp90 (Carver et al., 1998), whereas Meyer and Perdew showed that removal of the COOH-terminal 32 amino acid residues of ARA9/XAP2 prevented association with hsp90 (Meyer and Perdew, 1999).

Interestingly, in this thesis I have localised the binding site for rpde6 to the COOH-terminal half of RB3, amino acids 170-330 (sections 5.4.1). The co-localisation of the binding sites for hsp90 and rpde6 gives rise to a number of possibilities. Firstly, hsp90 may be required for the interaction between rpde6 and the COOH-terminal half of RB3, i.e. rpde6 may directly bind to hsp90, which in turn binds to the COOH-terminus of RB3. The work presented so far in this chapter does not exclude this possibility, as I have not proved that the interaction between rpde6 and RB3 is direct. In my analysis of the rpde6:RB3 interaction, I incubated purified GST-RB3 fusion proteins with cytosolic rpde6 from transfected COS-7 cells (Sections 5.3 and 5.4). Therefore, an indeterminate amount of endogenous COS-7 cell hsp90 would have been present in these pull-down assays. Endogenous hsp90 would also have been present in the yeast strain initially used to identify RB3 as an interaction partner for rpde6.

Secondly, hsp90 and rpde6 may both bind directly to the same site on RB3. We would therefore expect hsp90 and rpde6 to compete for binding to RB3 in a manner similar to the competition between Cyp40 and FKBP52 for association with the hsp90 (Ratajczak and Carrello, 1996). Finally, rpde6 and hsp90 may bind independently to separate sites

within the COOH-terminus of RB3 and the association of one may not affect the association of the other.

5.14.1 Interaction of hsp90 and rpde6 with RB3

The three possibilities described above suggest that hsp90 may enhance, inhibit or have no effect on the rpde6:RB3 interaction. A preliminary experiment was carried out to investigate these possibilities. The scheme for this experiment is illustrated in Figure 5.35. As this diagram shows, an attempt was made to saturate the hsp90 binding sites on GST-RB3$^{170-330}$ using a human hsp90 (GenBank accession number P08238) with a COOH-terminal V5 tag obtained from Prof. Graeme Bolger (the V5 tag is described in Methods, section 2.10). To do this, COS-1 cells were transfected with the plasmid encoding V5-hsp90. In the first stage (incubation 1) increasing amounts of the cytosolic (S) fraction from these cells was incubated with the GST-RB3$^{170-330}$ bound to glutathione Sepharose beads for 30min at 4°C. The beads were centrifuged and washed several times with complete KHEM buffer. The supernatants and washes were retained and pooled to form an unbound fraction (unbound fraction 1). In the second stage (incubation 2) the beads were incubated with the cytosol from rpde6 transfected COS-7 cells for 30min at 4°C. After incubation, the beads were centrifuged and washed as before. The supernatants and washes were retained and pooled to form a second unbound fraction (unbound fraction 2). GST-RB3$^{170-330}$ and associated proteins were then eluted from the beads with glutathione.

The extent of the association between hsp90 and GST-RB3$^{170-330}$ was assessed by immunoblotting samples of the final bound fraction and unbound fraction 1 for V5-hsp90 using an anti-V5 antibody. The results are shown in Figure 5.36. As this figure shows, the percentage binding of V5-hsp90 to GST-RB3$^{170-330}$ was low. However, the immunoblots of the bound fraction show that some binding of hsp90 to GST-RB3$^{170-330}$ took place that was resistant to washing with cKHEM buffer.

The total PDE activities in the bound and (second) unbound fractions were determined and used to calculate the percentage binding of rpde6 as shown in Figure 5.37. This figure shows that pre-incubation of GST-RB3$^{170-330}$ with increasing amounts of cytosolic hsp90 had no effect on the association of GST-RB3$^{170-330}$ with rpde6. This suggests that hsp90 and rpde6 bind to separate sites within the COOH-terminus of RB3.

However, there are a number of limitations to this preliminary experiment. The analysis of the binding of hsp90 to GST-RB3$^{170-330}$ shown in Figure 5.36 does not tell us

the stoichiometry for this interaction, as we do not know the percentage amount of V5-hsp90 in the COS-1 cell cytosol. Therefore, we cannot estimate the proportion of GST-RB3$^{170-330}$ molecules that have associated with hsp90. In addition, some endogenous hsp90 will be present in the COS cell cytosol. Therefore, GST-RB3$^{170-330}$ that has been exposed to both mock-transfected and V5-hsp90-transfected COS-1 cell cytosol may have become associated with an unknown amount of endogenous hsp90, which may affect the results.

A less ambiguous analysis of the effect of hsp90 on the rpde6:RB3 interaction would require purified hsp90 and purified rpde6 in addition to purified GST-RB3$^{170-330}$. We would then be able to assess the rpde6:RB3 interaction in the presence or total absence of hsp90. The results shown in Figure 5.36 suggest that the binding of hsp90 to GST-RB3$^{170-330}$ may be weak. After incubating purified GST-RB3$^{170-330}$ with varying amounts of the cytosolic fraction from V5-hsp90-tranfected COS-1 cells, only a small proportion of hsp90 appears to become associated. Therefore, purified AhR may also be necessary in this study to facilitate the hsp90:RB3 interaction. Unfortunately, an analysis of the direct interaction between purified affinity tagged forms of rpde6 and RB3 *in vitro* has been precluded by proteolytic degradation of full-length rpde6 when I attempted to express this in *E. coli*.

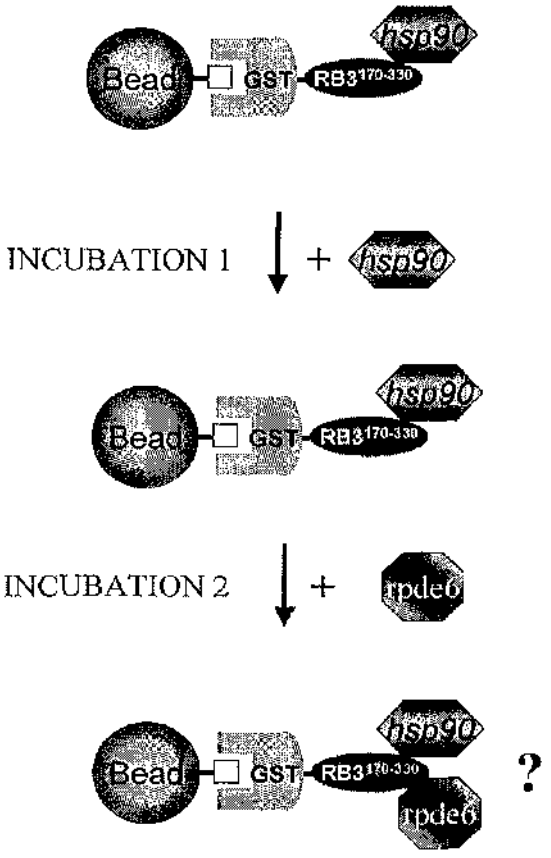

Figure 5.35 Scheme for an experiment to determine whether hsp90 competes with rpde6 for association with the COOH-terminal half of RB3

In the first stage (*incubation 1*) GST-RB3$^{170-330}$ bound to glutathione Sepharose beads is exposed to V5-tagged hsp90 (or untransfected COS-1 cell cytosol as a control) and then washed. The wash fraction is retained (unbound fraction 1). In the second stage (*incubation 2*), the beads are then exposed to rpde6. They are then washed again and this wash fraction is again retained (unbound fraction 2). The GST-RB3$^{170-330}$ and associated proteins are then eluted with glutathione to form a bound fraction. In order to calculate the percentage binding of rpde6 to GST-RB3$^{170-330}$ after exposure to hsp90, the PDE activities in the bound fraction and the unbound fraction 2 are determined. The extent of binding of V5-tagged hsp90 to GST-RB3$^{170-330}$ is determined by immunoblotting samples of the final bound fraction and unbound fraction 1 using an anti-V5 antibody.

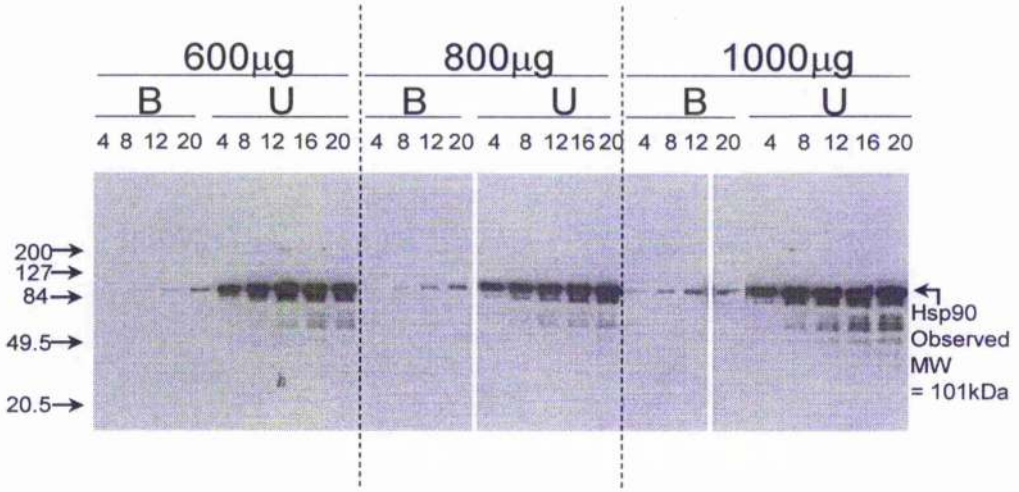

Figure 5.36 Association of hsp90 with GST-RB3$^{170-330}$.

This figure shows the association of hsp90 with GST-RB3$^{170-330}$. As described in the legend to Figure 5.37, samples of the cytosolic fraction (600, 800 or 1000µg) from V5-tagged hsp90 transfected COS-1 cells were incubated with GST-RB3$^{170-330}$ (200 µg) bound to glutathione Sepharose beads at 4°C for 30min. The beads were pelleted by centrifugation and washed with 3 x 400µl of cKHEM buffer. The supernatant and washes were retained and pooled to form an unbound fraction (unbound fraction 1). They were then incubated with cytosolic rpde6 from transfected COS-7 cells. After washing the beads again as described above, GST-RB3$^{170-330}$ and associated proteins were eluted with 3 x 100µl of 10mM glutathione, 50mM Tris-HCl, pH 8.0. Samples of this bound fraction and unbound fraction 1 were separated by SDS-PAGE (10% [w/v] acrylamide), transferred onto nitrocellulose and immunoblotted for V5-hsp90 with anti-V5 antibody as primary reagent. The numbers above the lanes refer to the volumes (in µl) of the fractions run on the gel. The immunoblots shown above were processed on one piece of nitrocellulose.
The calculated MW for V5-hsp90 is 85kDa.

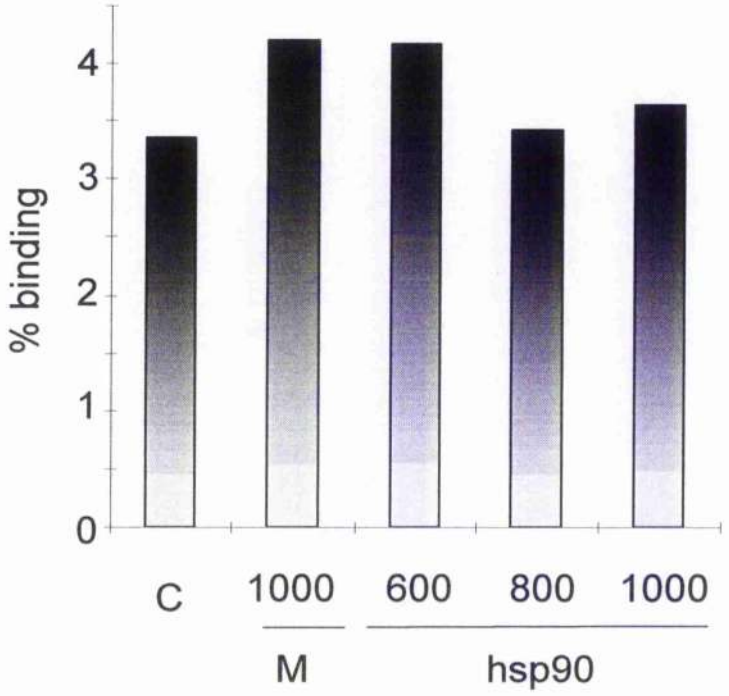

Figure 5.37 Hsp90 does not compete with rpde6 for binding to RB3.

The percentage binding of rpde6 to GST-RB3$^{170-330}$ that has previously been exposed to hsp90 is shown. Samples of GST-RB3$^{170-330}$ (200 μg) bound to glutathione Sepharose beads were incubated with various amounts of cytosolic hsp90 (hsp90), the cytosolic fraction of mock transfected COS-1 cells (M) or cKHEM buffer alone (C). The amounts of hsp90-transfected or mock-transfected COS-1 cell cytosol added are indicated in μg. After incubation, the beads were washed with 3 x 400μl cKHEM buffer. The beads were then incubated with samples of COS-7 cell expressed cytosolic rpde6 (100EU). The beads were centrifuged and washed with cKHEM as before. The supernatants and washes were retained and pooled to form an unbound fraction (unbound fraction 2). Bound protein was eluted with 10mM glutathione, 50mM Tris-HCl pH 8.0. The total PDE activities in the bound fraction and unbound fraction 2 were determined and used to calculate the percentage binding of rpde6 as described in the legend to Figure 5.29, section 5.11.

CHAPTER 5: CONCLUSIONS

5.15 Discussion and conclusions

5.15.1 RB3 can interact with rpde6: possible signalling mechanisms

In this chapter I have demonstrated that the PDE4A isoenzyme rpde6 can interact with an immunophilin-related protein, RB3 *in vitro*. I have thus confirmed an interaction that was initially discovered using the yeast two-hybrid system to probe a rat brain cDNA library with rpde6. In addition, I have shown that this RB3 interaction inhibits rpde6 catalytic activity. This is the first example of a protein-protein interaction that significantly inhibits the activity of a PDE4 isoenzyme.

As discussed in section 5.2, RB3 is the rat homologue of the human protein ARA9/XAP2 which is expressed in a broad range of tissues, including spleen, thymus and liver and brain (Carver and Bradfield, 1997; Meyer et al., 1998). In the liver, ARA9/XAP2 forms a cytoplasmic complex with the ligand-activated transcription factor AhR (the aryl hydrocarbon receptor). The latter binds to environmental toxins, such as polycyclic aromatic hydrocarbons (e.g. TCCD), halogenated dioxins and dibenzofurans. As a result of this binding, AhR translocates to the nucleus where it regulates the transcription of genes encoding the enzymes of xenobiotic metabolism, such as cytochrome P450 1A1 (Schmidt and Bradfield, 1996).

The results presented in this chapter may implicate rpde6 in AhR signalling. Indeed, the rpde6:RB3 interaction may serve as a monitor for xenobiotic cell stress. For instance, the binding of environmental toxins to AhR may cause a conformational change that is transmitted to rpde6 via RB3, causing a change in rpde6 activity. This may result in the activation or inhibition of various cAMP-dependent processes that prepare the cell for xenobiotic stress. It would be interesting to see whether the presence of AhR and a ligand such as TCCD would affect RB3 inhibition of rpde6.

An interesting example of a possible cAMP-dependent response to cell stress has recently been put forward by Anandatheerthavarada et al. This group shows that cAMP-dependent phosphorylation of cytochrome P4502B1 targets this enzyme to the mitochondria in preference to the ER (Anandatheerthavarada et al., 1999). The authors suggest that this may provide the mitochondria with protection from oxidative or chemical

damage. Therefore, cross-talk between cAMP-dependent signalling pathways and the response to chemical or oxidative stress may occur at a number of points. The rpde6:RB3 interaction may represent one such mechanism for this cross talk.

5.15.2 RB3 may protect rpde6 from proteolytic degradation

Meyer and Perdew show that over-expression of ARA9/XAP2 in COS-1 cells enhances the levels of cytosolic, endogenous AhR (Meyer and Perdew, 1999). This suggests that ARA9/XAP2 may stabilise AhR by protecting it from proteolytic degradation. The ability of ARA9/XAP2 to bind to AhR may be a requirement for this effect. A deletion mutant of ARA9/XAP2, lacking the COOH-terminal 67 amino acids, failed to cause an increase in the cytosolic levels of AhR.

RB3 may have a similar effect on the levels of rpde6. To test this, cells that express endogenous rpde6 could be transfected with RB3 and the levels of rpde6 in the various subcellular fractions could be monitored. It is known that the PDE4 isoenzymes are particularly susceptible to proteolytic degradation (Houslay et al., 1998). Therefore, RB3 protection may be an important mechanism whereby the levels of rpde6 are regulated.

5.15.3 RB3 inhibits rpde6 activity

I have shown that submicromolar concentrations of RB3 inhibited rpde6 *in vitro* ($IC_{50} \approx 0.2\mu M$). Inhibition was incomplete (~50-60%) suggesting that RB3 is a non-competitive inhibitor, i.e. it does not block the active site. Signal-induced inhibition of rpde6 by RB3 or a similar protein may have important physiological consequences *in vivo* and this may represent a new mechanism for the control of cAMP levels in cells. An equally important physiological event might be a signal-induced release and activation of rpde6 from an RB3-bound inhibited state.

Interesting, particulate fraction (P1 and P2) rpde6 was resistant to inhibition by exogenous RB3. Proteins similar to RB3 may be associated with subcellular structures represented in the particulate fractions, such as the cytoskeleton. These may sequester rpde6 in an inhibited state that is resistant to further inhibition by soluble RB3. In the P1 pellet fraction, rpde6 may interact with endogenous RB3. Alternatively, a completely different protein may interact with rpde6 in the P2 fraction. In agreement with this, the presence of an excess of Lyn-SH3, previously shown to associate with rpde6 (O' Connell et al., 1996), diminished the inhibitory effect of rpde6 on RB3 activity.

5.15.4 rpde6 interacts with the COOH-terminal half of RB3

I have shown that the COOH-terminal half of RB3 (amino acids 170-330) mediates binding and inhibition of rpde6. It should be noted that the residues and structures that mediate binding may be distinct from those that mediate inhibition. No binding of rpde6 was seen with the NH_2-terminal half of RB3, which contains regions of homology to FKBP12 and the FKBP-domain of FKBP52. In addition, FK506 and rapamycin, which bind to the FKBP domains of FKBP12 and FKBP52, had no effect on the inhibition of rpde6 by RB3. An alignment of RB3 with its closest relative, FKBP52, showed that only 3 out of 14 component residues of the FK506 binding/PPIase site of FKBP52 are conserved in RB3.

Collectively, these results indicated that the NH_2-terminal region was not directly involved in binding or inhibiting rpde6. However, the results did not exclude the possibility that the NH_2-terminal half of RB3 may exert an influence on the interaction with rpde6. The NH_2-terminal region may affect the accessibility of the COOH-terminal rpde6 binding region. In this way it may provide a 'switch' mechanism for the control of the rpde6:RB3 interaction by phosphorylation or protein-protein interactions.

5.15.5 RB3 interacts with the NH_2-terminal half of UCR2

By testing a series of NH_2-terminal deletions of rpde6 for interaction with the COOH-terminal half of RB3 expressed as a GST-fusion (GST-$RB3^{170-330}$) the region Ser218-Arg259 was shown to be necessary for interaction with rpde6. This region covers the NH_2-terminal half of UCR2. Confirmation that this region is required for RB3 binding will be obtained from experiments where a GST-fusion or peptide containing this region can block the interaction of rpde6 with RB3. If a peptide was discovered that disrupted the interaction of rpde6 with RB3 this would have enormous potential value in defining the functional significance of the rpde6:RB3 interaction *in vivo*. The RB3 binding site may extend downstream of Arg259. Therefore, COOH-terminal deletions of rpde6 will have to be employed in order to define the RB3 binding site from both sides.

This RB3 interaction region (Ser218-Arg259) has been implicated in various other fundamental properties of PDE4 isoenzymes. For instance, in PDE4D3 this region has been shown to contain three acidic residues that mediate interaction with UCR1. In rpde6 the equivalent residues are Glu231, Glu232 and Glu234. These negatively charged residues

may form electrostatic intramolecular interactions with two conserved arginine residues near the COOH-terminal end of UCR1.

UCR1 and UCR2 are believed to bind to one another within PDE4 isoenzymes (Beard et al., 2000). It has been suggested that this UCR1:UCR2 'module' integrates the effects of PKA phosphorylation at the NH_2-terminus of the isoenzyme (beginning of UCR1) and ERK2-dependent phosphorylation near the COOH-terminus of the catalytic unit (MacKenzie et al., 2000). ERK2 phosphorylates long and short form PDE4B, PDE4C and PDE4D splice variants. Whether ERK2 phosphorylation causes activation or inhibition of PDE activity depends on what UCR sequences are present in the splice variant concerned. The NH_2-terminal half of UCR2 appears to be crucial in this respect. ERK-dependent phosphorylation of PDE4D1, which has intact UCR2, caused activation of this short PDE4 isoenzyme (see Figure 5.38). However, PDE4D2, which lacks the NH_2-terminal 32 amino acids of UCR2 was mildly inhibited on ERK2 phosphorylation. Long PDE4 isoenzymes, with both UCR1 and UCR2, are strongly inhibited upon ERK2-dependent phosphorylation (MacKenzie et al., 2000). These results are summarised in Figure 5.38.

The interpretation of these results is as follows. In long PDE4 isoenzymes, UCR1 and UCR2 combine to amplify an inherent inhibitory effect of ERK2 phosphorylation on the catalytic unit. The presence of a lone, intact UCR2 in many short PDE4 isoenzymes, such as PDE4D1, causes stimulation of PDE activity upon ERK2-dependent phosphorylation. This effect of UCR2 is abolished by the removal of the NH_2-terminal 32 amino acids of this region in PDE4D2. Therefore, in addition to mediating interaction with UCR1, the NH_2-terminal half of UCR2 is specifically required to effect ERK2-dependent stimulation of short PDE4 isoenzymes (MacKenzie et al., 2000). Although PDE4A isoenzymes do not appear to be phosphorylated by ERK2, it would seem likely that an association of RB3, with the NH_2-terminal half of UCR2, would have a major effect on the mechanisms of regulation of rpde6.

Studies of the subcellular distribution of a series of NH_2-terminal deletions of rpde6 (shown in Figure 5.28) suggest that the 218-259 region in rpde6 can target rpde6 to cellular structures represented in the P2-particulate fraction of transfected COS-7 cells (M. B. Beard and M. D. Houslay, unpublished work). The co-localisation of regions on rpde6 required for P2-association and RB3 interaction suggests that a protein similar to RB3 may target rpde6 to the P2 fraction. Subcellular distribution studies have excluded RB3 itself

from this role as RB3 is absent from the P2 pellet fraction. However, a proportion of RB3 (~16%) is present in the P1 pellet fraction of transfected COS-7 cells (see Figure 5.15, section 5.5.2). One hypothesis proposed above was that endogenous RB3 itself might be involved in the association of rpde6 with the P1 pellet fraction of rpde6-transfected COS-7 cells. Therefore, it would be interesting to investigate whether co-transfection and expression of RB3 in rpde6-transfected cells increased the proportion of rpde6 that became associated with the P1-pellet fraction, when compared with cells that were singly transfected with rpde6. The presence of the P1 pellet-associated RB3 might increase the proportion of rpde6 that associates with this fraction. One could also assess the effect of mutations or deletions within the RB3 binding site on rpde6 on the subcellular distribution of this isoenzyme in transfected COS-7 cells. The results to these experiments would provide evidence for or against an *in vivo* interaction between RB3 and rpde6 in the P1-pellet fraction.

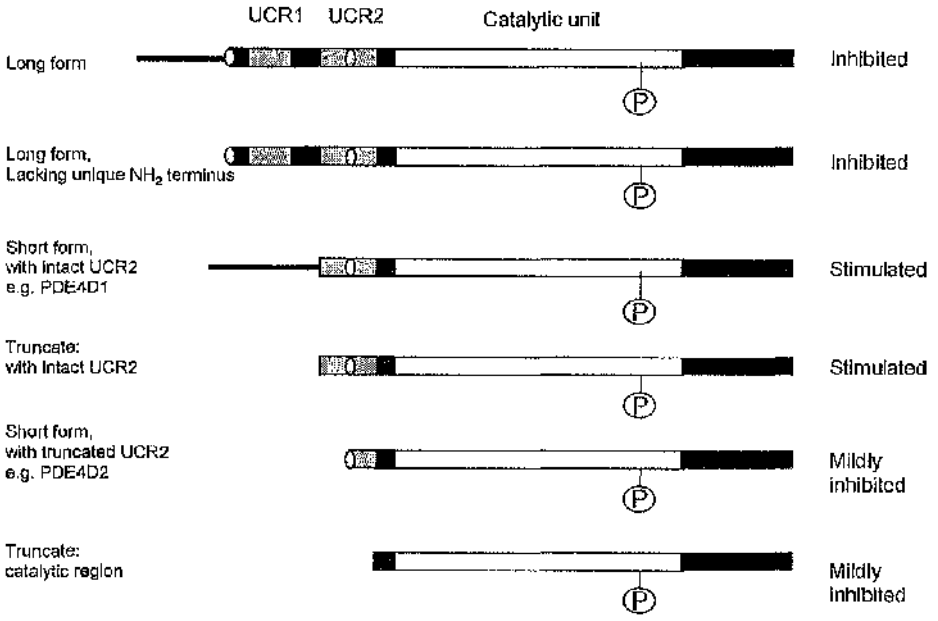

Figure 5.38 ERK2 mediated modulation of the activity of PDE4 splice variants
This figure summarises the effect of ERK2 phosphorylation on the activity of long and short PDE4 isoenzymes and NH_2-terminal PDE4 truncates. The position of the Serine residue phosphorylated by ERK2 is marked with an encircled P. Based on a diagram shown in (MacKenzie et al., 2000).

5.15.6 Interaction of rpde6 with other TPR domain containing proteins

An important question was whether rpde6 interacted only with RB3, or whether RB3 is one of a range of similar proteins that interact with rpde6. As the COOH-terminal half of RB3 mediates interaction with the rpde6, it was sensible to search for proteins that were similar to this half of RB3 rather than the protein as a whole. A striking feature of the COOH-terminal half RB3 was the presence of a TPR motif. Such TPR motifs are known to mediate protein-protein interactions (Lamb et al., 1995).

A plasmid was obtained that encoded a GST-fusion of a close homologue of RB3, FKBP52. Like GST-RB3, GST-FKBP52 produced a dose-dependent inhibition of cytosolic rpde6 activity. The IC_{50} for this inhibition (~0.16μM) was comparable to the value obtained for GST-$RB3^{1-330}$. This result suggested that RB3 might not be unique in its ability to interact with and inhibit rpde6. A structural feature common to both RB3 and FKBP52, such as a TPR motif may mediate inhibitory binding to rpde6.

5.15.7 TPR proteins involved in intracelluiar targeting

As discussed in the introduction, section 1.11.4, TPR proteins may be involved in the intracellular targeting of proteins. Pratt and co-workers showed that complexes containing a TPR protein in association with hsp90 and a steroid hormone receptor such as the glucocorticoid receptor (GR) had distinct patterns of intracellular targeting. These different subcellular distributions were determined by the TPR protein that they contained (Owens-Grillo et al., 1996).

Other experimental observations suggest a specific role for FKBP52 (RB3's closest relative) in protein transport and targeting. FKBP52 is believed to target GR to nucleus by facilitating its movement along cytoskeletal tracts. Cytosolic FKBP52 has been found to associate with microtubules and nuclear FKBP52 has the same distribution pattern as GR (Czar et al., 1994; Pratt et al., 1999). FKBP52 also co-immunoprecipitates with the molecular motor dynein (Pratt et al., 1999). Similarly, RB3 or a similar TPR protein may combine with hsp90 to direct rpde6 to a specific compartment within the cell. In this regard it is important to assess whether rpde6 associates with hsp90.

5.15.8 Future perspectives

An outstanding question is whether the interaction between rpde6 and RB3 is direct or whether it requires an additional component, such as hsp90. In order to answer this question, we need to be able to study the association of purified rpde6 with RB3. Unfortunately, my attempts to over-express and purify full-length rpde6 as an MBP-fusion have been hampered by the susceptibility of full-length rpde6 to degradation by bacterial proteases. However, my studies suggest that the site required for RB3-binding is contained within the NH_2-terminal region of rpde6. I have also shown that is possible to over-express and purify the NH_2-terminal region of rpde6 as the fusion GST-rpde6$^{1-256}$ (see Chapter 4, section 1.1). Therefore, it may be possible to study the interaction of purified MBP-RB3$^{1-330}$ with GST-rpde6$^{1-256}$ [note that MBP and GST do not interact, as shown in (Yarwood et al., 1999)]

In order to gain a deeper understanding of rpde6:RB3 interaction the association of these proteins needs to be demonstrated and studied *in vivo*. Such studies would allow us to determine whether the inhibitory effect of RB3 on rpde6 is physiologically significant. In addition, the idea that rpde6 might be involved in AhR signalling could be pursued by examining the inhibitory binding of rpde6 to RB3 in the presence of AhR (and the AhR ligand TCCD). I have shown that a number of cell lines, including MOLT3 monocytes and B-cells, express RB3 endogenously (section 5.6). These cell lines may be potential model systems for the above *in vivo* studies. The precise residues that are involved in the binding of RB3 to rpde6 need to be defined by the use of NH_2- and COOH-terminal truncations and site directed mutagenesis. This may allow the design of a peptide to disrupt the interaction and thus determine its function *in vivo*. A similar method was successfully used by Rosenmund et al to block the anchoring of PKA by AKAP79 in hippocampal neurones and to show that this interaction is essential for the modulation of AMPA/kainate receptor function (Rosenmund et al., 1994). Even if RB3 is not the true interaction partner for rpde6 *in vivo*, a peptide designed to mimic the RB3 binding site on rpde6 may disrupt the interaction of rpde6 with its true protein binding partner. Perfusion of such a peptide into the cell of interest might, for instance, prevent the correct intracellular targeting of RB3. A more accurate definition of the residues on RB3 required for interaction with rpde6 may allow other potential rpde6 interaction partners to be found. These proteins can then be tested for binding and regulation of rpde6.

CHAPTER 6
General discussion

6.General discussion

The ubiquitous second messenger cAMP transduces the action of a wide range of hormones and neurotransmitters and is involved in the regulation of numerous physiological processes. Complex multi-enzyme families of adenylyl cyclase (which generate cAMP) and PDEs (which degrade cAMP) control the intracellular levels of this second messenger. The elevation of cAMP above a certain threshold results in the activation of PKA, which can phosphorylate many different target proteins. Many of the components of the cAMP signalling system are targeted to specific regions of the cell. For instance, the PKA isoforms are targeted to a number of distinct intracellular compartments by their association with a diverse family of AKAP anchoring proteins (Colledge and Scott, 1999). Evidence has also accumulated for the specific targeting of isoforms of adenylyl cyclase and PDE. The spatial organisation of these cAMP-signalling components suggests the existence of differentially regulated pools of cAMP within cells. This theory provides one explanation for how different stimuli acting via cAMP can produce distinct physiological responses in the same cell (Hohl and Li, 1991).

The cAMP-specific PDE4 family is comprised of four genes which each generate multiple isoenzymes by 5' alternative mRNA splicing. This process generates 'long' and 'short' splice variants that have a shared central to COOH-terminal catalytic region and unique NH_2-terminal splice domains, which confer distinct modes of regulation and intracellular targeting. The PDE4 isoenzymes show tissue-specific patterns of expression and have been implicated in the regulation of the cAMP response and the compartmentalisation of cAMP in a number of cell types. The determination of the unique protein-protein interactions and regulatory properties of the individual PDE4 isoenzymes will aid our understanding of their physiological roles *in vivo*.

In the course of this work I have extended our knowledge of the properties of one particular long form, PDE4A5. Using RT-PCR and sequence analyses I have shown that PDE4A5 is the sole PDE4A isoenzyme expressed in mouse 3T3 F442A preadipocytes. Further studies showed that murine PDE4A5 has an essential role in the regulation of 3T3 F442A preadipocyte differentiation by growth hormone (GH) (MacKenzie et al., 1998). PDE4A5 is specifically activated by GH, via JAK2, PI3-kinase and p70S6 kinase and this has a negative effect on the process of differentiation. I have shown that GH-stimulation does not affect the level of the PDE4A transcript. However, the GH-dependent activation

of PDE4A5 is accompanied by its decreased mobility on SDS-PAGE (MacKenzie et al., 1998), which implies that it is phosphorylated. Further work is required in order to identify the site of phosphorylation and the kinase involved.

I have identified new sites within the NH_2-terminal region of the rat homologue of RNPDE4A5 (rpde6) for the intracellular targeting and regulation of this isoenzyme. Using a chimeric construct, I have shown that the NH_2-terminal region (amino acids 1-256) of rpde6 can confer high-speed P2-membrane fraction association on the normal soluble protein GST. The binding component in the P2-membrane fraction was susceptible to heat-denaturation, which suggested that it might be an unidentified anchoring protein. The region between Leu103 and Lys256 on rpde6 was sufficient for P2-membrane association. This region includes all of UCR1, LR1 and the NH_2-terminal half of UCR2 (see Figure 6.1) and is shared with the other long rat PDE4A isoenzyme RNPDE4A6 (rpde39) which also associates with the P2-membrane fraction. I have also demonstrated that the NH_2-terminal 100 amino acid region of the short form RNPDE4A1 (RD1) can confer P2-membrane fraction association when expressed as a fusion to the COOH-terminus of GST. In contrast to rpde6, the NH_2-terminal region of RD1 interacted with a thermostable component of the P2-membrane fraction, which may be a lipid species.

These studies and the recent work of Huston et al (Huston et al., 2000) suggest that two domains within the NH_2-terminal region of rpde6 are responsible for two different aspects of the intracellular targeting of this isoenzyme. The NH_2-terminal 67 amino acids of rpde6 contain three proline-rich motifs which are the putative binding sites for the SH3 domains of Src-family tyrosyl kinases such as Lyn (O' Connell et al., 1996). In contrast to full-length rpde6, an NH_2-terminal truncate of rpde6 (ΔP3-rpde6) which lacks the first 72 amino acids is unable to associate with Lyn SH3. Confocal immunofluorescence analysis of transfected COS-7 cells shows that rpde6 is targeted to both the membrane cortical region and a distinct perinuclear region where it co-localises with Lyn (Huston et al., 2000). In contrast, the truncate ΔP3-rpde6 localises with the membrane cortical regions but is absent from the perinuclear region (Huston et al., 2000). Therefore, a sequence downstream of Asp72 appears to be responsible for localising rpde6 to the membrane cortical region. This targeting sequence may occur within the P2 membrane-association region Leu103-Lys256 identified above (see Figure 6.1). The targeting of rpde6 may be crucial for its role in the compartmentalisation of cAMP in cells or for the specific regulation of signalling proteins that co-localise with rpde6. Further investigation is

necessary for the precise definition of the targeting sequence and the identification of the protein that anchors rpde6 to the membrane cortical region.

In Chapter 5 I have shown that rpde6 can interact with a novel immunophilin-like protein called RB3. RB3 is the rat form of the human protein ARA9/XAP2, which was originally identified as a protein binding partner for the ligand-activated cytoplasmic transcription factor AhR (Aryl hydrocarbon receptor) (Carver and Bradfield, 1997; Ma and Whitlock, 1997). RB3 is homologous to the high molecular weight FK506 binding proteins, notably FKBP52 and FKBP51. I have shown that a purified GST-fusion of RB3 (but not GST) could pull down rpde6 from the cytosolic fraction of transfected COS-7 cells. I have mapped the RB3-binding site on rpde6 to the NH_2-terminal half of UCR2 (Ser218 to Arg259). The interaction of RB3 with this region causes the inhibition of rpde6 activity (IC_{50} ~0.2μM). This lends further support to the hypothesis that UCR1 and UCR2 form an intramolecular module that is involved in the regulation of the catalytic unit (MacKenzie et al., 2000).

The COOH-terminal region of RB3 (amino acids 170-330) contains a 34 amino acid TPR motif (amino acids 265-298). TPR domains have been implicated in a number of protein-protein interactions. I have shown that the COOH-terminal half of RB3 is sufficient for the binding and inhibition of rpde6. The NH_2-terminal half of RB3 (amino acid 1-169) contains a region of homology known as the FKBP domain that is found in FK506 binding proteins such as FKBP12 and FKBP52. The NH_2-terminal half of RB3 did not pull down rpde6 or inhibit its catalytic activity, which suggests that it has no direct involvement in the interaction with rpde6. However, it is possible that protein-protein interactions or post-translational modifications in both halves of RB3 may result in a conformational change that affects the ability of the COOH-terminal half of RB3 to interact with rpde6. Challenge of rpde6-transfected COS-7 cells with PMA or forskolin had no effect on the inhibition of rpde6 with RB3. This implies that either rpde6 is not phosphorylated by PKA or PKC, or that phosphorylation has no effect on the interaction between rpde6 and RB3. Further studies will be needed in order to determine the factors which regulate the rpde6:RB3 interaction *in vivo*.

Subcellular distribution analysis of RB3-transfected COS-7 cells showed that RB3 is distributed between the cytosolic (S) and the P1-low speed pellet fraction, but is absent from the P2-membrane fraction, in contrast to rpde6 which was present in all three fractions. This suggests that the rpde6:RB3 interaction is confined to only certain subcellular compartments. In contrast to the cytosolic form of rpde6, the particulate (P1

and P2) forms of rpde6 from transfected COS-7 cells were resistant to inhibition with GST-RB3. This implies that interacting components in these fractions, such as cytoskeletal proteins, may prevent the association of soluble exogenous RB3 with rpde6. These interacting components may be SH3-domain proteins. Alternatively, they may be RB3-like TPR proteins, which associate with the 218-256 binding region. These proteins may sterically block the association of exogenous RB3 or retain rpde6 in an inhibited conformation that is resistant to further inhibition with exogenous RB3. It should be noted that in the P1-pellet fraction, rpde6 might actually interact with endogenous RB3.

As shown in Figure 6.1 the RB3 binding site on rpde6 is downstream of the proline-rich SH3 domain binding sites (Huston et al., 2000; O' Connell et al., 1996). Pre-incubation of cytosolic rpde6 with Lyn SH3 impeded the binding of RB3. Therefore, the binding of Lyn SH3 to the unique NH_2-terminal splice domain of rpde6 may sterically interfere with the binding of RB3 to the NH_2-terminal half of UCR2. The competition between proteins for interaction with the NH_2-terminal region of rpde6 may be an important factor in the dynamic regulation and intracellular targeting of this isoenzyme.

The above studies suggest that the association of RB3 may represent a new mechanism for the regulation and/or intracellular localisation of rpde6. This interaction could implicate rpde6 in the AhR signalling system. The binding of a ligand, such the dioxin TCCD to AhR may cause a conformational change in this receptor that affects its interaction with RB3. This may in turn affect the ability of RB3 to bind to or inhibit rpde6 *in vivo*. The RB3:rpde6 interaction may thus provide a means of cross-talk between the AhR signalling system and cAMP-dependent processes. Therefore, it would be interesting to determine the effect of TCCD-treatment on the subcellular distribution or activity of rpde6 in cells that express both RB3 and AhR.

I have demonstrated that a close homologue of RB3, FKBP52, which also contains a TPR domain in its COOH-terminal region, can also inhibit rpde6. This supports the hypothesis that other TPR domain-containing proteins may interact with rpde6 *in vivo* in addition to RB3. Interestingly, TPR proteins such as FKBP52, FKBP51 and Cyp40 have been implicated in the targeted trafficking of proteins in cells. For instance, FKBP52 appears to be involved in the rapid movement of the glucocorticoid receptor (GR) towards the nucleus along cytoskeletal tracks (Pratt et al., 1999). This then is consistent with the notion that RB3 or a similar protein may be involved in the intracellular targeting of rpde6.

Further work is required to define the precise residues on rpde6 and RB3 that are necessary for the association of these two proteins. In addition to binding AhR, the human

homologue of RB3, ARA9/XAP2 also associates with the molecular chaperone hsp90. A number of other TPR proteins, including protein phosphatase 5 (PP5) and FKBP52 interact with hsp90 (Barent et al., 1998; Carrello et al., 1999; Carver and Bradfield, 1997; Meyer et al., 1998; Nair et al., 1997; Ratajczak and Carrello, 1996). The mutation to alanine of Lys97 or Arg101 in the third TPR motif of PP5 abolishes its association with hsp90 (Russell et al., 1999). A recent paper has shown that the Lys266 in the TPR motif of ARA9/XAP2, which is analogous to Lys266 in PP5, is also essential for binding hsp90 (Bell and Poland, 2000). These conserved basic residues have been suggested to interact with the acidic EEVD motif at the COOH-terminus of hsp90, which is essential for its interaction with TPR proteins. This EEVD motif is strikingly similar to the EELD motif in the Ser218-Arg259 region of rpde6 (first half of UCR2). Therefore, electrostatic interactions may occur between conserved basic residues in the TPR motif of RB3 and conserved acidic residues in rpde6. This could be tested by determining the effect of the alanine substitution of the EELD motif on the association between rpde6 and RB3.

I have shown that a number of cell lines express endogenous RB3, including U937 monocytes which also express the human homologue of rpde6 (MacKenzie et al., 2000). Cell lines such as these could be used to as a model for studying the rpde6:RB3 interaction *in vivo*. New techniques have been devised for generating knock-out cell lines where both alleles for a particular gene are inactivated (Chan et al., 1999; Mortensen et al., 1992). These methods could be employed to replace endogenous wild type rpde6 with a mutant form that lacks the RB3 binding site. A direct comparison could then be made between the wild type and mutant cell lines in order to assess the effect of RB3-association on the activity or intracellular localisation of rpde6. This system could be used to investigate whether the interaction of RB3 stabilises rpde6 or protects it from proteolytic degradation (see section 5.15.2), which has been suggested for the interaction between ARA9/XAP2 and AhR (Meyer and Perdew, 1999). Alternatively, we could test whether rpde6 is involved in signalling downstream of AhR.

In the work presented in this thesis I have localised the binding site for RB3 and the P2-membrane association site to relatively short stretches of sequence within the NH_2-terminal region of rpde6. From this information it may be possible to design peptides or peptide-mimetic compounds that specifically block these interactions. These compounds would be extremely useful for determining the functional importance of these properties of rpde6. Furthermore, the development of PDE4 isoenzyme-specific compounds that block separate aspects of their function *in vivo* is a major goal in drug research. These

compounds may prove to be effective treatments for inflammatory diseases such as asthma and atopic dermatitis, with fewer side effects than the currently available PDE4 inhibitors.

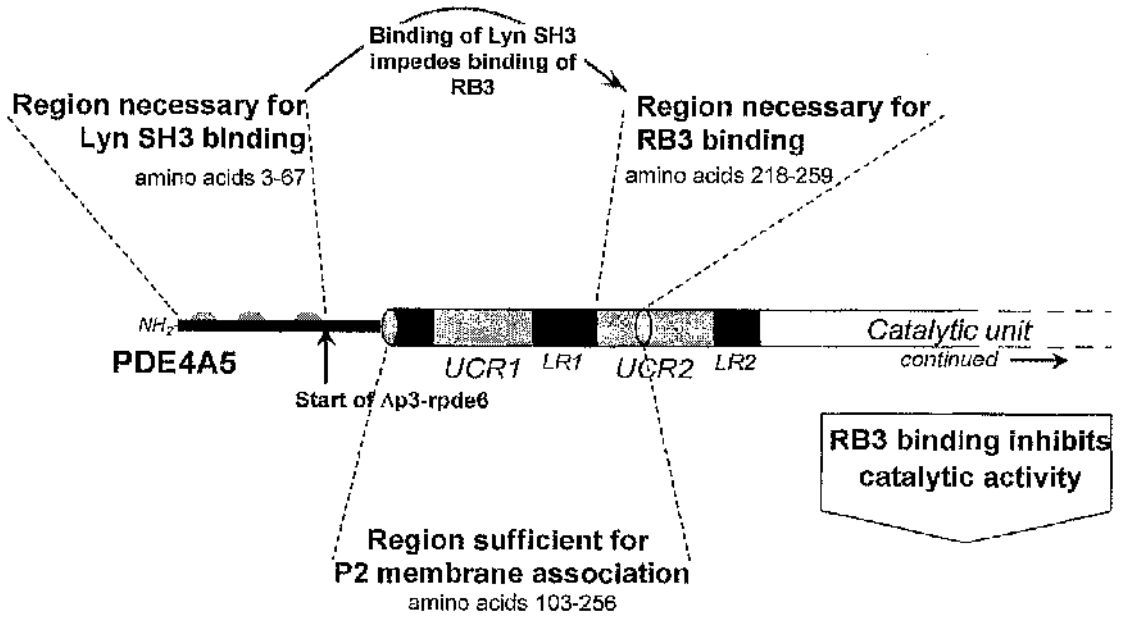

Figure 6.1 Summary of the protein-protein interactions and intracellular targeting of rat PDE4A5 (rpde6)

This figure shows the protein-protein interaction sites in the NH_2-terminal region of RNPDE4A5 (rpde6). The proline-rich putative SH3-domain binding motifs in the unique NH_2-terminal splice domain are indicated with grey semi-circles. This interaction site occurs upstream of the RB3-binding site, which has been mapped to the NH_2-terminal half of UCR2. The region sufficient for P2-membrane association occurs between the two splice junctions (grey circles) and is shared with the other long form RNPDE4A6 (rpde39).

7. References

Abram, C. L., and Courtneidge, S. A. (2000). Src family tyrosine kinases and growth factor signaling. Experimental Cell Research *254*, 1-13.

Aldape, R. A., Futer, O., DeCenzo, M. T., Jarrett, B. P., Murcko, M. A., and Livingston, D. J. (1992). Charged surface residues of FKBP12 participate in formation of the FKBP12-FK506-calcineurin complex. Journal of Biological Chemistry *267*, 16029-16032.

Alexandropoulos, K., Cheng, G., Baltimore, D. (1995). Proline-rich sequences that bind to Src homology 3 domains with individual specificities. Proceedings of the National Academy of Sciences of the United States of America *92*, 3110-3114.

Anandatheerthavarada, H. K., Biswas, G., Mullick, J., V.Sepuri, N. B., Otvos, L., Pain, D., and Avadhani, N. G. (1999). Dual targeting of cytochrome P4502B1 to endoplasmic reticulum and mitochondria involves a novel signal activation by cyclic AMP-dependent phosphorylation at Ser128. EMBO Journal *18*, 5494-5504.

Anderson, N. G. (1992). Growth hormone activates mitogen-activated protein kinase and S6 kinase and promotes intracellular tyrosine phosphorylation in 3T3-F442A preadipocytes. Biochemical Journal *284*, 649-652.

Aravind, L., and Ponting, C. P. (1997). The GAF domain: an evolutionary link between diverse phototransducing proteins. Trends in Biochemical Science *22*, 458-459.

Argetsinger, L. S., and Carter-Su, C. (1996). Mechanism of signaling by growth hormone receptor. Physiological Reviews *76*, 1089-1107.

Athenstaedt, K., and Daum, G. (1999). Phosphatidic acid, a key intermediate in lipid metabolism. European Journal of Biochemistry *266*, 1-16.

Barent, R. L., Nair, S. C., Carr, D. C., Ruan, Y., Rimerman, R. A., Fulton, J., Zhang, Y., and Smith, D. F. (1998). Analysis of FKBP51/FKBP52 chimeras and mutants for hsp90 binding and association with progesterone receptor complexes. Molecular Endocrinology *12*, 342-354.

Barnes, P. J. (1997). Molecular mechanisms of glucocorticoid action in asthma. Pulmonary Pharmacology and Therapeutics *10*, 3-19.

Barnette, M. S., Christensen, S. B., Essayan, D. M., Grous, M., Prabhakar, U., Rush, J. A., Kagey-Sobotka, A., and Torphy, T. J. (1998). SB 207499 (Ariflo), a potent and selective second-generation phosphodiesterase 4 inhibitor: *In vitro* anti-inflammatory actions. Journal of Pharmacology and Experimental Therapeutics *284*, 420-426.

Baughman, G., Wiederrecht, G. J., Campbell, N. F., Martin, M. M., and Bourgeois, S. (1995). FKBP51, a novel T-cell-specific immunophilin capable of calcineurin inhibition. Molecular & Cellular Biology *15*, 4395-4402.

Beard, M. B., O'Connell, J. C., Bolger, G. B., and Houslay, M. D. (1999). The unique N-terminal domain of the cAMP phosphodiesterase PDE4D4 allows for interaction with specific SH3 domains. FEBS Letters *460*, 173-177.

Beard, M. B., Olsen, A. E., Jones, R. E., Erdogan, S., Houslay, M. D., and Bolger, G. B. (2000). UCR1 and UCR2 domains unique to the cAMP-specific phosphodiesterase family form a discrete module via electrostatic interactions. Journal of Biological Chemistry *275*, 10349-10358.

Beavo, J. (1995). Cyclic nucleotide phosphodiesterases: functional implications of multiple isoforms. Physiological Reviews *75*, 725-748.

Beavo, J., Conti, M., and Heaslip, R. J. (1994). Multiple Cyclic Nucleotide Phosphodiesterases. Molecular Pharmacology *40*, 399-405.

Bell, D. R., and Poland, A. (2000). Binding of Aryl hydrocarbon Receptor (AhR) to AhR-interacting Protein (AIP): role of hsp90. Journal of Biological Chemistry *in press*.

Bierer, B. E., Mattila, P. S., Standaert, R. F., Herzenberg, L. A., Burakoff, S. J., Crabtree, G., and Schreiber, S. L. (1990). Two distinct signal transmission pathways in T lymphocytes are inhibited by complexes formed between an immunophilin and either FK506 or rapamycin. Proceedings of the National Academy of Sciences of the United States of America *87*, 9231-9235.

Bjorntorp, P., Karlsson, M., Pettersson, P., and Sypniewska, G. (1980). Differentiation and function of rat adipocyte precursor cells in primary culture. Journal of Lipid Research *21*, 714-23.

Blumer, K. J., and Johnson, G. L. (1994). Diversity in function and regulation of MAP kinase pathways. Trends in Biochemical Sciences *19*, 236-240.

Bolger, G., Michaeli, T., Martins, T., St John, T., Steiner, B., Rodgers, L., Riggs, M., Wigler, M., and Ferguson, K. (1993). A family of human phosphodiesterases homologous to the dunce learning and memory gene product of Drosophila melanogaster are potential targets for antidepressant drugs. Molecular and Cellular Biology *13*, 6558-6571.

Bolger, G., Rodgers, L., and Riggs, M. (1994). Differential CNS expression of alternative mRNA isoforms of the mammalian genes encoding cAMP-specific phosphodiesterases. Gene *149*, 237-244.

Bolger, G. B. (1994). Molecular biology of the cyclic AMP-specific cyclic nucleotide phosphodiesterases: a diverse family of regulatory enzymes. Cellular Signalling *6*, 851-859.

Bolger, G. B. (1998). Molecular Genetic Approaches 1: Two Hybrid Systems. In Protein Targeting Protocols, R. A. Clegg, ed. (Totowa, NJ: Humana Press Inc), pp. 101-131.

Bolger, G. B., Erdogan, S., Jones, R. E., Loughney, K., Scotland, G., Hoffmann, R., Wilkinson, I., Farrell, C., and Houslay, M. D. (1997). Characterization of five different proteins produced by alternatively spliced mRNAs from the human cAMP-specific phosphodiesterase PDE4D gene. Biochemical Journal *328*, 539-548.

Bolger, G. B., McPhee, I., and Houslay, M. D. (1996). Alternative splicing of cAMP-specific phosphodiesterase mRNA transcripts (characterisation of a novel tissue specific isoform, RNPDE4A8). Journal of Biological Chemistry *271*, 1065-1071.

Bradford, M. (1976). A rapid and sensitive method for the quantitation of microgram quantities of protein utilizing the principle of protein-dye binding. Analytical Biochemistry *72*, 248-254.

Bram, R. J., Hung, D. T., Martin, P. K., Schreiber, S. L., and Crabtree, G. R. (1993). Identification of the immunophilins capable of mediating inhibition of signal transduction by cyclosporin A and FK506: Roles of calcineurin binding and cellular location. Molecular & Cellular Biology *13*, 4760-4769.

Bregman, D. B., Bhattacharyya, N., and Rubin, C. S. (1989). High affinity binding protein for the regulatory subunit of cAMP-dependent protein kinase II-B. Journal of Biological Chemistry *264*, 4648-4656.

Brown, D. A., and London, E. (1998). Functions of lipid rafts in biological membranes. Annual Review of Cell Developmental Biology *14*, 111-136.

Brown, E. J., Beal, P. A., Keith, C. T., Chen, J., Shin, T. B., and Schreiber, S. L. (1995). Control of p70 S6 kinase by kinase activity of FRAP in vivo. Nature *377*, 441-446.

Brunn, G. J., Hudson, C. C., Sekulic, A., Williams, J. M., Hosoi, H., Houghton, P. J., Lawrence, J. C., Jr., and Abraham, R. T. (1997). Phosphorylation of the translational repressor PHAS-I by the mammalian target of rapamycin. Science *277*, 99-101.

Buday, L. (1999). Membrane-targeting of signalling molecules by SH2/SH3 domain-containing adaptor proteins. Biochimica et Biophysica Acta- Reviews on Biomembranes *1422*, 187-204.

Burton, K. A., Johnson, B. D., Hausken, Z. E., Westenbroek, R. E., Idzerda, R. L., Scheuer, T., Scott, J. D., Catterall, W. A., and McKnight, G. S. (1997). Type II regulatory subunits are not required for the anchoring-dependent modulation of Ca2+ channel activity by cAMP-dependent protein kinase. Proceedings of the National Academy of Sciences of the United States of America *94*, 11067-11072.

Byers, D., Davis, R. L., and Kiger, J. A. (1981). Defect in cyclic AMP phosphodiesterase due to the dunce mutation of learning in Drosophila melanogaster. Nature *289*, 79-81.

Callebaut, I., Renoir, J. M., Lebeau, M. C., Massol, N., Burny, A., Baulieu, E. E., and Mornon, J. P. (1992). An immunophilin that binds M(r) 90,000 heat shock protein: Main structural features of a mammalian p59 protein. Proceedings of the National Academy of Sciences of the United States of America *89*, 6270-6274.

Carr, D. W., Hausken, Z. E., Fraser, I. D. C., Stofkohahn, R. E., and Scott, J. D. (1992). Association of the Type-II cAMP-dependent protein kinase with a human thyroid RII-anchoring protein - cloning and characterization of the RII-binding domain. Journal of Biological Chemistry *267*, 13376-13382.

Carr, D. W., and Scott, J. D. (1992). Blotting and band-shifting: techniques for studying protein-protein interactions. Trends in Biological Science *17*, 246-249.

Carrello, A., Ingley, E., Minchin, R. F., Tsai, S., and Ratajczak, T. (1999). The common tetratricopeptide repeat acceptor site for steroid receptor- associated immunophilins and Hop is located in the dimerization domain of Hsp90. Journal of Biological Chemistry *274*, 2682-2689.

Carver, L. A., and Bradfield, C. A. (1997). Ligand-dependent interaction of the aryl hydrocarbon receptor with a novel immunophilin homolog in vivo. Journal of Biological Chemistry *272*, 11452-11456.

Carver, L. A., LaPres, J. J., Jain, S., Dunham, E. E., and Bradfield, C. A. (1998). Characterization of the Ah receptor-associated protein, ARA9. Journal of Biological Chemistry *273*, 33580-33587.

Chabot, B. (1996). Directing alternative splicing: cast and scenarios. Trends in genetics *12*, 472-477.

Chabre, M., and Deterre, P. (1989). Molecular mechanism of visual transduction. European Journal of Biochemistry *179*, 255-266.

Chan, T. A., Hermeking, H., Lengauer, C., Kinzler, K. W., and Vogelstein, B. (1999). 14-3-3Sigma is required to prevent mitotic catastrophe after DNA damage. Nature *401*, 616-620.

Chang, B. Y., Conroy, K. B., Machleder, E. M., and Cartwright, C. A. (1998). RACK1, a receptor for activated C kinase and a homolog of the beta subunit of G proteins, inhibits activity of src tyrosine kinases and growth of NIH 3T3 cells. Molecular and Cellular Biology *18*, 3245-3256.

Cheley, S., Panchal, R. G., Carr, D. W., Scott, J. D., and Bayley, H. (1994). Type II regulatory subunits of cAMP-dependent protein kinase and their binding proteins in the nervous system of Aplysia californica. Journal of Biological Chemistry *269*, 2911-2920.

Chen, C., Denome, S., and Davis, R. L. (1986). Molecular analysis of the cDNA clones and the corresponding genomic coding sequences of the *Drosophila* dunce$^+$ gene, the structural gene for cAMP phosphodiesterase. Proceedings of the National Academy of Sciences of the United States of America *83*, 9313-9317.

Chen, M. X., and Cohen, P. T. W. (1997). Activation of protein phosphatase 5 by limited proteolysis or by the binding of polyunsaturated fatty acids to the TPR domain. FEBS Letters *400*, 136-140.

Chen, M. X., McPartlin, A. E., Brown, L., Chen, Y. H., Barker, H. M., and Cohen, P. T. W. (1994). A novel human protein serine/threonine phosphatase, which possesses four tetratricopeptide repeate motifs and localises to the nucleus. EMBO Journal *13*, 4278-4290.

Chini, C. C. S., Chini, E. N., Williams, J. M., Matousovic, K., and Dousa, T. P. (1994). Formation of reactive oxygen metabolites in glomeruli is suppressed by inhibition of cAMP phosphodiesterase isozyme type-IV. Kidney International *46*, 28-36.

Chini, C. C. S., Grande, J. P., Chini, E. N., and Dousa, T. P. (1997). Compartmentalization of cAMP signaling in mesangial cells by phosphodiesterase isozymes PDE3 and PDE4. Journal of Biological Chemistry *272*, 9854-9859.

Clapham, D. E. (1996). The G-Protein Nanomachine. Nature *379*, 297-299.

Coghlan, V. M., Perrino, B. A., Howard, M., Langeberg, L. K., Hicks, J. B., Gallatin, W. M., and Scott, J. D. (1995). Association of protein kinase A and protein phosphatase 2B with a common anchoring protein. Science *267*, 108-111.

Cohan, V. L., Showell, H. J., Fisher, D. A., Pazoles, C. J., Watson, J. W., and Turner CR, C. J. (1996). In vitro pharmacology of the novel phosphodiesterase type 4 inhibitor, CP-80633. Journal of Pharmacology and Experimental Therapeutics *278*, 1356-1361.

Colledge, M., and Scott, J. D. (1999). AKAPs: from structure to function. Trends in Cell Biology *9*, 216-221.

Conti, M., and Jin, S. L. C. (2000). The molecular biology of cyclic nucleotide phosphodiesterases. Progress in Nucleic Acid Research and Molecular Biology *63*, 1-38.

Conti, M., Nemoz, G., Sette, C., and Vicini, E. (1995). Recent progress in understanding the hormonal-regulation of phosphodiesterases. Endocrine Reviews *16*, 370-389.

Cooper, J. A., and Howell, B. (1993). The when and how of src regulation. Cell *1993*, 1051-1054.

Corbin, J. D., and Francis, S. H. (1999). Cyclic GMP phosphodiesterase-5: Target of sildenafil. Journal of Biological Chemistry *274*, 13729-13732.

Czar, M. J., Owens-Grillo, J. K., Yem, A. W., Leach, K. L., Deibel Jr, M. R., Welsh, M. J., and Pratt, W. B. (1994). The hsp56 immunophilin component of untransformed steroid receptor complexes is localized both to microtubules in the cytoplasm and to the same nonrandom regions within the nucleus as the steroid receptor. Molecular Endocrinology *8*, 1731-1741.

Daniel, P. B., Walker, W. H., and Habener, J. F. (1998). Cyclic AMP signaling and gene regulation. Annual Review of Nutrition *18*, 353-383.

Das, A. K., Cohen, P. T. W., and Barford, D. (1998). The structure of the tetratricopeptide repeats of protein phosphatase 5: Implications for TPR-mediated protein-protein interactions. EMBO Journal *17*, 1192-1199.

Davis, R., L.,, Takayasu, H., Eberwine, M., and Myres, J. (1989). Cloning and characterization of mammalian homologs of the *Drosophila* dunce$^+$ gene. Proceedings of the National Academy of Sciences of the United States of America *86*, 3604-3608.

De Rooij, J., Zwartkruis, F. J. T., Verheijen, M. H. G., Cool, R. H., Nijman, S. M. B., Wittinghofer, A., and Bos, J. L. (1998). Epac is a Rap1 guanine-nucleotide-exchange factor directly activated by cyclic AMP. Nature *396*, 474-477.

Degerman, E., Belfrage, P., and Manganiello, V. C. (1997). Structure, localisation and regulation of the cGMP-inhibited phosphodiesterase (PDE3). Journal of Biological Chemistry *272*, 6823-6826.

Degerman, E., Smith, C. J., Tornqvist, H., Vasta, V., Belfrage, P., and Manganiello, V. C. (1990). Evidence that insulin and isoprenaline activate the cGMP-inhibited low-Km cAMP phosphodiesterase in rat fat cells by phosphorylation. Proceedings of the National Academy of Science of the United States of America *87*, 533-537.

Disatnik, M. H., Hernandezsotomayor, S. M. T., Jones, G., Carpenter, G., and Mochlyrosen, D. (1994). Phospholipase C gamma 1 binding to intracellular receptors for activated protein kinase C. Proceedings of the National Academy of Sciences of the United States of America *91*, 559-563.

Dousa, T. P. (1999). Cyclic-3',5'-nucleotide phosphodiesterase isozymes in cell biology and pathophysiology of the kidney. Kidney International *55*, 29-62.

Dudai, Y., Jan, Y., Byers, D., Quinn, W. G., and Benzer, S. (1976). *dunce*, a mutant of *Drosophila* deficient in learning. Proceedings of the National Academy of Sciences of the United States of America *73*, 1684-1688.

Dugan, L. L., Kim, J. S., Zhang, Y., Bart, R. D., Sun, Y., Holtzman, D. M., and Gutmann, D. H. (1999). Differential effects of cAMP in neurons and astrocytes. Role of B-raf. Journal of Biological Chemistry *274*, 25842-25848.

Edwards, A. E., and Scott, J. D. (2000). A-kinase anchoring proteins: protein kinase A and beyond. Current Opinion in Cell Biology *12*, 217-221.

El Benna, J., Dang, P. M. C., Andrieu, V., Vergnaud, S., Dewas, C., Cachia, O., Fay, M., Morel, F., Chollet-Martin, S., Hakim, J., and Gougerot-Pocidalo, M. A. (1999). P40(phox) associates with the neutrophil triton X-100-insoluble cytoskeletal fraction and PMA-activated membrane skeleton: A comparative study with p67(phox) and p47(phox). Journal of Leukocyte Biology *66*, 1014-1020.

ElBawab, S., Macovschi, O., Sette, C., Conti, M., Lagarde, M., Nemoz, G., and Prigent, A. F. (1997). Selective stimulation of a cAMP-specific phosphodiesterase (PDE4A5) isoform by phosphatidic acid molecular species endogenously formed in rat thymocytes. European Journal of Biochemistry *247*, 1151-1157.

Elks, M. L., and Manganiello, V. C. (1985). A role for soluble cAMP phosphodiesterases in differentiation of 3T3-L1 adipocytes. Journal of Cellular Physiology *124*, 191-8.

Engels, P., Fichtel, K., and Lubbert, H. (1994). Expression and regulation of the human and rat phosphodiesterase type IV isogenes. FEBS letters *350*, 291-295.

Erdogan, S., and Houslay, M. D. (1997). Challenge of human Jurkat T-cells with the adenylate cyclase activator forskolin elicits major changes in cAMP phosphodiesterase (PDE) expression by up-regulating PDE3 and inducing PDE4D1 and PDE4D2 splice variants as well as down-regulating a novel PDE4A splice variant. Biochemical Journal *321*, 165-175.

Erpel, T., and Courtneidge, S. A. (1995). Src family protein tyrosine kinases and cellular signal transduction pathways. Current Opinion in Cell Biology *7*, 176-182.

Essayan, D. M. (1999). Cyclic nucleotide phosphodiesterase (PDE) inhibitors and immunomodulation. Biochemical Pharmacology *57*, 965-973.

Ewton, D., and Florini, J. (1980). Relative effects of the somatomedins, multiplication-stimulating activity, and growth hormone on myoblasts and myotubes in culture. Endocrinology *106*, 577-583.

Fagan, K. A., Mahey, R., and Cooper, D. M. F. (1996). Functional co-localisation of transfected Ca^{2+}-stimulable adenylyl cyclases with capacitative Ca^{2+} entry sites. Journal of Biological Chemistry *271*, 12438-12444.

Faux, M. C., and Scott, J. D. (1996). Molecular glue: kinase anchoring and scaffold proteins. Cell *85*, 9-12.

Fawcett, L., Baxendale, R., Stacey, P., McGrouther, C., Harrow, I., Soderling, S., Hetman, J., Beavo, J. A., and Phillips, S. C. (2000). Molecular cloning and characterization of a distinct human phosphodiesterase gene family: PDE11A. Proceedings of the National Academy of Sciences of the United States of America *97*, 3702-3707.

FormanKay, J. D., and Pawson, T. (1999). Diversity in protein recognition by PTB domains. Current Opinion in Structural Biology *9*, 690-695.

Frank, D. A., and Greenberg, M. E. (1994). CREB: A mediator of long-term memory from mollusks to mammals. Cell *79*, 5-8.

Fraser, I. D. C., and Scott, J. D. (1999). Modulation of ion channels: A "Current" view of AKAPs. Neuron *23*, 423-426.

Fruman, D. A., Burakoff, S. J., and Bierer, B. E. (1994). Immunophilins in protein folding and immunosuppression. FASEB Journal *8*, 391-400.

Fukunaga, B. N., Probst, M. R., Reisz-Porszasz, S., and Hankinson, O. (1995). Identification of functional domains of the aryl hydrocarbon receptor. Journal of Biological Chemistry *270*, 29270-29278.

Futer, O., DeCenzo, M. T., Aldape, R. A., and Livingston, D. J. (1995). FK506 binding protein mutational analysis. Defining the surface residue contributions to stability of the calcineurin co-complex. Journal of Biological Chemistry *270*, 18935-18940.

Galat, A., Lane, W. S., Standaert, R. F., and Schreiber, S. L. (1992). A rapamycin-selective 25-kDa immunophilin. Biochemistry *31*, 2427-2434.

Giembycz, M. A. (1996). Phosphodiesterase 4 and tolerance to β_2-adrenoceptor agonists in asthma. Trends in Pharmacological Sciences *17*, 331-336.

Gluzman, Y. (1981). SV40-transformed simian cells support the replication of early SV40 mutants. Cell *23*, 175-182.

Goebl, M., and Yanagida, M. (1991). The TPR snap helix: a novel protein repeat motif from mitosis to transcription. Trends in Biochemical Sciences *16*, 173-177.

Granovsky, A. E., Natochin, M., McEntaffer, R. L., Haik, T. L., Francis, S. H., Corbin, J. D., and Artemyev, N. O. (1998). Probing Domain Functions of Chimeric PDE6'/PDE5 cGMP-Phosphodiesterase. Journal of Biological Chemistry *273*, 24485-24490.

Hamm, H. E., and Gilchrist, A. (1996). Heterotrimeric G proteins. Current Opinion in Cell Biology *8*, 189-196.

Han, J. W., Pearson, R. B., Dennis, P. B., and Thomas, G. (1995). Rapamycin, wortmannin, and the methylxanthine SQ20006 inactivate p70(s6k) by inducing dephosphorylation of the same subset of sites. Journal of Biological Chemistry *270*, 21396-21403.

Han, P., Zhu, X., and Michaeli, T. (1997). Alternative splicing of the high affinity cAMP-specific phosphodiesterase (PDE7A) mRNA in human skeletal muscle and heart. Journal of Biological Chemistry *272*, 16152-16157.

Harbinson, P. L., MacLeod, D., Hawksworth, R., O'Toole, S., Sullivan, P. J., Heath, P., Kilfeather, S., Page, C. P., Costello, J., Holgate, S. T., and Lee, T. H. (1997). The effect of a novel orally active selective PDE4 isoenzyme inhibitor (CDP840) on allergen-induced responses in asthmatic subjects. European Respiratory Journal *10*, 1008-1014.

Harris, M. (1998). Use of GST-fusion and Related Constructs for the Identification of Interacting Proteins. In Protein Targeting Protocols, R. Clegg, ed. (Totowa, NJ: Humana Press Inc), pp. 87-99.

Harrison, R. K., and Stein, R. L. (1990). Substrate specificities of the peptidyl prolyl cis-trans isomerase activities of cyclophilin and FK-506 binding protein: evidence for the existence of a family of distinct enzymes. Biochemistry *29*, 3813-3816.

Hartzell, H. C., Mery, P. F., Fischmeister, R., and Szabo, G. (1991). Sympathetic regulation of cardiac calcium current is due exclusively to cAMP-dependent phosphorylation. Nature *351*, 573-576.

Hayes, J. S., Bowling, N., King, K. L., and Boder, G. B. (1982). Evidence for the selective regulation of the phosphorylation of myocyte proteins by isoproterenol and prostaglandin E_1. Biochemica et Biophysica Acta *714*, 136-142.

Hayon, T., Dvilansky, A., Oriev, L., and Nathan, I. (1999). Non-steroidal antiestrogens induce apoptosis in HL60 and MOLT3 leukemic cells; Involvement of reactive oxygen radicals and protein kinase C. Anticancer Research *19*, 2089-2093.

Hengen, P. N. (1996). Methods and reagents - Purification of GST fusion proteins. Trends in Biochemical Sciences *21*, 400-401.

Henkel-Tigges, J., and Davis, R. (1989). Rat homologues of the *Drosophila dunce* gene code for cyclic AMP phosphodiesterases sensitive to rolipram and RO 20-1724. Molecular Pharmacology *37*, 7-10.

Hewitt, E. L., Ozanne, B. W., and Cushley, W. (1997). Negative regulation of the interleukin (IL)-2 receptor alpha chain (CD25) promoter region in human B lymphocytes. Cytokine *9*, 982-991.

Higgins, D. G., and Sharp, P. M. (1988). CLUSTAL: a package for performing multiple sequence alignment on a microcomputer. Gene *73*, 237-244.

Hirano, T., Kinoshita, N., Morikawa, K., and Yanagida, M. (1990). Snap helix with knob and hole: Essential repeats in S. pombe nuclear protein nuc2+. Cell *60*, 319-328.

Hoffmann, R., Baillie, G. S., MacKenzie, S. J., Yarwood, S. J., and Houslay, M. D. (1999). The MAP kinase ERK2 inhibits the cyclic AMP-specific phosphodiesterase HSPDE4D3 by phosphorylating it at ser579. EMBO Journal *18*, 893-903.

Hoffmann, R., Wilkinson, I. R., McCallum, J. F., Engels, P., and Houslay, M. D. (1998). cAMP-specific phosphodiesterase HSPDE4D3 mutants which mimic activation and changes in rolipram inhibition triggered by protein kinase A phosphorylation of Ser-54: Generation of a molecular model. Biochemical Journal *333*, 139-149.

Hohl, C., and Li, Q. (1991). Compartmentalization of cAMP in adult canine ventricular myocytes. Circulation Research *69*, 1369-1379.

Holowka, D., Sheets, E. D., and Baird, B. (2000). Interactions between FcepsilonRI and lipid raft components are regulated by the actin cytoskeleton. Journal of Cell Science *113*, 1009-1019.

Horton, Y. M., Sullivan, M., and Houslay, M. D. (1995). Molecular cloning of a novel splice variant of human type-IVA (PDE-IVA) cyclic AMP phosphodiesterase and localization of the gene to the p13.1-q12 region of human chromosome 19. Biochemical Journal *308*, 683-691.

Houslay, M., Scotland, G., Erdogan, S., Huston, E., Mackenzie, S., McCallum, J., McPhee, I., Pooley, L., Rena, G., Ross, A., Beard, M., Peden, A., Begg, F., Wilkinson, I., Yarwood, S., Ackerman, C., Houslay, E., Hoffman, R., Engels, P., Sullivan, M., and Bolger, G. (1997). Intracellular targeting, interaction with Src homology 3 (SH3) domains and rolipram-detected conformational switches in cAMP-specific PDE4A phosphodiesterase. Biochemical Society Transactions *25*, 374-381.

Houslay, M. D. (1995). Compartmentalization of cyclic AMP phosphodiesterases, signaling crosstalk, desensitization and the phosphorylation of G(i)-2 add cell specific personalization to the control of the levels of the second messenger cyclic AMP. Advances in Enzyme Regulation *35*, 303-338.

Houslay, M. D. (1996). N-terminal alternately spliced regions of PDE4A cAMP-specific phosphodiesterases determine intracellular targeting and regulation of catalytic activity. Biochemical Society Transactions *24*, 980-986.

Houslay, M. D., and Milligan, G. (1997). Tailoring cAMP-signalling responses through isoform multiplicity. Trends in Biochemical Sciences *22*, 217-224.

Houslay, M. D., Scotland, G., Pooley, L., Spence, S., Wilkinson, I., McCallum, F., Julien, P., Rena, N. G., Michie, A. M., Erdogan, S., Zeng, L., O'Connell, J. C., Tobias, E. S., and MacPhee, I. (1995). Alternative splicing of the type-IVA cyclic AMP phosphodiesterase gene provides isoform variants with distinct N-terminal domains fused to a common, soluble catalytic unit - designer changes in V-max, stability and membrane association. Biochemical Society Transactions *23*, 393-398.

Houslay, M. D., Sullivan, M., and Bolger, G. B. (1998). The multienzyme PDE4 cyclic adenosine monophosphate-specific phosphodiesterase family: intracellular targeting, regulation, and selective inhibition by compounds exerting anti-inflammatory and antidepressant actions. Advances in Pharmacology *44*, 225-342.

Huang, L. J., Durick, D., Weiner, J. A., Chun, J., and Taylor, S. S. (1997). Identification of a novel protein kinase A anchoring protein that binds both type I and type II regulatory subunits. Journal of Biological Chemistry *12*, 8057-8064.

Huang, Z. J., Curtin, K. D., and Rosbash, M. (1995). PER protein interactions and temperature compensation of a circadian clock in Drosophila. Science *267*, 1169-1172.

Huang, Z. J., Edery, I., and Rosbash, M. (1993). PAS is a dimerization domain common to Drosophila period and several transcription factors. Nature *364*, 259-262.

Hubbard, M. J., and Cohen, P. (1993). On target with a new mechanism for the regulation of protein phosphorylation. Trends in Biochemical Science *18*, 172-177.

Hulley, P., Hartikka, J., Abdel'Al S, E. P., Buerki, H. R., Wiederhold, K. H., Muller, T., Kelly, P., Lowe, D., and Lubbert, H. (1995). Inhibitors of type IV phosphodiesterases reduce the toxicity of MPTP in substantia nigra neurons in vivo. European Journal of Neuroscience *7*, 2431-2440.

Huston, E., Beard, M., McCallum, J., Pyne, N., Vandenabeele, P., Scotland, G., and Houslay, M. (2000). The cAMP-specific phosphodiesterase PDE4A5 is cleaved downstream of its SH3-interaction domain by caspase-3: consequences for altered intracellular distribution. Journal of Biological Chemistry *275*, 28063-28074.

Huston, E., Lumb, S., Russell, A., Catterall, C., Ross, A. H., Steele, M. R., Bolger, G. B., Perry, M. J., Owens, R. J., and Houslay, M. D. (1997). Molecular cloning and transient expression in COS7 cells of a novel human PDE4B cAMP-specific phosphodiesterase, HSPDE4B3. Biochemical Journal *328*, 549-558.

Huston, E., Pooley, L., Julien, P., Scotland, G., McPhee, I., Sullivan, M., Bolger, G., and Houslay, M. D. (1996). The human cyclic AMP-specific phosphodiesterase PDE-46 (HSPDE4A4B) expressed in transfected COS7 cells occurs as both particulate and cytosolic species that exhibit distinct kinetics of inhibition by the antidepressant rolipram. Journal of Biological Chemistry *271*, 31334-31344.

Jackson, S. P., Schoenwaelder, S. M., Yuan, Y. P., Rabinowitz, I., Salem, H. H., and Mitchell, C. A. (1994). Adhesion receptor activation of phosphatidylinositol 3-kinase - von- Willebrand factor stimulates the cytoskeletal association and activation of phosphatidylinositol 3-kinase and pp60(c-Src) in human platelets. Journal of Biological Chemistry *269*, 27093-27099.

Jacobitz, S., Ryan, M. D., McLaughlin, M. M., Livi, G. P., DeWolf, W. E., Jr., and Torphy, T. J. (1997). Role of conserved histidines in catalytic activity and inhibitor binding of human recombinant phosphodiesterase 4A. Molecular Pharmacology *51*, 999-1006.

Janes, P. W., Ley, S. C., and Magee, A. I. (1999). Aggregation of lipid rafts accompanies signaling via the T cell antigen receptor. Journal of Cell Biology *147*, 447-461.

Jin, S. L., Swinnen, J. V., and Conti, M. (1992). Characterization of the structure of a low Km, rolipram-sensitive cAMP phosphodiesterase. Mapping of the catalytic domain. Journal of Biological Chemistry *267*, 18929-18939.

Jin, S. L. C., Bushnik, T., Lan, L., and Conti, M. (1998). Subcellular localization of rolipram-sensitive, cAMP-specific phosphodiesterases. Differential targeting and activation of the splicing variants derived from the PDE4D gene. Journal of Biological Chemistry *273*, 19672-19678.

Johnson, J. A., Gray, M. O., Chen, C. H., and Mochlyrosen, D. (1996). A protein kinase C translocation inhibitor as an isozyme-selective antagonist of cardiac function. Journal of Biological Chemistry *271*, 24962-24966.

Joyal, J. L., Annan, R. S., Ho, Y. D., Huddleston, M. E., Carr, S. A., Hart, M. J., and Sacks, D. B. (1997). Calmodulin modulates the interaction between IQGAP1 and Cdc42:

Identification of IQGAP1 by nanoelectrospray tandem mass spectrometry. Journal of Biological Chemistry *272*, 15419-15425.

Juilfs, D. M., Fulle, H., Zhao, A. Z., Houslay, M. D., Garbers, D. L., and Beavo, J. A. (1997). A subset of olfactory neurons that selectively express cGMP-stimulated phosphodiesterase (PDE2) and guanylyl cyclase-D define a unique olfactory signal transduction pathway. Proceedings of the National Academy of Sciences of the United States of America *94*, 3388-3395.

Jung, S. M., and Moroi, M. (1988). Platelet cytoskeletal protein distributions in two triton-insoluble fractions and how they are affected by stimulants and reagents that modify cytoskeletal protein interactions. Thrombosis Research *50*, 775-787.

Jurevicius, J., and Fischmeister, R. (1996). cAMP compartmentation is responsible for a local activation of cardiac Ca^{2+} channels by beta-adrenergic agonists. Proceedings of the National Academy of Sciences of the United States of America *93*, 295-299.

Jurevicius, J., Skeberdis, A., and Fischmeister, R. (1997). Characterization of the phosphodiesterase isoforms involved in the compartmentation of cAMP following beta-adrenoceptor activation in frog cardiac myocytes. Biophysical Journal *72*, MPM10-MPM10.

Kassem, M., Okazaki, R., Harris, S. A., Spelsberg, T. C., Conover, C. A., and Riggs, B. L. (1998). Estrogen effects on insulin-like growth factor gene expression in a human osteoblastic cell line with high levels of estrogen receptor. Calcified Tissue International *62*, 60-66.

Kasuya, J., Goko, H., and Fujita-Yamaguchi, Y. (1995). Multiple transcripts for the human cardiac form of the cGMP-inhibited cAMP phosphodiesterase. Journal of Biological Chemistry *270*, 14305-14312.

Kawasaki, H., Springett, G. M., Mochizuki, N., Toki, M., Nakaya, M., Matsuda, M., Housman, D. E., and Graybiel, A. M. (1998). A family of cAMP-binding proteins that directly activate Rap1. Science *282*, 2275-2279.

Kay, J. E. (1996). Structure-function relationships in the FK506-binding protein (FKBP) family of peptidylproplyl cis-trans isomerases. Biochemical Journal *314*, 361-385.

Klauck, T. M., Faux, M. C., Labudda, K., Langeberg, L. K., Jaken, S., and Scott, J. D. (1996). Co-ordination of three signaling enzymes by AKAP79, a mammalian scaffold protein. Science *271*, 1589-1592.

Korschen, H. G., Beyermann, M., Muller, F., Heck, M., Vantler, M., Koch, K. W., Kellner, R., Wolfrum, U., Bode, C., Hofmann, K. P., and Kaupp, U. B. (1999). Interaction of glutamic-acid-rich proteins with the cGMP signalling pathway in rod photoreceptors. Nature *400*, 761-766.

Kostic, M. M., Erdogan, S., Rena, G., Borchert, G., Hoch, B., Bartel, S., Scotland, G., Huston, E., Houslay, M. D., and Krause, E. G. (1997). Altered expression of PDE1 and PDE4 cyclic nucleotide phosphodiesterase isoforms in 7-oxo-prostacyclin-preconditioned rat heart. Journal of Molecular and Cellular Cardiology *29*, 3135-3146.

Kovala, T., Lorimer, A. J., Brickenden, A. M. (1994). Protein kinase A regulation of cAMP Phosphodiesterase Expression. Journal of Biological Chemistry *269*, 8680-8685.

Kreppel, L. K., Blomberg, M. A., and Hart, G. W. (1997). Dynamic glycosylation of nuclear and cytosolic proteins: cloning and characterization of a unique O-GlcNAc transferase with multiple tetratricopeptide repeats. Journal of Biological Chemistry *272*, 9308-9315.

Kuzhandaivelu, N., Cong, Y. S., Inouye, C., Yang, W. M., and Seto, E. (1996). XAP2, a novel hepatitis B virus X-associated protein that inhibits X transactivation. Nucleic Acids Research *24*, 4741-4750.

Laemmli, U. K. (1970). Cleavage of structural proteins during the assembly of the head of the bacteriophage T4. Nature (London) *227*, 680-685.

Lalli, E., and Sassone-Corsi, P. (1994). Signal transduction and gene regulation: the nuclear response to cAMP. Journal of Biological Chemistry *269*, 17359-17362.

Lamb, J. R., Tugendreich, S., and Hieter, P. (1995). Tetratrico peptide repeat interactions: To TPR or not to TPR? Trends in Biochemical Sciences *20*, 257-259.

Lambright, D. G., Sondek, J., Bohm, A., Skiba, N. P., Hamm, H. E., and Sigler, P. B. (1996). The 2.0 A crystal structure of a heterotrimeric G protein. Nature *379*, 311-319.

Leroy, M. J., Degerman, E., Taira, M., Murata, T., Wang, L. H., Movsesian, M. A., Meacci, E., and Manganiello, V. C. (1996). Characterization of two recombinant PDE3 (cGMP-inhibited cyclic nucleotide phosphodiesterase) isoforms, RcGIP1 and HcGIP2, expressed in NIH 3006 murine fibroblasts and Sf9 insect cells. Biochemistry *35*, 10194-10202.

Lester, L. B., Langeberg, L. K., and Scott, J. D. (1997). Anchoring of protein kinase A facilitates hormone-mediated insulin secretion. Proceedings of the National Academy of Sciences of the United States of America *94*, 14942-14947.

Leverson, J. D., and Ness, S. A. (1998). Point mutations in v-Myb disrupt a cyclophilin-catalysed negative regulatory mechanism. Molecular Cell *1*, 203-211.

Liliental, J., and Chang, D. D. (1998). Rack1, a receptor for activated protein kinase C, interacts with integrin beta subunit. Journal of Biological Chemistry *273*, 2379-2383.

Lim, K., Ho, J. X., Keeling, K., Gilliland, G. L., Ji, X. H., Ruker, F., and Carter, D. C. (1994). 3-Dimensional structure of Schistosoma japonicum glutathione-S- transferase fused with a 6-amino acid conserved neutralizing epitope of Gp41 From HIV. Protein Science *3*, 2233-2244.

Linden, H., and Macino, G. (1997). White collar 2, a partner in blue-light signal transduction, controlling expression of light-regulated genes in Neurospora crassa. EMBO Journal *16*, 98-109.

Liu, F. H., Wu, S. J., Hu, S. M., Hsiao, C. D., and Wang, C. (1999). Specific interaction of the 70-kDa heat shock cognate protein with the tetratricopeptide repeats. Journal of Biological Chemistry *274*, 34425-34432.

Liu, J., Farmer Jr, J. D., Lane, W. S., Friedman, J., Weissman, I., and Schreiber, S. L. (1991). Calcineurin is a common target of cyclophilin-cyclosporin A and FKBP-FK506 complexes. Cell *66*, 807-815.

Livi, G. P., Kmetz, P., McHale, M. M., Cieslinski, L. B., Sathe, G. M., Taylor, D. P., Davis, R. L., Torphy, T. J., and Balcarek, J. M. (1990). Cloning and expression of cDNA for a human low-Km, rolipram-sensitive cyclic AMP phosphodiesterase. Molecular cell biology *10*, 2678-2686.

Lobban, M., Shakur, Y., Beattie, J., Houslay, M. D. (1994). Identifiction of two splice varient forms of type IV_B cyclic AMP phosphodiesterase, DPD (rPDE-IV_{B1}) and PDE-4 (rPDE -IV_{B2}) in brain: selective localization in membranes and and cytosolic compartments and differential expression in various brain regions. Biochemical Journal *304*, 399-406.

Lochhead, A., Nekrasova, E., Arshavsky, V. Y., and Pyne, N. J. (1997). The regulation of the cGMP-binding cGMP phosphodiesterase by proteins that are immunologically related to γ subunit of the photoreceptor cGMP phosphodiesterase. Journal of Biological Chemistry *272*, 18397-18403.

Lopez, A. J. (1998). Alternative splicing of pre-mRNA: Developmental consequences and mechanisms of regulation. Annual Review of Genetics *32*, 279-305.

Lu, P. J., Wulf, G., Zhou, X. Z., Davies, P., and Lu, K. P. (1999). The prolyl isomerase Pin1 restores the function of Alzheimer-associated phosphorylated tau protein. Nature *399*, 784-788.

Lubas, W. A., Frank, D. W., Krause, M., and Hanover, J. A. (1997). O-linked GlcNAc transferase is a conserved nucleocytoplasmic protein containing tetratricopeptide repeats. Journal of Biological Chemistry *272*, 9316-9324.

Luttrel, L. M., Ferguson, S. S. G., Daaka, Y., Miller, W. E., Maudsley, S., Della Rocca, G. J., Lin, F. T., Kawakatsu, H., Owada, K., Luttrell, D. K., Caron, M. G., and Lefkowitz, R. J. (1999). beta-arrestin-dependent formation of beta2 adrenergic receptor-src protein kinase complexes. Science *283*, 655-661.

Ma, Q., and Whitlock, J. P., Jr. (1997). A novel cytoplasmic protein that interacts with the Ah receptor, contains tetratricopeptide repeat motifs, and augments the transcriptional response to 2,3,7,8-tetrachlorodibenzo-p-dioxin. Journal of Biological Chemistry *272*, 8878-8884.

MacKenzie, S., Baillie, G. S., McPhee, I., Bolger, G. B., and Houslay, M. D. (2000). ERK2 mitogen-activated protein kinase binding, phosphorylation, and regulation of the PDE4D cAMP-specific phosphodiesterases. The involvement of COOH-terminal docking sites and NH2-terminal UCR regions. Journal of Biological Chemistry *275*, 16609-16617.

MacKenzie, S., Fleming, I., Houslay, M. D., Anderson, N. G., and Kilgour, E. (1997). Growth hormone and phorbol esters require specific protein kinase C isoforms to activate mitogen-activated protein kinases in 3T3-F442A cells. Biochemical Journal *324*, 159-165.

MacKenzie, S. J., and Houslay, M. D. (2000). Action of rolipram on specific PDE4 cAMP phosphodiesterase isoforms and on the phosphorylation of cAMP-response-element-binding protein (CREB) and p38 mitogen-activated protein (MAP) kinase in U937 monocytic cells. Biochemical Journal *347*, 571-578.

MacKenzie, S. J., Yarwood, S. J., Peden, A. H., Bolger, G. B., Vernon, R. G., and Houslay, M. D. (1998). Stimulation of p70S6 kinase via a growth hormone-controlled phosphatidylinositol 3-kinase pathway leads to the activation of a PDE4A cyclic AMP-specific phosphodiesterase in 3T3-F442A preadipocytes. Proceedings of the National Academy of Sciences of the United States of America *95*, 3549-3554.

Manganiello, V. C., Degerman, E., Taira, M., Kono, T., and Belfrage, P. (1996). Type III cyclic nucleotide phosphodiesterases and insulin action. Current Topics in Cellular Regulation *34*, 63-100.

Marchmont, R. J., and Houslay, M. D. (1980). A peripheral and an intrinsic enzyme constitute the cyclic AMP phosphodiesterase activity of rat liver plasma membranes. Biochemical Journal *187*, 381-392.

Marks, A. R. (1996). Cellular function of Immunophilins. Physiological reviews *76*, 631-649.

Mayer, B. J., Baltimore, D. (1993). Signalling through SH2 and SH3 domains. Trends in Cell Biology *3*, 8-13.

Mayer, B. J., and Eck, M. J. (1995). SH3 Domains - Minding Your Ps and Qs. Current Biology *5*, 364-367.

Mayer, B. J., and Gupta, R. (1998). Functions of SH2 and SH3 domains. Current Topics in Microbiology and Immunology *228*, 1-22.

McGuire, J., Whitelaw, M. L., Pongratz, I., Gustafsson, J. A., and Poellinger, L. (1994). A cellular factor stimulates ligand dependent release of Hsp90 from the basic helix-loop-helix dioxin receptor. Molecular and Cellular Biology *14*, 2438-2446.

McLaughlin, M. M., Cieslinski, L. B., Burman, M., Torphy, T. J., and Livi, G. P. (1993). A low-Km, rolipram-sensitive, cAMP-specific phosphodiesterase from human brain. Cloning and expression of cDNA, biochemical characterization of recombinant protein, and tissue distribution of mRNA. Journal of Biological Chemistry *268*, 6470-6476.

McPhail, L. C. (1994). SH3-dependent assembly of the phagocyte NADPH oxidase. Journal of Experimental Medicine *180*, 2011-2015.

McPhee, I., Pooley, L., Lobban, M., Bolger, G., and Houslay, M. D. (1995). Identification, characterization and regional distribution in brain of RPDE-6 (RNPDE4A5), a novel splice variant of the PDE4A cyclic AMP phosphodiesterase family. Biochemical Journal *310*, 965-974.

McPhee, I., Yarwood, S. J., Scotland, G., Huston, E., Beard, M. B., Ross, A. H., Houslay, E. S., and Houslay, M. D. (1999). Association with the SRC family tyrosyl kinase LYN triggers a conformational change in the catalytic region of human cAMP-specific phosphodiesterase HSPDE4A4B: Consequences for rolipram inhibition. Journal of Biological Chemistry *274*, 11796-11810.

Meacci, E., Taira, M., Moos, M. J., Smith, C. J., Movsesian, M. A., Degerman, E., Belfrage, P., and Manganiello, V. (1992). Molecular cloning and expression of human myocardial cGMP-inhibited cAMP phosphodiesterase. Proceedings of the National Academy of Sciences of the United States of America *89*, 3721-3725.

Meyer, B. K., and Perdew, G. H. (1999). Characterization of the AhR-hsp90-XAP2 core complex and the role of the immunophilin-related protein XAP2 in AhR stabilization. Biochemistry *38*, 8907-8917.

Meyer, B. K., Pray-Grant, M. G., Heuvel, J. P. V., and Perdew, G. H. (1998). Hepatitis B virus X-associated protein 2 is a subunit of the unliganded aryl hydrocarbon receptor core complex and exhibits transcriptional enhancer activity. Molecular & Cellular Biology *18*, 978-988.

Michnick, S. W., Rosen, M. K., Wandless, T. J., Karplus, M., and Schreiber, S. L. (1991). Solution structure of FKBP, a rotamase enzyme and receptor for FK506 and rapamycin. Science *252*, 836-839.

Milatovich, A., Bolger, G., Michaeli, T., and Francke, U. (1994). Chromosome localizations of genes for five cAMP-specific phosphodiesterases in man and mouse. Somatic Cell & Molecular Genetics *20*, 75-86.

Miyata, Y., Chambraud, B., Radanyi, C., Leclerk, J., Lebeau, M. C., Renoir, J. M., Shirai, R., Catelli, M. G., Yahara, I., and Baulieu, E. E. (1997). Phosphorylation of the immunosuppressant FK506-binding protein FKBP52 by casein kinase II: Regulation of HSP90-binding activity of FKBP52. Proceedings of the National Academy of Sciences of the United States of America *94*, 14500-14505.

Mochly-Rosen, D. (1995). Localisation of protein kinases by anchoring proteins; a theme in signal transduction. Science *268*, 247-251.

Mochly-Rosen, D., Khaner, H., and Lopez, J. (1991). Identification of intracellular receptor proteins for activated protein kinase C. Proceedings of the National Academy of Sciences of the United States of America *88*, 3997-4000.

Monaco, L., Vicini, E., and Conti, M. (1994). Structure of two rat genes coding for closely related rolipram sensitive cAMP phosphodiesterases - multiple messenger RNA variants originate from alternative splicing and multiple start sites. Journal of Biological Chemistry *269*, 347-357.

Moreland, R. B., Goldstein, I., Kim, N. N., and Traish, A. (1999). Sildenafil citrate, a selective phosphodiesterase type 5 inhibitor: Research and clinical implications in erectile dysfunction. Trends in Endocrinology and Metabolism *10*, 97-104.

Mortensen, R. M., Conner, D. A., Chao, S., Geisterferlowrance, A. A. T., and Seidman, J. G. (1992). Production of Homozygous Mutant Es Cells with a Single Targeting Construct. Molecular and Cellular Biology *12*, 2391-2395.

Muller, T., Engels, P., and Fozard, J. R. (1996). Subtypes of type 4 cAMP phosphodiesterases: structure, regulation and selective inhibition. Trends in Pharmacological Sciences *17*, 294-298.

Muniz, M., Alonso, M., Hidalgo, J., and Velasco, A. (1996). A regulatory role for cAMP-dependent protein kinase in protein traffic along the exocytotic route. Journal of Biological Chemistry *271*, 30935-30941.

Nair, S. C., Rimerman, R. A., Toran, E. J., Chen, S., Prapapanich, V., Butts, R. N., and Smith, D. F. (1997). Molecular cloning of human FKBP51 and comparisons of immunophilin interactions with Hsp90 and progesterone receptor. Molecular & Cellular Biology *17*, 594-603.

Neer, E. J., Schmidt, C. J., Nambudripad, R., and Smith, T. F. (1994). The ancient regulatory-protein family of WD-repeat proteins. Nature *371*, 297-300.

Nemoz, G., Sette, C., and Conti, M. (1997). Selective activation of rolipram-sensitive, cAMP-specific phosphodiesterase isoforms by phosphatidic acid. Molecular Pharmacology *51*, 242-249.

Nieba, L., Krebber, A., and Pluckthun, A. (1996). Competition BIAcore for measuring true affinities: large differrences from values determined from binding kinetics. Analytical Biochemistry *234*, 155-165.

Nishiyama, K., Sugimoto, T., Kaji, H., Kanatani, M., Kobayashi, T., and Chihara, K. (1996). Stimulatory effect of growth hormone on bone resorption and osteoclast differentiation. Endocrinology *137*, 35-41.

Norstedt, G., and Palmiter, R. (1984). Secretory rhythm of growth-hormone regulates sexual differentiation of mouse liver. Cell *36*, 805-812.

O' Connell, J. C., McCallum, J. F., McPhee, I., Wakefield, J., Houslay, E. S., Wishart, W., Bolger, G., Frame, M., and Houslay, M. D. (1996). The SH3 domain of src tyrosyl protein-kinase interacts with the N- terminal splice region of the PDE4A cAMP-specific phosphodiesterase RPDE-6 (RNPDE4A5). Biochemical Journal *318*, 255-261.

Obernolte, R., Bhakta, S., Alvarez, R., Bach, C., Zuppan, P., Mulkins, M., Jarnagin, K., and Shelton, E. R. (1993). The cDNA of a human lymphocyte cyclic-AMP phosphodiesterase (PDE IV) reveals a multigene family. Gene *129*, 239-247.

Obernolte, R., Ratzliff, J., Baecker, P. A., Daniels, D. V., Zuppan, P., Jarnagin, K., and Shelton, E. R. (1997). Multiple splice variants of phosphodiesterase PDE4C cloned from human lung and testis. Biochim Biophys Acta *1353*, 287-297.

Ollendorff, V., and Donoghue, D. J. (1997). The serine/threonine phosphatase PP5 interacts with CDC16 and CDC27, two tetratricopeptide repeat-containing subunits of the anaphase-promoting complex. Journal of Biological Chemistry *272*, 32011-32018.

Owens, R. J., Lumb, S., ReesMilton, K., Russell, A., Baldock, D., Lang, V., Crabbe, T., Ballesteros, M., and Perry, M. J. (1997). Molecular cloning and expression of a human phosphodiesterase 4C. Cellular Signalling *9*, 575-585.

Owens-Grillo, J. K., Czar, M. J., Hutchison, K. A., Hoffmann, K., Perdew, G. H., and Pratt, W. B. (1996). A model of protein targeting mediated by immunophilins and other proteins that bind to hsp90 via tetratricopeptide repeat domains. Journal of Biological Chemistry *271*, 13468-13475.

Park, S. T., Aldape, R. A., Futer, O., Decenzo, M. T., and Livingston, D. J. (1992). PPIase catalysis by human FK506-binding protein proceeds through a conformational twist mechanism. Journal of Biological Chemistry *267*, 3316-3324.

Pawson, T. (1995). Protein modules and signalling networks. Nature *373*, 573-579.

Pawson, T., and Gish, G. D. (1992). SH2 and SH3 domains: from structure to function. Cell *71*, 35-362.

Pawson, T., and Nash, P. (2000). Protein-protein interactions define specificity in signal transduction. Genes and Development *14*, 1027-1047.

Pawson, T., and Scott, J. D. (1997). Signaling through scaffold, anchoring, and adaptor proteins. Science *278*, 2075-2080.

Peattie, D. A., Harding, M. W., Fleming, M. A., DeCenzo, M. T., Lippke, J. A., Livingston, D. J., and Benasutti, M. (1992). Expression and characterization of human FKBP52, an immunophilin that associates with the 90-kDa heat shock protein and is a component of steroid receptor complexes. Proceedings of the National Academy of Sciences of the United States of America *89*, 10974-10978.

Perrot-Applanat, M., Cibert, C., Geraud, G., Renoir, J. M., and Baulieu, E. E. (1995). The 59 kDa FK506-binding protein, a 90 kDa heat shock protein binding immunophilin

(FKBP59-HBI), is associated with the nucleus, the cytoskeleton and mitotic apparatus. Journal of Cell Science *108*, 2037-2051.

Perrot-Applanat, M., Lescop, P., and Milgrom, E. (1992). The cytoskeleton and the cellular traffic of the progesterone receptor. Journal of Cell Biology *119*, 337-348.

Plant, P. J., Yeger, H., Staub, O., Howard, P., and Rotin, D. (1997). The C2 domain of the ubiquitin protein ligase Nedd4 mediates Ca^{2+}-dependent plasma membrane localisation. Journal of Biological Chemistry *272*, 32329-32336.

Polson, J. B., and Strada, S. J. (1996). Cyclic nucleotide phosphodiesterases and vascular smooth muscle. Annual Review of Pharmacology and Toxicology *36*, 403-427.

Ponting, C. C. P., and Phillips, C. (1996). Rapsyn's knobs and holes: eight tetratricopeptide repeates. Biochemical Journal *314*, 1053-1054.

Ponting, C. P. (1996). Novel domains in NADPH oxidase subunits, sorting nexins, and PtdIns 3- kinases: Binding partners of SH3 domains? Protein Science *5*, 2353-2357.

Pooley, L., Shakur, Y., Rena, G., and Houslay, M. D. (1997). Intracellular localization of the PDE4A cAMP-specific phosphodiesterase splice variant RD1 (RNPDE4A1A) in stably transfected thyroid carcinoma FTC cell lines. Biochemical Journal *321*, 177-185.

Pratt, W., Silverstein, A., and Galigniana, M. (1999). A model for the cytoplasmic trafficking of signaling proteins involving the hsp90-binding immunophilins and $p50^{cdc37}$. Cellular Signalling *11*, 839-851.

Prodromou, C., Siligardi, G., O'Brien, R., Woolfson, D. N., Regan, L., Panaretou, B., Ladbury, J. E., Piper, P. W., and Pearl, L. H. (1999). Regulation of Hsp90 ATPase activity by tetratricopeptide repeat (TPR)-domain co-chaperones. EMBO Journal *18*, 754-762.

Proud, C. G. (1996). p70 S6 kinase: an enigma with variations. Trends in Biochemical Science *21*, 181-185.

Pryzwansky, K. B., Kidao, S., and Merricks, E. (1998). Compartmentalization of type 4 phosphodiesterase and cyclic AMP dependent protein kinase in neutrophils and macrophages during phagocytosis. Cell Biochemistry and Biophysics *28*, 251-275.

Qui, Y., Chen, C. N., Malone, T., Richter, L., Beckendorf, S. K., and Davis, R. L. (1991). Characterisation of the memory gene dunce of *Drosophila melanogaster*. Journal of Molecular Biology *222*.

Radanyi, C., Chambraud, B., and Baulieu, E. E. (1994). The ability of the immunophilin FKBP59-HBI to interact with the 90-kDa heat shock protein is encoded by its tetratricopeptide repeat domain. Proceedings of the National Academy of Sciences of the United States of America *91*, 11197-11201.

Ratajczak, T., and Carrello, A. (1996). Cyclophilin 40 (CyP-40), mapping of its hsp90 binding domain and evidence that FKBP52 competes with CyP-40 for hsp90 binding. Journal of Biological Chemistry *271*, 2961-2965.

Roesler, W. J., Vandenbark, G. R., and Hanson, R. W. (1988). Cyclic AMP and the induction of eukaryotic gene transcription. Journal of Biological Chemistry *263*, 9063-9066.

Ron, D., Chen, C. H., Caldwell, J., Jamieson, L., Orr, E., and Mochly-Rosen, D. (1994). Cloning of an intracellular receptor for protein kinase C: a homolog of the beta subunit of G proteins. Proceedings of the National Academy of Sciences of the United States of America *91*, 839-843.

Rosenmund, C., Carr, D. W., Bergeson, S. E., Nilaver, G., Scott, J. D., and Westbrook, G. L. (1994). Anchoring of protein kinase A is required for modulation of AMPA/kainate receptors on hippocampal neurones. Nature *368*, 853-856.

Rosenthal, E., Hunt, T., and Ruderman, J. (1980). Selective translation of mRNA controls the pattern of protein synthesis during early development of the surf clam, Spisula solidissima. Cell *20*, 487-494.

Russell, L. C., Whitt, S. R., Chen, M., and Chinkers, M. (1999). Identification of conserved residues required for the binding of a tetratricopeptide repeat domain to heat shock protein 90. Journal of Biological Chemistry *274*, 20060-20063.

Russell, T. R., and Ho, R. (1976). Conversion of 3T3 fibroblasts into adipose cells: triggering of differentiation by prostaglandin F2alpha and 1-methyl-3-isobutyl xanthine. Proceedings of the National Academy of Sciences of the United States of America *73*, 4516-20.

Rutten, W. J., Schoot, B. M., and Dupont, J. S. H. (1973). Biochemica et Biophysica Acta *315*, 378-383.

Sambrook, J., Fritsch, E. F., and Maniatis, J. (1989). Molecular cloning- a laboratory manual, Second Edition, C. Nolan, ed. (New York: Cold Spring Habour Laboratory Press).

Savany, A., Abrait, C., Nemoz, G., Legarde, M., and Prigent, A. (1996). Activation of cyclic nucleotide phosphodiesterase 4 (PDE4) from rat thymocytes by phosphatidic acid. Cellular Signalling *8*, 511-516.

Schillace, R. V., and Scott, J. D. (1999). Organization of kinases, phosphatases, and receptor signaling complexes. Journal of Clinical Investigation *103*, 761-765.

Schmidt, J. V., and Bradfield, C. A. (1996). AH receptor signaling pathways. Annual Review of Cell Developmental Biology *12*, 55-89.

Scotland, G., Beard, M., Erdogan, S., Huston, E., McCallum, F., MacKenzie, S. J., Peden, A. H., Pooley, L., Rena, N. G., Ross, A. H., Yarwood, S. J., and Houslay, M. D. (1998). Intracellular compartmentalization of PDE4 cyclic AMP-specific phosphodiesterases. Methods (Duluth) *14*, 65-79.

Scotland, G., and Houslay, M. D. (1995). Chimeric constructs show that the unique N-terminal domain of the cyclic AMP specific phosphodiesterase RD1 (RNPDE4A1A, RPDE-IV$_{A1}$) can confer membrane association upon the normally cytosolic protein chloramphenicol acetyltransferase. Biochemical Journal *308*, 673-681.

Scotland, G., and Houslay, M. D. (1998). Molecular genetic approaches III. In Protein targeting protocols, R. A. Clegg, ed. (Totowa, NJ: Humana Press Inc.), pp. 141-149.

Scott, V. E. S., and Gurnett, C. A. (1998). Overlay and bead assay. In Protein Targeting Protocols, R. A. Clegg, ed. (Totowa, NJ: Humana Press Inc), pp. 71-85.

Sette, C., and Conti, M. (1996). Phosphorylation and activation of a cAMP-specific phosphodiesterase by the cAMP-dependent protein kinase. Journal of Biological Chemistry *271*, 16526-16534.

Sette, C., Iona, S., and Conti, M. (1994). The short-term activation of a rolipram-sensitive, cAMP-specific phosphodiesterase by thyroid-stimulating hormone in thyroid FRTL-5 cells is mediated by a cAMP-dependent phosphorylation. Journal of Biological Chemistry *269*, 9245-9252.

Sette, C., Vicini, E., and Conti, M. (1994). The rat phosphodiesterase PDE3/IVd gene codes for multiple proteins differentially activated by cAMP-dependent protein kinase. Journal of Biological Chemistry *269*, 18271-18274.

Seybold, J., Newton, R., Wright, L., Finney, P. A., Suttorp, N., Barnes, P. J., Adcock, I. M., and Giembycz, M. A. (1998). Induction of phosphodiesterases 3B, 4A4, 4D1, 4D2, and 4D3 in Jurkat T- cells and in human peripheral blood T-lymphocytes by 8-bromo-cAMP and G(s)- coupled receptor agonists: Potential role in beta2-adrenoreceptor desensitization. Journal of Biological Chemistry *273*, 20575-20588.

Shakur, Y., Pryde, J. G., and Houslay, M. D. (1993). Engineered deletion of the unique N-terminal domain of the cyclic AMP-specific phosphodiesterase RD1 prevents plasma membrane association and the attainment of enhanced thermostability without altering its sensitivity to inhibition by rolipram. Biochemical Journal *292*, 677-686.

Shakur, Y., Wilson, M., Pooley, L., Lobban, M., Griffiths, S. L., Campbell, A. M., Beattie, J., Daly, C., and Houslay, M. D. (1995). Identification and characterization of the type-IVA

cyclic AMP- specific phosphodiesterase RD1 as a membrane bound protein expressed in cerebellum. Biochemical Journal *306*, 801-809.

Shi, P. Y., Maizels, N., and Weiner, A. M. (1997). Recovery of soluble, active recombinant protein from inclusion bodies. Biotechniques *23*, 1036-1038.

Short, D. B., Trotter, K. W., Reczek, D., Kreda, S. M., Bretscher, A., Boucher, R. C., Stutts, M. J., and Milgram, S. L. (1998). An apical PDZ protein anchors the cystic fibrosis transmembrane conductance regulator to the cytoskeleton. Journal of Biological Chemistry *273*, 19797-19801.

Sicheri, F., Moarefi, I., and Kuriyan, J. (1997). Crystal structure of the Src family tyrosine kinase Hck. Nature *385*, 602-609.

Sikorski, R. S., Boguski, M. S., Goebl, M., and Hieter, P. (1990). A repeating amino acid motif in CDC23 defines a family of proteins and a new relationship among genes required for mitosis and RNA synthesis. Cell *60*, 307-317.

Silverstein, A. M., Galigniana, M. D., Chen, M. S., Owens-Grillo, J. K., Chinkers, M., and Pratt, W. B. (1997). Protein phosphatase 5 is a major component of glucocorticoid receptor.hsp90 complexes with properties of an FK506-binding immunophilin. Journal of Biological Chemistry *272*, 16224-16230.

Slusarewicz, P., Nilsson, T., Hui, N., Watson, R., and Warren, G. (1994). Isolation of a matrix that binds medial golgi enzymes. Journal of Cell Biology *124*, 405-413.

Smit, L. S., Meyer, D. J., Billestrup, N., Norstedt, G., Schwartz, J., and Carter-Su, C. (1996). The role of the growth hormone (GH) receptor and JAK1 and JAK2 kinases in the activation of Stats 1, 3, and 5 by GH. Molecular Endocrinology *10*, 519-33.

Smith, C. J., Krall, J., Manganiello, V. C., and Movsesian, M. A. (1993). Cytosolic and sarcoplasmic reticulum-associated low Km, cGMP-inhibited cAMP phosphodiesterase in mammalian myocardium. Biochemical and Biophysical Research Communications *190*, 516-521.

Smith, D. B., and Johnson, K. S. (1988). Single-step purfication of polypeptides expressed in *Escherichia coli* as fusions with glutathione-S-transferase. Gene *67*, 31-40.

Smith, K. J., Scotland, G., Beattie, J., Trayer, I. P., and Houslay, M. D. (1996). Determination of the structure of the N-terminal splice region of the cyclic AMP-specific phosphodiesterase RD1 (RRNPDE4A1) by H1-NMR and identification of the membrane association domain using chimeric constructs. Journal of Biological Chemistry *271*, 16703-16711.

Soderling, S. H., Bayuga, S. J., and Beavo, J. A. (1998). Cloning and characterization of a cAMP-specific cyclic nucleotide phosphodiesterase. Proceedings of the National Academy of Sciences of the United States of America *95*, 8991-8996.

Soderling, S. H., Bayuga, S. J., and Beavo, J. A. (1999). Isolation and characterization of a dual-substrate phosphodiesterase gene family: PDE10A. Proceedings of the National Academy of Sciences of the United States of America *96*, 7071-7076.

Soderling, S. H., and Beavo, J. A. (2000). Regulation of cAMP and cGMP signalling: new phosphodiesterases and new functions. Current Opinion in Cell Biology *12*, 174-179.

Soldati, T., and Perriard, J. C. (1991). Intracompartmental sorting of essential myosin light chains: molecular dissection and *in vivo* monitoring by epitope tagging. Cell *66*, 277-289.

Souness, J. E., and Scott, L. C. (1993). Stereospecificity of rolipram actions on eosinophil cyclic AMP-specific phosphodiesterase. Biochemical Journal *291*, 389-395.

Spence, S., Rena, G., Sullivan, M., Erdogan, S., and Houslay, M. D. (1997). Receptor-mediated stimulation of lipid signaliing pathways in CHO cells elicits the rapid transient induction of the PDE1B isoform of $Ca2^{+}$/Calmodulin-stimulated cAMP phosphodiesterase. Biochemical Journal *321*, 157-163.

Spence, S., Rena, G., Sweeney, G., and Houslay, M. D. (1995). Induction of Ca^{2+}/calmodulin stimulated cyclic-AMP phosphodiesterase (PDE1) activity in chinese-

hamster ovary cells (CHO) by phorbol 12- myristate 13-acetate and by the selective overexpression of protein kinase C isoforms. Biochemical Journal *310*, 975-982.

Spiegelman, B. M., and Green, H. (1981). Cyclic AMP-mediated control of lipogenic enzyme synthesis during adipose differentiation of 3T3 cells. Cell *24*, 503-510.

Spina, D., Landells, L. D., and Page, C. P. (1998). The role of phosphodiesterase enzymes in allergy and asthma. Advances in Pharmacology *44*, 33-83.

Stryer, L. (1991). Visual excitation and recovery. Journal of Biological Chemistry *266*, 10711-10714.

Sullivan, M., Egerton, M., Shakur, Y., Marquardsen, A., and Houslay, M. D. (1994). Molecular cloning and expression, in both COS-1 cells and Saccharomyces cerevisiaea of a human cytosolic type-IVA, cyclic-AMP specific phosphodiesterase (hPDE $IV_{A\text{-}h6.1}$). Cellular Signalling *6*, 793-812.

Sullivan, M., Olsen, A. S., and Houslay, M. D. (1999). Genomic organisation of the human cyclic AMP-specific phosphodiesterase PDE4C gene and its chromosomal localisation to 19p13.1, between RAB3A and JUND. Cellular Signalling *11*, 735-742.

Sullivan, M., Rena, G., Begg, F., Gordon, L., Olsen, A. S., and Houslay, M. D. (1998). Identification and characterization of the human homologue of the short PDE4A cAMP-specific phosphodiesterase RD1 (PDE4A1) by analysis of the human HSPDE4A gene locus located at chromosome 19p13.2. Biochemical Journal *333*, 693-703.

Swinnen, J. V., Joseph, D. R., and Conti, M. (1989). Molecular cloning of rat homologues of the *Drosophila melanogaster* dunce cAMP phosphodiesterase: Evidence for a family of genes. Proceedings of the National Academy of Science of the United States of America *86*, 5325-5329.

Swinnen, J. V., Tsikalas, K. E., and Conti, M. (1991). Properties and hormonal regulation of two structurally related cAMP phosphodiesterases from the rat sertoli cell. Journal of Biological Chemistry *266*, 18370-18377.

Szpirer, C., Szpirer, J., Riviere, M., Swinnen, J., Vicini, E., and Conti, M. (1995). Chromosomal localization of the human and rat genes (PDE4D and PDE4B) encoding the cAMP specific phosphodiesterases 3 and 4. Cytogenetics & Cell Genetics *69*, 11-14.

Taira, M., Hockman, S. C., Calvo, J. C., Taira, M., Belfrage, P., and Manganiello, V. C. (1993). Molecular cloning of the rat adipocyte hormone-sensitive cyclic GMP-inhibited cyclic nucleotide phosphodiesterase. Journal of Biological Chemistry *268*, 18573-18579.

Takeda, S., Lin, C. T., Morgano, P. G., McIntyre, S. J., and Dousa, T. P. (1991). High activity of low-Michaelis-Menten constant 3', 5'-cyclic adenosine monophosphate-phosphodiesterase isozymes in renal inner medulla of mice with hereditary nephrogenic diabetes insipidus. Endocrinology *129*, 287-294.

Tatosyan, A. G., and Mizenina, O. A. (2000). Kinases of the Src family: structure and functions. Biochemistry (Mosc) *65*, 49-58.

Taussig, R., and Gilman, A. G. (1995). Mammalian membrane-bound adenylyl cyclases. Journal of Biological Chemistry *270*, 1-4.

Terlecky, S. R., Nuttley, W. M., McCollum, D., Sock, E., and Subramani, S. (1995). The Pichia pastoris peroxisomal protein PAS8p is the receptor for the C-terminal tripeptide peroxisomal targeting signal. EMBO Journal *14*, 3627-3634.

Thompson, W. J., and Appleman, M. M. (1971). Multiple cyclic nucleotide phosphodiesterase activities from rat brain. Biochemistry *10*, 311-316.

Tibbs, V. C., Gray, P. C., Catterall, W. A., and Murphy, B. J. (1998). AKAP15 anchors cAMP-dependent protein kinase to brain sodium channels. Journal of Biological Chemistry *273*, 25783-25788.

Torphy, T. J. (1998). Phosphodiesterase isozymes, molecular targets for novel antiasthma agents. American Journal of Respiratory & Critical Care Medicine *157*, 351-370.

Torphy, T. J., Zhou, H., Foley, J. J., Sarau, H. M., Manning, C. D., and Barnette, M. S. (1995). Salbutamol up-regulates PDE4 activity and induces a heterologous desensitization of U937 cells to prostaglandin E_2. Journal of Biochemistry Chemistry *270*, 23598-23604.

Turko, I. V., Francis, S. H., and Corbin, J. D. (1998). Binding of cGMP to both allosteric sites of cGMP-binding cGMP-specific phosphodiesterase (PDE5) is required for its phosphorylation. Biochemical Journal *329*, 505-510.

Van Duyne, G. D., Standaert, R. F., Karplus, P. A., Schreiber, S. L., and Clardy, J. (1991). Atomic structure of FKBP-FK506, an immunophilin-immunosuppressant complex. Science *252*, 839-842.

VanderKuur, J. A., Wang, X., Zhang, L., Allevato, G., Billestrup, N., and Carter-Su, C. (1995). Growth hormone-dependent phosphorylation of tyrosine 333 and/or 338 of the growth hormone receptor. Journal of Biological Chemistry *270*, 21738-21744.

Verghese, M. W., McConnell, R. T., Lenhard, J. M., Hamacher, L., and Jin, S. L. C. (1995). Regulation of distinct cyclic AMP-specific phosphodiesterase (phosphodiesterase type 4) isozymes in human monocytic cells. Molecular Pharmacology *47*, 1164-1171.

Vicini, E., and Conti, M. (1997). Characterisation of an intronic promoter of a cyclic adenosine 3', 5'-monophosphate (cAMP)-specific phosphodiesterase gene that confers hormone and cAMP inducibility. Molecular Endocrinology *11*, 839-850.

Von Manteuffel, S. R., Gingras, A. C., Ming, X. F., Sonenberg, N., and Thomas, G. (1996). 4E-BP1 phosphorylation is mediated by the FRAP-p70(s6k) pathway and is independent of mitogen-activated protein kinase. Proceedings of the National Academy of Sciences of the United States of America *93*, 4076-4080.

Vossler, M. R., Yao, H., York, R. D., Pan, M. G., Rim, C. S., and Stork, P. J. S. (1997). cAMP activates MAP kinase and Elk-1 through a B-Raf- and Rap1-dependent pathway. Cell *89*, 73-82.

Walden, W. E., Danielsmequeen, S., Brown, P. H., Gaffield, L., Russell, D. A., Bielser, D., Bailey, L. C., and Thach, R. E. (1988). Translational repression in eukaryotes - partial purification and characterization of a repressor of ferritin messenger RNA translation. Proceedings of the National Academy of Sciences of the United States of America *85*, 9503-9507.

Walden, W. E., and Thach, R. E. (1986). Translational control of gene expression in a normal fibroblast - characterization of a subclass of messenger-RNAs with unusual kinetic properties. Biochemistry *25*, 2033-2041.

Wall, M., Coleman, D., Lee, E., Iniguez-Lluhi, J., Posner, B., Gilman, A., and Sprang, S. (1995). The structure of the G protein heterotrimer Gi alpha 1 beta 1 gamma 2. Cell *83*, 1047-1058.

Wang, D., Deng, T., and Shaw, G. (1997). Membrane binding and enzymatic activation of a dbl homology domain require the neighboring pleckstrin homology domain. Biochemical and Biophysical Research Communications *234*, 183-189.

Wang, H. Y., Watkins, D. C., and Malbon, C. C. (1992). Antisense oligodeoxynucleotides to G(S) protein alpha-subunit sequence accelerate differentiation of fibroblasts to adipocytes. Nature *358*, 334-337.

Weng, Q. P., Andrabi, K., Klippel, A., Kozlowski, M. T., Williams, L. T., and Avruch, J. (1995). Phosphatidylinositol 3-kinase signals activation of p70 S6 kinase in situ through site-specific p70 phosphorylation. Proceedings of the National Academy of Sciences of the United States of America *92*, 5744-5748.

Westphal, R. S., Tavalin, S. J., Lin, J. W., Alto, N. M., Fraser, I. D., Langeberg, L. K., Sheng, M., and Scott, J. D. (1999). Regulation of NMDA receptors by an associated phosphatase-kinase signaling complex. Science *285*, 93-96.

Xu, B. C., Chen, W. Y., Gu, T., Ridgway, D., Wiehl, P., Okada, S., and Kopchick, J. J. (1995). Effects of growth hormone antagonists on 3T3-F442A preadipocyte differentiation. Journal of Endocrinology *146*, 131-9.

Yamazaki, A., Bartucca, F., Ting, A., and Bitensky, M. W. (1982). Reciprocal effects of an inhibitory factor on catalytic activity and noncatalytic cGMP binding sites of rod phosphodiesterase. Proceedings of the National Academy of Sciences of the United States of America *79*, 3702-3706.

Yan, C., Zhao, A. Z., Bentley, J. K., and Beavo, J. A. (1996). The calmodulin-dependent phosphodiesterase gene PDE1C encodes several functionally different splice variants in a tissue-specific manner. Journal of Biological Chemistry *271*, 25699-25706.

Yan, S. R., Fumagalli, L., Dusi, S., and Berton, G. (1995). Tumor necrosis factor triggers redistribution to a Triton X-100-insoluble, cytoskeletal fraction of beta2 integrins, NADPH oxidase components, tyrosine phosphorylated proteins, and the protein tyrosine kinase p58(fgr) in human neutrophils adherent to fibrinogen. Journal of Leukocyte Biology *58*, 595-606.

Yano, M., Kanazawa, M., Terada, K., Takeya, M., Hoogenraad, N., and Mori, M. (1998). Functional analysis of human mitochondrial receptor Tom20 for protein import into mitochondria. Journal of Biological Chemistry *273*, 26844-26851.

Yarfitz, S., and Hurley, J. B. (1994). Transduction mechanisms of vertebrate and invertebrate photoreceptors. Journal of Biological Chemistry *269*, 14329-14332.

Yarwood, S. J., Kilgour, E., and Anderson, N. G. (1998). Cyclic AMP potentiates growth hormone-dependent differentiation of 3T3-F442A preadipocytes: Possible involvement of the transcription factor CREB. Molecular & Cellular Endocrinology *138*, 41-50.

Yarwood, S. J., Sale, E. M., Sale, G. J., Houslay, M. D., Kilgour, E., and Anderson, N. G. (1999). Growth hormone-dependent differentiation of 3T3-F442a preadipocytes requires Janus kinase/signal transducer and activator of transcription but not mitogen-activated protein kinase or p70 S6 kinase signaling. Journal of Biological Chemistry *274*, 8662-8668.

Yarwood, S. J., Steele, M. R., Scotland, G., Houslay, M. D., and Bolger, G. B. (1999). The RACK1 signaling scaffold protein selectively interacts with the cAMP-specific phosphodiesterase PDE4D5 isoform. Journal of Biological Chemistry *274*, 14909-14917.

Yedovitzky, M., MochlyRosen, D., Johnson, J. A., Gray, M. O., Ron, D., Abramovitch, E., Cerasi, E., and Nesher, R. (1997). Translocation inhibitors define specificity of protein kinase C isoenzymes in pancreatic beta-cells. Journal of Biological Chemistry *272*, 1417-1420.

Young, J. C., Obermann, W. M. J., and Hartl, F. U. (1998). Specific binding of tetratricopeptide repeat proteins to the C-terminal 12-kDa domain of hsp90. Journal of Biological Chemistry *273*, 18007-18010.

Zezulak, K. M., and Green, H. (1986). The generation of insulin-like growth factor-1--sensitive cells by growth hormone action. Science *233*, 551-3.

Zhao, A. Z., Zhao, H., Teague, J., Fujimoto, W., and Beavo, J. A. (1997). Attenuation of insulin secretion by insulin-like growth factor 1 is mediated through activation of phosphodiesterase 3B. Proceedings of the National Academy of Sciences of the United States of America *94*, 3223-3228.